2019

Molecularly imprinted nanoparticles (MINPs) for molecular recognition and bio-mimetic catalysis in water

Md Arifuzzaman
Iowa State University

Molecularly imprinted nanoparticles (MINPs) for molecular recognition and bio-mimetic catalysis in water

by

MD Arifuzzaman

A dissertation submitted to the graduate faculty

in partial fulfillment of the requirements for the degree of

DOCTOR OF PHILOSOPHY

Major: Organic Chemistry

Program of Study Committee:
Yan Zhao, Major Professor
Levi Stanley
Kirill Kovnir
Wenyu Huang
Brett VanVeller

The student author, whose presentation of the scholarship herein was approved by the program of study committee, is solely responsible for the content of this dissertation. The Graduate College will ensure this dissertation is globally accessible and will not permit alterations after a degree is conferred.

Iowa State University

Ames, Iowa

2019

DEDICATION

Every challenging work needs self-efforts as well as guidance of elders especially those who were very close to my heart.

My humble effort I dedicate to my sweet and loving

Father & Mother

Whose affection, love, encouragement and help make me able to get such success and honor,

Along with all hardworking and respected

Teachers

TABLE OF CONTENTS

Page

ACKNOWLEDGMENTS

I am extremely delightful to express my indebtedness and deepest sense of gratitude and sincere thanks to my honorable supervisor Dr. Yan Zhao, for his encouragement, indispensable guidance, untiring efforts, keen interest and thoughtful advice throughout the progress of my research work. To him I owe entire success.

I would like to express my deepest sense of appreciation to Dr. William S. Jenks, Dr. Levi Stanley, Dr. Kirill Kovnir, Dr. Wenyu Huang, and Dr. Brett VanVeller to serve as my committee members and advisors. They generously devoted their time in providing me with constant ideas and direction during my study.

I would like to pay my respect and thanks to all of my honorable members of Chemistry Department, Iowa State University, for their encouragement and help during the course of this work. I offer my special thanks to Dr. Kamel Harrata for his help in carrying out mass spectroscopic analysis. I'd also like to give my thanks to Dr. Shu Xu and Dr. Sarah Cady for their support in NMR spectroscopy. Many thanks also go to the members of Yan Zhao group for healthy discussion, collaboration, and providing a good working environment in the research laboratory.

Finally, I would like to specially thank my wife for her patience and sacrifice that she showed throughout this work. Her help and encouragement were exceptionally unparalleled. I would also like to acknowledge with gratitude, the support and love of my family–my daughter (Aanaya), my parents (mother & father), my brothers, my sister, my parents in-law, my brother in-law, relatives, and friends.

ABSTRACT

Water-soluble molecularly imprinted nanoparticles (MINPs) were produced easily by double cross-linking of surfactant micelles in the presence of suitable template molecules. The micellar surface could be modified with different groups to help the binding of guest molecules. The core could be tuned though usage of amide-containing surfactants that gave a layer of hydrogen-bonding groups in the interior. The location and the orientation of these surface and internal functional groups were important to the molecular recognition of MINPs as receptors.

It remains difficult to construct mimics of enzymatic active sites with accurately positioned catalytic groups and tunable selectivity for substrates. Artificial zinc esterases were prepared through molecular imprinting a substrate-like amino template coordinated to a polymerizable zinc complex inside cross-linked micelles. The resulting catalysts were able to distinguish substrates that differed by the position of a single methyl group, chain length of the acyl chain, and substitution of the phenyl ring. The activity of the substrate was enhanced through inclusion of a thiourea functional group as an oxyanion hole to stabilize the transition state of the ester during hydrolysis.

CHAPTER 1: GENERAL INTRODUCTION

Molecularly imprinted nanoparticles (MINPs) have only been reported by the Zhao group in recent years. This dissertation presents an extended experimental investigation into the design and applications of molecularly imprinted nanoparticles as mimics of antibodies and enzymes.

The dissertation comprises of five chapters. Chapter 1 is a review of the artificial catalyst and their application as esterases. Chapter 2 is a completed research project focusing on water-soluble MINP receptors with hydrogen-bond-assisted hydrophobic binding. The study was published in the *Journal of Organic Chemistry* in 2016. The cross-linkable surfactant plays an important role in micellar imprinting. The alkyne-containing polar head group defines the boundary for the imprinting and allows surface decoration of the cross-linked micelle. It binds the template through hydrophobic and electrostatic interactions and thus acts as a functional monomer (FM). When an amide functionality was introduced into the surfactant, it strongly impacted how it interacts with template molecules, especially those containing hydrogen-bonding groups in their structures.

Chapter 3 is a completed research project focusing on the surface ligands used in the imprinting and binding of MINPs. The study was published in the ***Supramolecular Chemistry*** as a full paper in 2018. The surface groups on the MINPs can not only increase their hydrophilicity but also be used to enhance the binding of MINPs. Fortunately, these groups can be changed easily because of the click reaction used for surface functionalization. The surface ligand of MINP was found to play a significant role in the molecular recognition, but the magnitude of the effect strongly depended on the template used. The surface-cross-

linking density in MINP was tuned by the structure of the surface cross-linker, and was especially important for templates with relatively small/narrow hydrophobes.

Chapter 4 is a completed research project focusing on artificial zinc enzymes with fine-tuned active sites for highly selective hydrolysis of activated esters. The study was published in ***ACS Catalysis*** in 2018. Zinc enzymes are frequently used by nature to catalyze the hydrolysis of esters, peptides, and amides. However, it is still challenging to construct active sites with accurately positioned catalytic groups and tunable substrate selectivity. Water-soluble nanoparticles with well-defined active sites were obtained by imprinting a substrate-like amino template coordinated to a polymerizable zinc complex. The activity of the resulting artificial zinc enzyme could be tuned by the position of the amino nitrogen in the template and by the shape of the active site. Cross-linking density in the MINP core was found to impact the performance of the catalysts. The catalysts could distinguish activated esters with different acyl chains and linear vs. branched structures.

Chapter 4 is a completed research project focusing on artificial esterases with combination of noncovalent templating and post-modification enabled systematic, fine-tuning of the active site that selectively hydrolyzed aryl esters with minute structural differences under neutral conditions. The study will be submitted for publication in 2019. One of the most remarkable features of enzymes is their ability to use ordinary functional groups to achieve extraordinary catalysis. Despite tremendous interest in such synthetic catalysts, it has been difficult for chemists to construct synthetic catalysts with active sites with molecular recognition features and multiple catalytic groups working in cooperation. Molecular imprinting in the nanospace of a cross-linked micelle using easy-to-synthesize small-molecule templates served as a convenient method to build a multifunctionalized,

modifiable active site within the micellar core. A combination of noncovalent templating and post-modification enabled systematic, fine-tuning of the active site, yielding artificial esterases that selectively hydrolyzed aryl esters with minute structural differences under neutral conditions.

CHAPTER 2: WATER-SOLUBLE MOLECULARLY IMPRINTED NANOPARTICLE RECEPTORS WITH HYDROGEN-BOND-ASSISTED HYDROPHOBIC BINDING

Modified from a paper published in *Journal of Organic Chemistry* **2016**, 81, 7518−7526

MD Arifuzzaman and Yan Zhao

Department of Chemistry, Iowa State University, Ames, Iowa 50011-3111, United States

Abstract

Molecularly imprinted nanoparticles (MINPs) were prepared when surfactants with a tripropargylammonium headgroup and a methacrylate-functionalized hydrophobic tail were cross-linked in the micelle form on the surface and in the core in the presence of hydrophobic template molecules. With the surfactants containing an amide bond near the headgroup, the MINPs had a layer of hydrogen-bonding groups in the interior that strongly influenced their molecular recognition. Templates/guests with strong hydrogen-bonding groups in the midsection of the molecule benefited most, especially if the hydrophobe of the template could penetrate the amide layer to reach the hydrophobic core of the cross-linked micelles. The location and the orientation of the hydrophilic groups were also important, as they determined how the template interacted with the surfactant micelles and, ultimately, with the MINP receptors.

Introduction

Molecular recognition is at the heart of nearly every biological process, be it enzymatic catalysis, ligand–receptor binding, selective transport of nutrients across membranes, or gene expression. To recognize a guest molecule with high affinity and selectivity, the host needs to possess a binding interface complementary to the guest in size, shape, and distribution of functional groups. Over the last several decades, a great number of synthetic hosts with such features have been prepared, often through molecular synthesis.[1-3] The benefit of molecular synthesis is that well-defined host molecules can be obtained and numerous methods (spectroscopic or otherwise) may be used to study the host–guest complexes. On the other hand, molecular hosts, typically larger and more complex than the guest molecules, require significant synthetic efforts to prepare. For guest molecules with complex functionality and shape, designing hosts with good (let alone perfect) complementarity can be extremely challenging.

Molecular imprinting is a conceptually different method to create guest-complementary hosts.[4-14] In a typical procedure, free radical polymerization is induced in a mixture of template molecules, functional monomers (FMs) that bind the templates by noncovalent or covalent bonds, and cross-linkers to maintain rigidity of the resulting polymer. The cross-linked material, after removal of the templates by washing or bond cleavage, is left with cavities complementary to the templates and thus considered "molecularly imprinted" with the templates. The method has been adopted by numerous researchers for a wide range of applications in molecular recognition, separation, enzyme-mimetic catalysis, and chemical sensing. In addition to traditional macroporous polymers, imprinting could occur on surface and even unimolecularly within dendrimers.[15,16]

An extremely attractive feature of molecular imprinting is the simplicity in the design and preparation of molecularly imprinted polymers (MIPs). Free radical polymerization is easy to perform and guest-complementary binding sites are created by the imprinting process, without the need of custom design for each individual guest. As a result, the method can be used by scientists without substantial training in supramolecular chemistry and organic synthesis.

Nonetheless, there remain a number of challenges in this technique. For example, it is generally accepted that binding sites in MIPs are heterogeneous and poorly defined in structure.[4-6,8-12,17,18] Conventional MIPs are intractable macroporous polymers and limited methods are available to understand their structure and binding properties.[19] Template molecules are frequently trapped deep inside the cross-linked and polymeric matrix and difficult to be removed. Although soluble nanoparticle MIPs have been reported,[20-28] aqueous compatibility remains a challenge.[29]

We have been interested in the design and synthesis of functional receptors through biomimetic strategies. Recently, we reported a method to imprint within cross-linked surfactant micelles to create molecularly imprinted nanoparticles (MINPs). Our method worked well for a number of water-soluble molecules including bile salt derivatives,[30] aromatic carboxylates and sulfonates,[31-33] and nonsteroidal anti-inflammatory drugs (NSAIDs).[34] In addition, we could install specific functional groups in the MINP binding site and chemically modify the functional groups.[32] Because the MINPs are fully soluble in water and similar to protein in size (40–60 KD in MW), we could study their binding by techniques used for molecular receptors such as fluorescence titration, isothermal titration calorimetry (ITC), and chemical derivatization. They are similar to water-soluble proteins in topology,

having a hydrophilic exterior and a hydrophobic core with guest-complementary binding sites.

The most important building block in the MINP synthesis is the cross-linkable surfactant that serves multiple roles in the molecular imprinting. Its micellization defines the boundary for polymerization and cross-linking, and enables the highly cross-linked MINPs to be fully soluble due to their nanosize and solubilizing ligands on the surface. It serves as the FM to bind the template (mainly through hydrophobic and electrostatic interactions), as well as one of the cross-linkers to maintain integrity of the binding site. Its alkynyl headgroup allows facile surface-decoration of the nanoparticles with different functional groups.

In this paper, we report two new cross-linkable surfactants synthesized from more readily available, less expensive starting materials than the previously reported surfactant. Importantly, their amide group within the structure enables the surfactants to interact with the template or guest molecules by hydrogen bonds, in additional to hydrophobic and electrostatic interactions. Our study also yielded interesting insight into how the position of the amide bond affects the imprinting process and molecular recognition of the MINPs. The binding pockets in the MINPs were found to be highly discriminating, even toward very similar guest molecules.

Result and Discussion

Design, Synthesis of MINPs and Characterization of cross-Linkable Surfactants

Our previously reported MINPs were prepared using cross-linkable surfactant **1**.[30-32,34] Its tripropargylammonium headgroup enables facile cross-linking and decoration of the micellar surface by the alkyne–azide click reaction (Scheme 1).[35,36] The hydrophobic C12 chain provides necessary amphiphilicity to the surfactant. The methacrylate allows the

surfactant to be cross-linked in the core (with DVB) by free radical polymerization. Dynamic light scattering (DLS) showed that each MINP contained approximately 50 (cross-linked) surfactant molecules. Thus, with a surfactant/template ratio of 50:1 in the preparation, the MINPs obtained typically have on average one binding site per nanoparticle. Doubling the amount of template resulted in two binding sites per nanoparticle, as demonstrated in a previous study.[30]

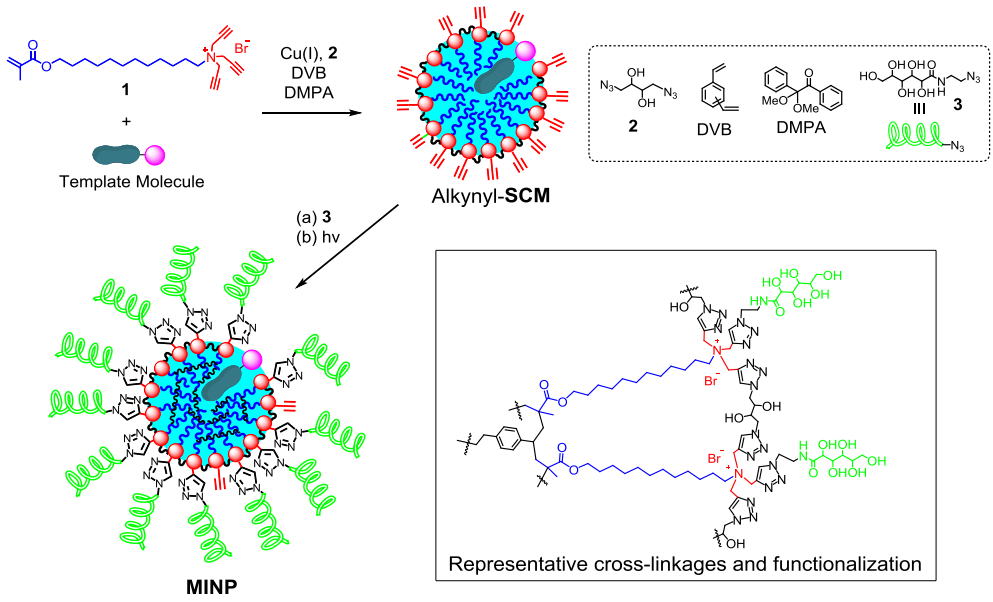

Scheme 1. Preparation of MINP by surface-cross-linking of micelle of **1**, surface decoration of resulting alkynyl-surface-cross-linked micelle (alkynyl-SCM) by ligand **3**, and core-cross-linking of the resulting material to afford MINP with an internal binding site complementary to the template molecule.

Surfactant **1** was synthesized in a three-step reaction from 1,12-dodecanediol—i.e., monomethacrylation of the diol, conversion of the remaining alcohol to trifluoromethansulfonate (triflate) with triflic anhydride, and nucleophilic substitution of the triflate with tripropargylamine. Although the synthetic route is short, it requires two expensive reagents (i.e., triflic anhydride and tripropargylamine), and a final ion exchange must be done to replace triflate with a more soluble anion such as bromide.[30]

In this study, we have designed two new cross-linkable surfactants prepared from commercially available δ-undecalactone (Scheme 2). Ring opening of the lactone by 5 equiv ethylenediamine or butylenediamine at room temperature afforded amine **5a** and **5b**, respectively. The amine could be used in the next step simply after removing the excess ethylenediamine or butylenediamine by co-evaporation with methanol under vacuum. Propargylation of **5a** or **5b** occurred readily in acetonitrile with propargyl bromide and sodium bicarbonate, thus avoiding the more expensive tripropargylamine. The ammonium salt **6a** or **6b** was treated with methacryloyl chloride, which converted the hydroxyl group on the hydrophobic tail into methacrylate to yield the final surfactant **4a** and **4b**.

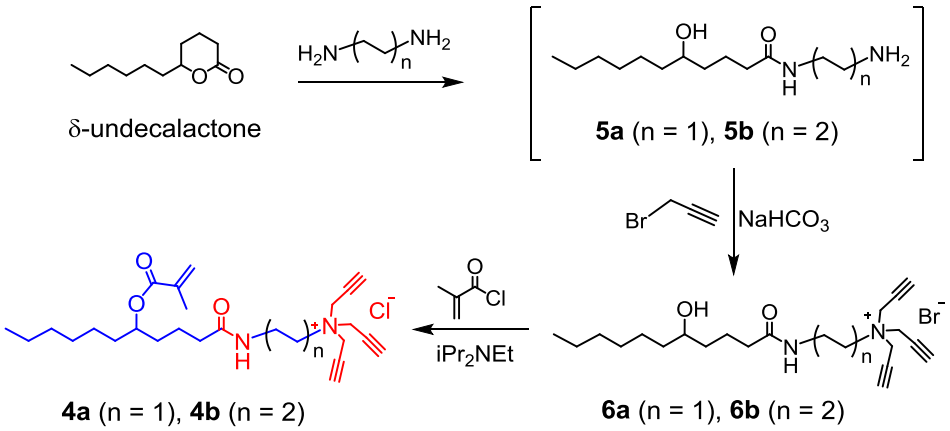

Scheme 2. Synthesis of cross-linkable surfactants **4a** and **4b** from δ-undecalactone.

In addition to easier synthesis from less expensive starting materials, the new surfactants (**4a** and **4b**) have an internal amide bond on the hydrophobic backbone. Although one might think hydrogen bonds in aqueous solution does not contribute too much to guest-binding, the hydrogen bonds in our case are located within the micelle and ultimately within the hydrophobic core of the MINP. The local hydrophobicity around the amide bonds should increase the strength of the hydrogen bonds significantly and make them potentially important to guest binding. Surfactants **4a** and **4b** differ in the number of carbons between

the amide bond and the tripropargylammonium headgroup. Because the ammonium headgroup has to stay on the surface of the micelle/MINP, in contact with water, the hydrogen bonds are deeper within the hydrophobic core of $MINP_{\mathbf{4b}}$ (i.e., MINP prepared with **4b** as the cross-linkable surfactant) than within the core of $MINP_{\mathbf{4a}}$.

One of the most important properties of a surfactant is its critical micelle concentration (CMC), above which micelles begin to form. To determine the CMC, we used the method of pyrene solubilization.[37] The method afforded similar CMC values as those determined from the reduction of surface tension for analogous surfactants.[35,38] Briefly, we prepared aqueous solutions of the surfactants in different concentrations, with 0.1 μM of pyrene in water. Pyrene is an environmentally sensitive fluorescent probe with five vibronic bands. The first band (I_1) near 372 nm becomes stronger in a more polar environment and the third (I_3) near 384 nm changes little. The I_3/I_1 ratio thus increases with decreasing environmental polarity.

As shown in Figure 1a,b, the I_3/I_1 ratio initially showed very small change but began to rise sharply as the surfactant concentration increased beyond a certain point. The probe apparently was in the aqueous phase in the beginning but entered a nonpolar environment at higher surfactant concentrations. The inflection point of the curve normally is considered the CMC of the surfactant, and was 0.41 mM for **4a** and 0.27 mM for **4b**. The lower CMC for the latter was reasonable given its higher hydrophobicity. It is also possible that the deeper location of the amide in the hydrophobic core of the micelle strengthens the hydrogen bonds among the amide groups and stabilize the micelle in the meantime.

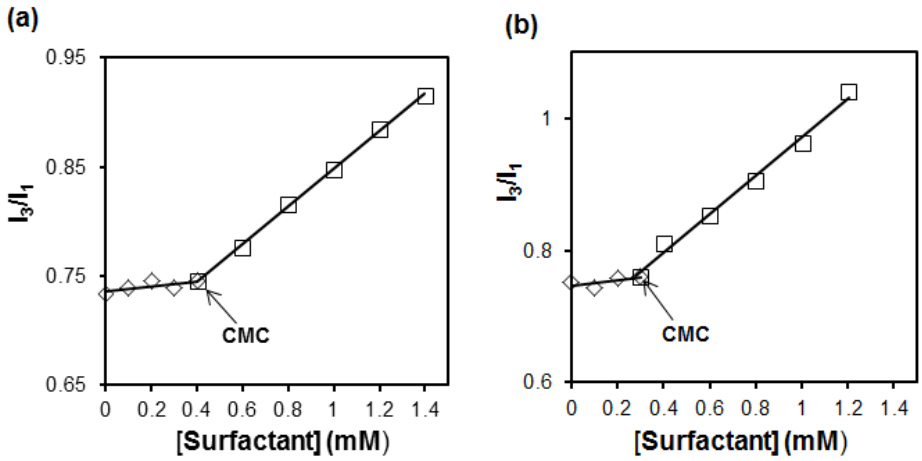

Figure 1. (a) Pyrene I_3/I_1 ratio as a function of [**4a**]. (b) Pyrene I_3/I_1 ratio as a function of [**4b**]. [pyrene] = 0.1 μM

Contribution of Hydrogen-Bonds to Molecular Imprinting and Guest-Binding

To understand whether the amide group in **4a** and **4b** could enhance the guest binding of MINPs by hydrogen bonds, we designed three template molecules **7**–**9** whose syntheses are shown in Scheme 3. The templates all have a fluorescent dansyl group connected to an aminobenzoate derivative through sulfonamide. The benefit of using dansyl as the hydrophobic group is its environmentally sensitive emission that enables us to study the binding by fluorescence spectroscopy, in addition to ITC (vide infra). The choice of having a carboxylate in the template is two-fold. First, its anionic nature makes it electrostatically attracted to the cationic micelle and the final MINP. Second, incomplete template removal is frequently a problem in conventional imprinting.[19] Being ionic, the carboxylate has to stay on the surface of the micelle to be solvated by water, while the dansyl group will prefer to stay inside the micelle due to its hydrophobicity. The carboxylate then serves as an anchor to keep the template near the micelle surface, making the binding site easily vacated after imprinting and readily accessible to guest molecules during re-binding.[30]

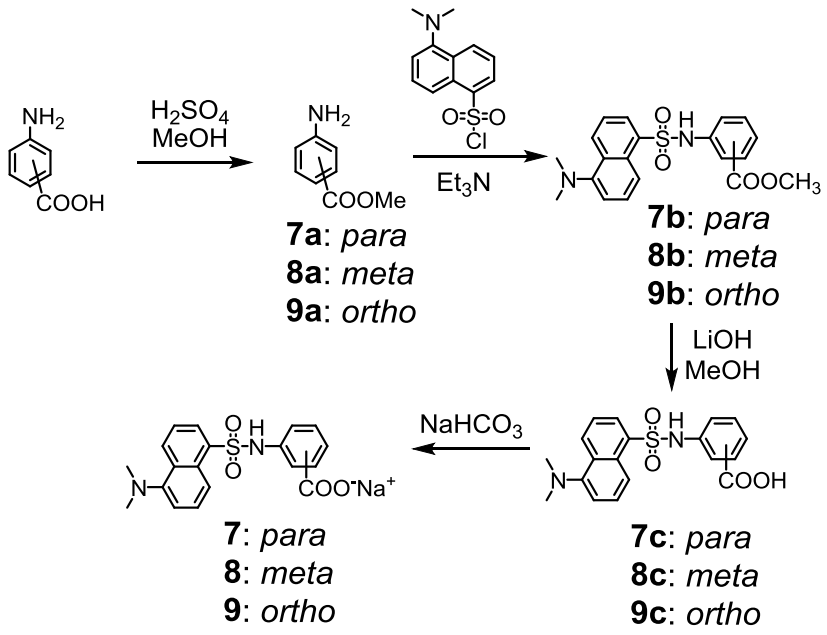

Scheme 3. Syntheses of templates **7**–**9** from the corresponding aminobenzoic acids.

The three templates differ in the substitution of the aminobenzoate moiety. The different substitutions keep the carboxylate and the sulfonamide in different distances. Since we expect the carboxylate of the template to interact with the ammonium headgroup of the surfactant electrostatically and the sulfonamide of the template with the amide of the surfactant by hydrogen bonds, it might be beneficial to match the distance between the ionic and the hydrogen-bonding functional group in the two.

Preparation of MINPs followed Scheme 1 and detailed procedures are found in the Experimental Section. In general, the surface-cross-linking and core-polymerization were monitored by ^{1}H NMR spectroscopy and DLS.[30] ^{1}H NMR spectroscopy normally shows broadening/disappearance of characteristic signals as the surfactant and DVB (core-cross-linker) undergo free radical polymerization. DLS gives the size of the nanoparticles and allows us to estimate the molecular weight of the MINP and the number of (cross-linked) surfactants within a MINP. The surface-cross-linked micelles previously were characterized

also by transmission electron microscopy (TEM) and mass spectrometry (after cleaving the surface-cross-linkages).[35]

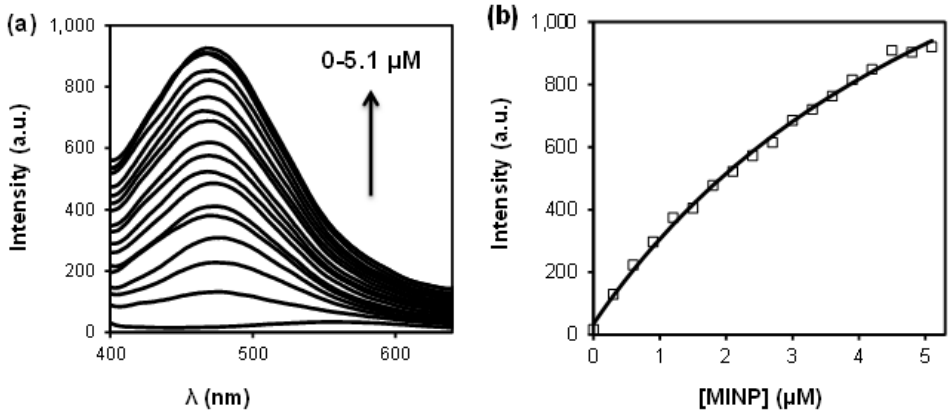

Figure 2. (a) Emission spectra of compound **7** in the presence of 0–5.1 μM of MINP$_1$(**7**) in Millipore water. [**7**] = 0.2 μM. λ_{ex} = 340 nm. (b) Nonlinear least squares curve fitting of the fluorescence intensity at 463 nm to a 1:1 binding isotherm.

Figure **2a** shows the emission spectra of template **7** upon titration with MINP$_1$(**7**), i.e., MINP prepared with cross-linkable surfactant **1** and template **7**. The addition of MINP caused a large blue shift in the emission maximum of dansyl from ~550 to ~470 nm, while greatly enhancing the emission intensity. Dansyl is known to fluoresce weakly in water but strongly in nonpolar environments; its emission wavelength typically increases with increasing environmental polarity.[39] The blue shift and stronger emission indicate that the probe entered a nonpolar microenvironment during titration, in agreement with its binding by MINP. The fluorescence data fit well to a 1:1 binding model and afforded a binding constant (K_a) of (15.3 ± 1.1) × 10^4 M^{-1} in water (Figure 2b).

The binding was also studied by ITC, one of the most reliable ways to study intermolecular interactions.[40] By measuring the heat change during the titration, ITC yields a wealth of information on the binding, including the binding constant (K_a), enthalpy (ΔH), and

the number of binding sites per particle (N). The binding free energy (ΔG) can be calculated from K_a using equation $-\Delta G = RT\ln(K_a)$, and ΔS can be calculated from ΔG and ΔH. As shown in Figure 2, the binding exhibited a negative/favorable enthalpy, with $K_a = (12.8 \pm 0.3) \times 10^4\ M^{-1}$. The binding constant agreed well with the value obtained by fluorescence titration. The average number of binding site per nanoparticle (N) was 1.3 ± 0.2, also consistent with the 1:1 binding model.

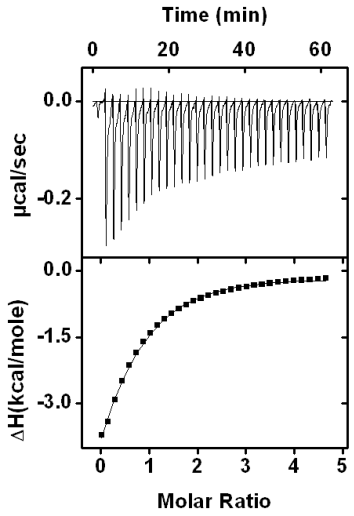

Figure 3. ITC curve obtained at 298.15 K from titration of $MINP_1$(**7**) with **7** in water. $MINP_1$(**7**) = 10 µM in the cell. The concentration of **7** in the syringe was 0.2 mM.

Table 1 summarizes the binding data obtained for the three model templates by different MINPs. Entries 1–3 compare the effectiveness of molecular imprinting of the same template (**7**) by the three different surfactants. The binding data, whether those from ITC or fluorescence titration, all point to **4a** as the most effective cross-linkable surfactant among the three. $MINP_{4a}$(**7**) bound template **7** nearly one order of magnitude stronger than $MINP_1$(**7**) prepared from the original cross-linkable surfactant. Although $MINP_{4b}$(**7**) showed weaker binding than $MINP_{4a}$(**7**), both amide-functionalized surfactants clearly outperformed **1** as far as the binding affinity of the MINP was concerned.

Table 1. Binding data for MINPs (obtained by ITC unless indicated otherwise) [a]

Entry	MINP[b]	Guest	-Δ*G* (kcal/mol)	*N*	K_a (10^4 M^{-1})	-Δ*H* (kcal/mol)	TΔ*S* (kcal/mol)
1	$MINP_1$(7)	7	6.8	1.3 ± 0.2	12.8 ± 0.3 (15.3 ± 1.1)	4.7 ± 0.9	2.2
2	$MINP_{4a}$(7)	7	8.1	1.0 ± 0.1	90.4 ± 2.8 (99.3 ± 1.6)	7.99 ± 0.95	0.1
3	$MINP_{4b}$(7)	7	7.2	1.5 ± 0.1	46.6 ± 3.9 (40.2 ± 2.6)	4.66 ± 0.1	3.1
4	$MINP_1$(8)	8	6.6	1.0 ± 0.3	7.70 ± 0.30 (8.2 ± 1.0)	3.15 ± 1.0	2.8
5	$MINP_{4a}$(8)	8	7.7	0.5 ± 0.1	42.6 ± 0.8 (35.6 ± 2.1)	2.45 ± 0.24	5.2
6	$MINP_{4b}$(8)	8	6.2	0.8 ± 0.1	22.3 ± 1.2 (25.7 ± 1.9)	1.36 ± 0.4	5.9
7	$MINP_1$(9)	9	6.7	0.8 ± 0.1	12.0 ± 1.2 (11.0± 1.3)	2.15 ± 0.6	4.8
8	$MINP_{4a}$(9)	9	6.2	1.1 ± 0.1	34.0 ± 1.2 (33.0 ± 1.7)	3.28 ± 0.6	4.3
9	$MINP_{4b}$(9)	9	7.0	0.8 ± 0.2	14.7 ± 0.5 (21.7 ± 1.8)	3.15 ± 0.92	3.9
10	$MINP_{1:4a=1:3}$(7)	7	7.8	0.7 ± 0.1	51.6 ± 3.5	9.54 ± 0.15	-1.8
11	$MINP_{1:4a=1:1}$ (7)	7	7.5	1.5 ± 0.1	32.5 ± 2.7	3.80 ± 0.05	3.7
12	$MINP_{1:4a=3:1}$ (7)	7	6.9	1.4 ± 0.1	12.6 ± 1.4	1.3 ± 0.04	5.7
13	$MINP_{4a}$(7)	8	6.8	1.6 ± 0.1	9.40 ± 0.17	0.70 ± 0.03	6.1
14	$MINP_{4a}$(7)	9[c]	-	-	-	-	-
15	$MINP_{4a}$(8)	7	6.2	1.6 ± 0.1	9.07 ± 1.36	0.25 ± 0.02	6.5
16	$MINP_{4a}$(8)	9	6.5	0.7 ± 0.1	5.72 ± 0.13	1.6 ± 0.09	4.9
17	$MINP_{4a}$(9)	7[c]	-	-	-	-	-
18	$MINP_{4a}$(9)	8	5.2	1.4 ± 0.3	7.87 ± 0.95	7.4 ± 0.2	0.6

[a] The titrations were generally performed in duplicates in Millipore water and the errors between the runs were <20%. The binding constants in parentheses were from fluorescence titration and thus the number of binding sites and binding enthalpy/entropy were not available. [b] The subscript denotes the cross-linkable surfactant used in the MINP synthesis and the number in parentheses the template molecule. [c] Binding was too weak to be detected by ITC.

The same trend was maintained for templates **8** and **9** (Table 1, entries 4–6 and 7–9), with the binding affinity displaying a consistent order of $MINP_{\mathbf{4a}}$ > $MINP_{\mathbf{4b}}$ > $MINP_{\mathbf{1}}$. Thus, the two amide-functionalized surfactants clearly worked better than the original **1** for the model templates, regardless of their substitution pattern. The data also suggest that hydrogen bonds between the template and the cross-linkable surfactants were important to the binding.

We also prepared the nonimprinted nanoparticles from surfactant **1**, **4a**, and **4b**, respectively, and found none of the guest molecules (**7**–**9**) could bind the nanoparticles (Figure 15–17). The results further confirmed the molecular imprinting and ruled out nonspecific interactions between the MINPs and the guests.

If we compare the binding affinities of MINPs prepared from the same surfactant for different templates, $MINP_{\mathbf{1}}$ was practically insensitive to the substitution pattern of the template, with ITC-measured K_a = 12.8, 7.70, and 12.0 × 10^4 M^{-1} for **7**, **8**, and **9**, respectively (Table 1, entries 1, 4, and 7). $MINP_{\mathbf{4a}}$ and $MINP_{\mathbf{4b}}$, on the other hand, showed a consistent trend in their affinities, i.e., **7** > **8** > **9** (Table 1, compare entries 2, 5, 8, or 3, 6, 9). Note that the different K_a values do NOT reflect the binding selectivity of the MINPs (which will be discussed later), as they are the binding constants between three different template molecules and their corresponding MINPs.

Overall, two consistent trends were observed for the amide-functionalized MINPs regarding their binding affinity: $MINP_{\mathbf{4a}}$ > $MINP_{\mathbf{4b}}$ for all three templates (**7**–**9**) and templates **7** > **8** > **9** for both MINPs. These results, first of all, suggest there is no special benefit in matching the distance between the ionic and the hydrogen-bonding functional group in the surfactant and the template. This is because the better surfactant (**4a**) of the two

has a shorter distance between these groups and the best template (**7**) among the three has the longest distance.

One possible reason for the observed binding trend of **7** > **8** > **9** is the depth of the hydrophobic dansyl group. Compound **7** has the dansyl and carboxylate *para* to each other. Since the carboxylate has to stay on the surface of the micelle/MINP, **7** is expected to have its dansyl deeper in the MINP hydrophobic core than either the *meta* (**8**) or *ortho* (**9**) derivative. When both hydrogen-bonding and hydrophobic interactions are involved in guest-binding, we need to maximize both interactions to have the highest binding affinity.[41] To engage in hydrogen-bonds, the sulfonamide of the template needs to be close to the amide groups in the final MINP. Such an arrangement seems easily achievable for all three templates, by their tilting to different degrees with the carboxylate anchored on the MINP surface. To maximize the hydrophobic interactions, however, dansyl needs to penetrate the amide layer and reach into the hydrocarbon core, and template **7** seems to have a clear advantage over the other two due to its *para* substitution.

Why didn't substitution pattern of the template influence the binding of $MINP_1$, prepared from the amide-free surfactant? The most likely reason is the solvation of the sulfonamide group. Being highly hydrophilic, the sulfonamide can be "solvated" properly either by water or through interactions with the amide bonds of the surfactants. Since there are no amide groups in the micellar core of $MINP_1$, the only way for the sulfonamide to be properly solvated is to stay on the micellar surface, exposed to water. When both the carboxylate and sulfonamide need to stay on the micellar surface, the aminobenzoate moiety of the template is exposed to water and thus contributes little to binding. What is most important to the binding under such a circumstance are the hydrophobic interactions from

burying the dansyl from solvent exposure and the electrostatic interactions between the oppositely charged host and guest—both are fairly constant among the three templates.

We also prepared MINPs using a mixture of **1** and **4a** in different ratios (Table 1, entries 10–12). The original idea was that, in doing so, the hydrogen bonds between **4a** and the template would be formed in a "background" (or microenvironment) of hydrocarbon and might be stronger. Essentially, surfactant **1** would create a hydrocarbon-based micellar core, which could be drier and helpful to the hydrogen-bonding interactions between **4a** and the template. Instead, our data showed a monotonous decrease of K_a with decreasing **4a** in the MINP formulation (compare entries 2, 10, 11, 12, and 1), suggesting that the hypothesis was incorrect.

A key feature of molecularly imprinted polymers is their binding selectivity toward structural analogues. To understand this property, we titrated our MINPs with the "wrong" guest molecules, e.g., MINP$_{\mathbf{4a}}$(**7**) with **8** and **9** and likewise for the other MINPs. Our imprinted cross-linked micelles showed good selectivity consistently. For example, MINP$_{\mathbf{4a}}$(**7**) bound its template **7** most strongly among the three isomeric guests (entry 2). The binding constant decreased by nearly 10-fold for the *meta* derivative **8** (entry 13) and was undetectable for the *ortho* guest **9** (entry 14). For MINP$_{\mathbf{4a}}$(**9**) imprinted against the *ortho* derivative, the strongest binding was observed for **9** as expected (entry 8). Binding for the *meta* derivative **8** was about 1/4 as strong (entry 18) and undetectable for the *para* derivative **7** (entry 17). For MINP$_{\mathbf{4a}}$(**8**) imprinted against the *meta* derivative, its best guest was certainly its own template (entry 5) but, interestingly, both the *para* and *ortho* derivatives showed binding, albeit with a lower affinity (entries 15 and 16). These data suggest the MINPs overall were very selective and bind their own templates the best. In their binding of

the "wrong" constitutional isomers, a mismatch of substitution by 1 (from 1,4 to 1,3; from 1,2 to 1,3; or from 1,3 to 1,2 or 1,4) gave weaker but measurable binding, whereas a mismatch by 2 (from 1,2 to 1,4 or vice versa) could not be tolerated at all.

Binding of Other Guests

The above studies gave us a good understanding of how amide-functionalized MINPs bind model guests containing hydrogen-bonding groups in the structure. Both $MINP_{\mathbf{4a}}$ and $MINP_{\mathbf{4b}}$ clearly outperformed the original $MINP_{\mathbf{1}}$ without internal hydrogen-bonding capabilities. To see whether the advantage is maintained with other templates, we generated MINPs using **4a** (the best surfactant in this study) for four other templates (**10**–**13**). All four templates have been imprinted previously with surfactant **1**. Among the four templates, bile salt **10** had multiple hydrogen-bonding groups (hydroxyl and sulfonamide) arranged in a facially amphiphilic fashion.[30] 1-Naphthoic acid sodium salt **11** had a hydrocarbon aryl hydrophobe but no (heteroatom) hydrogen-bonding functionalities in the hydrophobe (other than the carboxylate).[31] Naproxen and Indomethacin are both nonsteroidal anti-inflammatory drugs (NSAIDs), with Indomethacin **13** having a strong hydrogen-bonding amide group in the midsection of the molecule (as opposed to the ether in **12**).[34]

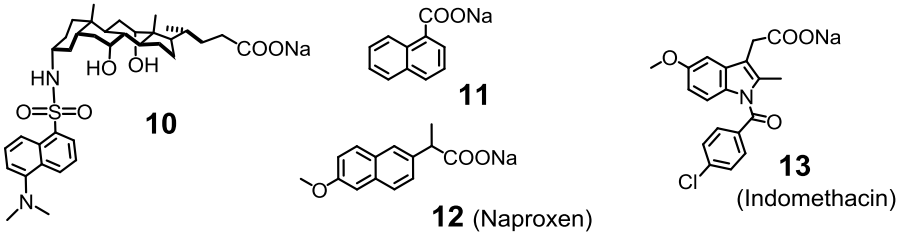

A quick glance of the binding data in Table 2 shows that the amide-containing surfactant (**4a**) was not always a winner. For the two NSAIDs (**12** and **13**), $MINP_{\mathbf{4a}}$ showed 30–40% stronger binding than $MINP_{\mathbf{1}}$, but for templates **10** and **11**, the opposite was true. Overall, the binding data are consistent with the earlier notion that templates with internal

hydrogen-bonding functionalities benefit most from the amide-containing **4a**. For example, as far as internal hydrogen-bonding capabilities are concerned, templates **11**–**13** should follow the order of **11** < **12** < **13**, as the template possesses an increasing number of ether and amide. The relative binding constant of MINP$_{\mathbf{4a}}$ to MINP$_{\mathbf{1}}$ (i.e., K_{rel} in Table 2) increased steadily from 0.2 to 1.3 to 1.4 for the three templates.

Table 2. Binding data for MINPs obtained by ITC[a]

Entry	MINP	Guest	-Δ*G* (kcal/mol)	*N*	K_a (10^4 M^{-1})	K_{rel}[b]	-Δ*H* (kcal/mol)	TΔ*S* (kcal/mol)
1	MINP$_{4a}$(10)	10	8.3	0.9 ± 0.1	126 ± 6	0.4	7.67 ± 0.3	0.6
2	MINP$_1$(10)	10	8.9	1.0 ± 0.1	347 ± 23	1	33.1 ± 2.6	-24.2
3	MINP$_{4a}$(11)	11	6.8	0.7 ± 0.1	9.8 ± 0.6	0.2	5.67 ± 0.9	1.1
4	MINP$_1$(11)	11	7.7	1.1 ± 0.1	42.9 ± 1.3	1	6.7 ± 0.2	1.0
5	MINP$_{4a}$(12)	12	8.3	0.7 ± 0.1	115 ± 5	1.3	1.20 ± 0.14	7.1
6	MINP$_1$(12)	12	8.1	0.6 ± 0.1	91 ± 4	1	28.1 ± 6.0	-20.0
7	MINP$_{4a}$(13)	13	8.4	0.5 ± 0.1	140 ± 9	1.4	1.48 ± 0.18	6.9
8	MINP$_1$(13)	13	8.2	1.1 ± 0.1	98 ± 5	1	26.9 ± 1.0	-18.7

[a] Binding was measured in 50 mM Tris buffer (pH = 7.4). The titrations were generally performed in duplicates and the errors between the runs were <20%. The binding data for MINP$_{\mathbf{4a}}$ were obtained in the current study and those for MINP$_{\mathbf{1}}$ were taken from previous publications for templates **10**,[30] **11**,[31] and **12**–**13**.[34] [b] K_{rel} is the binding affinity of MINP$_{\mathbf{4a}}$ relative to MINP$_{\mathbf{1}}$ for the same template.

Our model compounds **7**–**9** have stronger internal hydrogen-bonding capabilities than **11**–**13**, with the sulfonamide group possessing both hydrogen-bond donors and acceptors. Indeed, K_{rel} was even higher and was calculated to be 2.8 for **9**, 5.5 for **8**, and 7.1 for **7** from the binding data in Table 1. The continuous increase of K_{rel} from the *ortho* to *meta* to *para* template indicates that the template benefiting most from the amide-containing surfactant had its hydrogen-bonding sulfonamide deepest in the MINP hydrophobic core. The result is very

reasonable: the deeper the hydrogen-bonding group into the hydrophobic core, the more it can be shielded from water and the stronger the hydrogen bonds will be.

Once the above picture is made clear, it becomes quite obvious why the amide-functionalized surfactant did not help bile salt derivative **10**. Although the template has many hydrogen-bonding groups, they are all on the α face of the cholate, opposite to the hydrophobic β face. Because hydrophobic interactions are key to the incorporation of the hydrophobic template into the micelle, **10** could lie flat on the micellar surface, having the hydrophilic face toward water and hydrophobic face toward the interior of the micelle. With such an orientation, the amide groups inside the micelle of **4a** would have little chance interacting with the template through hydrogen bonds. To make things worse, the layer of amide bonds near the surface of the micelle would weaken the hydrophobic interactions between **10** and the micelle (ultimately $MINP_{\mathbf{4a}}$). This could be the reason why $MINP_{\mathbf{4a}}$(**10**) displayed much weaker binding toward the template than $MINP_{\mathbf{1}}$(**10**) (Table 2, entries 1 and 2). The same could the reason why template **11** was bound more strongly by $MINP_{\mathbf{1}}$(**11**) than $MINP_{\mathbf{4a}}$(**11**).

Conclusions

Our study so far gives a consistent mechanistic picture in the binding of amide-functionalized MINPs. Surfactant **4a** with two methylene groups between the tripropargylammonium headgroup and the amide outperformed surfactant **4b** with four methylene groups. In general, **4a** was most effective in the molecular imprinting of template molecules with strong hydrogen-bonding functionalities but the location of these functional groups was also critical. Overall, the binding between amide-functionalized MINPs and the templates are driven by a combination of hydrophobic and hydrogen-bonding interactions (in

addition to electrostatic interactions in our case). To maximize the hydrophobic interactions, the template/guest molecule needs to possess a sizable hydrophobe but it is best for the hydrophobe to penetrate the amide layer to reach into the hydrophobic core of the MINP. To maximize the hydrogen-bonding interactions, the templates should possess strong hydrogen-bonding groups that can favorably interact with the internal amide bonds geometrically.

The most significant learning in this work is a detailed understanding of how different intermolecular interactions can be used rationally to enhance the binding of molecularly imprinted nanoparticle receptors. MIPs are traditionally intractable cross-linked polymers that prohibit detailed study of their binding mechanisms. The water-solubility, nanodimension, and fine-tunability of our MINPs gave us tremendous opportunities to examine the details of binding. The knowledge generated will enable better designs of these protein-mimetic "plastic antibodies" that could find many applications in chemistry and biology.

Acknowledgement

We thank the National Institute of General Medical Sciences of the National Institutes of Health (R01GM113883) and NSF (DMR-1464927) for financial support of this research.

Experimental Section

General Method

All reagents and solvents were of ACS-certified grade or higher, and were used as received from commercial suppliers. Routine ^{1}H and ^{13}C NMR spectra were recorded on a Bruker DRX-400 or on a Varian VXR-400 spectrometer or a Bruker Avance III 600 spectrometer. MALDI-TOF mass was recorded on a Thermobioanalysis Dynamo mass spectrometer. Dynamic light scattering (DLS) was performed on a PD2000DLS+ dynamic

light scattering detector. Fluorescence spectra were recorded at ambient temperature on a Varian Cary Eclipse Fluorescence spectrophotometer. ITC was performed using a MicroCal VP-ITC Microcalorimeter with Origin 7 software and VPViewer2000 (GE Healthcare, Northampton, MA).

Syntheses

Syntheses of compounds **1**, **2**, **3**, **4**, and **10** were previously reported.[40]

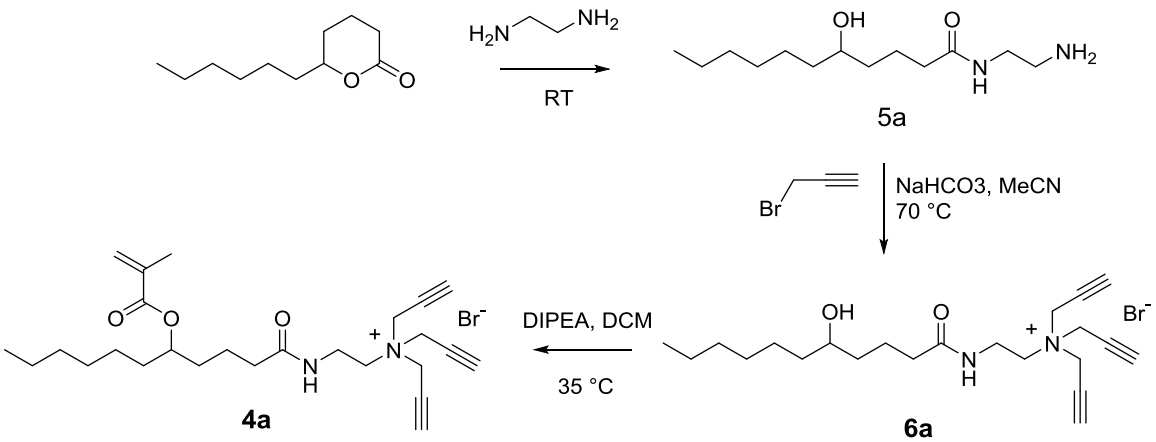

Scheme 4. Syntheses of compound **4a**

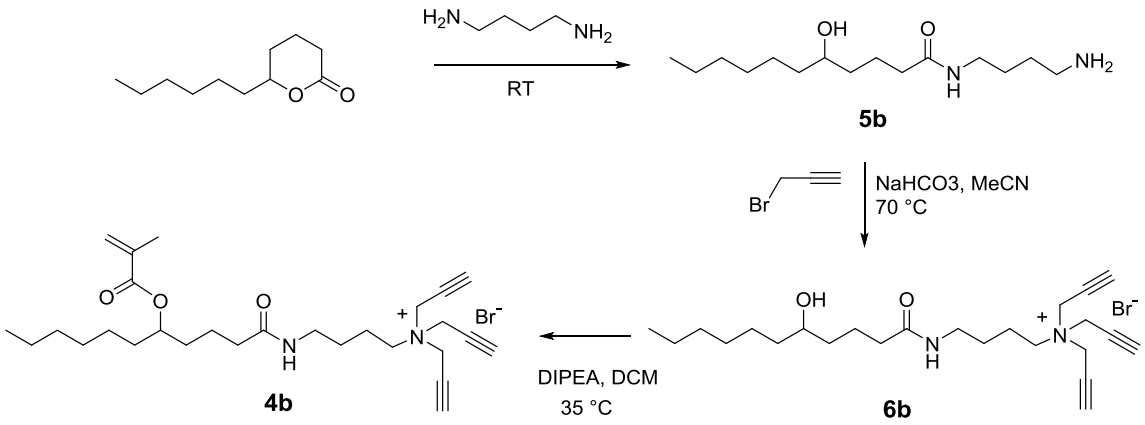

Scheme 5. Syntheses of compound **4b**

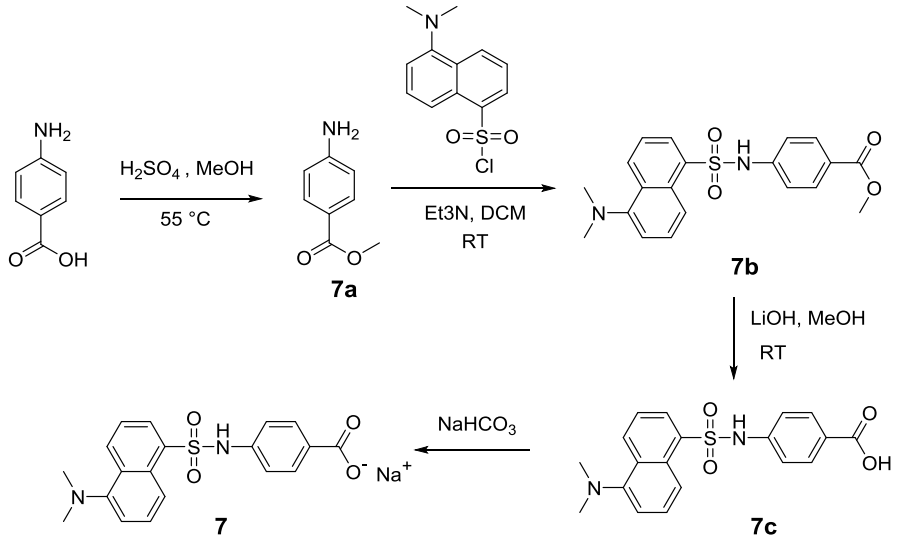

Scheme 6. Syntheses of compound **7**

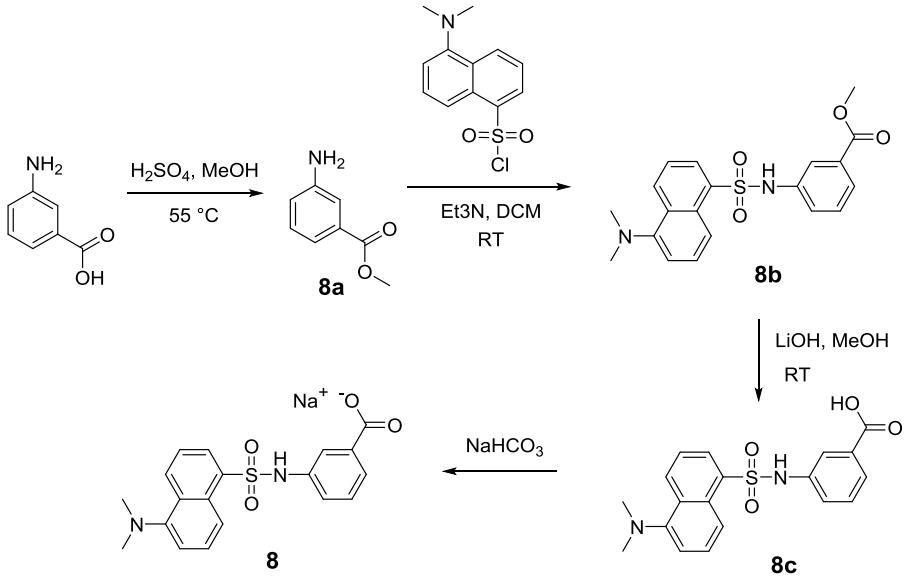

Scheme 7. Syntheses of compound **8**

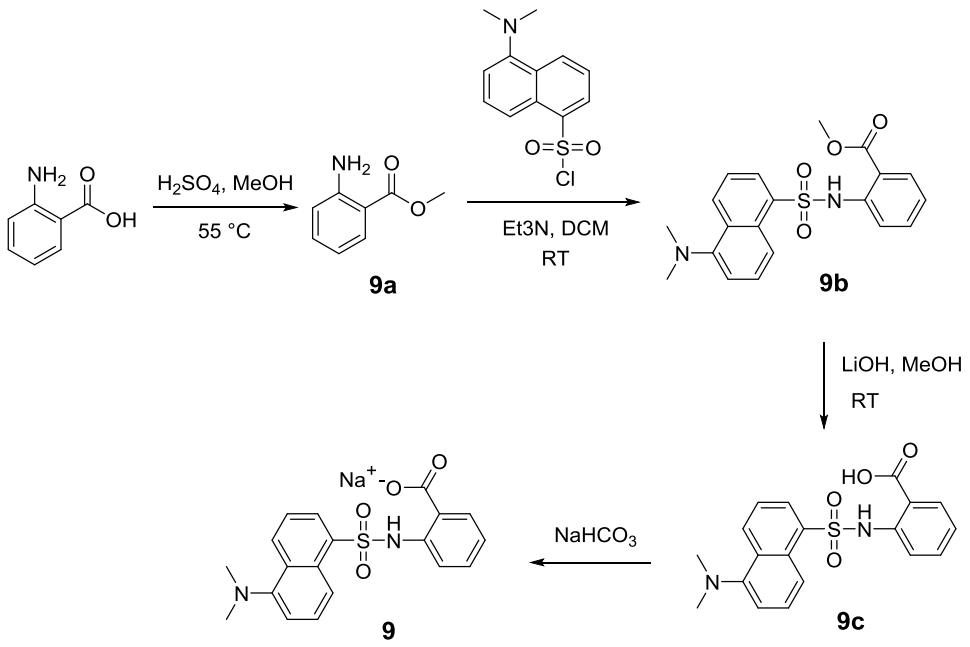

Scheme 8. Syntheses of compound **9**

N-(2-Aminoethyl)-5-hydroxyundecanamide (5a). δ-Undecalactone (1.0 mL, 5 mmol) and ethylenediamine (1.5 g, 25 mmol) were stirred for 4 h at room temperature. The excess amine was removed by co-evaporation with methanol (5 × 2 mL) in a rotary evaporator. The residual was combined with ether (50 mL) and kept overnight. The precipitate was recovered by vacuum filtration and washed with ether (3 × 30 mL) to afford a white powder (1.10 g, 84 %). ^{1}H NMR (400 MHz, $CDCl_3$, δ): 6.11 (br, 1H, N-H), 3.62 (m, 1H), 3.30 (t, *J* = 8.0 Hz, 2H), 2.84 (t, *J* = 8.0 Hz, 2H), 2.37 (t, *J* = 8.0 Hz, 2H), 1.88 (m, 2H), 1.67 (m, 2H), 1.43 (m, 2H), 1.26 (m, 8H), 0.85 (t, *J* = 8.0 Hz, 3H). ^{13}C NMR (100 MHz, CD_3OD, δ): 176.5, 71.7, 42.0, 41.6, 38.3, 33.9, 33.3, 32.8, 30.6, 30.3, 26.6, 23.5, 14.2. ESI-HRMS (*m/z*): $[M+H]^+$ calcd for $C_{13}H_{28}N_2O_2$ 245.2224; found, 245.2219.

5-Hydroxy-N-(2-(tri(prop-2-yn-1-yl)-l4-azanyl)ethyl)undecanamide (6a). A mixture of **5a** (0.80 g, 3.3 mmol) and $NaHCO_3$ (0.87 g, 10.82 mmol) in CH_3CN (2.00 mL) was stirred at 70 °C while a solution of propargyl bromide (1.0 mL, 10.82 mmol) in dry CH_3CN (2.0 mL)

was added dropwise over 10 min. The mixture was stirred for 16 h at 70 °C before another batch of propargyl bromide (0.33 mL) and $NaHCO_3$ (0.30 g) were added. The mixture was stirred another 4 h. The inorganic salts were removed by filtration. After the solvent was removed by rotary evaporation, the residue was purified by column chromatography over silica gel using 30:1 dichloromethane/methanol as the eluent to afford yellowish oil (0.65 g, 77 %). ^{1}H NMR (400 MHz, $CDCl_3$, δ): 8.52 (br, 1H, N-H), 4.88 (m, 1H), 4.78 (s, 6H), 3.93 (t, *J* = 8.0 Hz, 2H), 3.84 (t, *J* = 8.0 Hz, 2H), 3.59 (t, *J* = 8.0 Hz, 2H), 3.13 (s, 3H), 2.39 (m, 2H), 1.77 (m, 2H), 1.46 (m, 4H), 1.26 (m, 6H), 0.88 (t, *J* = 8.0 Hz, 3H) ppm. ^{13}C NMR (100 MHz, $CDCl_3$, δ): 175.2, 83.1, 71, 70, 58.5, 50.8, 37.6, 36.7, 36, 34.1, 31.8 29.4, 25.8, 22.64, 21.5, 14.1 ppm. ESI-HRMS (*m/z*): $[M-Br]^+$ calcd for $C_{22}H_{35}N_2O_2$, 359.2693; found, 359.2696.

1-Oxo-1-((2-(tri(prop-2-yn-1-yl)-l4-azanyl)ethyl)amino)undecan-5-yl methacrylate (4a). A solution of methacryloyl chloride (0.1 mL, 1.0 mmol) in dry CH_2Cl_2 (0.5 mL) was added dropwise over 10 min to a solution of **6a** (0.193 g, 0.60 mmol) and diisopropylethylamine (DIPEA , 0.14 mL. 1.5 mmol) in dry CH_2Cl_2 (10 mL) at 0 °C temperature. After 30 min at 0 °C, the mixture was stirred for 5 h at room temperature before second batch of methacryloyl chloride (0.05 mL, 0.5 mmol) was added. The third batch of methacryloyl chloride (0.05 mL, 0.5 mmol) was added after another 5 h and the mixture was stirred at 40 °C for additional 5 h. After the solvent was removed by rotary evaporation, the residue was purified by column chromatography over silica gel using 4:1 ethyl acetate/methanol as the eluent to afford yellowish oil (0.10 g, 45%).^{1}H NMR (400 MHz, $CDCl_3$, δ): 8.44 (br, 1H, N-H), 6.1(s,1H), 5.5 (s, 1H), 4.90 (m, 1H), 4.80 (s, 6H), 4.12 (t, *J* = 8.0 Hz, 2H), 3.90 (t, *J* = 8.0 Hz, 2H), 3.84 (t, *J* = 8.0 Hz, 2H),3.03 (s, 3H), 2.30 (m, 2H), 2.04 (m, 2H), 1.92 (s, 3H), 1.62 (m, 4H), 1.26 (m, 6H), 0.88 (t, *J* = 8.0 Hz, 3H) ppm. ^{13}C NMR (100 MHz, $CDCl_3$, δ):

174.5, 167.3, 136.6, 125.2, 82.9, 74.3, 69.8, 60.4, 58.8, 50.8, 37.8, 35.9, 34, 31.7, 29.2, 25.2, 22.5,21.3, 18.4, 14 ppm. ESI-HRMS (*m/z*): $[M\text{-}Br]^+$ calcd for $C_{26}H_{39}N_2O_3$, 427.2955; found, 427.2961.

N-(4-Aminobutyl)-5-hydroxyundecanamide (5b). δ-Undecalactone (3.0 mL, 15 mmol) and 1,4-diaminobutane (6.6 g, 75 mmol) were stirred for 4 h at room temperature. The excess amine was removed by co-evaporation with methanol (5 × 4 mL) in a rotary evaporator. The residual was combined with ether (100 mL) and kept overnight. The precipitate was recovered by vacuum filtration and washed with ether (3 × 30 mL) to afford a white powder (3.5 g, 80 %).The compound was used in the next step directly. ^{1}H NMR (400 MHz, $CDCl_3$, δ): 6.0 (br, 1H, N-H), 3.50 (m, 1H), 3.18 (t, *J* = 8.0 Hz, 2H), 2.66 (t, *J* = 8.0 Hz, 2H), 2.14 (t, *J* = 8.0 Hz, 2H), 1.67 (m, 6H), 1.44 (m, 4H), 1.35 (m, 4H), 1.20 (m, 4H), 0.80 (t, *J* = 8.0 Hz, 3H) ppm. ^{13}C NMR (100 MHz, CD_3OD, δ): 175.9, 71.8, 41.3, 39.7, 38.2, 37.6,36.9, 32.9, 30.3, 29.1, 27.5, 26.6, 23.5, 23.2, 14.2 ppm. ESI-HRMS (*m/z*): $[M\text{-}Br]^+$ calcd for $C_{26}H_{39}N_2O_3$, 273.2537; found, 273.2541.

5-Hydroxy-N-(4-(tri(prop-2-yn-1-yl)-l4-azanyl)butyl)undecanamide (6b). A mixture of **5b** (0.40 g, 1.4 mmol) and $NaHCO_3$ (0.41 g, 5.7 mmol) in CH_3CN (5.00 mL) was stirred at 70 °C while a solution of propargyl bromide (0.46 mL, 5.7 mmol) in dry CH_3CN (2.0 mL) was added dropwise over 10 min. The mixture was stirred for 16 h at 70 °C before another batch of propargyl bromide (0.2 mL) and $NaHCO_3$ (0.30 g) were added. The mixture was stirred another 4 h. The inorganic salts were removed by filtration. After the solvent was removed by rotary evaporation, the residue was purified by column chromatography over silica gel using 7:3 ethyl acetate/methanol as the eluent to afford yellowish oil (0.40 g, 72 %). ^{1}H NMR (400 MHz, $CDCl_3$, δ): 7.68 (br, 1H, N-H), 4.72 (s, 6H), 3.71 (t, *J* = 8.0 Hz, 2H),

3.60 (t, *J* = 8.0 Hz, 2H), 3.58 (m, 1H), 3.2 (m, 4H), 3.2 (m,4H), 3.03 (s, 3H), 2.15 (m, 2H), 1.76 (m, 2H), 1.70 (m, 4H), 1.40 (m, 4H), 0.86 (t, *J* = 8.0 Hz, 3H) ppm. ^{13}C NMR (100 MHz, $CDCl_3$, δ): 175.5, 82.6, 71, 70.5, 69.9, 60.5, 50.3, 37.8, 37.3, 36.5, 36.1, 31.7, 29.5, 29.3, 25.9, 25.7, 22.5, 21.9, 3.9 ppm. ESI-HRMS (*m/z*): $[M-Br]^+$ calcd for $C_{24}H_{39}N_2O_2$ 387.3006; found, 387.2999.

1-Oxo-1-((4-(tri(prop-2-yn-1-yl)-l4-azanyl)butyl)amino)undecan-5-yl methacrylate (4b). A solution of methacryloyl chloride (0.5 mL, 4.12 mmol) in dry CH_2Cl_2 (0.5 mL) was added dropwise over 10 min to a solution of **6b** (0.71 g, 1.82 mmol) and DIPEA (0.45 mL, 4.5 mmol) in dry CH_2Cl_2 (30 mL) at 0 °C temperature. After 30 min at 0 °C, the mixture was stirred for 5 h at room temperature before second batch of methacryloyl chloride (0.23 mL, 1.88 mmol) was added. The mixture was stirred at 40 °C for additional 8h. After the solvent was removed by rotary evaporation, the residue was purified by column chromatography over silica gel using 4:1 ethyl acetate/methanol as the eluent to afford yellowish oil (0.47 g, 56%).^{1}H NMR (400 MHz, $CDCl_3$ δ): 6.0 (s,1H), 5.5 (s, 1H), 4.77 (s, 6H), 4.08 (t, *J* = 8.0 Hz, 2H), 3.60 (m, 2H), 2.81 (s, 3H) ,1.98 (m, 4H), 1.89 (s, 3H), 1.61 (m, 4H), 1.58 (m, 6H), 1.52 (m, 8H), 0.88 (t, *J* = 8.0 Hz, 3H) ppm. ^{13}C NMR (100 MHz, $CDCl_3$ & CH^3OD, δ): 180.30, 171.57, 145.8, 129.4, 86.0, 78.1, 73.7, 58.6, 54.2, 46.8, 42.0, 37.8, 35.8, 33.0, 30.0, 29.1, 26.4, 24.3, 22.7, 22.4, 21.1, 17.8 ppm. ESI-HRMS (*m/z*): $[M-Br]^+$ calcd for $C_{28}H_{43}N_2O_3$ 455.3268; found, 455.3255.

Methyl 4-aminobenzoate (7a).[42] To a solution of 4-amino benzoic acid (2.0 g, 14.6 mmol) in 40 mL MeOH, concentrated H_2SO_4 (1.75 mL, 33 mmol) was added dropwise. After the mixture was heated to reflux for 8 h, the solvent was removed under reduced pressure. Water (25 mL) was added and the solution pH was adjusted to 3 with 2M NaOH. The precipitate

formed was collected by filtration and washed with water (20 mL) to afford a white solid (1.94 g, 86%). ^{1}H NMR (400 MHz, $CDCl_3$, δ): 7.85 (dd, *J* = 8 & 4 Hz, 2H), 6.64 (dd, *J* = 8 & 4 Hz, 2H), 4.05 (br, NH_2), 3.85 (s, 3H).

Methyl 4-((5-(dimethylamino)naphthalene)-1-sulfonamido)benzoate (7b).[43] To a solution of dansyl chloride (0.09 g, 0.33 mmol) in dry dichloromethane (20 mL) was added to a solution of compound **7a** (0.05 g, 0.33 mmol) and trimethylamine (0.07 mL, 0.66 mmol) in 3 mL dry dichloromethane. The mixture was stirred at room temperature for 6 h under N_2. After the solvent was removed by rotary evaporation, the residue was purified by column chromatography over silica gel using 2:1 ethyl acetate/hexane as the eluent to afford a white powder (0.10 g, 77%).^{1}H NMR (400 MHz, $CDCl_3$, δ): 8.53 (d, *J* = 8 Hz, 1H), 8.21 (d, *J* = 8 Hz, 1H), 7.77 (dd, *J* = 8 & 4 Hz, 2H), 7.41 (dd, *J* = 8 & 4 Hz, 2H), 7.09 (m,4H), 3.84 (s, 3H), 2.81 (s, 6H).

4-((5-(Dimethylamino)naphthalene)-1-sulfonamido)benzoic acid (7c).[44] LiOH (5.0 mL, 2M) was added to a solution of compound **7b** (0.17 g, 0.44 mmol) in MeOH (15 mL).The mixture was stirred for 12 h at room temperature. The mixture was concentrated under reduced pressure and acidified by 2M HCl. The precipitate formed was collected by filtration and dried in air to afford a white powder (0.10 g, 77%). To obtain the sodium salt of this compound, the above acid was mixed with saturated sodium bicarbonate (2.0 mL) and methanol (5 mL). The reaction mixture was stirred for 2 h. After the solvents were removed by rotary evaporation, the residue was dissolved in methanol (5 mL). The solution was filtered and then concentrated by rotary evaporation to give the sodium salt as a white powder. ^{1}H NMR (400 MHz, CD_3OD, δ): 8.81 (d, *J* = 8 Hz, 1H), 8.67 (d, *J* = 8 Hz, 1H), 8.56

(d, *J* = 8 Hz, 1H), 8.03 (dd, *J* = 8 & 4 Hz, 2H), 7.85 (m, 2H),7.55 (d, *J* = 8 Hz, 1H), 7.35 (dd, *J* = 8 & 4 Hz, 2H), 3.13 (s, 6H).

Methyl 3-aminobenzoate (8a).[45] To a solution of 3-amino benzoic acid (3.0 g, 22 mmol) in 40 mL MeOH, concentrated H_2SO_4 (2.5 mL, 47 mmol) was added dropwise. After the mixture was heated to reflux for 8 h, the solvent was removed under reduced pressure. Water (25 mL) was added and the solution pH was adjusted to 3 with 2M NaOH. The precipitate formed was collected by filtration and washed with water (20 mL) to afford a white solid (2.71g, 82%).^{1}H NMR (400 MHz, $CDCl_3$, δ): 7.42 (dd, *J* = 8 & 4 Hz, 1H), 7.35 (s, 1H), 7.21 (t, *J* = 8 Hz, 1H), 6.85 (dd, *J* = 8 & 4 Hz, 1H), 3.89 (s, 3H).

Methyl 3-((5-(dimethylamino)naphthalene)-1-sulfonamido)benzoate (8b).[46] To a solution of dansyl chloride (0.3 g, 1.1 mmol) in dry dichloromethane (20 mL) was added to a solution of compound **8a** (0.15 g, 1.0 mmol) and trimethylamine (0.22 mL, 2.0 mmol) in 3 mL dry dichloromethane. The mixture was stirred at room temperature for 6 h under N_2. After the solvent was removed by rotary evaporation, the residue was purified by column chromatography over silica gel using 2:1 ethyl acetate/hexane as the eluent to afford white powder (0.10 g, 77%). ^{1}H NMR (400 MHz, $CDCl_3$, δ): 8.6 (d, *J* = 8 Hz, 1H), 8.3 (d, *J* = 8 Hz, 1H), 8.00 (m, 2H), 7.79 (d, *J* = 8 Hz, 1H), 7.68 (m, 2H), 7.48 (dd, *J* = 8 & 4 Hz, 1H), 7.20 (m, 2H), 5.30 (s, 3H), 2.89 (s, 6H).

3-((5-(Dimethylamino)naphthalene)-1-sulfonamido)benzoic acid (8c).[45] LiOH (5.0 mL, 2M) was added to a solution of compound **8b** (0.17 g, 0.44 mmol) in MeOH (15 mL). The mixture was stirred for 12 h at room temperature. The mixture was concentrated under reduced pressure and acidified by 2M HCl. The precipitate was collected by filtration and dried in air to afford a white powder (0.14 g, 93%). To obtain the sodium salt of this

compound, the above acid was mixed with saturated sodium bicarbonate (2.0 mL) and methanol (5 mL). The reaction mixture was stirred for 2 h. After the solvents were removed by rotary evaporation, the residue was dissolved in methanol (5 mL). The solution was filtered and then concentrated by rotary evaporation to give the sodium salt as a white powder.^{1}H NMR (600 MHz, CD_3OD, δ): 8.83 (d, *J* = 8 Hz, 1H), 8.57 (d, *J* = 8 Hz, 1H), 8.41 (m, 1H), 8.21 (m, 1H), 7.61(m,1H), 7.49 (m, 2H), 7.24 (m, 1H), 7.06 (m, 1H), 6.95 (t, *J* = 8 Hz, 1H), 2.89 (s, 3H), 2.86(s, 3H).

Methyl 2-aminobenzoate (9a).[47] To a solution of 2-amino benzoic acid (2.0 g, 14.6 mmol) in 30 mL MeOH, concentrated H_2SO_4 (1.6 mL, 30 mmol) was added dropwise. After the mixture was heated to reflux for 8 h, the solvent was removed under reduced pressure. Water (20 mL) was added and the solution pH was adjusted to 3 with 2M NaOH. The precipitate formed was collected by filtration and washed with water (20 mL) to afford a white solid (2.10 g, 95%). ^{1}H NMR (400 MHz, $CDCl_3$, δ): 7.79 (d, *J* = 8 Hz, 2H), 7.18 (t, *J* = 8 Hz, 1H), 6.53 (m, 2H), 3.72 (s, 3H).

Methyl 2-((5-(dimethylamino)naphthalene)-1-sulfonamido)benzoate (9b).[47] To a solution of dansyl chloride (0.22 g, 0.8 mmol) in dry dichloromethane (15 mL) was added to a solution of compound **9a** (0.12 g, 0.8 mmol) and trimethylamine (0.17 mL, 1.6 mmol) in 3 mL dry dichloromethane. The mixture was stirred at room temperature for 6 h under N_2. After the solvent was removed by rotary evaporation, the residue was purified by column chromatography over silica gel using 2:1 ethyl acetate/hexane as the eluent to afford white powder (0.25 g, 83%). ^{1}H NMR (400 MHz, $CDCl_3$, δ):11.1 (br, 1H), 8.5 (m, 1H), 8.35 (3, 2H), 7.84 (m, 1H), 7.59 (m, 1H), 7.50 (m, 2H), 7.36 (m, 1H), 7.20 (m, 1H), 6.92 (m, 1H), 3.85 (s, 3H), 3.50 (s, 6H).

***2-((5-(Dimethylamino)naphthalene)-1-sulfonamido)benzoic acid* (9c).**[47] LiOH (5.0 mL, 2M) was added to a solution of compound **9b** (0.2 g, 0.40 mmol) in MeOH (15 mL). The mixture was stirred for 12 h at room temperature. The mixture was concentrated under reduced pressure and acidified by 2M HCl. The precipitate was collected by filtration and dried in air to afford white powder (0.14 g, 93%). To obtain the sodium salt of this compound, the above acid was mixed with saturated sodium bicarbonate (2.0 mL) and methanol (5 mL). The reaction mixture was stirred for 2 h. After the solvents were removed by rotary evaporation, the residue was dissolved in methanol (5 mL). The solution was filtered and then concentrated by rotary evaporation to give the sodium salt as a white powder. ^{1}H NMR (600 MHz, $CDCl_3$, δ): 10.93 (br, 1H), 8.4 (m, 1H), 7.91 (m, 1H), 7.62 (m, 4H), 7.48 (m, 2H), 6.99 (m, 2H), 3.85 (s, 6H).

Preparation of Molecularly Imprinted Nanoparticles (MINPs). To a micellar solution of compound **4a** (10.2 mg, 0.02 mmol) in D_2O (2.0 mL), divinylbenzene (DVB, 2.8 μL, 0.02 mmol), compound **7** in D_2O (10 μL of a solution of 15.68 mg/mL, 0.0004 mmol), and 2,2-dimethoxy-2-phenylacetophenone (DMPA,10 μL of a 12.8 mg/mL solution in DMSO, 0.0005 mmol) were added. (D_2O instead of H_2O was used in the preparation so that the cross-linking and polymerization of the micelles could by monitored by ^{1}H NMR spectroscopy) The mixture was subjected to ultrasonication for 10 min before compound **2** (4.13 mg, 0.024 mmol), $CuCl_2$ (10 μL of a 6.7 mg/mL solution in D_2O, 0.0005 mmol), and sodium ascorbate (10 μL of a 99 mg/mL solution in D_2O, 0.005 mmol) were added. After the reaction mixture was stirred slowly at room temperature for 12 h, compound **3** (10.6 mg, 0.04 mmol), $CuCl_2$ (10 μL of a 6.7 mg/mL solution in D_2O, 0.0005 mmol l), and sodium ascorbate (10 μL of a 99 mg/mL solution in D_2O, 0.005 mmol) were added. After being stirred for another 6 h at

room temperature, the reaction mixture was transferred to a glass vial, purged with nitrogen for 15 min, sealed with a rubber stopper, and irradiated in a Rayonet reactor for 12 h. ^{1}H NMR spectroscopy was used to monitor the progress of reaction. The reaction mixture was poured into acetone (8 mL). The precipitate was collected by centrifugation and washed with a mixture of acetone/water (5 mL/1 mL) three times. The crude produce was washed by methanol/acetic acid (5 mL/0.1 mL) three times until the emission peak at 480 nm (for the dansyl) disappeared and then with excess methanol. The off white powder was dried in air to afford the final MINPs (12 mg, 70%).

Determination of Critical Micelle Concentration (CMC) of Surfactants. A typical procedure is as follows. A stock solution was prepared by adding surfactant **4a** (10.2 mg, 0.02 mmol) to 2.0 mL of an aqueous solution of pyrene (1.0×10^{-7} M). To 11 separate vials, 100, 90, 80, 70, 60, 50, 40, 30, 20, 15, 10, and 5 μL of the above stock solution were added. Millipore water was added to each vial to make the total volume 2.0 mL. Fluorescence spectra were recorded with the excitation wavelength at 336 nm. The final results were based on duplicate experiments with separately prepared solutions.

Determination of Binding Constants by Fluorescence Titration. A typical procedure is as follows. A stock solution containing MINP$_1$(**7**) (150 μM) was prepared in Millipore water. Aliquots (2.0 μL) of the MINP stock solution were added to 2.00 mL of the solution of **7** in Millipore water (0.2 μM). After each addition, the sample was allowed to sit for 1 min at room temperature before the fluorescence spectrum was collected. The excitation wavelength (λ_{ex}) was 340 nm. The excitation slit width was 10 nm, and the emission slit width was 10 nm.

Determination of Binding Constants by ITC. The determination of binding constants by ITC followed standard procedures.[48-50] In general, a solution of an appropriate guest in

Millipore water was injected in equal steps into 1.43 mL of the corresponding MINP in the same solution. The top panel shows the raw calorimetric data. The area under each peak represents the amount of heat generated at each ejection and is plotted against the molar ratio of the MINP to the guest. The smooth solid line is the best fit of the experimental data to the sequential binding of *N* binding site on the MINP. The heat of dilution for the guest, obtained by titration carried out beyond the saturation point, was subtracted from the heat released during the binding. Binding parameters were auto-generated after curve fitting using Microcal Origin 7.

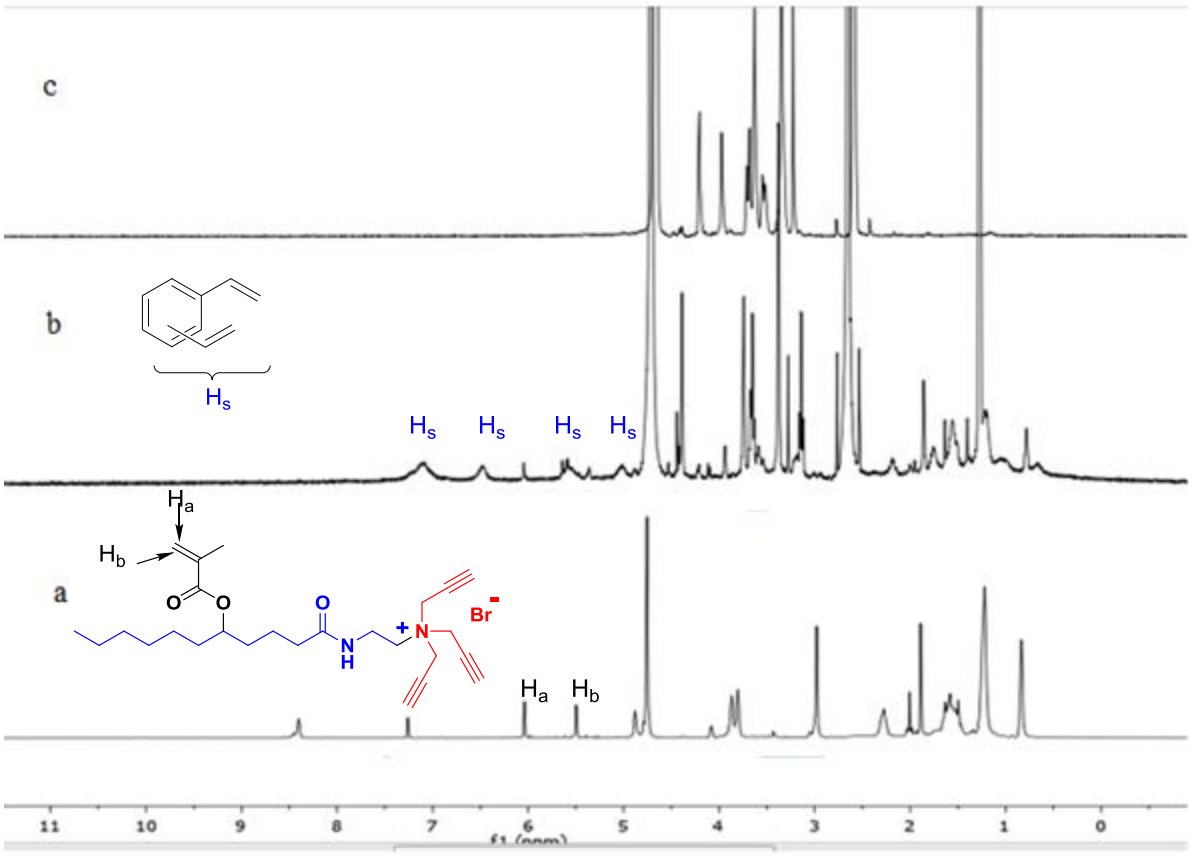

Figure 4. ^{1}H NMR spectra of (a) **4a** in $CDCl_3$, (b) alkynyl-SCM in D_2O, (c) $MINP_{\mathbf{4a}}$ (**7**) in D_2O.

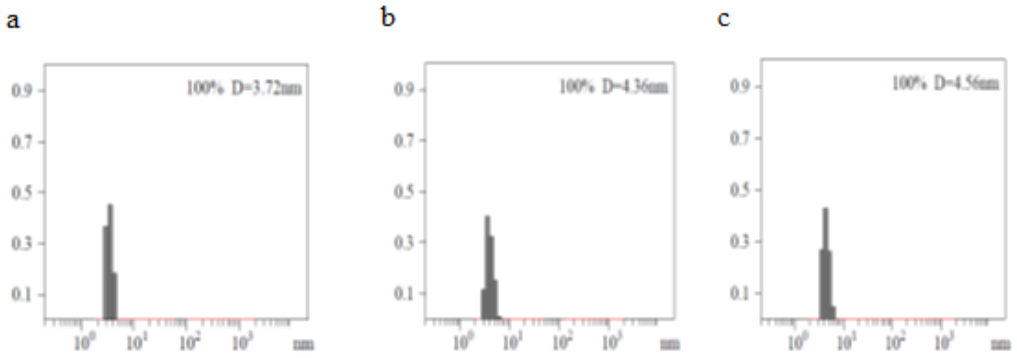

Figure 5. Distribution of the hydrodynamic diameters of the nanoparticles in water as determined by DLS for (a) alkynyl-SCM (b) surface-functionalized SCM, and (c) $MINP_{\mathbf{4a}}$ (**7**) after purification.

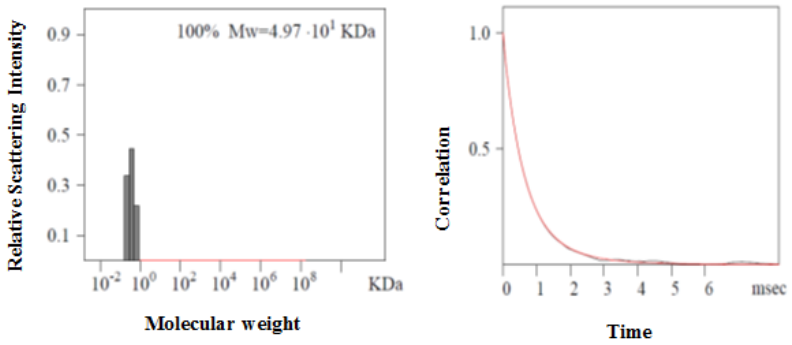

Figure 6. Distribution of the molecular weights of the alkynyl-SCMs and the correlation curve for DLS. The molecular weight distribution was calculated by the PRECISION DECONVOLVE program assuming the intensity of scattering is proportional to the mass of the particle squared. If each unit of building block for the alkynyl-SCM is assumed to contain one molecule of compound **4a** (MW = 520 g/mol), 1.2 molecules of compound **2** (MW = 172 g/mol), and one molecule of DVB (MW = 130 g/mol), the molecular weight of the alkynyl-SCM translates to 62 [= 53100/(520+1.2×172+130)] of such units.

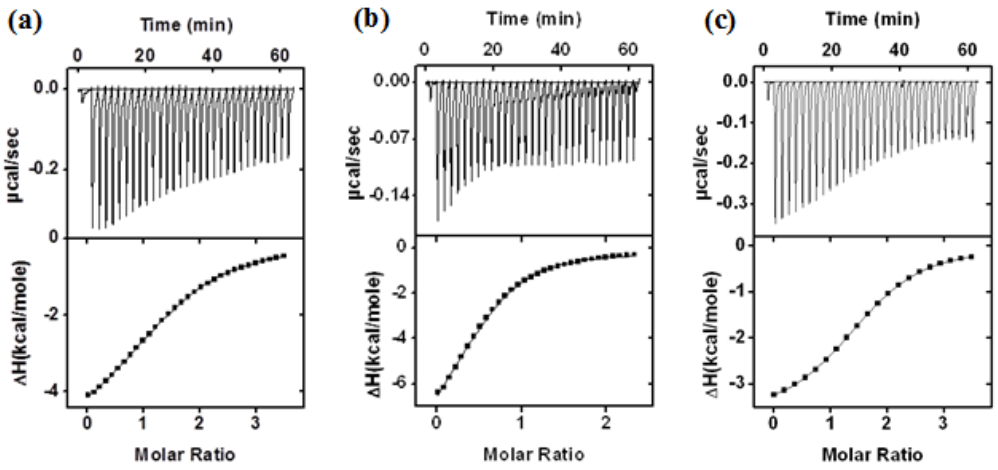

Figure 7. ITC titration curves obtained at 298 K for the binding of **7** by MINP$_{\mathbf{1}}$(**7**) (a), MINP$_{\mathbf{4a}}$(**7**) (b), MINP$_{\mathbf{4b}}$(**7**) (c), prepared with 1 equivalent of DVB. The data correspond to entries 1, 2, and 3, respectively in Table 1. The top panel shows the raw calorimetric data. The area under each peak represents the amount of heat generated at each ejection and is plotted against the molar ratio of guest to the MINP. The solid line is the best fit of the experimental data to the sequential binding of N equal and independent binding sites on the MINP. The heat of dilution for the guest, obtained by adding the guest to the water, was subtracted from the heat released during the binding. Binding parameters were auto-generated after curve fitting using Microcal Origin 7.

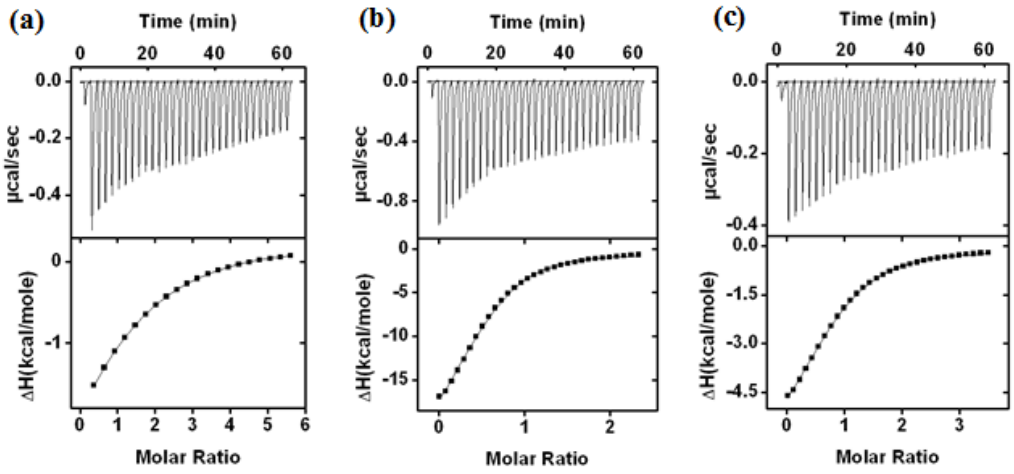

Figure 8. ITC titration curves obtained at 298 K for the binding of **8** by MINP$_{1}$(**8**) (a), MINP$_{4a}$(**8**) (b), MINP$_{4b}$(**8**) (c),prepared with 1 equivalent of DVB. The data correspond to entries 4, 5, and 6, respectively in Table 1. The top panel shows the raw calorimetric data. The area under each peak represents the amount of heat generated at each ejection and is plotted against the molar ratio of guest to the MINP. The solid line is the best fit of the experimental data to the sequential binding of N equal and independent binding sites on the MINP. The heat of dilution for the guest, obtained by adding the guest to the water, was subtracted from the heat released during the binding. Binding parameters were auto-generated after curve fitting using Microcal Origin 7.

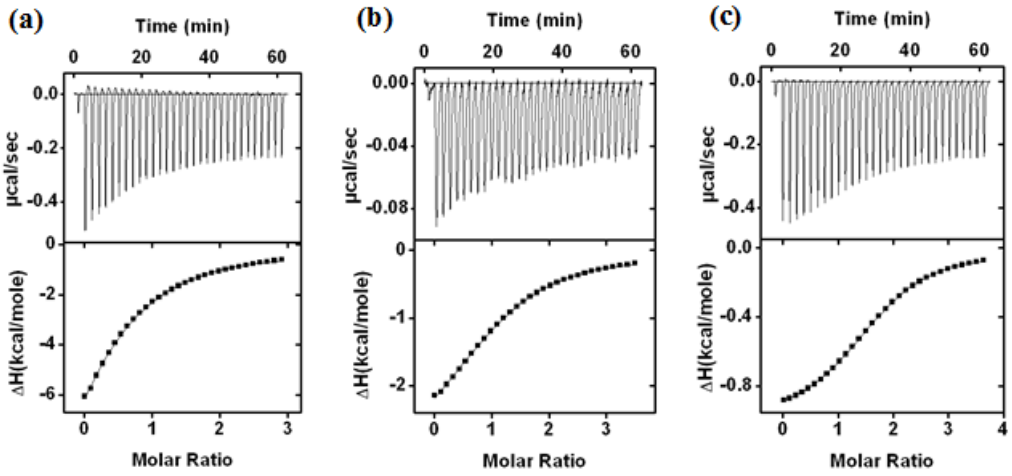

Figure 9. ITC titration curves obtained at 298 K for the binding of **9** by MINP$_1$(**9**) (a), MINP$_{4a}$(**9**) (b), MINP$_{4b}$(**9**) (c), prepared with 1 equivalent of DVB. The data correspond to entries 7, 8, and 9, respectively in Table 1. The top panel shows the raw calorimetric data. The area under each peak represents the amount of heat generated at each ejection and is plotted against the molar ratio of guest to the MINP. The solid line is the best fit of the experimental data to the sequential binding of N equal and independent binding sites on the MINP. The heat of dilution for the guest, obtained by adding the guest to the water, was subtracted from the heat released during the binding. Binding parameters were auto-generated after curve fitting using Microcal Origin 7.

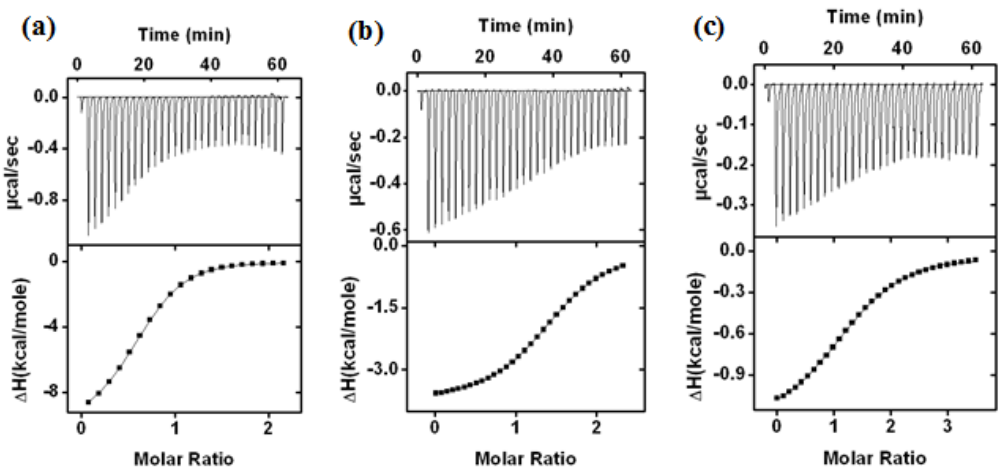

Figure 10. ITC titration curves obtained at 298 K for the binding of **7** by $MINP_{\mathbf{1:4a=1:3}}$(**7**) (a), $MINP_{\mathbf{1:4a=1:1}}$ (**7**) (b), $MINP_{\mathbf{1:4a=3:1}}$ (**7**) (c), prepared with 1 equivalent of DVB. The data correspond to entries 10, 11, and 12, respectively in Table 1. The top panel shows the raw calorimetric data. The area under each peak represents the amount of heat generated at each ejection and is plotted against the molar ratio of guest to the MINP. The solid line is the best fit of the experimental data to the sequential binding of N equal and independent binding sites on the MINP. The heat of dilution for the guest, obtained by adding the guest to the water, was subtracted from the heat released during the binding. Binding parameters were auto-generated after curve fitting using Microcal Origin 7.

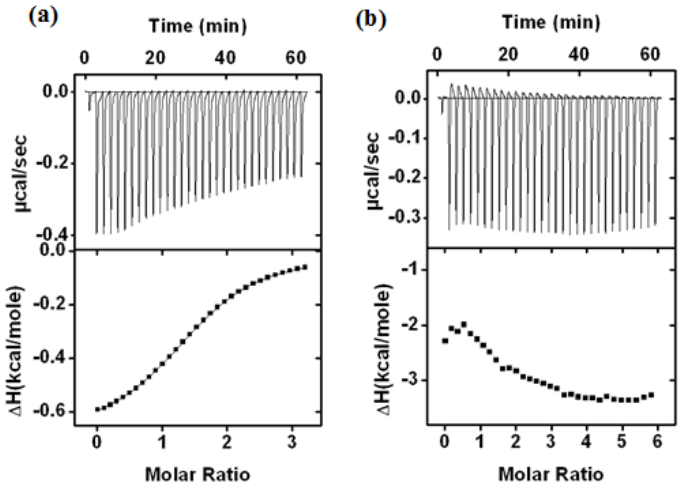

Figure 11. ITC titration curves obtained at 298 K for the binding of **8** (a) and **9** (b) by $MINP_{\mathbf{4a}}$ (**7**) prepared with 1 equivalent of DVB. The data correspond to entries 13 and 14 in Table 1. The top panel shows the raw calorimetric data. The area under each peak represents the amount of heat generated at each ejection and is plotted against the molar ratio of guest to the MINP. The solid line is the best fit of the experimental data to the sequential binding of N equal and independent binding sites on the MINP. The heat of dilution for the guest, obtained by adding the guest to the water, was subtracted from the heat released during the binding. Binding parameters were auto-generated after curve fitting using Microcal Origin 7.

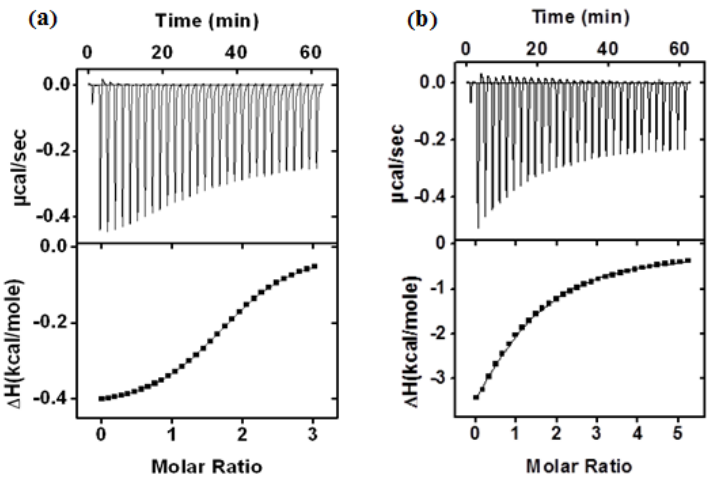

Figure 12. ITC titration curves obtained at 298 K for the binding of **7** (a) and **9** (b) by $MINP_{\mathbf{4a}}$ (**8**) prepared with 1 equivalent of DVB. The data correspond to entries 15 and 16 in Table 1. The top panel shows the raw calorimetric data. The area under each peak represents the amount of heat generated at each ejection and is plotted against the molar ratio of guest to the MINP. The solid line is the best fit of the experimental data to the sequential binding of N equal and independent binding sites on the MINP. The heat of dilution for the guest, obtained by adding the guest to the water, was subtracted from the heat released during the binding. Binding parameters were auto-generated after curve fitting using Microcal Origin 7.

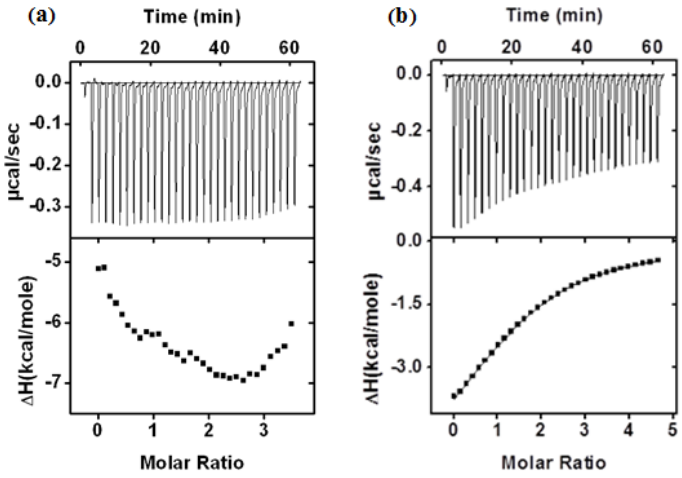

Figure 13. ITC titration curves obtained at 298 K for the binding of **7** (a) and **8** (b) by $MINP_{\mathbf{4a}}$ (**9**) prepared with 1 equivalent of DVB. The data correspond to entries 17 and 18 in Table 1. The top panel shows the raw calorimetric data. The area under each peak represents the amount of heat generated at each ejection and is plotted against the molar ratio of guest to the MINP. The solid line is the best fit of the experimental data to the sequential binding of N equal and independent binding sites on the MINP. The heat of dilution for the guest, obtained by adding the guest to the water, was subtracted from the heat released during the binding. Binding parameters were auto-generated after curve fitting using Microcal Origin 7.

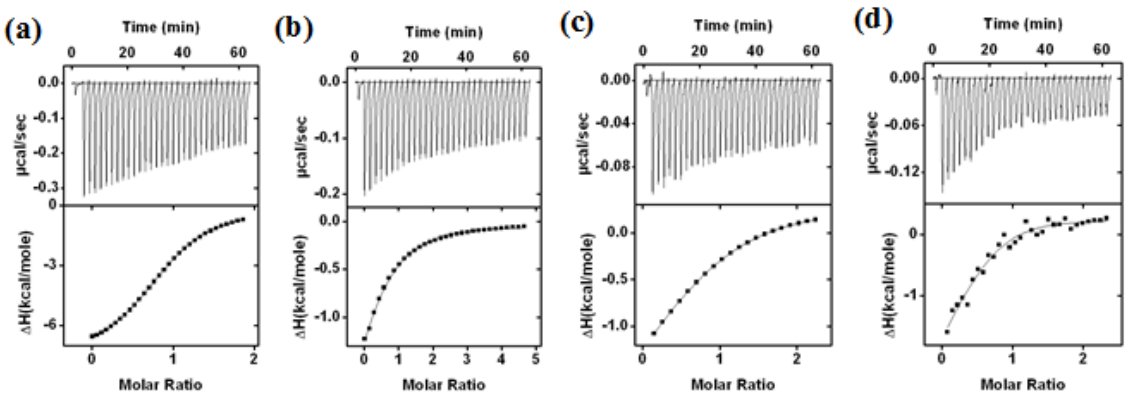

Figure 14. ITC titration curves obtained at 298 K for the binding of **10** (a), **11** (b), **12** (c), and **13** (d) by $MINP_{4a}$ (**10**), $MINP_{4a}$ (**11**), $MINP_{4a}$ (**12**), and $MINP_{4a}$ (**13**), respectively prepared with 1 equivalent of DVB. The data correspond to entries 1, 3, 5, and 7, respectively in Table 2. The top panel shows the raw calorimetric data. The area under each peak represents the amount of heat generated at each ejection and is plotted against the molar ratio of guest to the MINP. The solid line is the best fit of the experimental data to the sequential binding of N equal and independent binding sites on the MINP. The heat of dilution for the guest, obtained by adding the guest to the water, was subtracted from the heat released during the binding. Binding parameters were auto-generated after curve fitting using Microcal Origin 7.

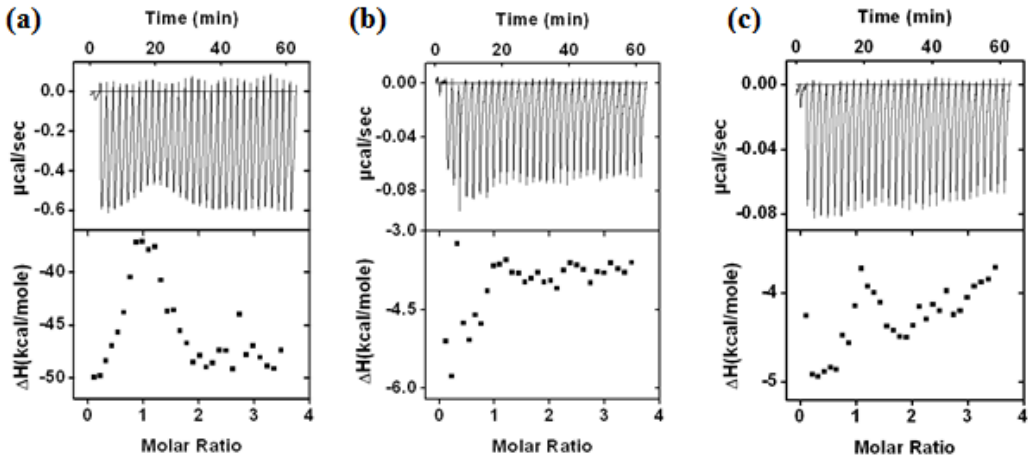

Figure 15. ITC titration curves obtained at 298 K for the binding of **7** (a), **8** (b) and **9** (c) by $NINP_1$ prepared with 1 equivalent of DVB. The area under each peak represents the amount of heat generated at each ejection and is plotted against the molar ratio of guest to the MINP. The solid line is the best fit of the experimental data to the sequential binding of N equal and independent binding sites on the MINP. The heat of dilution for the guest, obtained by adding the guest to the water, was subtracted from the heat released during the binding. Binding parameters were auto-generated after curve fitting using Microcal Origin 7.

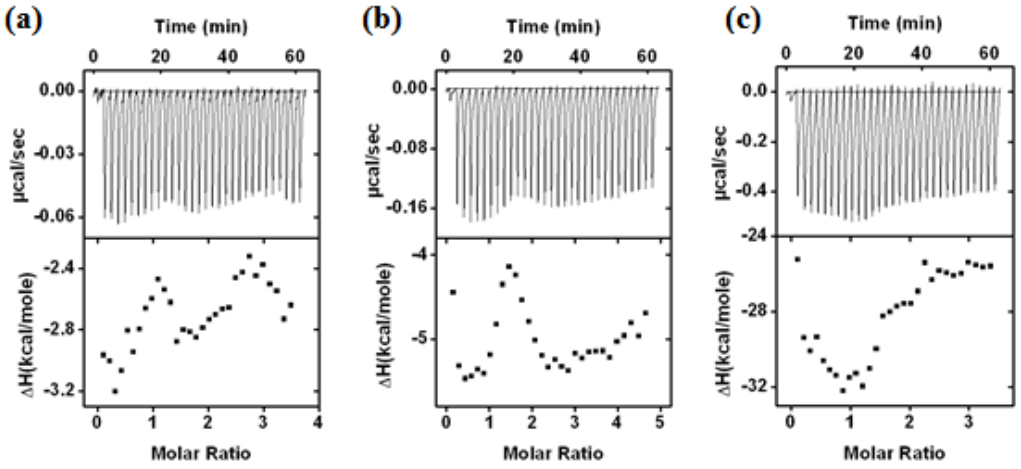

Figure 16. ITC titration curves obtained at 298 K for the binding of **7** (a), **8** (b) and **9** (c) by $NINP_{\mathbf{4a}}$ prepared with 1 equivalent of DVB. The area under each peak represents the amount of heat generated at each ejection and is plotted against the molar ratio of guest to the MINP. The solid line is the best fit of the experimental data to the sequential binding of N equal and independent binding sites on the MINP. The heat of dilution for the guest, obtained by adding the guest to the water, was subtracted from the heat released during the binding. Binding parameters were auto-generated after curve fitting using Microcal Origin 7.

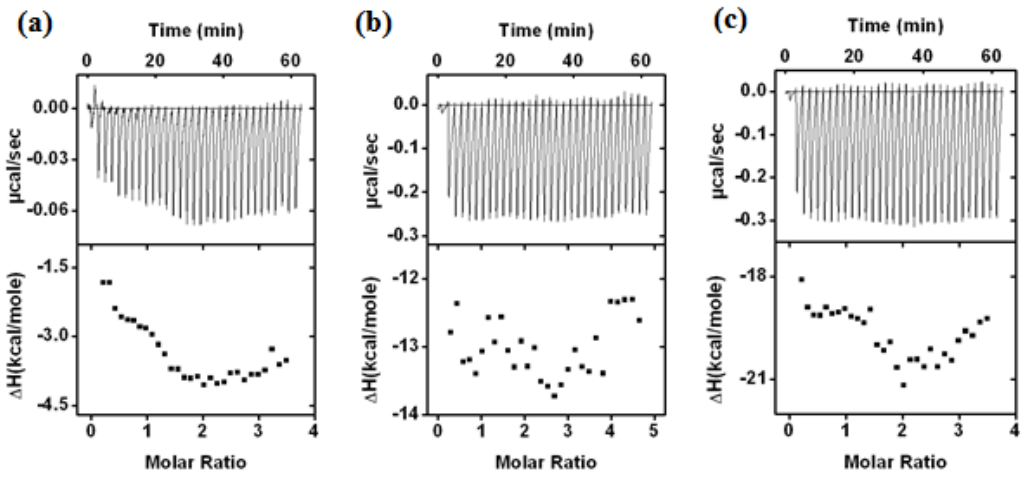

Figure 17. ITC titration curves obtained at 298 K for the binding of **7** (a), **8** (b) and **9** (c) by $NINP_{\mathbf{4b}}$ prepared with 1 equivalent of DVB. The area under each peak represents the amount of heat generated at each ejection and is plotted against the molar ratio of guest to the MINP. The solid line is the best fit of the experimental data to the sequential binding of N equal and independent binding sites on the MINP. The heat of dilution for the guest, obtained by adding the guest to the water, was subtracted from the heat released during the binding. Binding parameters were auto-generated after curve fitting using Microcal Origin 7.

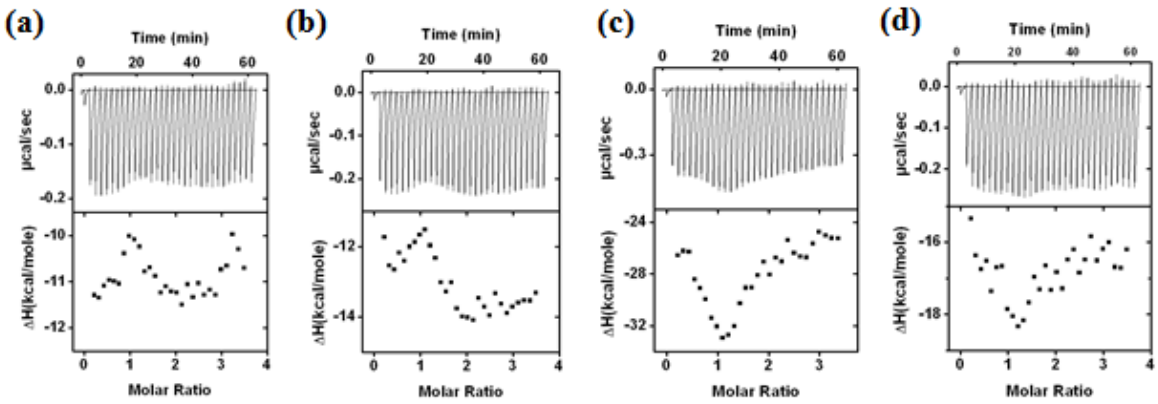

Figure 18. ITC titration curves obtained at 298 K for the binding of **10** (a), **11** (b), **12** (c) and **13** (d) by $NINP_{\mathbf{4a}}$ prepared with 1 equivalent of DVB. The area under each peak represents the amount of heat generated at each ejection and is plotted against the molar ratio of guest to the MINP. The solid line is the best fit of the experimental data to the sequential binding of N equal and independent binding sites on the MINP. The heat of dilution for the guest, obtained by adding the guest to the water, was subtracted from the heat released during the binding. Binding parameters were auto-generated after curve fitting using Microcal Origin 7.

^{1}H NMR of compound **5a**

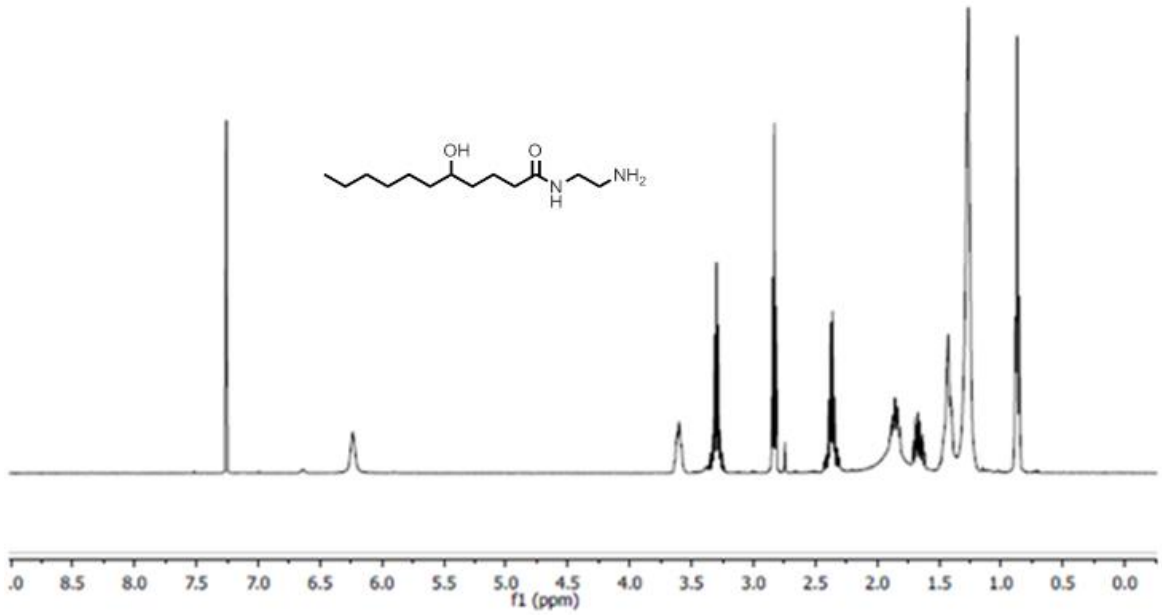

^{13}C NMR of compound **5a**

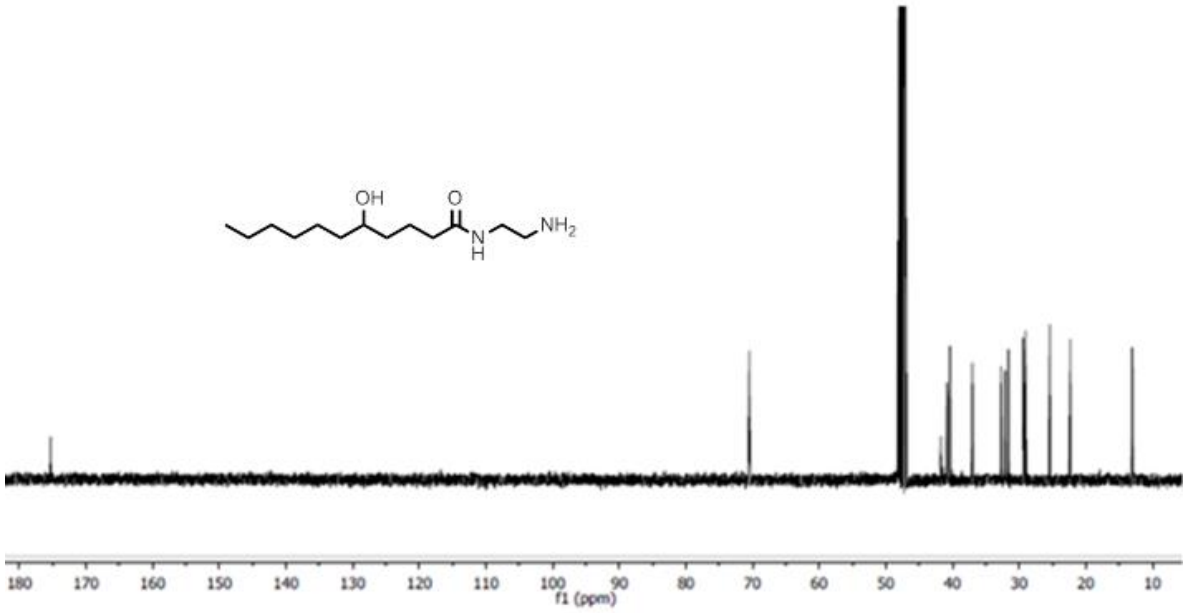

Mass spectrum of compound **5a**

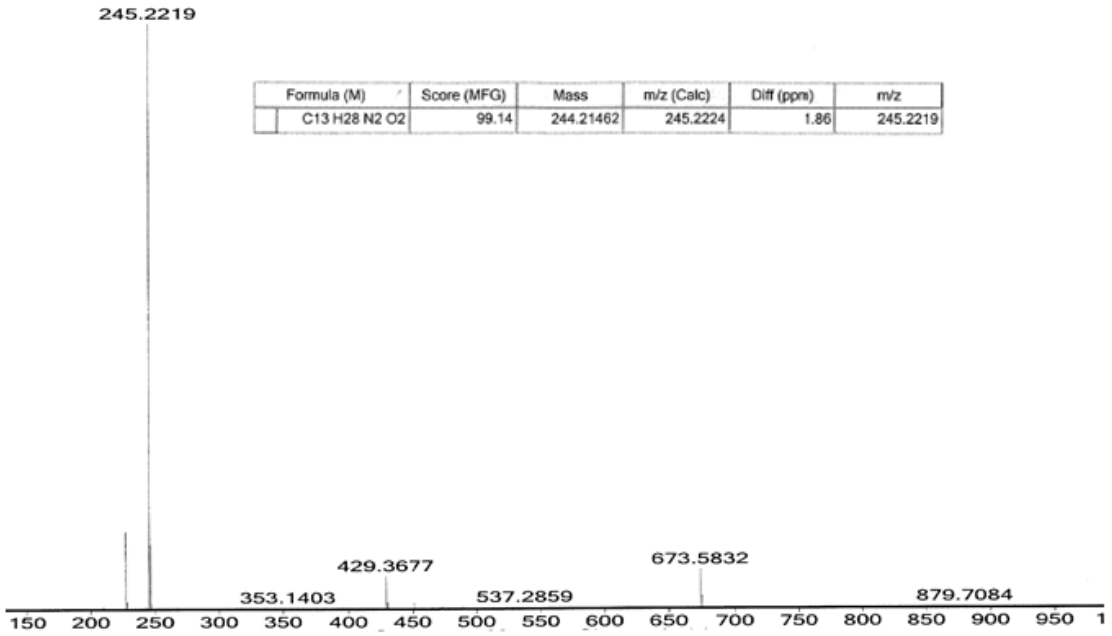

^{1}H NMR of compound **6a**

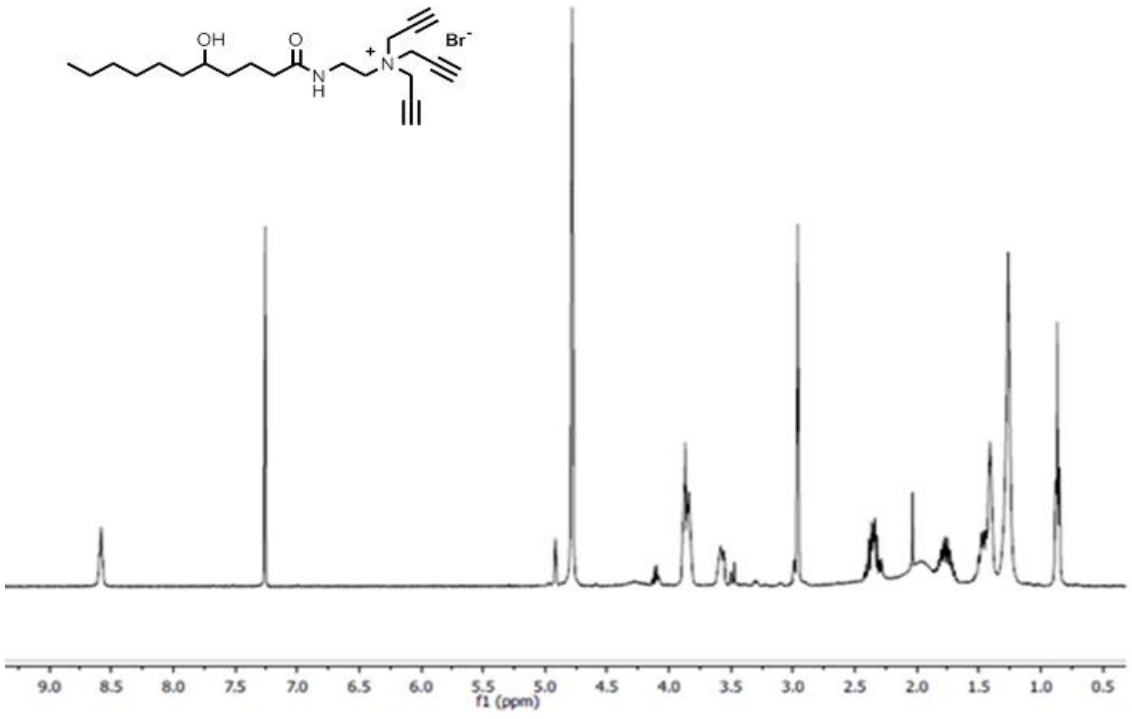

^{13}C NMR of compound **6a**

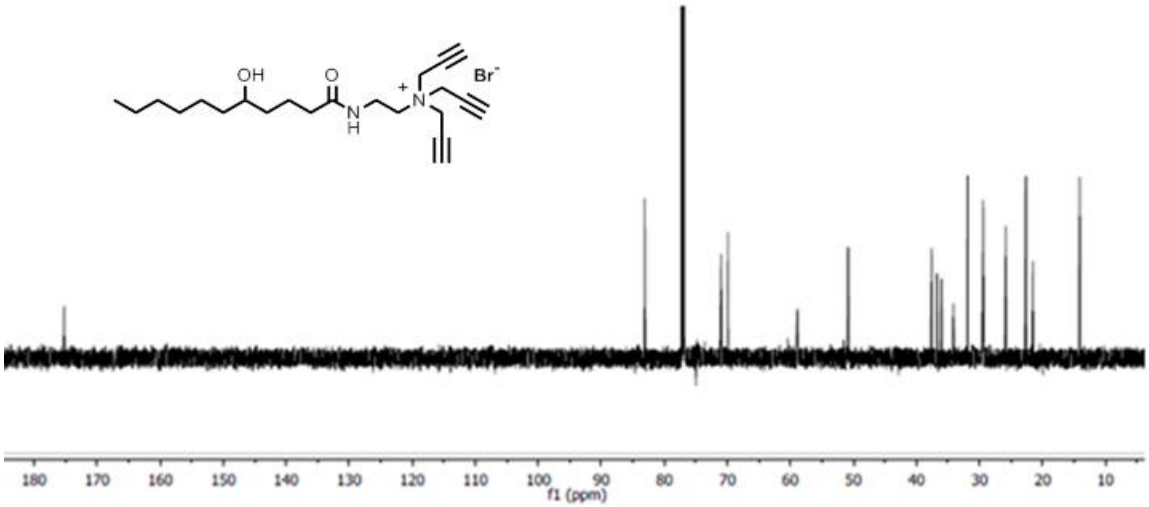

Mass spectrum of compound **6a**

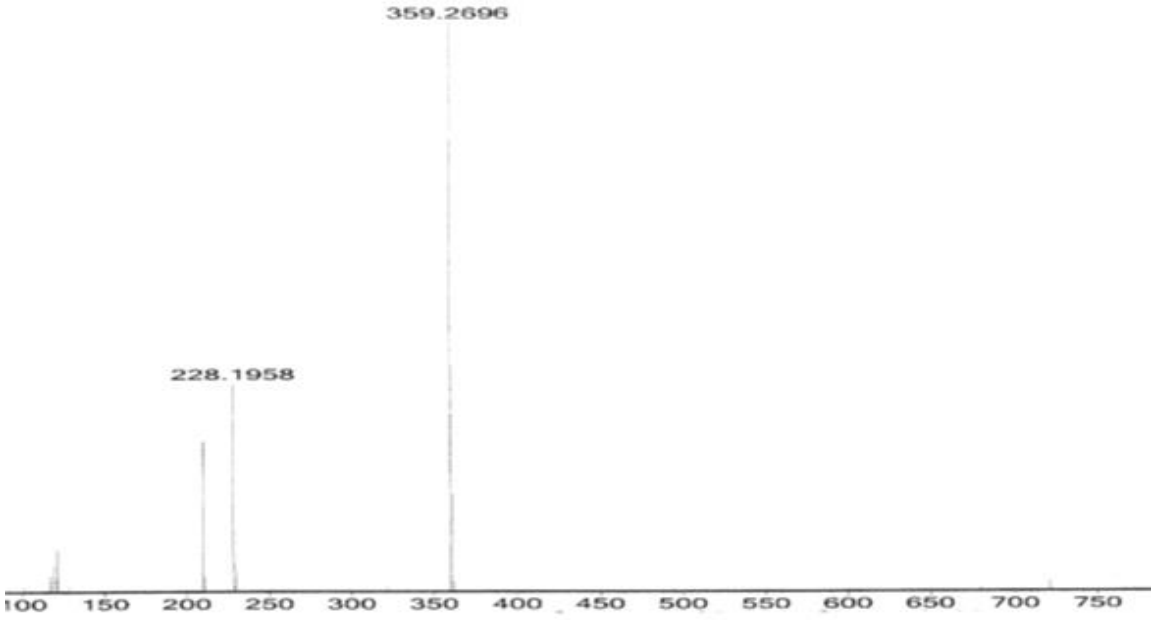

^{1}H NMR of compound **4a**

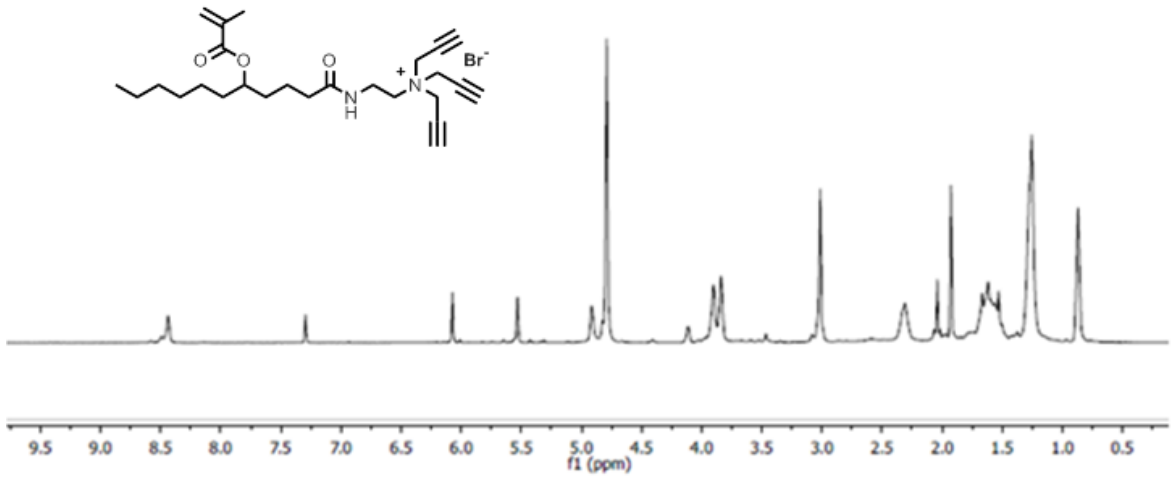

^{13}C NMR of compound **4a**

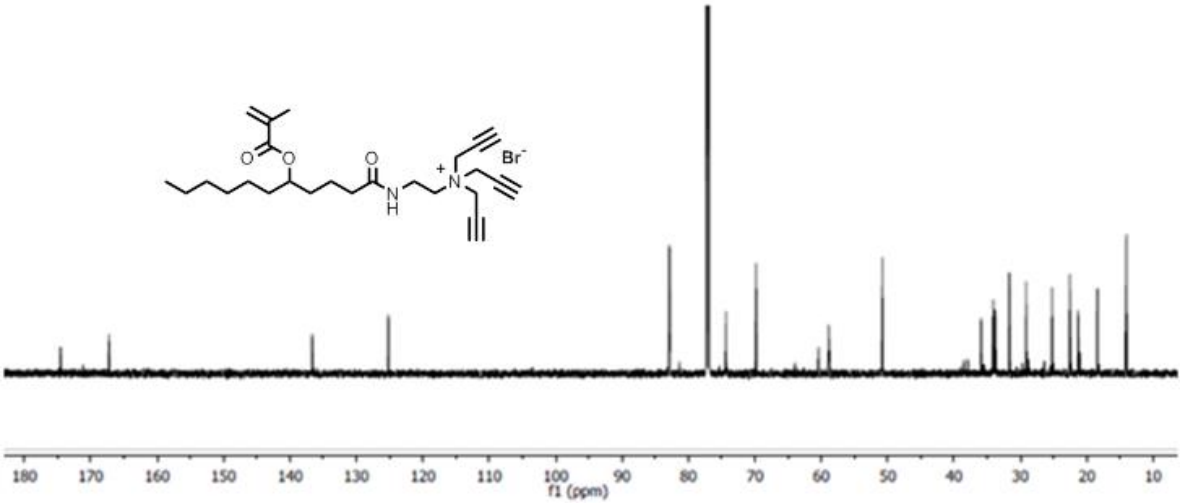

Mass spectrum of compound **4a**

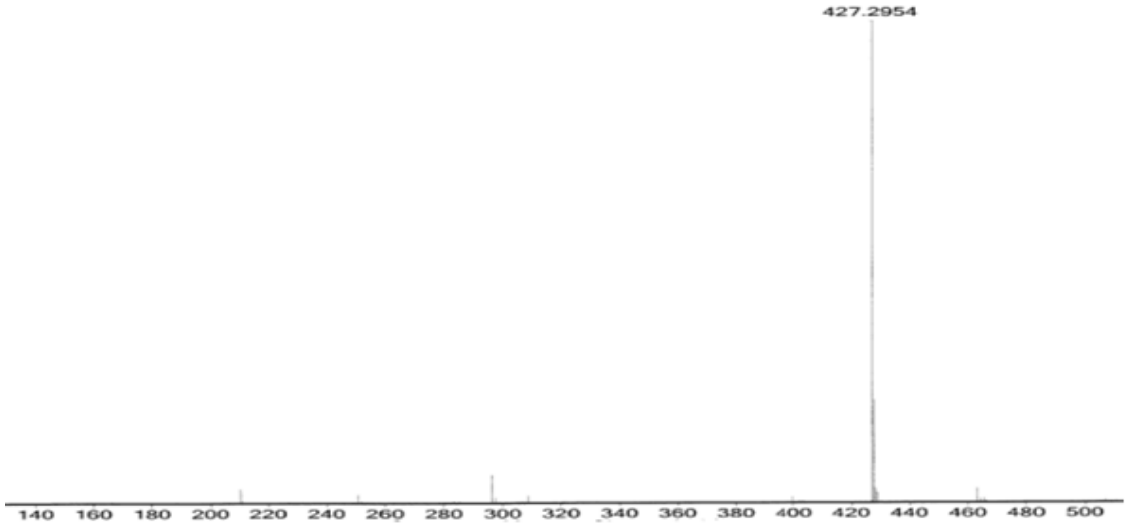

^{1}H NMR of compound **5b**

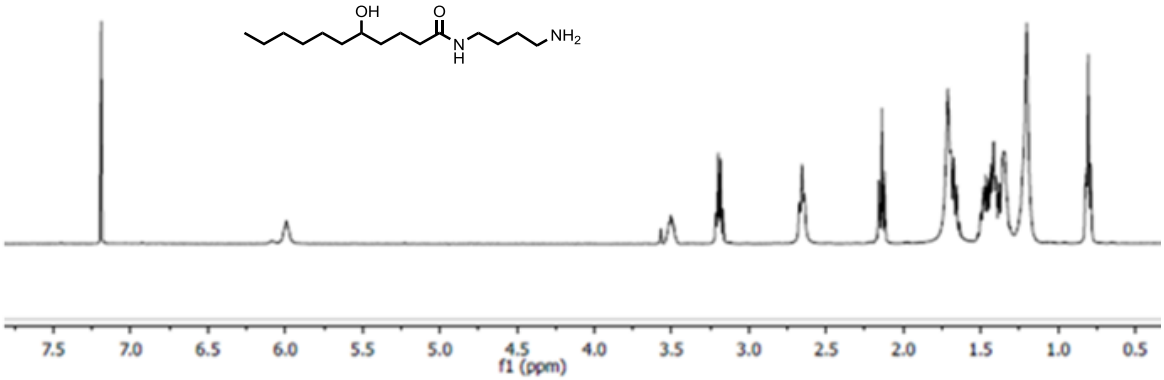

^{1}H NMR of compound **6b**

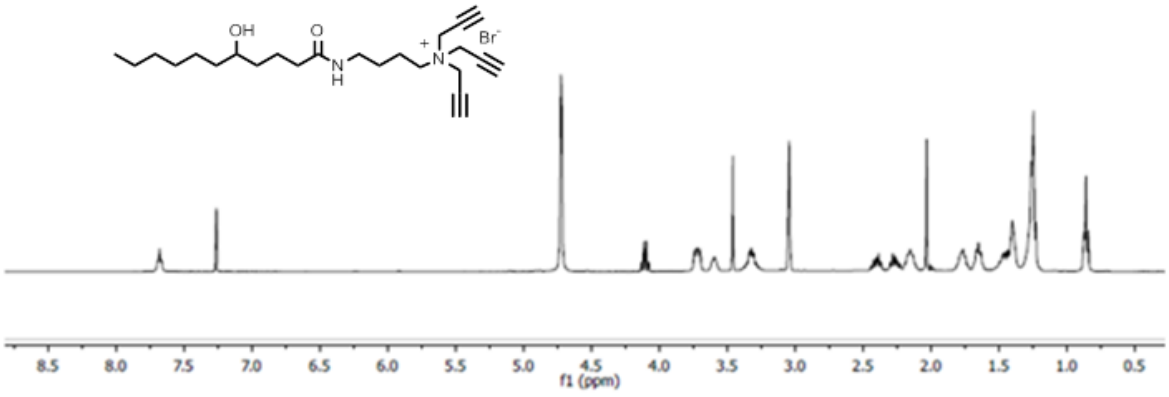

^{13}C NMR of compound **6b**

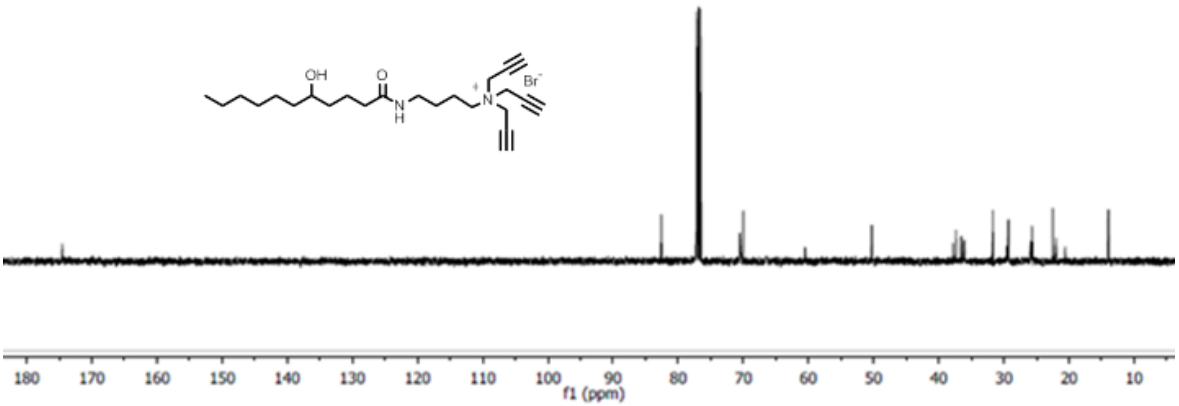

Mass spectrum of compound **6b**

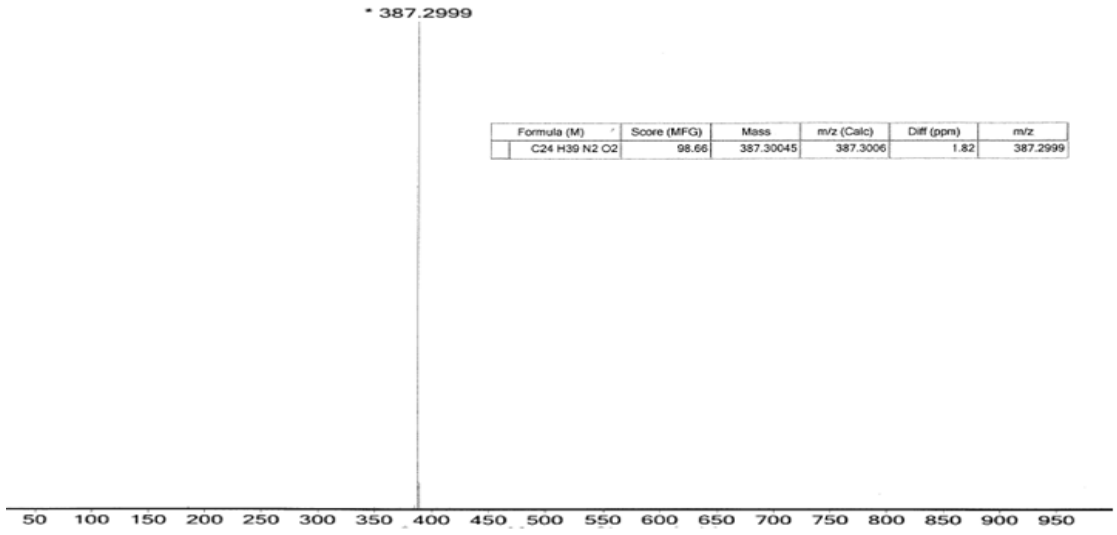

^{1}H NMR of compound **4b**

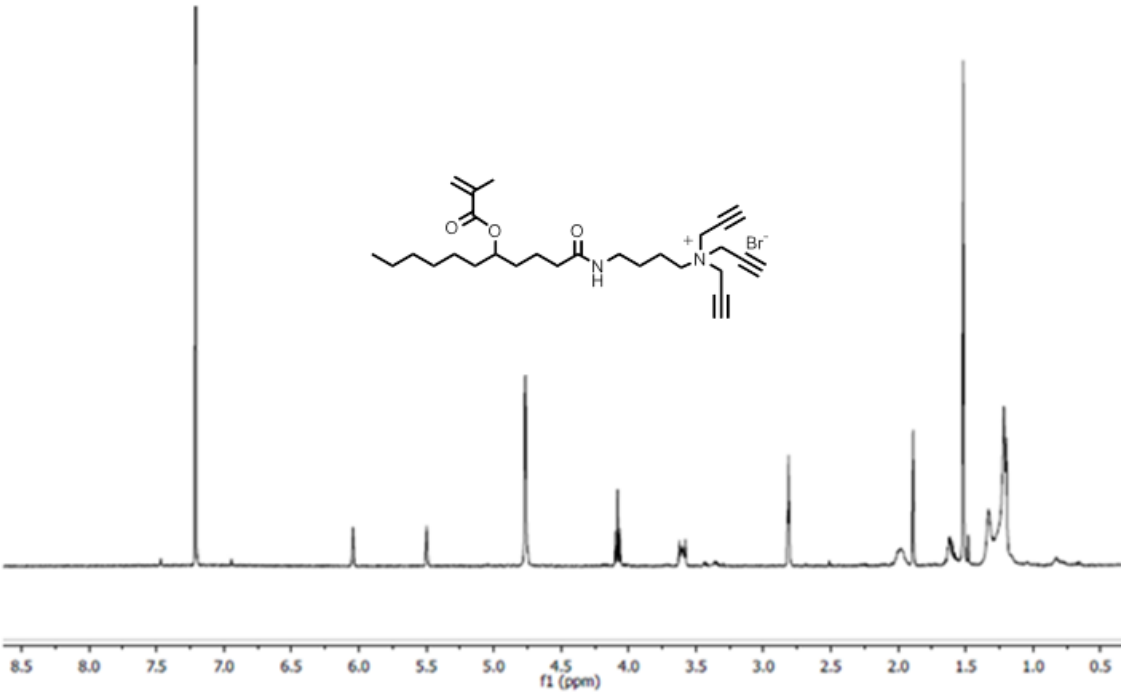

^{13}C NMR of compound **4b**

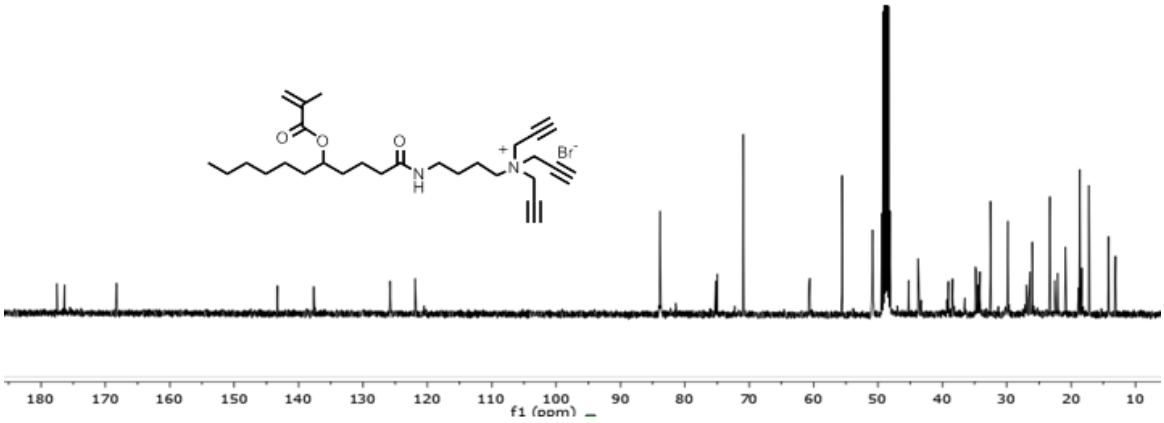

Mass spectrum of compound 4b

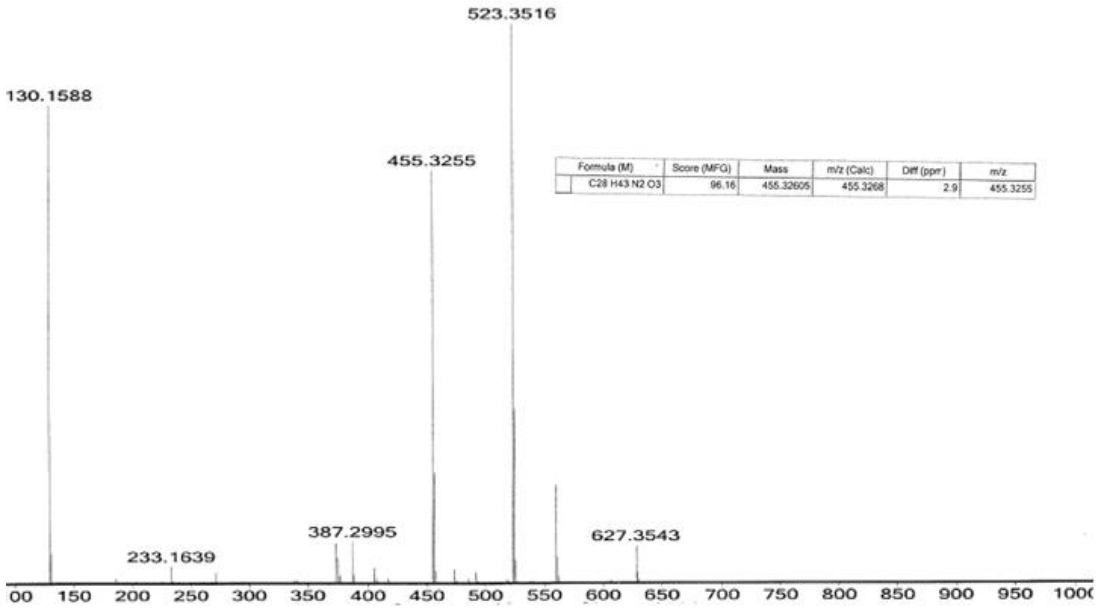

Formula (M)	Score (MFG)	Mass	m/z (Calc)	Diff (ppm)	m/z
C28 H43 N2 O3	96.16	455.32605	455.3268	2.9	455.3255

^{1}H NMR of compound **7a**

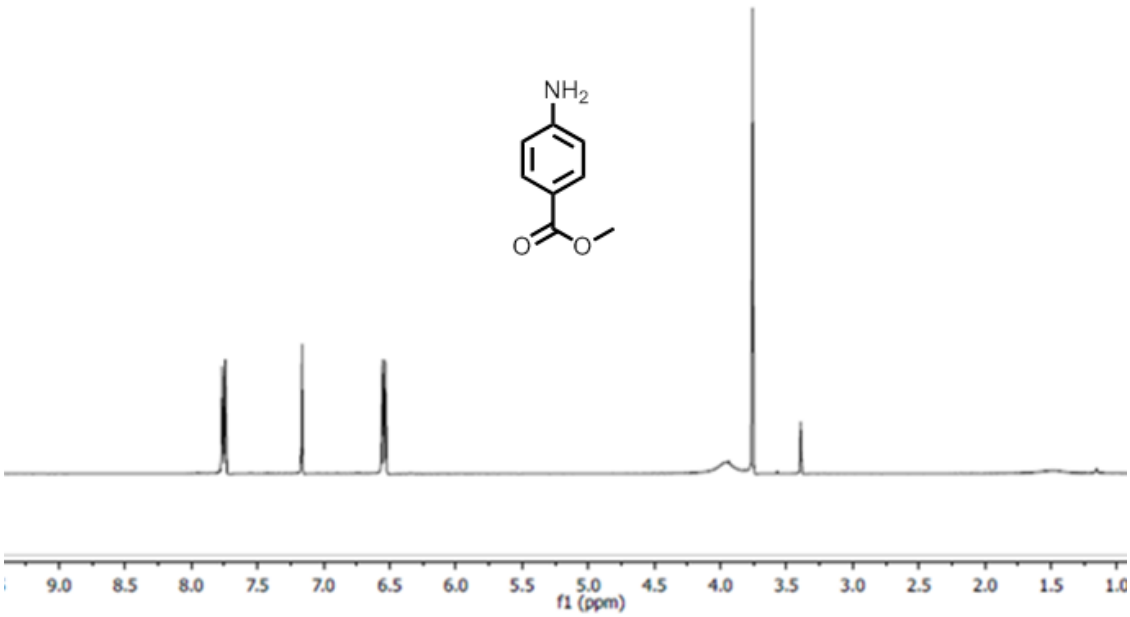

^{1}H NMR of compound **7b**

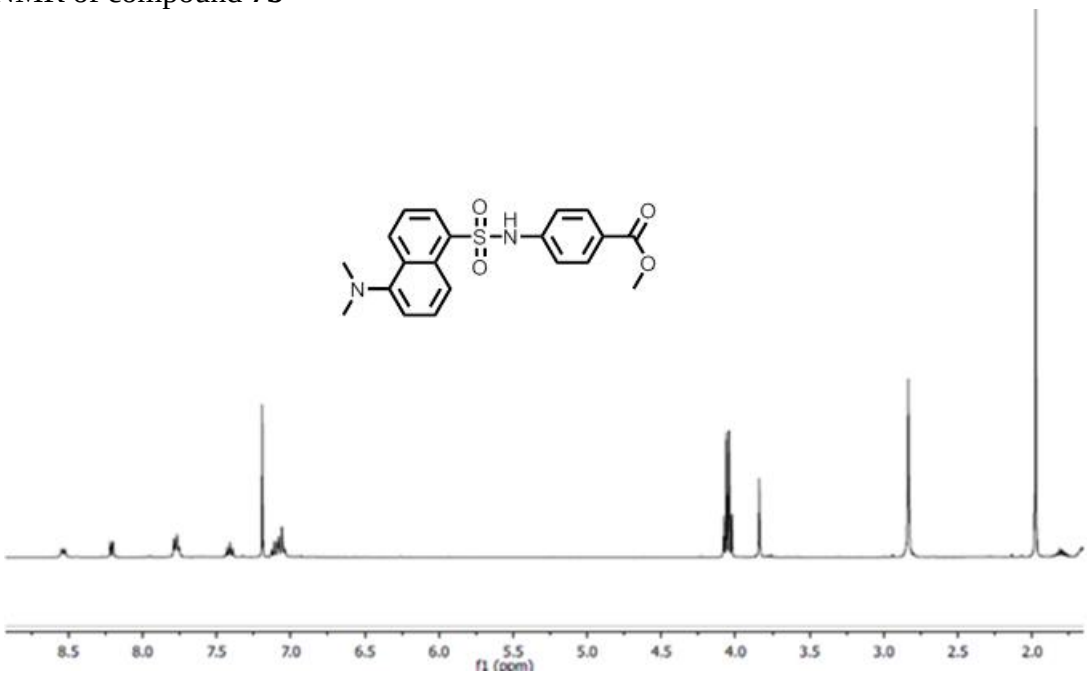

^{1}H NMR of compound **7c**

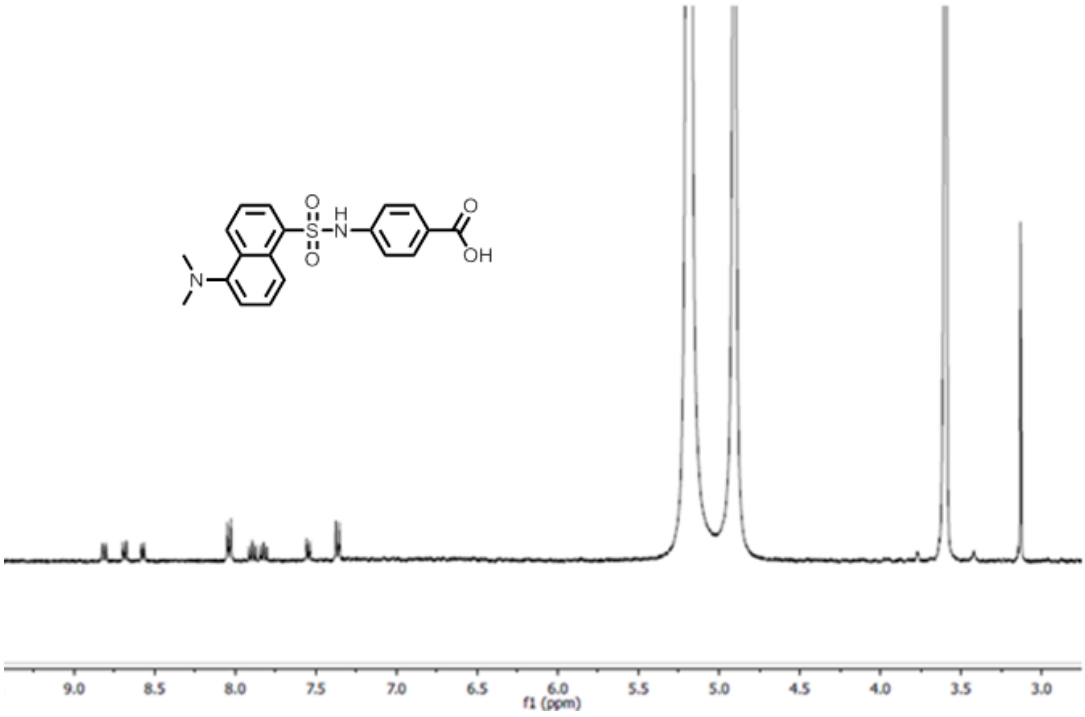

^{1}H NMR of compound **8a**

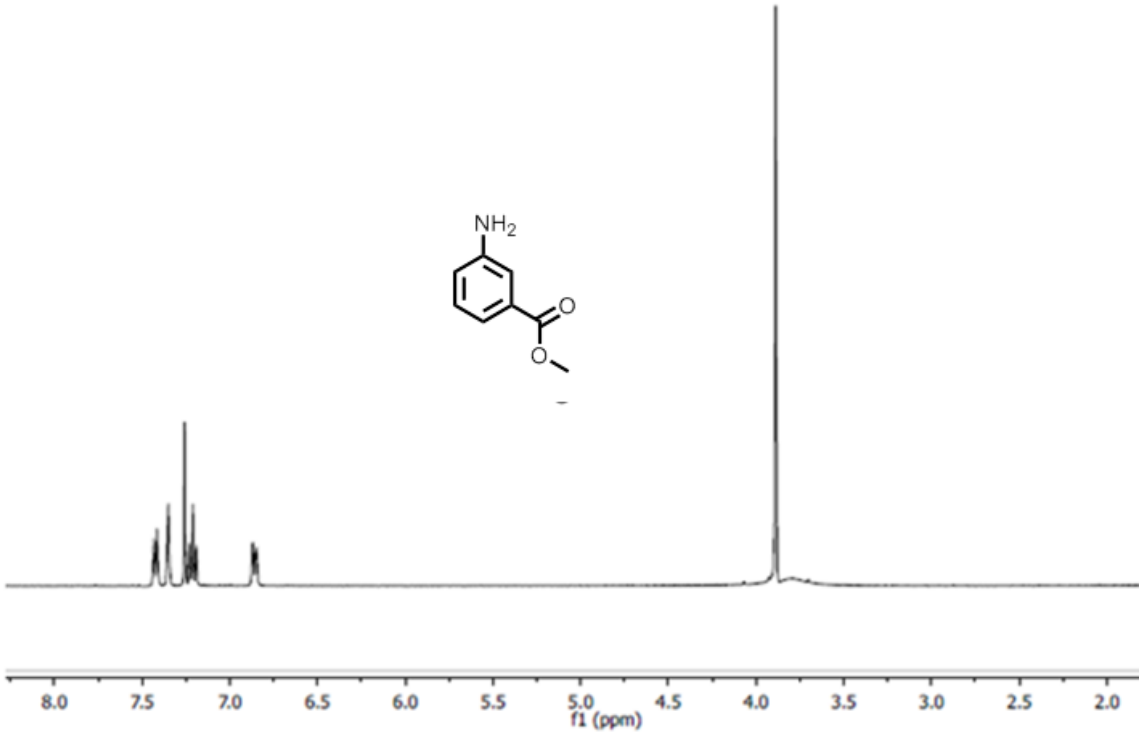

^{1}H NMR of compound **8b**

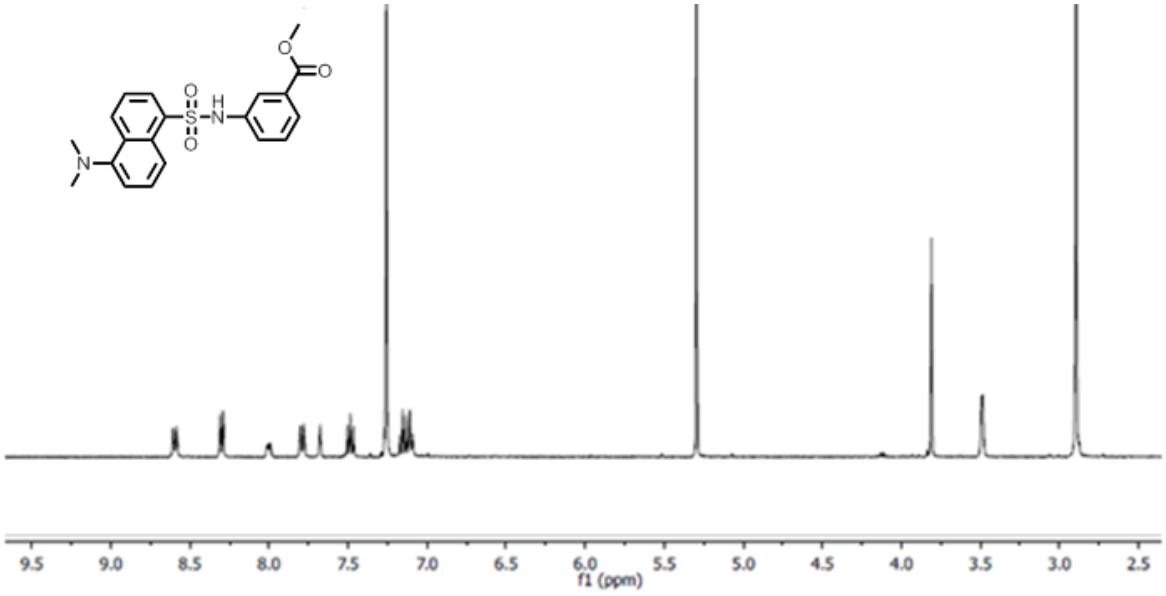

^{1}H NMR of compound **8c**

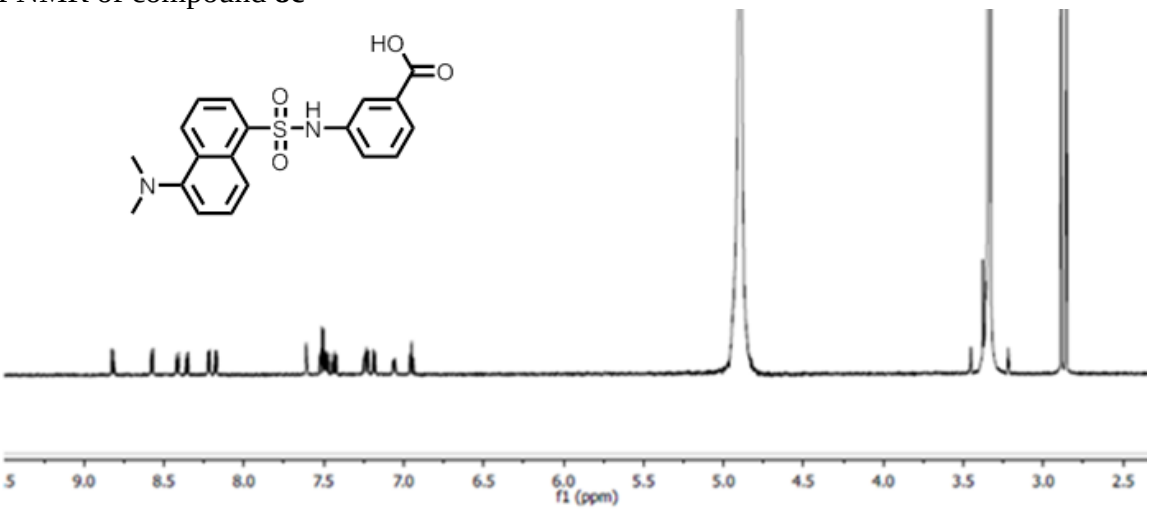

^{1}H NMR of compound **9a**

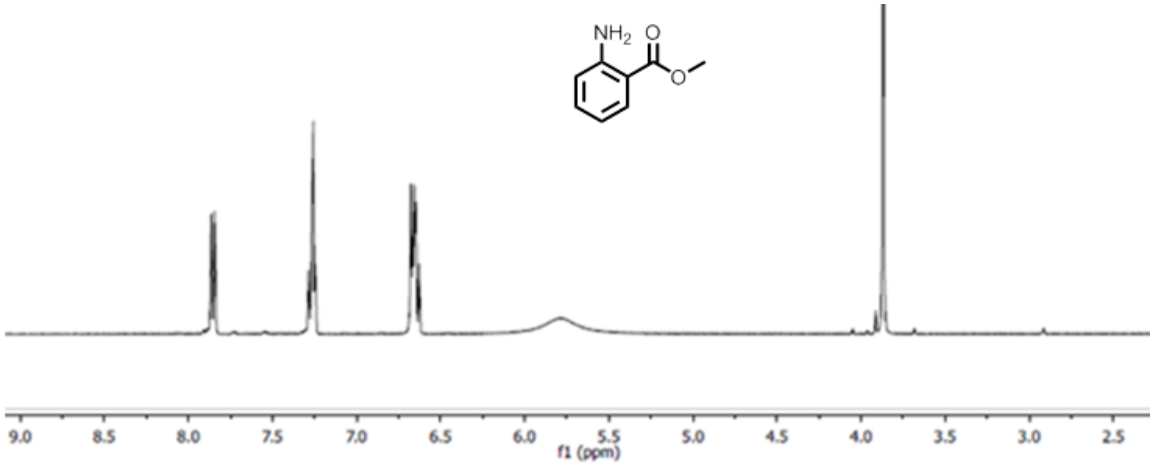

^{1}H NMR of compound **9b**

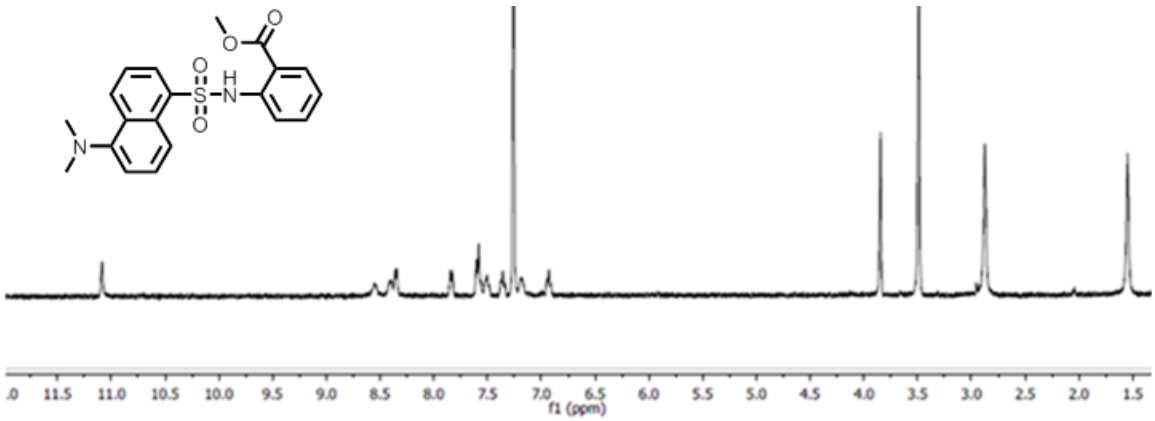

^{1}H NMR of compound **9c**

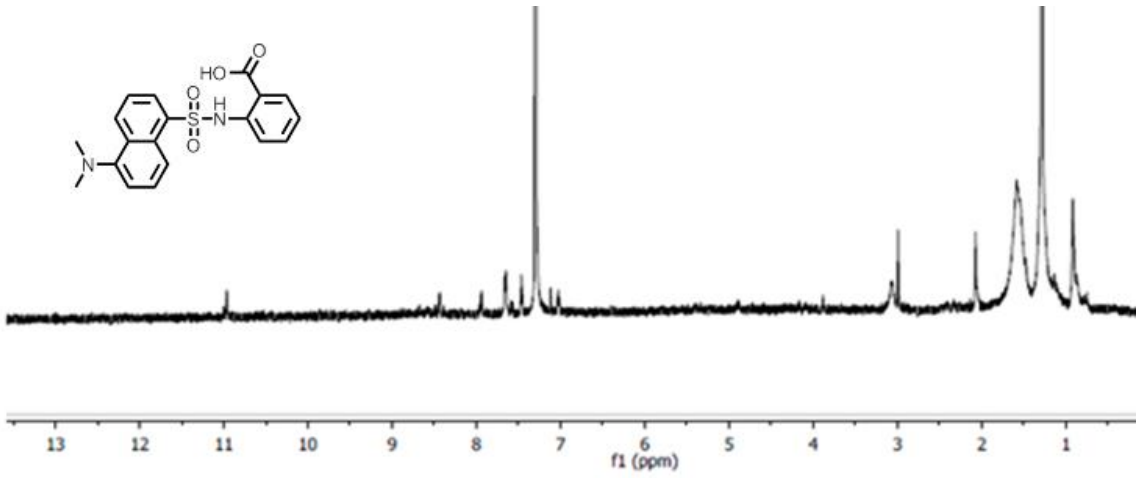

References

(1) Atwood, J. L.; Lehn, J. M. *Comprehensive Supramolecular Chemistry*; Pergamon: New York, 1996.

(2) Steed, J. W.; Gale, P. A. *Supramolecular Chemistry: From Molecules to Nanomaterials*; Wiley: Weinheim, 2012.

(3) Schneider, H.-J.; Yatsimirsky, A. K. *Principles and methods in supramolecular chemistry*; Wiley: New York, 2000.

(4) Wulff, G. *Angew. Chem. Int. Ed. Engl.* **1995**, *34*, 1812.

(5) Wulff, G. *Chem. Rev.* **2001**, *102*, 1.

(6) Haupt, K.; Mosbach, K. *Chem. Rev.* **2000**, *100*, 2495.

(7) Ye, L.; Mosbach, K. *Chem. Mater.* **2008**, *20*, 859.

(8) Shea, K. J. *Trends Polym. Sci.* **1994**, *2*, 166.

(9) Sellergren, B. *Molecularly imprinted polymers: man-made mimics of antibodies and their applications in analytical chemistry*; Elsevier: Amsterdam, **2001**.

(10) Komiyama, M. *Molecular imprinting: from fundamentals to applications*; Wiley-VCH: Weinheim, **2003**.

(11) Yan, M.; Ramström, O. *Molecularly imprinted materials: science and technology*; Marcel Dekker: New York, 2005.

(12) Alexander, C.; Andersson, H. S.; Andersson, L. I.; Ansell, R. J.; Kirsch, N.; Nicholls, I. A.; O'Mahony, J.; Whitcombe, M. J. *J. Mol. Recognit.* **2006**, *19*, 106.

(13) Sellergren, B.; Hall, A. J. In *Supramol Chem*; John Wiley & Sons, Ltd: 2012.

(14) Haupt, K.; Ayela, C. *Molecular Imprinting*; Springer: Heidelberg ; New York, 2012.

(15) Zimmerman, S. C.; Wendland, M. S.; Rakow, N. A.; Zharov, I.; Suslick, K. S. *Nature* **2002**, *418*, 399.

(16) Zimmerman, S. C.; Zharov, I.; Wendland, M. S.; Rakow, N. A.; Suslick, K. S. *J. Am. Chem. Soc.* **2003**, *125*, 13504.

(17) Sellergren, B. *Angew. Chem. Int. Ed.* **2000**, *39*, 1031.

(18) Wu, X.; Carroll, W. R.; Shimizu, K. D. *Chem. Mater.* **2008**, *20*, 4335.
(19) Zimmerman, S. C.; Lemcoff, N. G. *Chem. Commun.* **2004**, 5.

(20) Li, Z.; Ding, J.; Day, M.; Tao, Y. *Macromolecules* **2006**, *39*, 2629.

(21) Hoshino, Y.; Kodama, T.; Okahata, Y.; Shea, K. J. *J. Am. Chem. Soc.* **2008**, *130*, 15242.

(22) Priego-Capote, F.; Ye, L.; Shakil, S.; Shamsi, S. A.; Nilsson, S. *Anal. Chem.* **2008**, *80*, 2881.

(23) Cutivet, A.; Schembri, C.; Kovensky, J.; Haupt, K. *J. Am. Chem. Soc.* **2009**, *131*, 14699.

(24) Yang, K. G.; Berg, M. M.; Zhao, C. S.; Ye, L. *Macromolecules* **2009**, *42*, 8739.

(25) Zeng, Z. Y.; Patel, J.; Lee, S. H.; McCallum, M.; Tyagi, A.; Yan, M. D.; Shea, K. J. *J. Am. Chem. Soc.* **2012**, *134*, 2681.

(26) Ma, Y.; Pan, G. Q.; Zhang, Y.; Guo, X. Z.; Zhang, H. Q. *Angew. Chem. Int. Ed.* **2013**, *52*, 1511.

(27) Çakir, P.; Cutivet, A.; Resmini, M.; Bui, B. T.; Haupt, K. *Adv. Mater.* **2013**, *25*, 1048.

(28) Zhang, Y.; Deng, C.; Liu, S.; Wu, J.; Chen, Z.; Li, C.; Lu, W. *Angew. Chem. Int. Ed.* **2015**, *54*, 5157.

(29) Chen, L. X.; Xu, S. F.; Li, J. H. *Chem. Soc. Rev.* **2011**, *40*, 2922.

(30) Awino, J. K.; Zhao, Y. *J. Am. Chem. Soc.* **2013**, *135*, 12552.

(31) Awino, J. K.; Zhao, Y. *Chem. Commun.* **2014**, *50*, 5752.

(32) Awino, J. K.; Zhao, Y. *Chem.-Eur. J.* **2015**, *21*, 655.

(33) Awino, J. K.; Hu, L.; Zhao, Y. *Org. Lett.* **2016**, *18*, 1650.

(34) Awino, J. K.; Zhao, Y. *ACS Biomater. Sci. Eng.* **2015**, *1*, 425.

(35) Zhang, S.; Zhao, Y. *Macromolecules* **2010**, *43*, 4020.

(36) Peng, H.-Q.; Chen, Y.-Z.; Zhao, Y.; Yang, Q.-Z.; Wu, L.-Z.; Tung, C.-H.; Zhang, L.-P.; Tong, Q.-X. *Angew. Chem. Int. Ed.* **2012**, *51*, 2088.

(37) Kalyanasundaram, K.; Thomas, J. K. *J. Am. Chem. Soc.* **1977**, *99*, 2039.

(38) Zhang, S.; Zhao, Y. *J. Am. Chem. Soc.* **2010**, *132*, 10642.

(39) Li, Y. H.; Chan, L. M.; Tyer, L.; Moody, R. T.; Himel, C. M.; Hercules, D. M. *J. Am. Chem. Soc.* **1975**, *97*, 3118.

(40) Schmidtchen, F. P. In *Supramol Chem*; John Wiley & Sons, Ltd: 2012.

(41) Electrostatic interactions between the positively charged MINP and the negatively charged template should be fairly constant within the series and thus not discussed here.

(42) Takamatsu, D.; Fukui, K.-i.; Aroua, S.; Yamakoshi, Y. *Org. Biomol. Chem.* **2010**, *8*, 3655.

(43) Wu, H.; Zhou, P.; Wang, J.; Zhao, L.; Duan, C. *New J. Chem.* **2009**, *33*, 653.

(44) Himel, C. M.; Aboul-Saad, W. G.; Uk, S. *J. Agric. Food Chem.* **1971**, *19*, 1175.

(45) Hejesen, C.; Petersen, L. K.; Hansen, N. J. V.; Gothelf, K. V. *Org. Biomol. Chem.* **2013**, *11*, 2493.

(46) Sosic, I.; Turk, S.; Sinreih, M.; Trost, N.; Verlaine, O.; Amoroso, A.; Zervosen, A.; Luxen, A.; Joris, B.; Gobec, S. *Acta Chim. Slov.* **2012**, *59*, 380.

(47) Carrillo-Arcos, U. A.; Rojas-Ocampo, J.; Porcel, S. *Dalton transactions (Cambridge, England : 2003)* **2016**, *45*, 479.

(48) Wiseman, T.; Williston, S.; Brandts, J. F.; Lin, L. N. *Anal. Biochem.* **1989**, *179*, 131.

(49) Jelesarov, I.; Bosshard, H. R. *J. Mol. Recognit.* **1999**, *12*, 3.

(50) Velazquez-Campoy, A.; Leavitt, S. A.; Freire, E. *Methods Mol. Biol.* **2004**, *261*, 35.

CHAPTER 3. SURFACE LIGANDS IN THE IMPRINTING AND BINDING OF MOLECULARLY IMPRINTED CROSS-LINKED MICELLES

Modified from a paper published in *Supramolecular Chemistry* **2018**, 30(11), 929-939

MD Arifuzzaman, Wei Zhao and Yan Zhao

Department of Chemistry, Iowa State University, Ames, Iowa 50011-3111, United States

Abstract

Molecular recognition in water is challenging but water-soluble molecularly imprinted nanoparticle (MINP) receptors were produced readily by double cross-linking of surfactant micelles in the presence of suitable template molecules. When the micellar surface was decorated with different polyhydroxylated ligands, significant interactions could be introduced between the surface ligands and the template. Flexible surface ligands worked better than rigid ones to interact with the polar moiety of the template, especially for those template molecules whose water-exposed surface is not properly solvated by water. The importance of these hydrophilic interactions was examined in the context of different substrates, density of the surface ligands, and surface-cross-linking density of the MINP. Together with the hydrophobic interactions in the core, the surface hydrophilic interactions can be used to enhance the binding of guest molecules in water.

Introduction

In molecular recognition, molecules interact with one another by noncovalent forces to form specific supramolecular complexes. The process can occur between small and large molecules, and is essential to many biological processes including ligand–receptor binding,

enzymatic catalysis, and selective transport of nutrients across membranes. For molecular recognition to occur, the host molecule needs to possess a guest-complementary binding surface, ideally poorly solvated prior to binding. Traditionally, a concave structure is synthesized, preorganized by the covalent framework to engage multiple noncovalent forces with the guest molecule. This approach has led to countless small-molecule hosts[1-3] including macrocycles such as cyclodextrin, crown ether, and calixarene, as well as more flexible hosts[4-10] that utilize guest-triggered conformational changes to amplify guest binding.[11,12] As the guest molecule becomes larger in size and more complex in structure, however, design and synthesis of its molecular host become increasingly challenging, because the guest-complementary binding surface increases exponentially not only in size but also in complexity of the binding functionalities.

Molecular imprinting[13, 14] takes a different approach to creating guest-complementary hosts.[15-26] In this technique, the guest molecule (or surrogate) is used as the template. Functional monomers (FMs) interact with the template through noncovalent or cleavable covalent bonds. The template–FM complex is copolymerized and cross-linked with a large amount of a cross-linker to yield a polymer matrix with embedded template molecules. Removal of the templates leaves behind binding sites formed through the template polymerization, complementary to the template. The method is conceptually simple and highly attractive, because complementarity between the imprinted host and the guest does not require elaborate synthesis of complex organic molecules but, instead, relies on facile template–FM complexation and covalent capture by polymerization and cross-linking. Molecularly imprinted polymers (MIPs), indeed, have found broad applications in molecular recognition, separation, enzyme-mimetic catalysis, and chemical sensing.[13-26] In addition to

traditional macroporous polymers, imprinting could occur on surface and unimolecularly within dendrimers.[27,28] Traditional MIPs are insoluble macroporous materials but soluble materials could be prepared by imprinting on polymeric nanoparticles[29-36] and within micro/nanogels.[37-42]

Our group has been interested in the creation of functional receptors through biomimetic strategies.[43-45] Recently, we reported a method to perform templated polymerization within cross-linked surfactant micelles to create molecularly imprinted nanoparticles (MINPs).[46] The method allowed us to prepare protein-sized nanoparticles with a controllable number of binding sites, thus bridging the gap between molecular receptors and macroscopic MIPs. The water-solubility of MINPs enabled us to study their binding by techniques typically used for molecular receptors, including fluorescence titration, isothermal titration calorimetry (ITC), and chemical derivatization.[47]

In our previous studies, the binding functionalities were installed exclusively in the hydrophobic binding pocket created in the core of the MINP. Although the method worked successfully for many guests including nonsteroidal anti-inflammatory drugs (NSAIDs) [48], carbohydrates, [49,50] and peptides, [51-53] further improvement in binding affinity and selectivity is needed, particularly for molecules whose hydrophobic interactions are insufficient. In this paper, we report that the surface ligands on the MINP could contribute significantly to its binding but the interactions varied largely depending on the nature of the substrate and the structure of the surface ligands. The study thus revealed a previously neglected aspect of molecular recognition in our imprinted materials. Because the hydrophilic interactions provide additional driving force to the binding, they could be used rationally to enhance the binding of substrates with strong hydrophilicity.

Results and Discussion

Design and Synthesis of Surface-Functionalized MINPs

Synthesis of MINPs is shown in Scheme 1. Surfactant **1** has two sets of orthogonal cross-linkable groups: the tripropargylammonium headgroup can be cross-linked with diazide **2** through the click reaction, [54-55] and the methacrylate at the end of the hydrophobic tail can be co-polymerized with divinylbenzene (DVB) by free radical polymerization. The cross-linked micelle is typically functionalized by an azide-containing surface ligand (**3**) to enhance its water-solubility. The double cross-linking covalently fixes the micelle around the solubilized template molecule, converting the micelle into the molecularly imprinted nanoparticle (MINP). We often use a surfactant/template ratio of 50:1 in the preparation, as dynamic light scattering (DLS) estimated that each MINP contained approximately 50 (cross-linked) surfactant molecules. The 50:1 surfactant/template ratio would then afford one binding site per nanoparticle on average. As shown in a previous work of ours, the number of binding site could be tuned using different surfactant/template ratios in the preparation.[46]

Surface ligand **3**, prepared from δ-gluconolactone and 2-azidoethylamine, is used in all our previous MINP syntheses. It is installed for two primary purposes. First, it creates a hydrophilic layer on the surface of the MINP, enhancing its solubility in water. Second, due to its poor solubility in typical organic solvents, we can recover the MINP conveniently by pouring the aqueous reaction mixture into acetone and wash off the template and other impurities using acetone/water and methanol.[46]

In principle, we can decorate the surface of MINP with any azide-containing ligands.[54] Because we had used different surface ligands on the cross-linked micelles to modulate their interactions with lipid bilayer membranes, [56] we thought the surface ligands

might be made to interact with the hydrophilic moiety of the template molecule to further strengthen the binding. In this study, we synthesized azido sugars **4**–**6** from glucose, cellobiose, and maltose, respectively, and employed them as surface ligands for the MINPs. The sugars vary in length and have different curvatures for **5** and **6**, due to the β and α glycosidic linkage between the two monosaccharides, respectively. We reasoned that, together with the linear and flexible **3**, ligands **4**–**6** would provide enough diversity for us to identify the important factors in the hydrophilic interactions on the micelle surface.

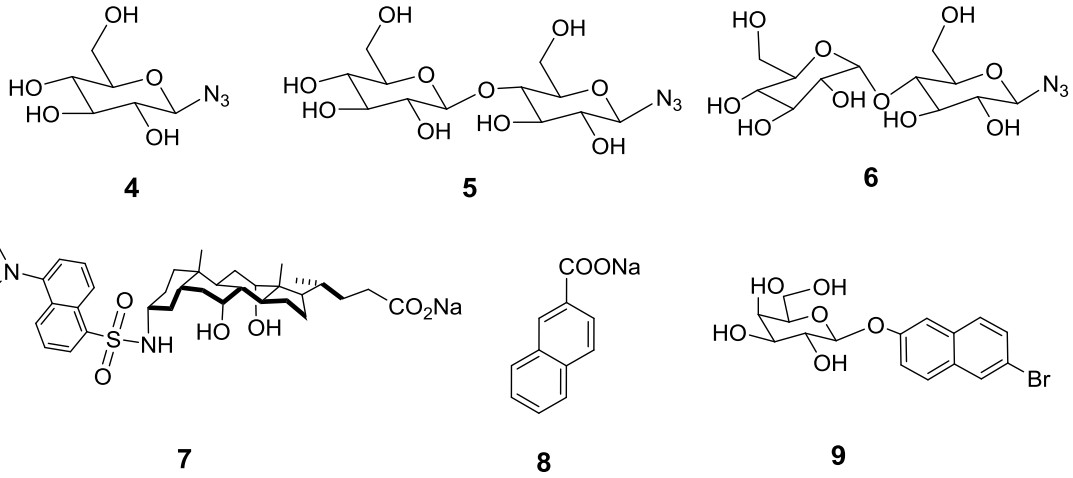

For our investigation, we used three templates (**7**–**9**). Compound **8** and **9** are commercially available and **7** was reported by us previously.[46] These templates have different size, shape, and, importantly, distribution of hydrophobic/hydrophilic groups. Compound **7** is a facially amphiphilic derivative of bile salt; its hydrophilic and hydrophobic groups are on two opposite faces.[57] Similar to **7**, compound **8** has an anionic carboxylate but contains an aromatic hydrophobe. Compound **9** is similar to **8** in its aromatic hydrophobic group but has a nonionic hydrophilic sugar moiety. Our idea was that the different hydrophilic groups of these templates would interact with the surface ligands of the MINP differently and help us

understand the key factors influencing the surface interactions. Previously, our study typically focused on the binding interactions in the hydrophobic core of the micelles.[46]

The preparation of MINPs followed Scheme 1 and the detailed procedures are reported in the Experimental Section. In general, we monitored the surface-cross-linking and core-polymerization/cross-linking by ^{1}H NMR spectroscopy and DLS (Supplementary Material).[46] ^{1}H NMR spectroscopy showed disappearance of alkenic protons as the surfactant and DVB (core-cross-linker) underwent free radical polymerization. DLS showed an increase in size of the nanoparticles as surface ligands were attached and a slight decrease in size when core-polymerization shrank the cross-linked micelles. DLS also allowed us to estimate the molecular weight of the MINP and the number of (cross-linked) surfactants within the MINP. The surface-cross-linking has been confirmed by mass spectrometry (after cleaving the surface-cross-linkages)[58] and the DLS size by transmission electron microscopy (TEM).[51]

Effects of Surface Ligands on the Imprinting and Binding of MINPs

Because the templates are fluorescent, we could determine the binding properties of the MINPs by fluorescence titration. Figure 1 shows the emission spectra of compound **7** upon titration with the MINP prepared with **7** as the template and **3** as the surface ligand, i.e., MINP$_3$(**7**). Addition of the MINP shifted the emission maximum of dansyl from ~550 to ~490 nm. Meanwhile, the emission intensity increased significantly. This was expected behavior for dansyl when it migrated from a polar to a nonpolar environment[59] and supports the binding of **7** by its MINP. The fluorescence data fit well to a 1:1 binding model and gave a binding constant (K_a) of (230 ± 40) × 10^4 M^{-1} in water (Figure 1b).

ITC is another commonly used technique to study binding.[60] In addition to the binding constant; it affords a number of other important parameters including binding

enthalpy (ΔH) and the number of binding sites per particle (N). The binding free energy (ΔG) can be calculated from K_a using equation $-\Delta G = RT\ln(K_a)$, and ΔS from ΔG and ΔH. Our ITC titration of $MINP_3$(**7**) by template **7** showed a negative/favorable enthalpy. The data afforded a K_a value of $(230 \pm 31) \times 10^4\ M^{-1}$ (Table 1, entry 1), in excellent agreement with the value from the fluorescence titration.

Table 1 summarizes the binding data obtained for all three templates by the different MINPs. Entries 1–3 show the selectivity of our imprinted materials. Among the three template/guests studied, $MINP_3$ (7) bound the template most strongly, with **8** and **9** showing 1/9 and 1/35 of the Ka value of **7**. The selectivity was expected, as our previous work has shown that the hydrophobic pocket generated through imprinting tends to be highly discriminating .[61]

The surface ligands indeed had a very pronounced effect on the MINPs prepared from template 7. The binding for the template was the strongest with surface ligand **3** ($K_a = 230 \times 10^4\ M^{-1}$, entry 1) and the weakest with ligand **6** ($K_a = 22.6 \times 104M^{-1}$, entry 6). The difference was thus 10- fold even though the binding pocket inside the core stayed the same. For templates **8** and **9**, however, although ligand remained the best, the strongest/weakest ratiowas much smaller, only 2.7 and 1.2, respectively. Therefore, the surface ligand of MINP could play quite a significant role in the molecular recognition, but the magnitude of the effect strongly depended on the template used.

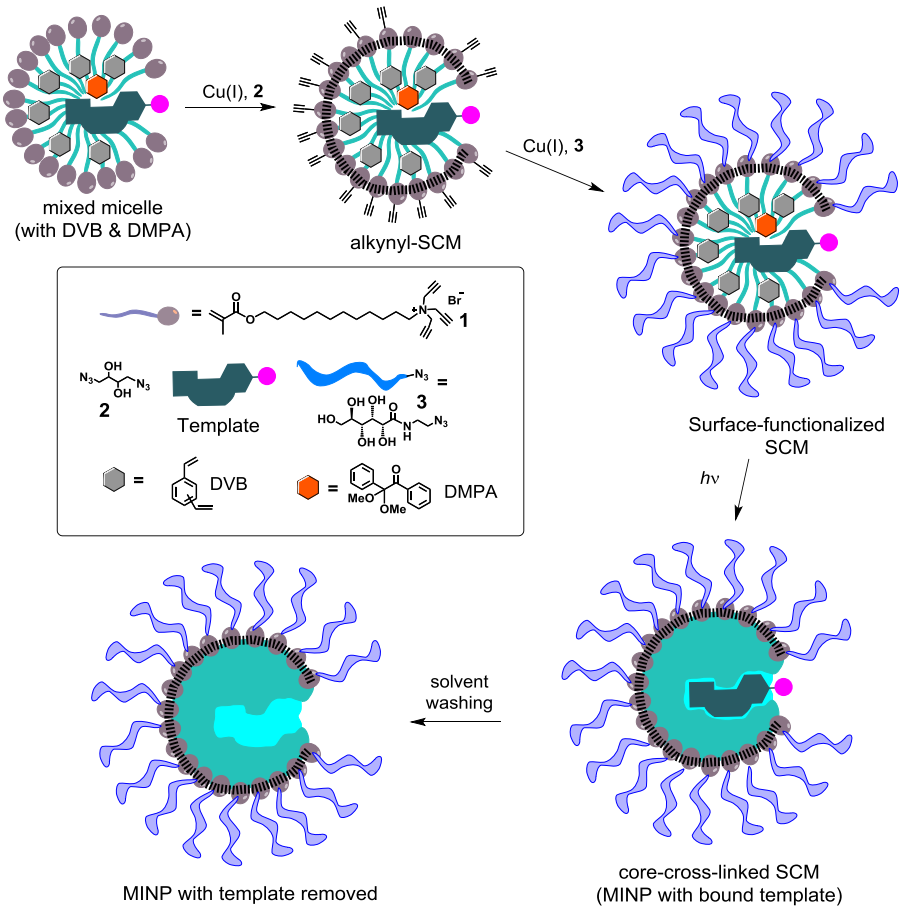

Scheme 1. Preparation of MINP by surface-cross-linking of the micelle of **1**, surface decoration of the alkynyl-surface-cross-linked micelle (alkynyl-SCM) by ligand **3**, and core-cross-linking of the resulting material.

The difference between the three templates is in the nature and size of their hydrophobe and the distribution of functional groups. Templates **8** and **9** both have a relatively small aromatic naphthyl group but possess an anionic and a nonionic hydrophilic group, respectively. The charge character was reflected in the overall stronger binding of **8** over **9**, presumably due to the electrostatic interactions between the negatively charged **8** and the positively charged MINP. These two templates are similar to a head/tail surfactant in their hydrophilic/hydrophobic arrangement, locating on the opposite ends of the molecule.

As the hydrophobic group resides in the hydrophobic core of the cross-linked micelle, the hydrophilic groups are expected to point into the water and be solvated by water molecules.

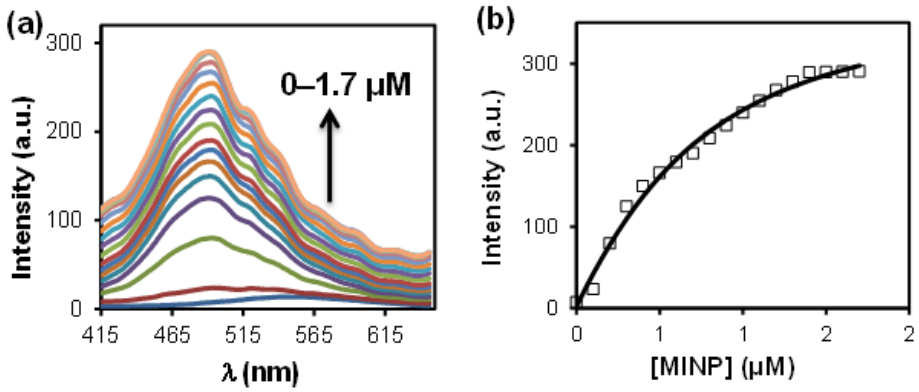

Figure 1. (a) Emission spectra of compound **7** in the presence of 0–1.7 μM of $MINP_3$(**7**) in Millipore water. [**7**] = 0.5 μM. λ_{ex} = 340 nm. (b) Nonlinear least squares curve fitting of the fluorescence intensity at 491 nm to a 1:1 binding isotherm.

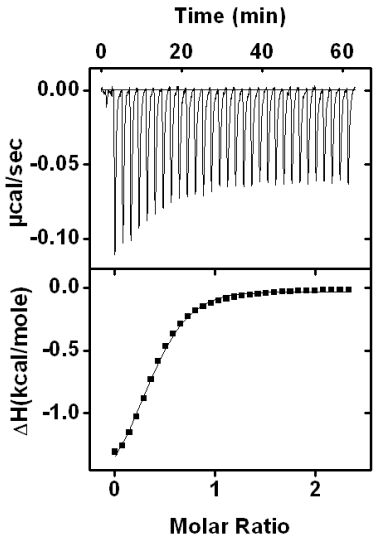

Figure 2. ITC curve obtained at 298 K from titration of $MINP_3$(**7**) with **7** in Millipore water. $MINP_3$(**7**) = 10 μM in the cell. The concentration of **7** in the syringe was 0.20 mM.

For template **7**, the situation is different. In addition to the anionic carboxylate at the end of the molecule, the hydrophilic groups (hydroxyl and sulfonamide) are located on the opposite side of a very large hydrophobic steroidal surface. The large hydrophobic surface

(including that from the dansyl group) gives a strong driving force for the template to interact with the nonpolar core of the micelle. The anionic group, with its strong tendency to stay in water, is expected to anchor the template near the surface of the micelle.[46] Given the strong effect of the hydrophilic surface ligands on the imprinting/binding of MINP(**7**), the hydrophilic groups of **7** most likely faced the bulk water, interacting with the hydrophilic ligand through hydrogen-bonds (directly or mediated by water molecules), shown schematically in Figure 3. Although the "hydrophilic" face of **7** contains three hydrophilic groups, the rest of the structure on this face remains hydrophobic, being made of hydrocarbon. The arrangement proposed in Figure 3 allows the hydroxyl groups of the attached **3** to interact with the hydrophilic face of **7**, thus avoiding a complete exposure of partially hydrophobic surface to water—this likely was the reason for the enhanced binding of $MINP_3$(**7**) in comparison to the MINPs prepared with other surface ligands. Being cyclic, ligands **4**–**6** have significantly higher rigidity than **3**, and are expected to have difficulty adopting the "folded" conformation shown in Figure 3 to interact with the bound template **7**.

Bile salts are well-known to form mixed micelles with head/tail surfactants and lipids.[62] In the most accepted model, the bile salt has its hydrophilic groups facing water, with its steroidal backbone facing the hydrocarbon core of the micelle, [63] as we have proposed in Figure 3. In the same model, cholates can insert their steroidal backbone into the hydrophobic core of the mixed micelle, usually as dimers with their hydroxyl groups hydrogen-bonded to one another to avoid unfavorable hydroxyl–hydrocarbon contact.

The latter scenario is not supported by our binding data, since the surface ligands exerted a strong influence on the binding of **7**, indicating significant interactions between the two—dimers with buried hydroxyl groups should not be able to do so. Furthermore, our ITC

titrations revealed the number of binding site on average was close to 1 (Table 1), a result from the surfactant/template ratio of 50. The dimer model of the bile salt would predict at least two binding sites per nanoparticle with cooperative binding behavior. In a previous work of ours, we have shown that, even when two binding sites were generated for template **7** (with a surfactant/template ratio of 25), they are independent, possessing identical binding affinities within experimental error.[46]

Table 1. Binding data for the MINPs prepared with different surface ligands.[a]

Entry	MINPs	Guest	K_a ($\times 10^4$ M^{-1})	*N*	ΔG (kcal/mol)	ΔH (kcal/mol)	$T\Delta S$ (kcal/mol)
1	$MINP_3$(**7**)	**7**	230 ± 31.1 (230 ± 40)	0.71 ± 0.05	-8.7	-0.28 ± 0.04	8.4
2	$MINP_4$(**7**)	**7**	42.1 ± 1.12 (44.3 ± 0.9)	0.83 ± 0.04	-7.7	-1.02 ± 0.11	6.6
3	$MINP_5$(**7**)	**7**	30.1 ± 1.04 (31.5 ± 1.9)	0.68 ± 0.09	-7.5	-9.23 ± 0.17	-1.8
4	$MINP_6$(**7**)	**7**	22.6 ± 1.05 (21.6 ± 1.1)	1.14 ± 0.27	-7.8	-4.15 ± 0.14	3.1
5	$MINP_3$(**8**)	**8**	50.9 ± 4.70	0.98 ± 0.03	-7.8	-1.63 ± 0.14	6.2
6	$MINP_4$(**8**)	**8**	21.8 ± 1.05	0.80 ± 0.03	-7.3	-1.74 ± 0.33	5.5
7	$MINP_5$(**8**)	**8**	27.4 ± 1.4	0.98 ± 0.02	-7.4	-6.94 ± 0.25	0.5
8	$MINP_6$(**8**)	**8**	18.7 ± 1.66	0.72 ± 0.07	-7.2	-7.66 ± 0.14	-0.3
9	$MINP_3$(**9**)	**9**	8.27 ± 1.60	1.20 ± 0.05	-6.7	-1.46 ± 0.09	5.3
10	$MINP_4$(**9**)	**9**	5.26 ± 0.14	1.21 ± 0.10	-6.4	-0.60 ± 0.05	5.9
11	$MINP_5$(**9**)	**9**	3.46 ± 0.57	1.19 ± 0.06	-6.2	-0.71 ± 0.05	5.7
12	$MINP_6$(**9**)	**9**	6.60 ± 0.13	1.22 ± 0.07	-6.6	-1.31± 0.1	5.3

[a] The titrations were performed in duplicates in Millipore water and the errors between the runs were <20%. The binding constants in parentheses were from fluorescence titration. [b] The subscript denotes the surface-ligand (**3**–**6**) used in the MINP synthesis and the number in parentheses (**7**–**9**) the template molecule.

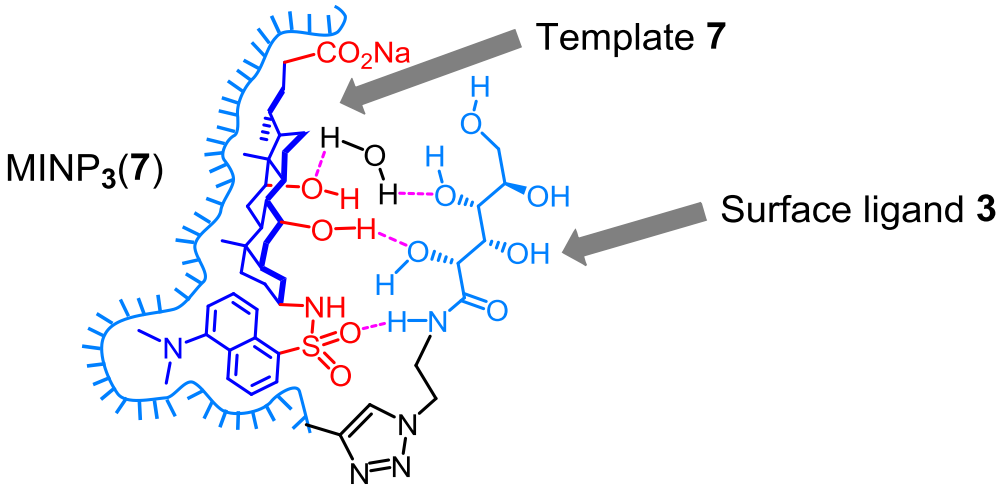

Figure 3. Proposed binding of template **7** by MINP$_3$(**7**), with possible hydrogen bonds between the surface ligand and the hydrophilic groups of the template, possibly also mediated by water molecules.

The binding model in Figure 3 is also consistent with the weak effect of surface ligands on templates **8** and **9**. These templates have their hydrophilic groups opposite to the aromatic hydrophobe, immersed in water. Being well-solvated, they have a much smaller need to interact with the hydroxyl groups of **3**.

Effects of Double Surface-Functionalization

In this study, the ratio of **1** to **2** was 1:1.2, leaving on average 0.8 alkyne per surfactant if the surface cross-linking happened quantitatively. The surface ligand was attached to the cross-linked surfactant by the click reaction to the quaternary ammonium headgroup. A previous study of ours indicated that the click functionalization was extremely efficient. Even for a polymeric azide (i.e., PEG 2000), 70–80% of the residual alkynes on the micelle surface could be successfully functionalized.[54] For smaller surface ligands used in this study, we assumed the surface functionalization was quantitative.

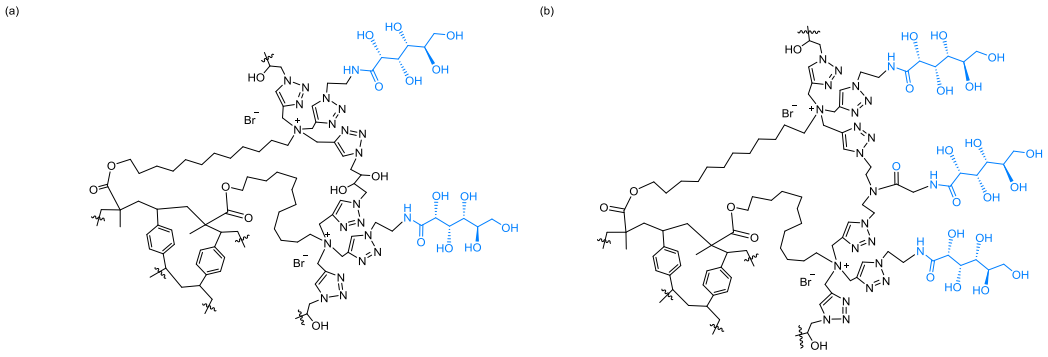

Figure 4. Schematic representation of the cross-linking and surface ligands in $MINP_{3,2}$ (a) and $MINP_{3,10}$ (b).

The usage of cross-linker **2** translates to a significant distance between neighboring surface ligands, due to the many bonds in between the two ammonium headgroups (Figure 4a). We hypothesized that an increase in the density of the hydrophilic ligands might strengthen their interactions with the guest, particularly **9**, which has an abundance of hydroxyl groups. We thought the carboxylate of template **8** might be too small and thus might not benefit as much from such a change.

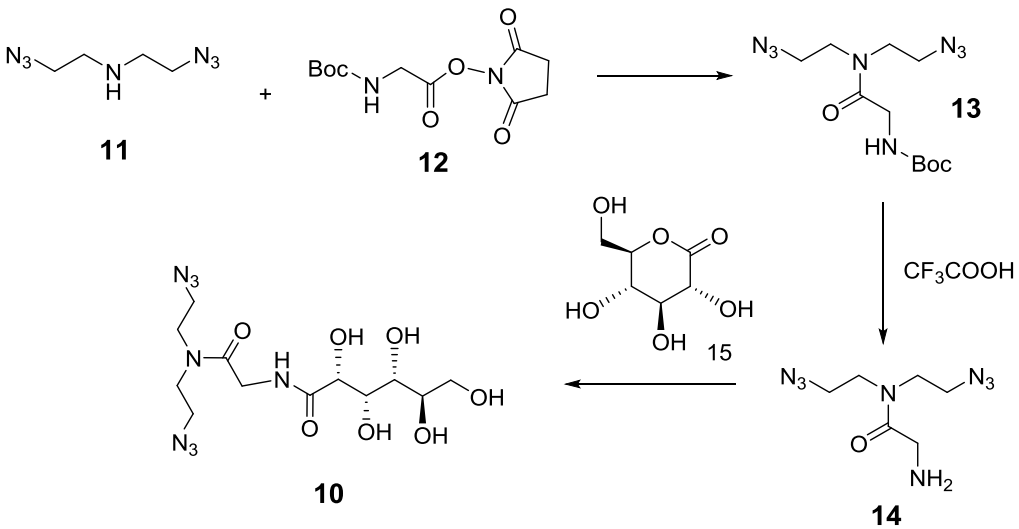

Scheme 2. Synthesis of cross-linker **10** containing a sugar-derived group.

To increase the density of hydrophilic ligands, we designed and synthesized a new diazide cross-linker (**10**). As shown in Scheme 2, the compound was prepared in three simple steps from diazidoamine **11** and Boc-protected glycine *N*-hydroxylsuccinimide ester **12**. Similar to surface ligand **3**, compound **10** carries a hydroxylated moiety derived from δ-gluconolactone (**15**).

We then prepared MINP using cross-linker **10** instead of diazide **2**. As a result, the MINP would have a layer of hydrophilic groups from the cross-linker itself. At the end of the surface cross-linking, we decorated the surface-cross-linked micelles with ligand **3** as usual, using the click reaction. Overall, we nearly doubled the surface hydrophilic groups because both the cross-linker (**10**) and the surface ligand (**3**) installed a δ-gluconolactone-derived hydrophilic ligand (Figure 4b). Since the linear and flexible ligand (**3**) was the best in our studies above, we did not use the cyclic azides (**4**–**6**) in these doubly surface-functionalized MINPs.

Table 2. Binding data for the MINPs prepared with surface ligand **3** and diazide cross-linker **10**.[a]

Entry	MINPs	Guest	K_a ($\times 10^4$ M^{-1})	*N*	ΔG (kcal/mol)	ΔH (kcal/mol)	$T\Delta S$ (kcal/mol)
1	$MINP_{3,10}$(**7**)	**7**	26.2 ± 1.79 (26.9 ± 1.5)	0.95 ± 0.24	-7.4	-2.77 ± 0.15	4.6
2	$MINP_{3,10}$(**8**)	**8**	-[b]	-	-	-	-
3	$MINP_{3,10}$(**9**)	**9**	61.3 ± 1.98 (68.4 ± 2.6)	0.95 ± 0.24	-7.9	-5.76 ± 0.17	2.1

[a]The titrations were performed in duplicates in Millipore water and the errors between the runs were <20%. The binding constants in parentheses were from fluorescence titration. The subscript denotes the diazide cross-linker (**10**) and the surface-ligand (**3**) used in the MINP synthesis and the number in parentheses the template molecule. [b]The binding was too weak to be measured.

Table 2 summarizes the binding data for the MINPs prepared in this approach. Template **9**, indeed, benefited significantly from the double surface-functionalization. The binding constant for the template went from 8.30×10^4 M^{-1} (Table 1, entry 9) to 65.8×10^4 M^{-1} (Table 2, entry 3), an increase of 8-fold. However, the K_a value for both **7** and **8** by their own MINPs decreased upon double surface-functionalization (Table 2, entries 1 and 2). In fact, the binding for **8** was so weak that it could not even be measured in our hands.

Thus, as expected, a higher density of hydrophilic surface ligands enhanced the binding of MINP for template **9**, possibly due to multiple hydrogen bonds formed between the sugar moiety of the template and the amide/hydroxyl groups of **3** and **10**. Even though these groups are exposed to water, crowding them on the surface of the micelle should facilitate their noncovalent interactions.

Why did the other two templates suffer under the same condition? One possibility is the reduced surface cross-linking density. Cross-linker **2** has 4 carbons in between the two azido groups but **10** has 4 carbons and 1 nitrogen in between. Thus, at the same stoichiometry (surfactant/cross-linker = 1:1.2), the effective surface-cross-linking density should be lower in the MINPs prepared with **10** than with **2** as the surface cross-linker. A lower surface-cross-linking density is expected to decrease the rigidity of the binding pocket, detrimental to the binding.

If the lower surface cross-linking density is indeed the reason for the weaker binding for **7** and **8** (*64*), our results also imply that this parameter was more critical to the binding of guests with a smaller hydrophobe (i.e., **8**) than those with larger ones (i.e., **7**). The substitution of **2** by **10**, for example, lowered the K_a value of **7** by 9-fold (compare entry 1 of Table 1 and 2) but reduced that of **8** to undetectable. The result does make sense. Without the

proposed hydrophilic interactions—due to its small-sized carboxylate—compound **8** needs to rely heavily on the hydrophobic interactions between the imprinted binding site and its naphthyl group. A poorly formed, narrow hydrophobic binding pocket for the naphthyl group (due to the low surface cross-linking density) could easily collapse in water, preventing the binding of the guest. For a template (i.e., **7**) with a much larger hydrophobic group, complete collapse of a correspondingly large binding pocket would cause too much stress to the cross-linked network—this could be the reason why the bile salt retained a reasonable binding affinity despite a lower surface-cross-linking density.

Conclusions

Molecular recognition in water is a very challenging topic in supramolecular chemistry because directional noncovalent interactions are often weakened significantly by competition from the solvent (*65-66*). MINPs, on the other hand, can bind various guests strongly and selectively in water (*48-52, 67*). Our previous studies focused exclusively on the molecular recognition between the template and the binding site in the hydrophobic core of the cross-linked micelle. Although the strategy worked quite successfully for a number of different templates, this work suggested there is an important, overlooked opportunity for additional improvement. Since the surface ligands could interact with the hydrophilic groups of the templates significantly, we could install different surface ligands—not limited to the ones studied in this work—to interact with the templates by design. We have reported a strategy to double the density of the surface ligands in this work. We expect similar approaches could increase the density further and magnify the hydrophilic interactions.

Another important learning from this study comes from the realization that the contribution of different intermolecular forces could be tuned quite rationally in our system.

For example, Table 1 shows that binding of **8** by its MINPs was generally higher than that of **9**, most likely due to the electrostatic interactions present in the former that are absent in the latter. However, with the double surface-functionalization, binding of **9** was enhanced while that of **8** disappeared. Since the lower surface-cross-linking density deteriorated the bindings of **7** and **8**, the enhancement of binding in **9** was even more significant, as the lower surface cross-linking density probably decreased the hydrophobic contribution to the binding of **9** just as it did to **7** and **8**.

Finally, this work shows that the surface-cross-linking density in MINP played a significant role in the imprinting and can be very sensitive to minute changes in structure of the surface cross-linker, especially for templates with relatively small/narrow hydrophobes. The learning will be useful in the design of future MINPs with improved binding properties.

Acknowledgments

This work was supported by the Division of Materials Research [DMR-1464927] and NIGMS [R01GM113883]

Experimental Section

General Method

Routine ^{1}H and ^{13}C NMR spectra were recorded on a Bruker DRX-400, on a Bruker AV II 600 or on a Varian VXR-400 spectrometer. ESI-MS mass was recorded on Shimadzu LCMS-2010 mass spectrometer. Dynamic light scattering (DLS) data were recorded at 25°C using PDDLS/ CoolBatch 90T with PD2000DLS instrument. Fluorescence spectra were recorded at ambient temperature on a Varian Cary Eclipse Fluorescence spectrophotometer. Isothermal titration calorimetry (ITC) was performed using a MicroCal VP-ITC

Microcalorimeter with Origin 7 software and VPViewer2000 (GE Healthcare, Northampton, MA).

Syntheses

Syntheses of compounds **1**, **2**, **3**, and **7** were previously reported.[46] Compounds **4**–**6**, [68] **11**, [69] and **12**[70] were synthesized according to literature procedures.

Compound 13. A mixture of **11** (6.21g, 40.0 mmol) and **12** (5.425g, 20.0 mmol) in 100 mL dry CH_3CN was stirred at 70°C for 24 h. The solvent was removed by rotary evaporator and the residue was purified by column chromatography over silica gel using 20:1 methylene chloride/methanol as the eluent to afford an oily product (5.43 g, 87%). ^{1}H NMR (400 MHz, $CDCl_3$, δ): 4.03 (d, *J* = 4.6 Hz, 2H), 3.59-3.53 (m, 4H), 3.53 – 3.45 (m, 4H), 1.45 (s, 9H). ^{13}C NMR (100 MHz, $CDCl_3$, δ): 169.6, 156.1, 80.1, 50.0, 49.6, 47.5, 46.7, 42.7, 28.7. ESI-HRMS (*m/z*): $[M+H]^+$ calcd for $C_{11}H_{21}N_8O_3$, 313.1732; found 313.1728.

Compound 10. A mixture of δ-gluconolactone (0.30g, 1.68 mmol) and **13 (**1.07g 5.04 mmol**)** in pyridine (15 mL) was stirred at 65 °C for 16 h. The mixture was poured into water and washed with chloroform (3 × 20 mL) and ethyl ether (3 × 20 mL). The aqueous phase was concentrated to afford a white powder (0.64 g, 98%). ^{1}H NMR (400 MHz, D_2O, δ) : 4.40 (d, *J* = 4.0 Hz, 1H), 4.31 (d, *J* = 3.6 Hz, 1H), 4.12 (dt, *J* = 3.9, 2.4 Hz, 1H), 3.98-3.73 (m, 3H), 3.71-3.49 (m, 10H). ^{13}C NMR (100 MHz, D_2O, δ): 174.6, 170.9, 73.3, 71.9, 71.0, 70.3, 62.6, 48.9, 48.3, 46.7, 45.3, 40.8. ESI-HRMS (*m/z*): $[M+H]^+$ calcd for $C_{12}H_{23}N_8O_7$, 391.1684; found 391.1681.

Preparation of Molecularly Imprinted Nanoparticles (MINPs) of compound 1. A typical procedure is as follows.[46] To a micellar solution of compound **1** (9.3 mg, 0.02 mmol) in H_2O (2.0 mL), divinylbenzene (DVB, 2.8 μL, 0.02 mmol), compound **7** in H_2O (10 μL of a

solution of 26.5 mg/mL, 0.0004 mmol), and 2,2-dimethoxy-2-phenylacetophenone (DMPA,10 μL of a 12.8 mg/mL solution in DMSO, 0.0005 mmol) were added. The mixture was subjected to ultrasonication for 10 min before compound **2** (4.13 mg, 0.024 mmol), $CuCl_2$ (10 μL of a 6.7 mg/mL solution in H_2O, 0.0005 mmol), and sodium ascorbate (10 μL of a 99 mg/mL solution in H_2O, 0.005 mmol) were added. After the reaction mixture was stirred slowly at room temperature for 12 h, compound **3** (10.6 mg, 0.04 mmol), $CuCl_2$ (10 μL of a 6.7 mg/mL solution in H_2O, 0.0005 mmol l), and sodium ascorbate (10 μL of a 99 mg/mL solution in H_2O, 0.005 mmol) were added. After being stirred for another 6 h at room temperature, the reaction mixture was transferred to a glass vial, purged with nitrogen for 15 min, sealed with a rubber stopper, and irradiated in a Rayonet reactor for 12 h. ^{1}H NMR spectroscopy was used to monitor the progress of reaction. The reaction mixture was poured into acetone (8 mL). The precipitate was collected by centrifugation and washed with a mixture of acetone/water (5 mL/1 mL) three times. The crude produce was washed by methanol/acetic acid (5 mL/0.1 mL) three times until the emission peak at 480 nm (for the dansyl) disappeared and then with excess methanol. The off white powder was dried in air to afford the final MINP (16 mg, 80%).

Determination of Binding Constants by Fluorescence Titration. A typical procedure is as follows. A stock solution containing $MINP_3$(**7**) (150 μM) was prepared in Millipore water. Aliquots (2.0 μL) of the MINP stock solution were added to 2.00 mL of the solution of **7** in Millipore water (0.2 μM). After each addition, the sample was allowed to sit for 1 min at room temperature before the fluorescence spectrum was collected. The excitation wavelength (λ_{ex}) was 340 nm. The excitation slit width was 10 nm, and the emission slit width was 10 nm.

The binding constant was obtained by nonlinear least squares curve fitting of the fluorescence intensity at 491 nm to a 1:1 binding isotherm.

Determination of Binding Constants by ITC. The determination of binding constants by ITC followed standard procedures.[71-73] In general, a solution of an appropriate guest in Millipore water was injected in equal steps into 1.43 mL of the corresponding MINP in the same solution. The top panel shows the raw calorimetric data. The area under each peak represents the amount of heat generated at each ejection and is plotted against the molar ratio of the MINP to the guest. The smooth solid line is the best fit of the experimental data to the sequential binding of *N* binding site on the MINP. The heat of dilution for the guest, obtained by titration carried out beyond the saturation point, was subtracted from the heat released during the binding. Binding parameters were auto-generated after curve fitting using Microcal Origin 7.

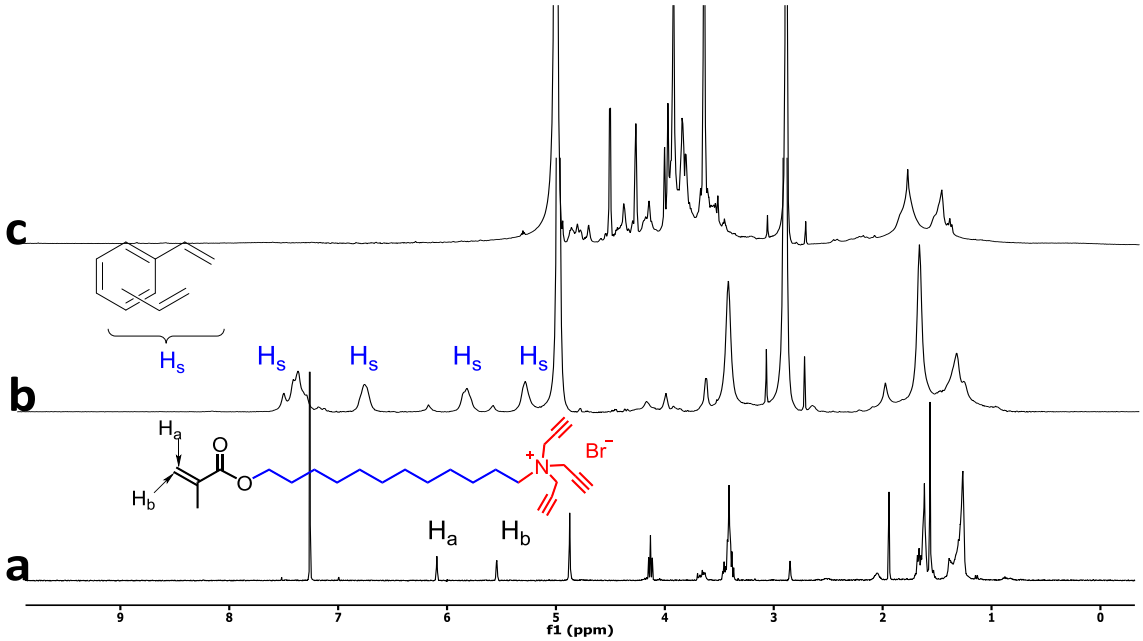

Figure 5. ^{1}H NMR spectra of (a) **1** in $CDCl_3$, (b) alkynyl-SCM in D_2O, (c) $MINP_3$(**7**) in D_2O at 25 °C.

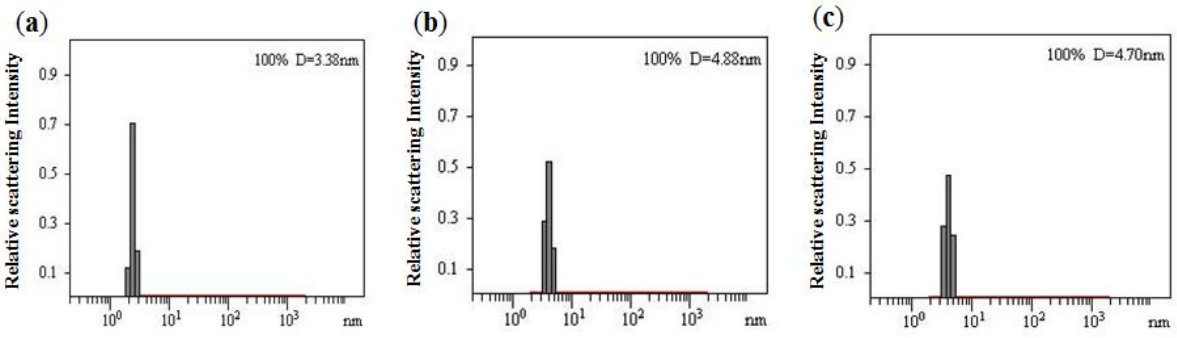

Figure 6. Distribution of the hydrodynamic diameters of the nanoparticles in water as determined by DLS for (a) alkynyl-SCM (b) surface-functionalized SCM and (c) $MINP_3$(**7**) after purification

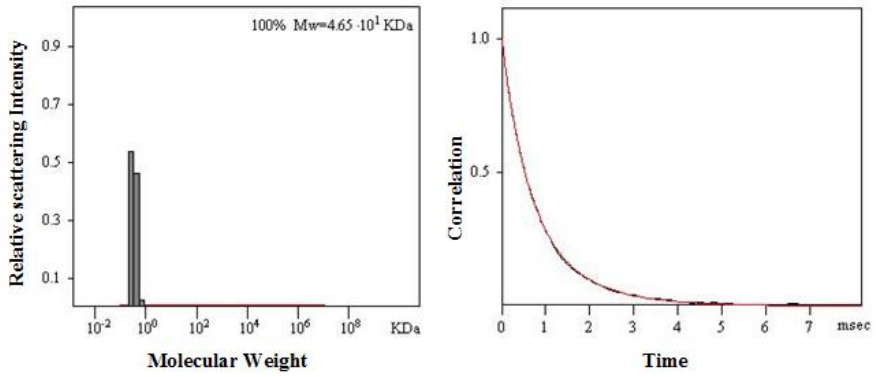

Figure 7. Distribution of the molecular weights of $MINP_3$(**7**) and the correlation curves for DLS. The molecular weight distribution was calculated by the PRECISION DECONVOLVE program assuming the intensity of scattering is proportional to the mass of the particle squared. If each unit of building block for the $MINP_3$(**7**) is assumed to contain one molecule of compound **1** (MW = 465 g/mol), 1.2 molecules of compound **2** (MW = 172 g/mol), one molecule of DVB (MW = 130 g/mol), and 0.8 molecules of compound **3** (MW = 264 g/mol), the molecular weight of $MINP_3$(**7**) translates to 46 [= 46500/(465+1.2×172+130+0.8×264)] of such units.

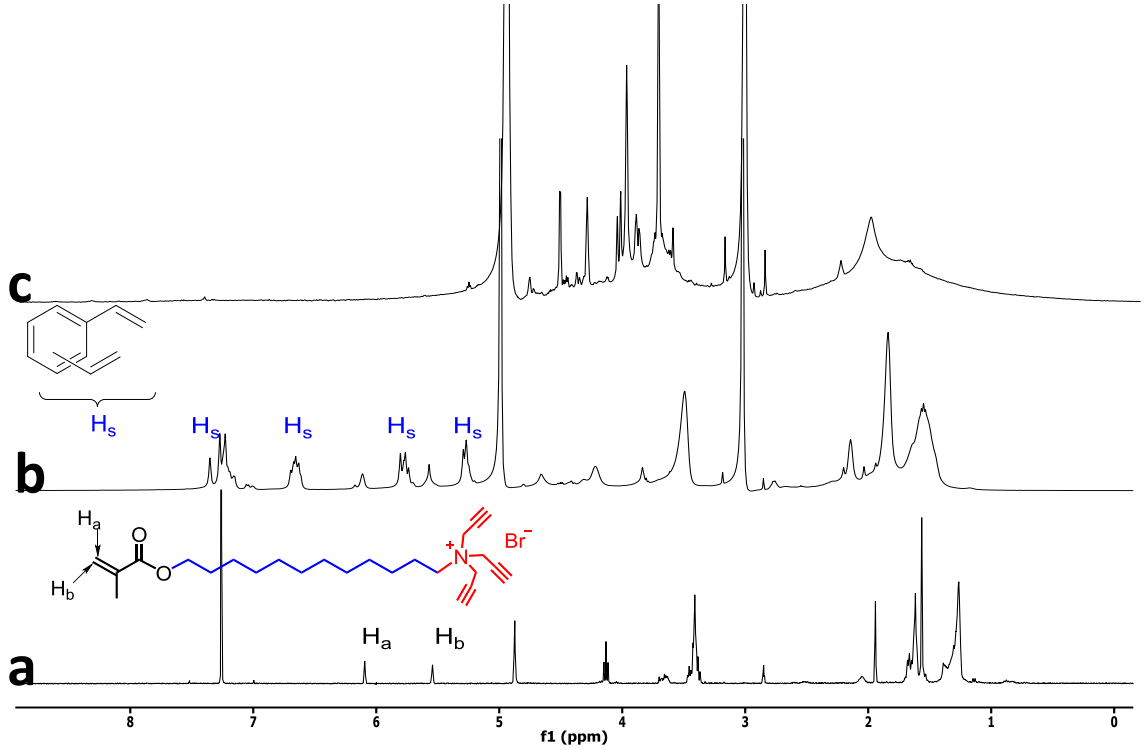

Figure 8. ^{1}H NMR spectra of (a) **1** in $CDCl_3$, (b) alkynyl-SCM in D_2O, (c) $MINP_4$(**7**) in D_2O at 25 °C.

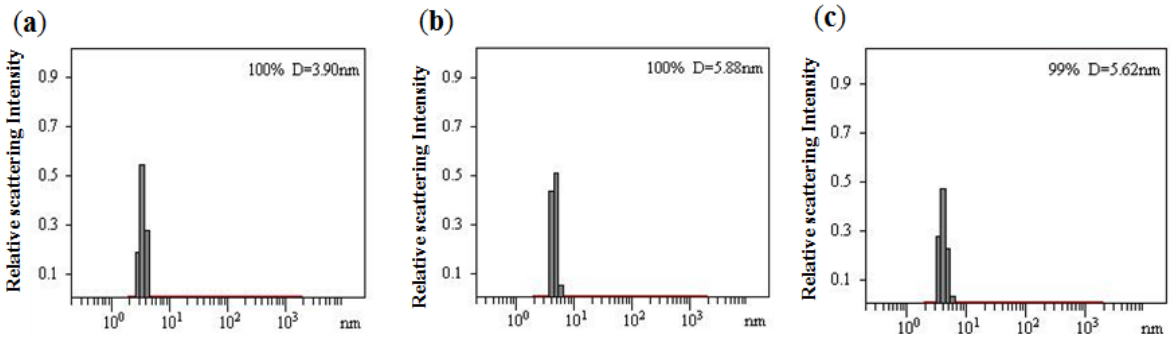

Figure 9. Distribution of the hydrodynamic diameters of the nanoparticles in water as determined by DLS for (a) alkynyl-SCM (b) surface-functionalized SCM and (c) $MINP_4$(**7**) after purification **.**

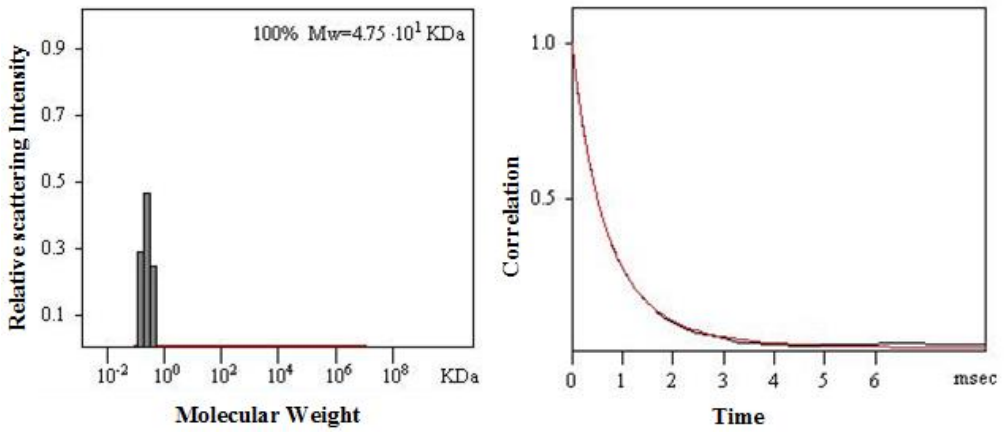

Figure 10. Distribution of the molecular weights MINP$_4$(**7**)) and the correlation curves for DLS. The molecular weight distribution was calculated by the PRECISION DECONVOLVE program assuming the intensity of scattering is proportional to the mass of the particle squared. If each unit of building block for the MINP$_4$(**7**) is assumed to contain one molecule of compound **1** (MW = 465 g/mol), 1.2 molecules of compound **2** (MW = 172 g/mol), one molecule of DVB (MW = 130 g/mol), and 0.8 molecules of compound **4** (MW = 205 g/mol), the molecular weight of MINP$_4$(**7**) translates to 49 [= 47500/(465+1.2×172+130+0.8×205)] of such units.

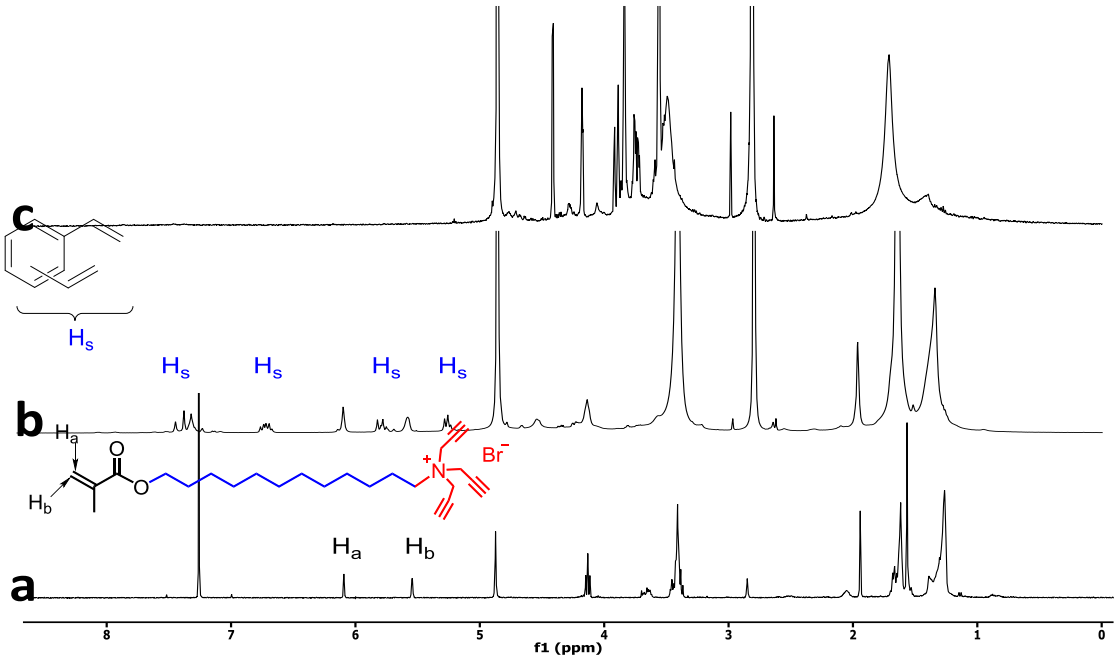

Figure 11. ^{1}H NMR spectra of (a) **1** in $CDCl_3$, (b) alkynyl-SCM in D_2O, (c) MINP$_5$(**7**) in D_2O at 25 °C.

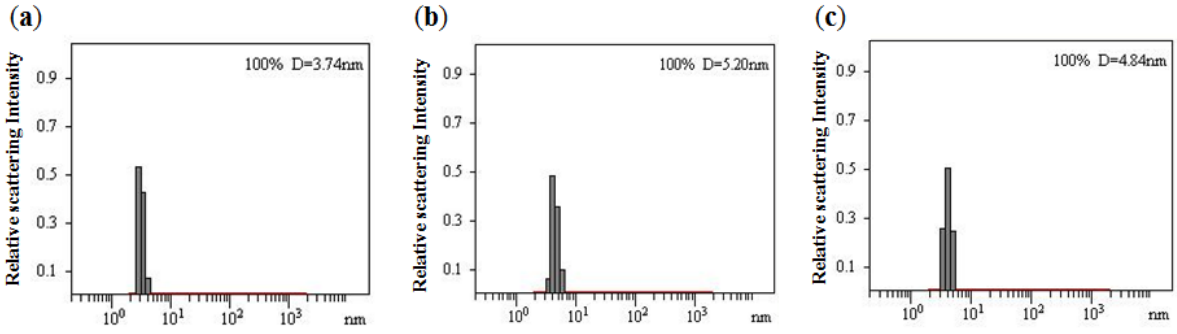

Figure 12. Distribution of the hydrodynamic diameters of the nanoparticles in water as determined by DLS for (a) alkynyl-SCM (b) surface-functionalized SCM, and (c) $MINP_5$(**7**) after purification.

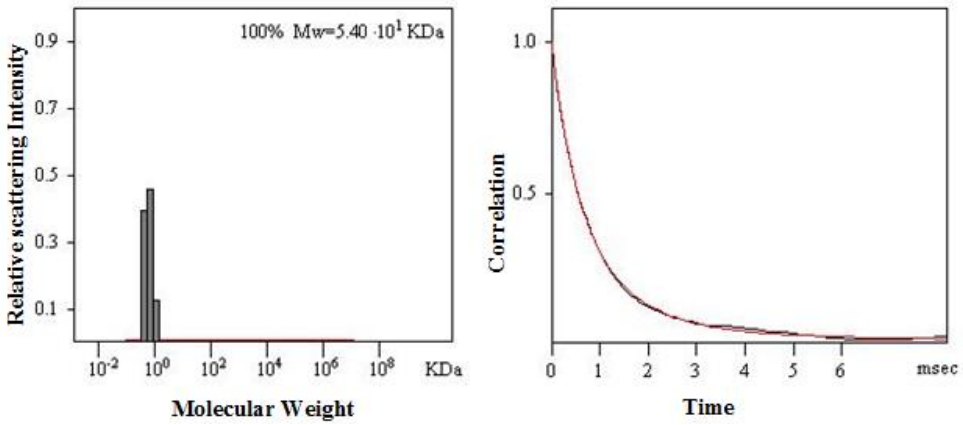

Figure 13. Distribution of the molecular weights of $MINP_5$(**7**) and the correlation curves for DLS. The molecular weight distribution was calculated by the PRECISION DECONVOLVE program assuming the intensity of scattering is proportional to the mass of the particle squared. If each unit of building block for the $MINP_5$(**7**) is assumed to contain one molecule of compound **1** (MW = 465 g/mol), 1.2 molecules of compound **2** (MW = 172 g/mol), one molecule of DVB (MW = 130 g/mol), and 0.8 molecules of compound **5** (MW = 367 g/mol), the molecular weight of $MINP_5$(**7**) translates to 49 [= 54000/(465+1.2×172+130+0.8×367)] of such units.

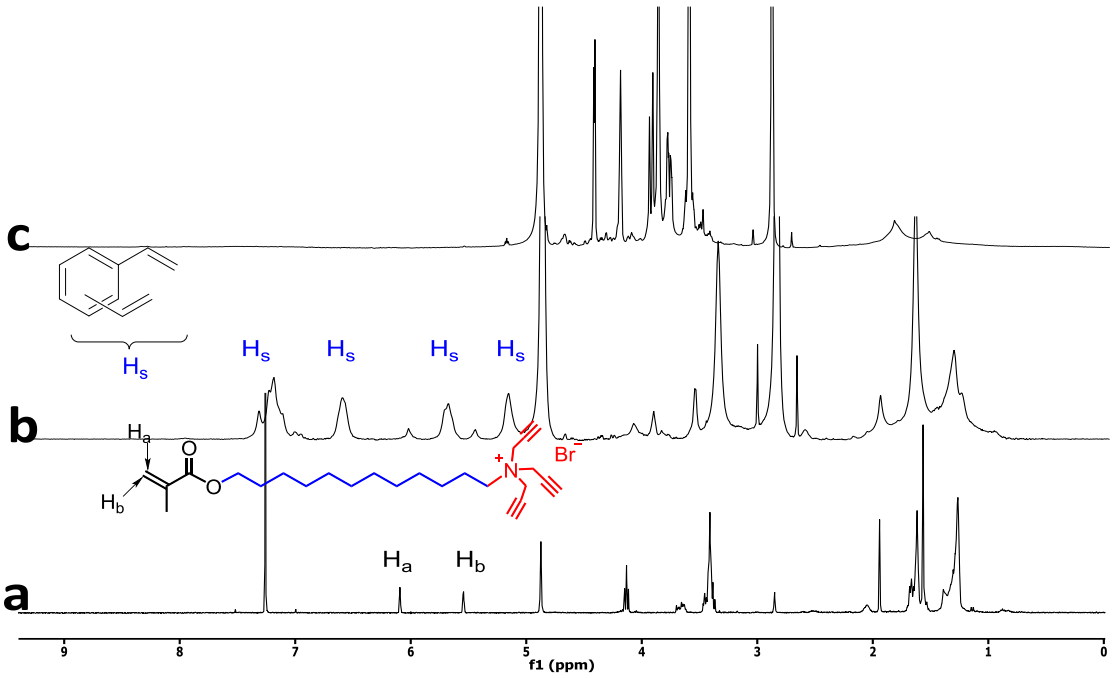

Figure 14. ^{1}H NMR spectra of (a) **1** in $CDCl_3$, (b) alkynyl-SCM in D_2O (c) $MINP_6$(**7**) in D_2O at 25 °C.

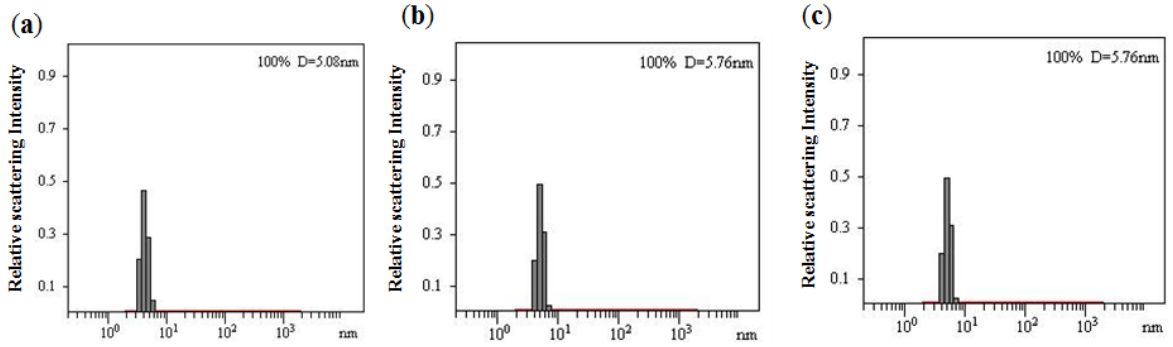

Figure 15. Distribution of the hydrodynamic diameters of the nanoparticles in water as determined by DLS for (a) alkynyl-SCM (b) surface-functionalized SCM, and (c) $MINP_6$(**7**) after purification.

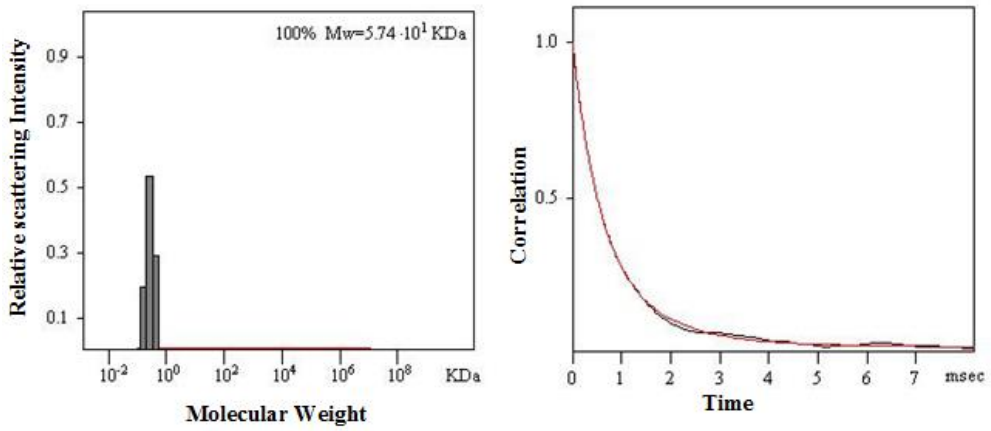

Figure 16. Distribution of the molecular weights of MINP$_6$(**7**) and the correlation curves for DLS. The molecular weight distribution was calculated by the PRECISION DECONVOLVE program assuming the intensity of scattering is proportional to the mass of the particle squared. If each unit of building block for the MINP$_6$(**7**) is assumed to contain one molecule of compound **1** (MW = 465 g/mol), 1.2 molecules of compound **3** (MW = 172 g/mol), one molecule of DVB (MW = 130 g/mol), and 0.8 molecules of compound **6** (MW = 367 g/mol), the molecular weight of MINP$_6$(**7**) translates to 52 [= 57400/(465+1.2×172+130+0.8×367)] of such units.

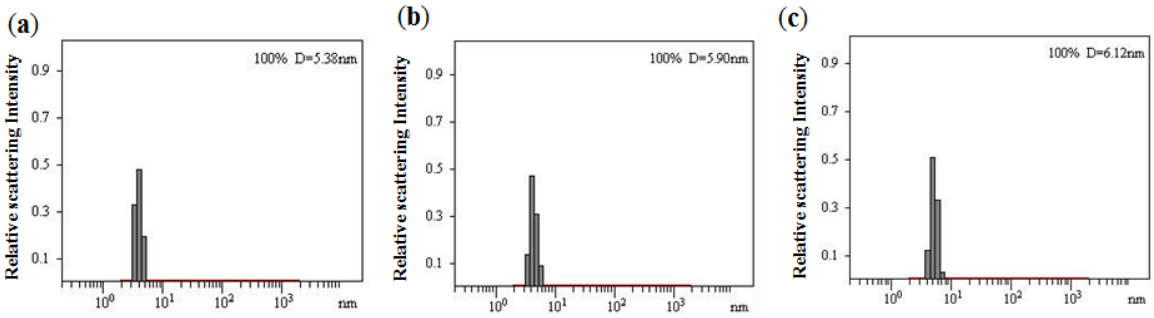

Figure 17. Distribution of the hydrodynamic diameters of the nanoparticles in water as determined by DLS for (a) alkynyl-SCM (b) surface-functionalized SCM, and (c) MINP$_{3,10}$(**7**) after purification.

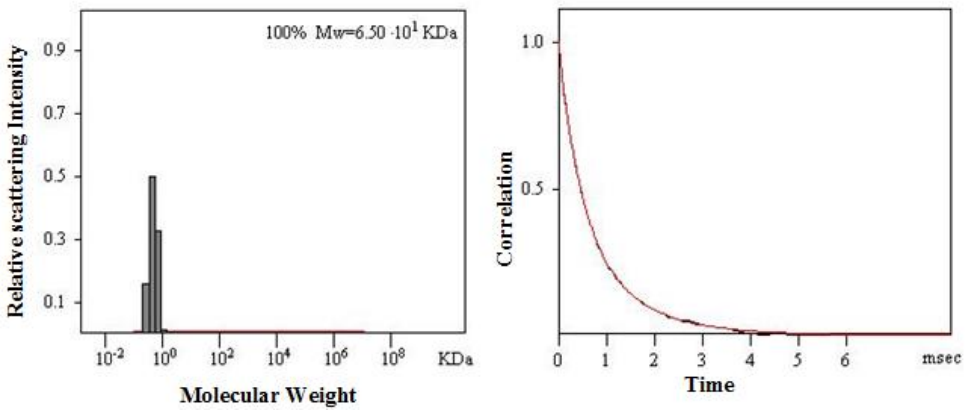

Figure 18. Distribution of the molecular weights of $MINP_{3,10}$(**7**) and the correlation curves for DLS. The molecular weight distribution was calculated by the PRECISION DECONVOLVE program assuming the intensity of scattering is proportional to the mass of the particle squared. If each unit of building block for the $MINP_{3,10}$(**7**) is assumed to contain one molecule of compound **1** (MW = 465 g/mol), 1.2 molecules of compound **10** (MW = 390 g/mol), one molecule of DVB (MW = 130 g/mol), and 0.8 molecules of compound **3** (MW = 264 g/mol), the molecular weight of $MINP_{3,10}$(**7**) translates to 51 [= 65000/(465+1.2×390+130+0.8×264)] of such units.

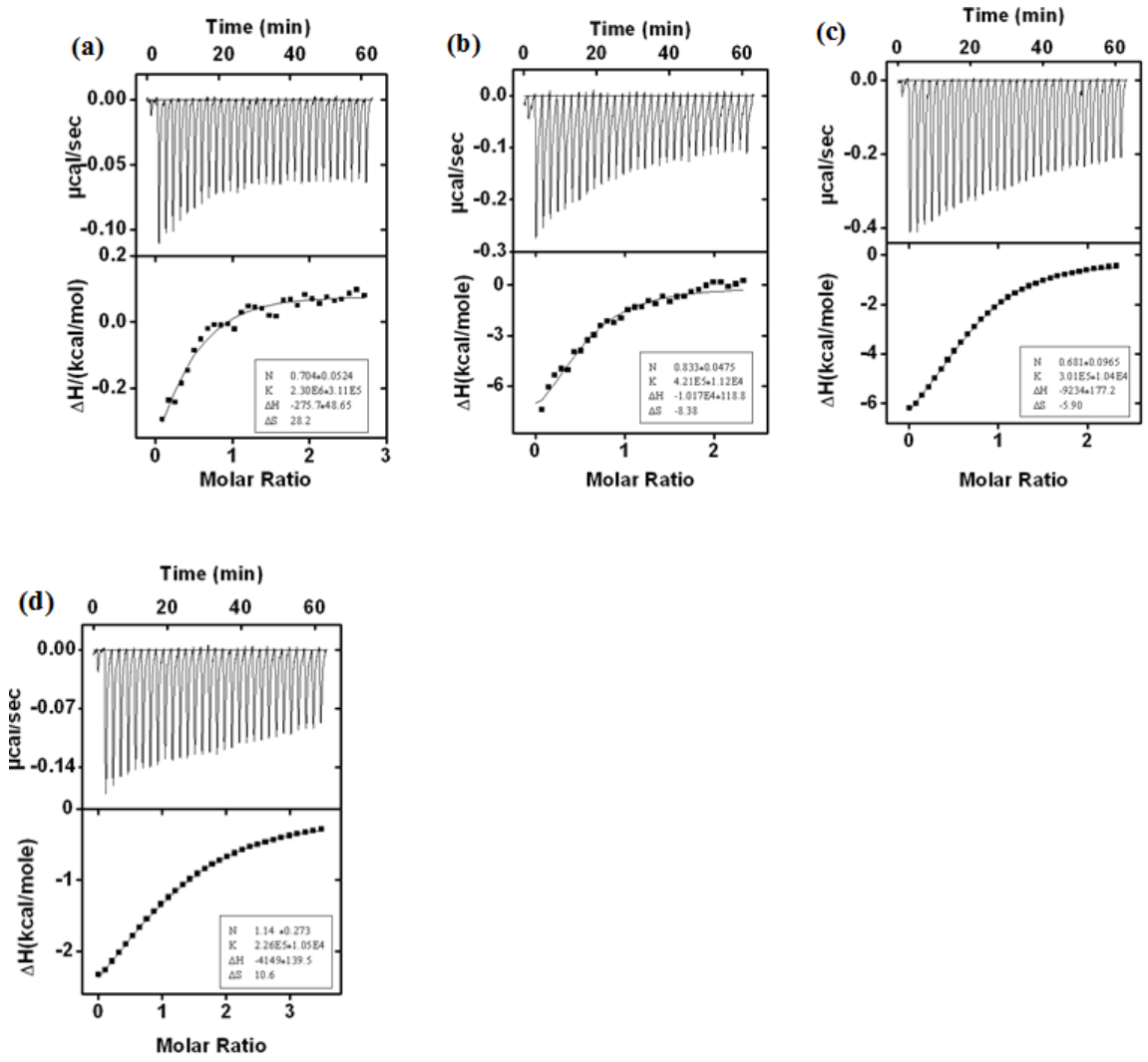

Figure 19. ITC titration curves obtained at 298 K for the binding of **7** by (a) $MINP_3$(**7**), (b) $MINP_4$(**7**), (c) $MINP_5$(**7**), and (d) $MINP_6$(**7**) prepared with 1 equiv of DVB. In general, an aqueous solution of an appropriate bile salt in Tris buffer (50 mM Tris, 150 mM NaCl, pH = 7.4) was injected in equal steps into 1.428 mL of the corresponding MINP solution (4.0 mg/mL) in the same buffer. The top panel shows the raw calorimetric data. The area under each peak represents the amount of heat generated at each ejection and is plotted against the molar ratio of the bile salt to the MINP. The smooth solid line is the best fit of the experimental data to the sequential binding of *N* equal and independent binding sites on the

MINP. The heat of dilution for the bile salt, obtained by adding the bile salt to the buffer, was subtracted from the heat released during the binding. Binding parameters were auto-generated after curve fitting using Microcal Origin 7.

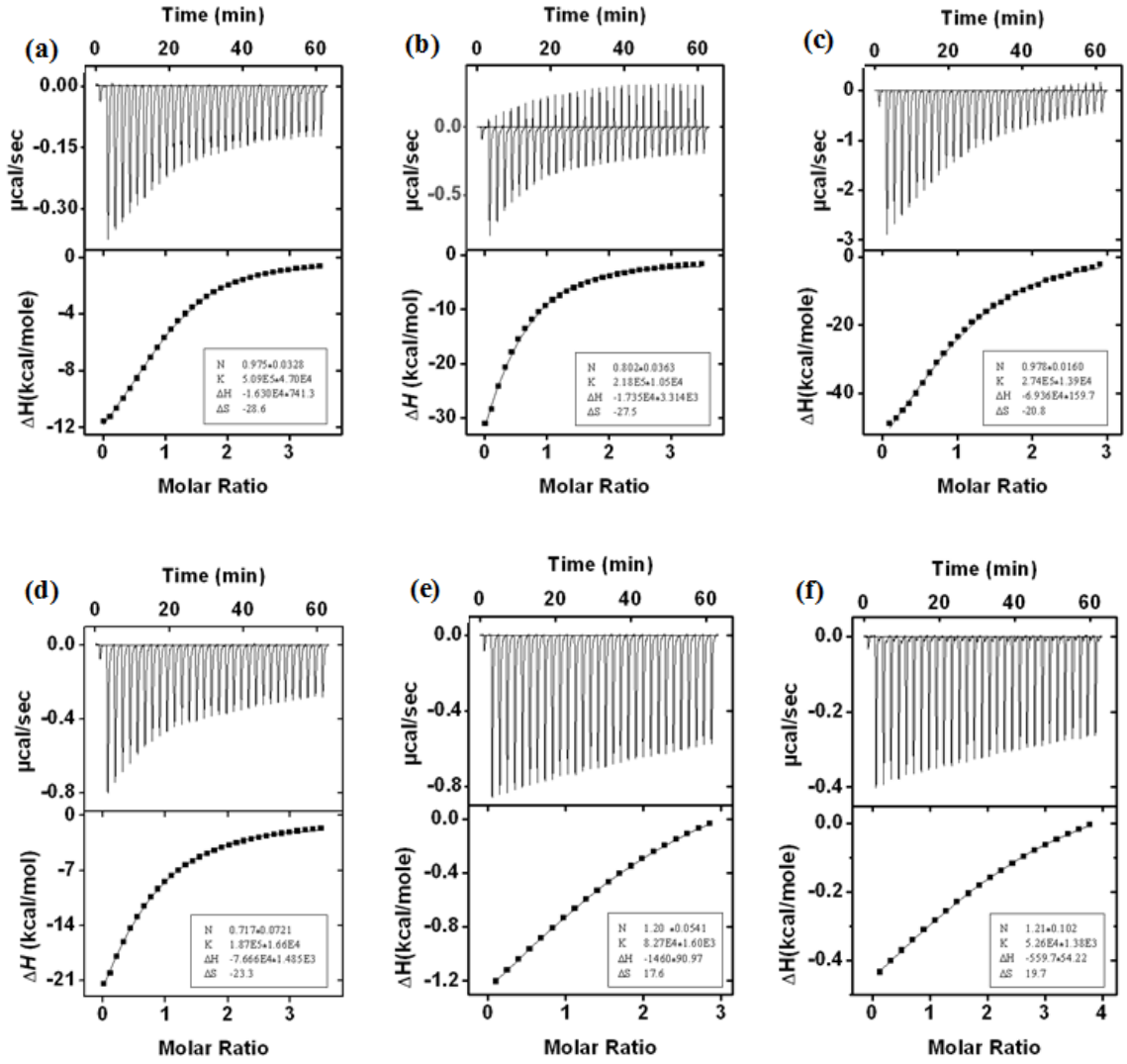

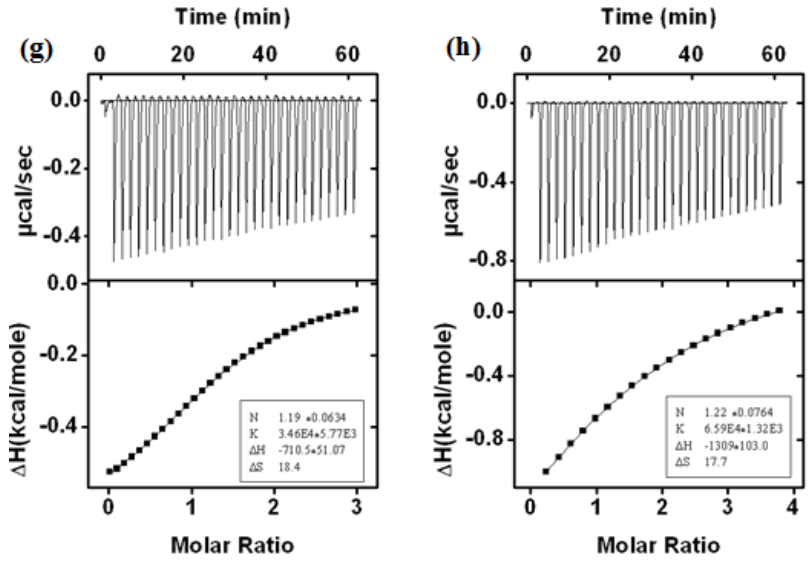

Figure 20. ITC titration curves obtained at 298 K for the binding of **8** by (a) $MINP_3$(**8**), (b) $MINP_4$(**8**), (c) $MINP_5$(**8**), (d) $MINP_6$(**8**), and **9** by (e) $MINP_3$(**9**), (f) $MINP_4$(**9**), (g) $MINP_5$(**9**), (h) $MINP_6$(**9**) prepared with 1 equiv of DVB. In general, an aqueous solution of an appropriate bile salt in Tris buffer (50 mM Tris, 150 mM NaCl, pH = 7.4) was injected in equal steps into 1.428 mL of the corresponding MINP solution in the same buffer. The top panel shows the raw calorimetric data. The area under each peak represents the amount of heat generated at each ejection and is plotted against the molar ratio of the bile salt to the MINP. The smooth solid line is the best fit of the experimental data to the sequential binding of *N* equal and independent binding sites on the MINP. The heat of dilution for the bile salt, obtained by adding the bile salt to the buffer, was subtracted from the heat released during the binding. Binding parameters were auto-generated after curve fitting using Microcal Origin 7.

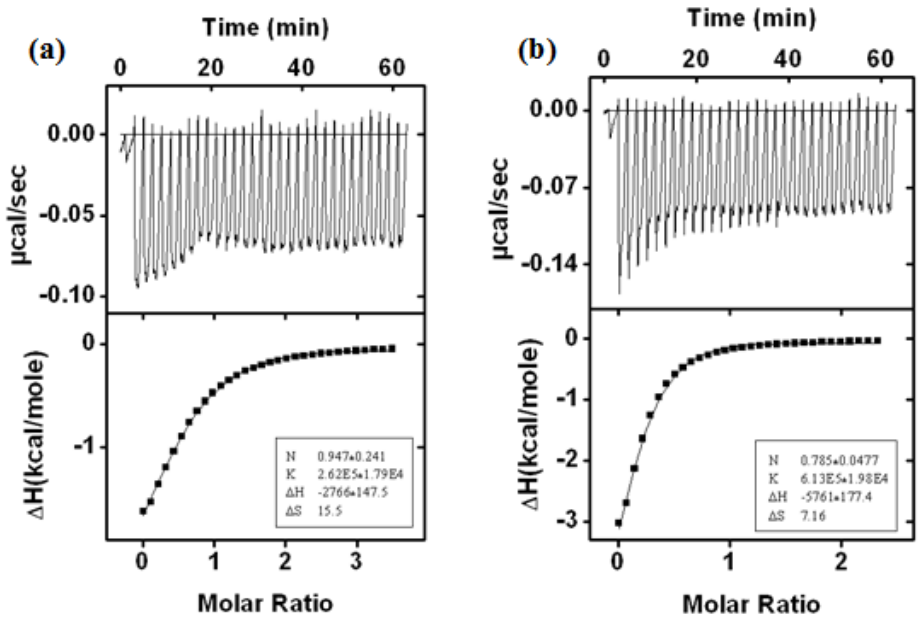

Figure 21**.** ITC titration curves obtained at 298 K for the binding of **7** by (a) $MINP_{3,10}$(**7**), and **9** by (b) $MINP_{3,10}$(**9**) prepared with 1 equiv of DVB. In general, an aqueous solution of an appropriate bile salt in Tris buffer (50 mM Tris, 150 mM NaCl, pH = 7.4) was injected in equal steps into 1.428 mL of the corresponding MINP solution in the same buffer. The top panel shows the raw calorimetric data. The area under each peak represents the amount of heat generated at each ejection and is plotted against the molar ratio of the bile salt to the MINP. The smooth solid line is the best fit of the experimental data to the sequential binding of *N* equal and independent binding sites on the MINP. The heat of dilution for the bile salt, obtained by adding the bile salt to the buffer, was subtracted from the heat released during the binding. Binding parameters were auto-generated after curve fitting using Microcal Origin 7.

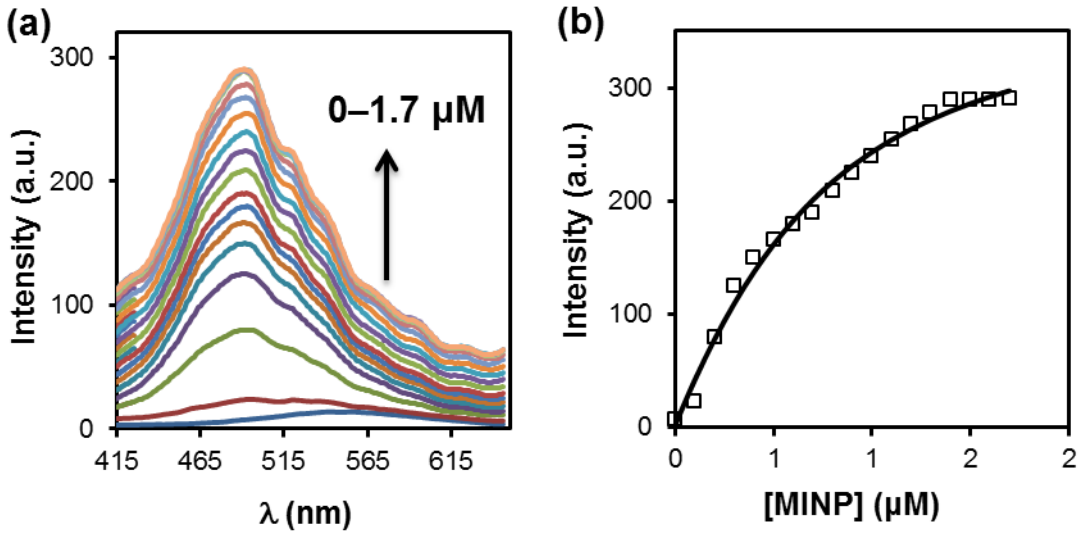

Figure 22. (a) Emission spectra of compound **7** in the presence of 0-1.7 μM of MINP$_3$(**7**) in Millipore water. [**7**] = 0.5 μM. λ_{ex} = 340 nm. (b) Nonlinear least squares curve fitting of the fluorescence intensity at 491 nm to a 1:1 binding isotherm.

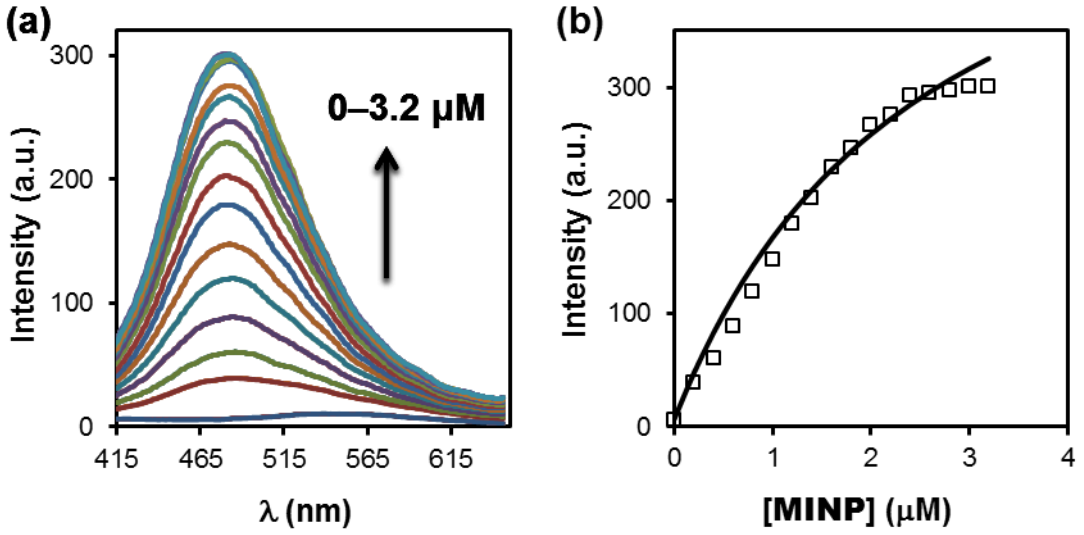

Figure 23. (a) Emission spectra of compound **7** in the presence of 0-3.2 μM of MINP$_4$(**7**) in Millipore water. [**7**] = 0.3 μM. λ_{ex} = 340 nm. (b) Nonlinear least squares curve fitting of the fluorescence intensity at 483 nm to a 1:1 binding isotherm.

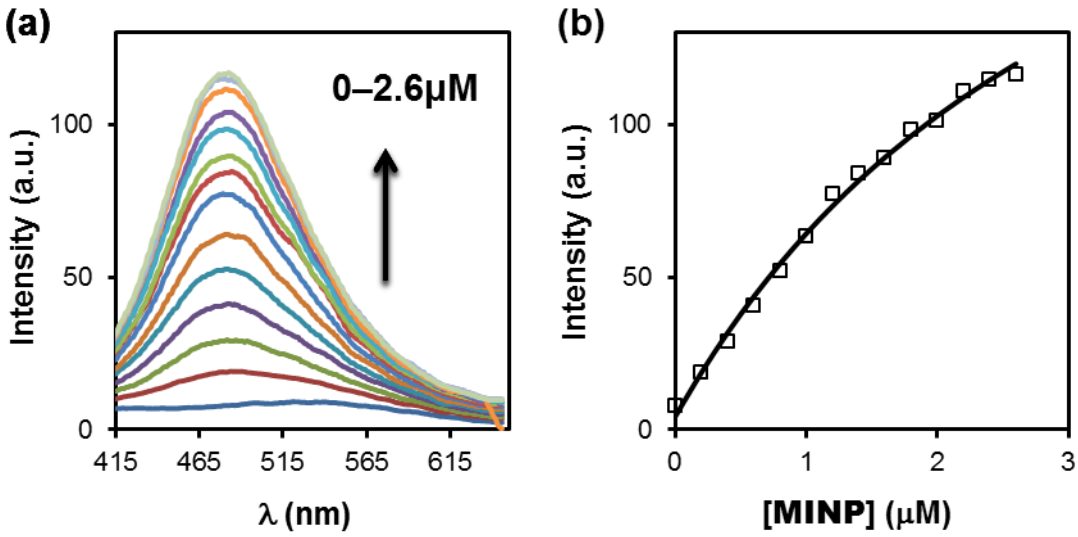

Figure 24. (a) Emission spectra of compound **7** in the presence of 0-2.6 μM of $MINP_5$(**7**) in Millipore water. [**7**] = 0.3 μM. λ_{ex} = 340 nm. (b) Nonlinear least squares curve fitting of the fluorescence intensity at 478 nm to a 1:1 binding isotherm.

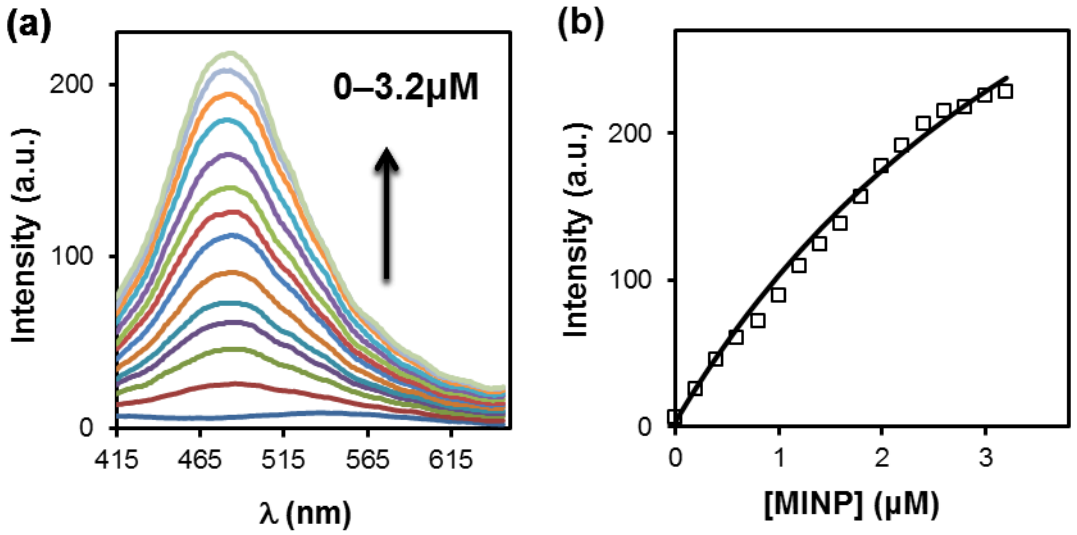

Figure 25. (a) Emission spectra of compound **7** in the presence of 0-2.6 μM of $MINP_6$(**7**) in Millipore water. [**7**] = 0.3 μM. λ_{ex} = 340 nm. (b) Nonlinear least squares curve fitting of the fluorescence intensity at 475 nm to a 1:1 binding isotherm.

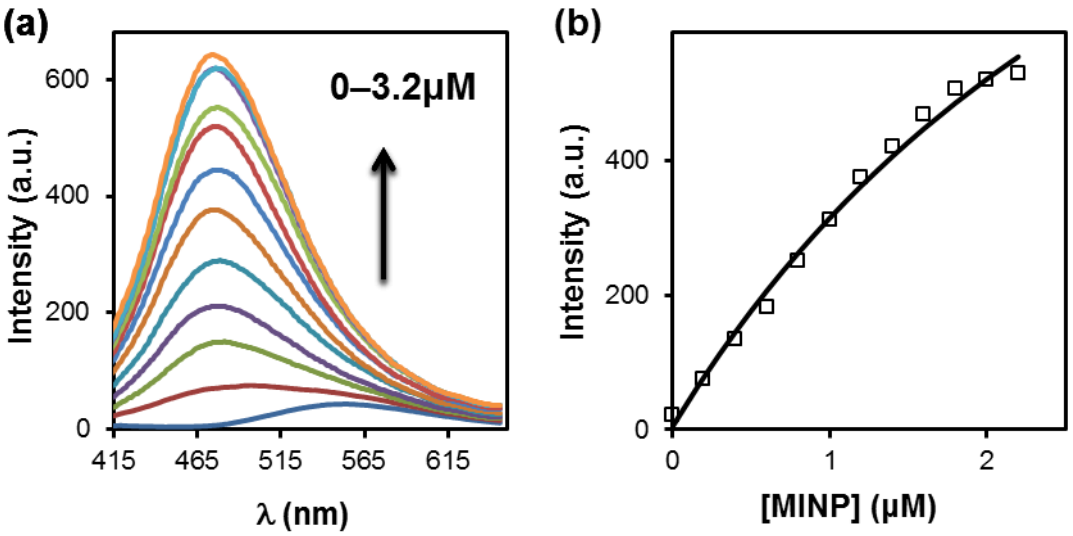

Figure 26. (a) Emission spectra of compound **7** in the presence of 0-3.2 μM of $MINP_{3,10}$(**7**)in Millipore water. [**7**] = 0.2 μM. λ_{ex} = 340 nm. (b) Nonlinear least squares curve fitting of the fluorescence intensity at 503 nm to a 1:1 binding isotherm.

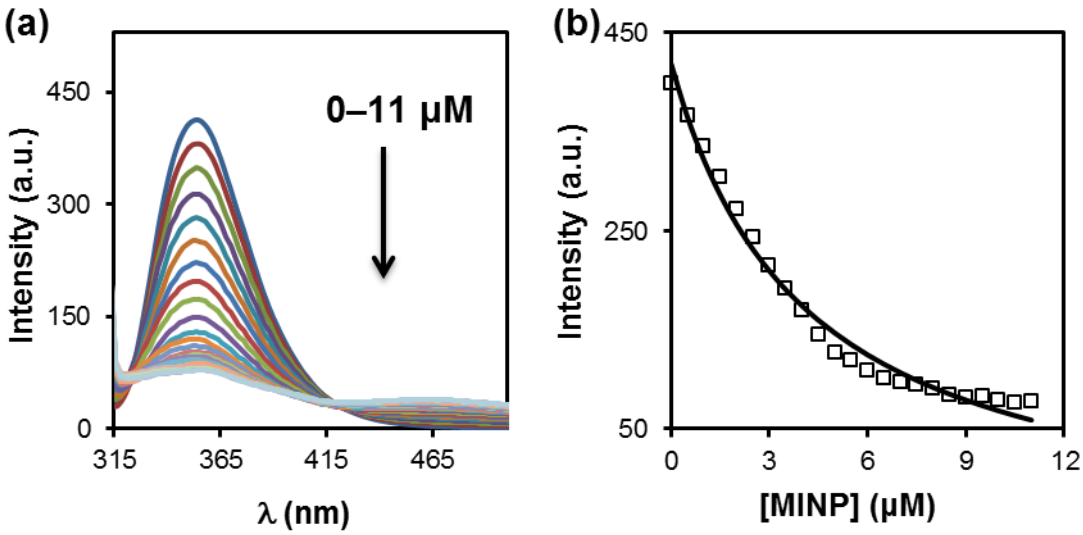

Figure 27. (a) Emission spectra of compound **8** in the presence of 0-11 μM of $MINP_3$(**7**)in Millipore water. [**8**] = 1.0 μM. λ_{ex} = 295 nm. (b) Nonlinear least squares curve fitting of the fluorescence intensity at 348 nm to a 1:1 binding isotherm.

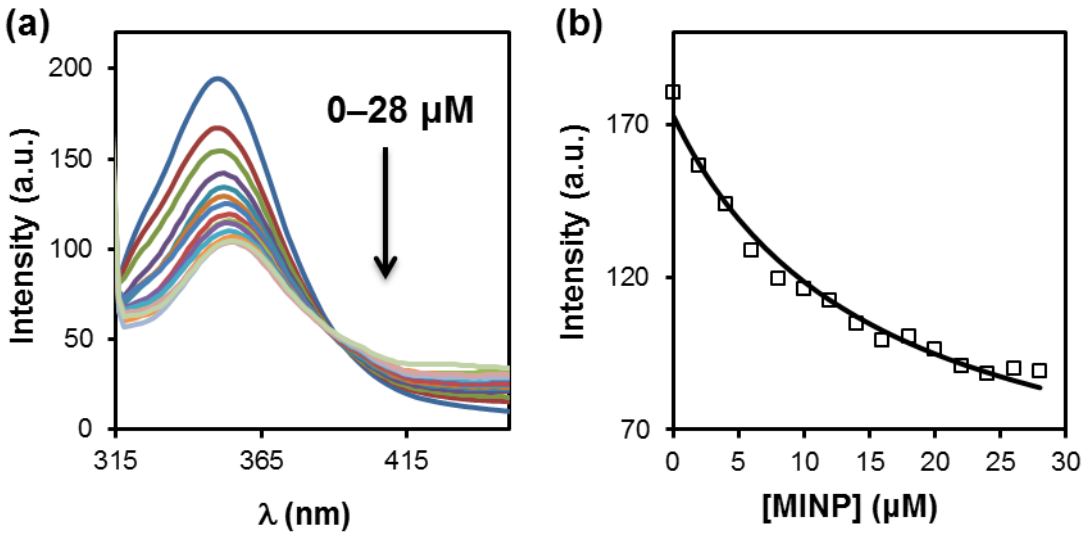

Figure 28. (a) Emission spectra of compound **9** in the presence of 0-28 μM of $MINP_3$(**7**)in Millipore water. [**9**] = 1.0 μM. λ_{ex} = 295 nm. (b) Nonlinear least squares curve fitting of the fluorescence intensity at 342 nm to a 1:1 binding isotherm.

^{1}H NMR spectra of compound **13**

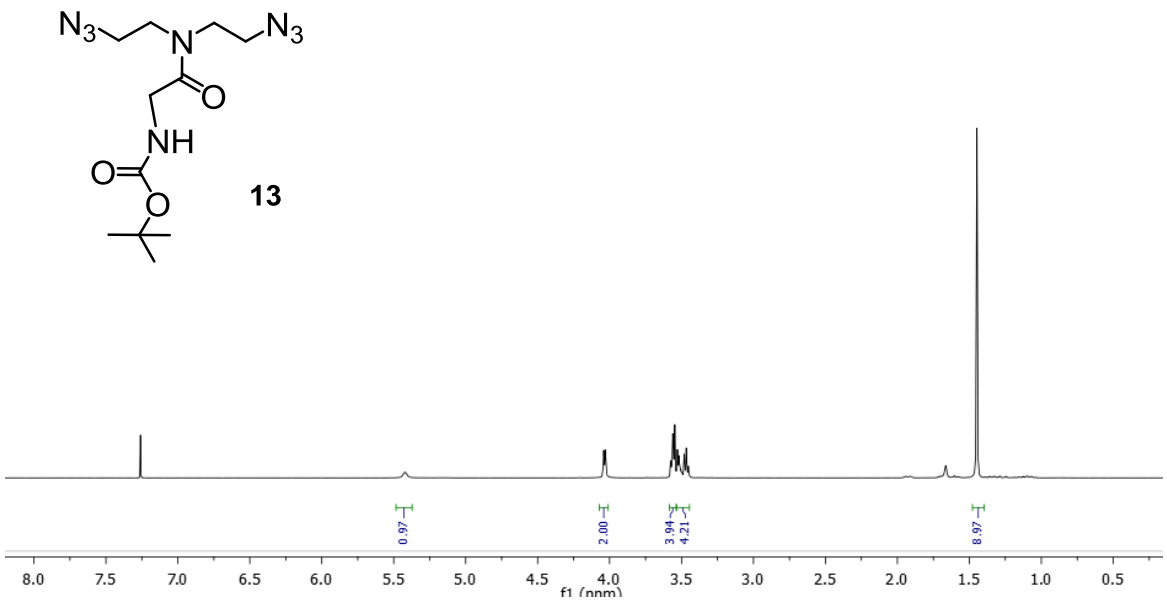

^{13}C NMR spectra of compound **13**

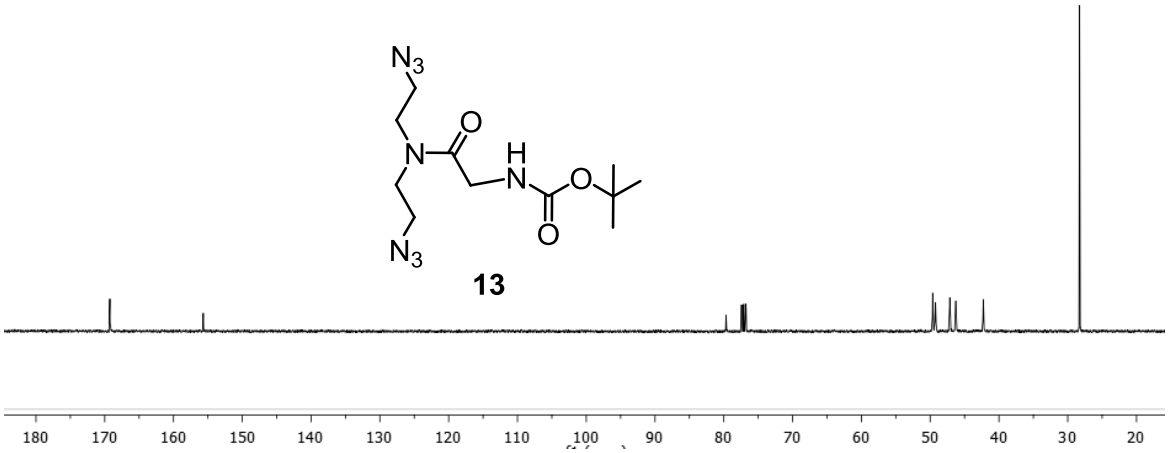

^{1}H NMR spectra of compound **10**

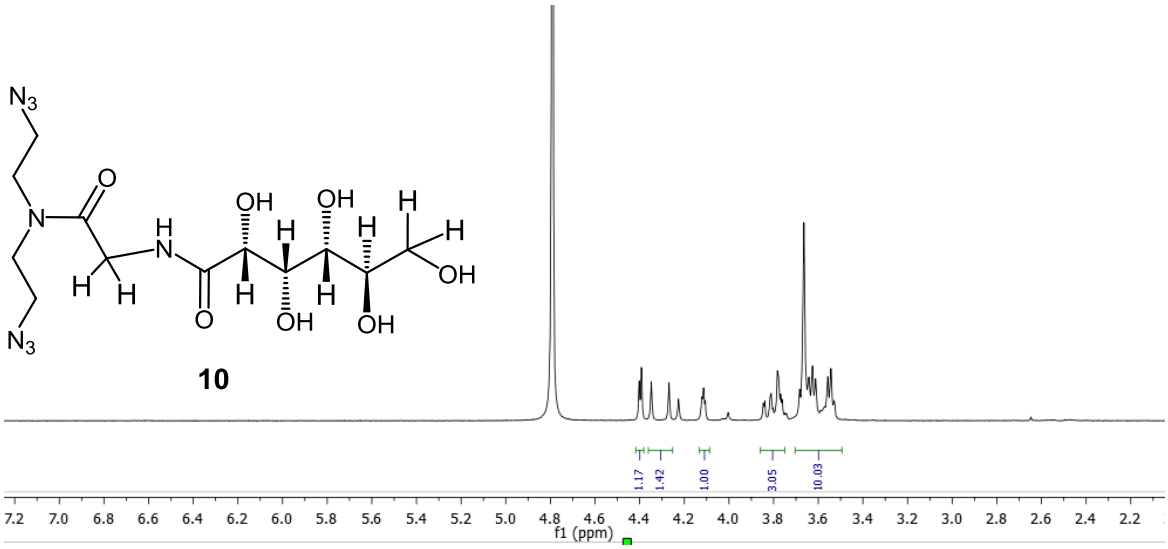

^{13}C NMR spectra of compound **10**

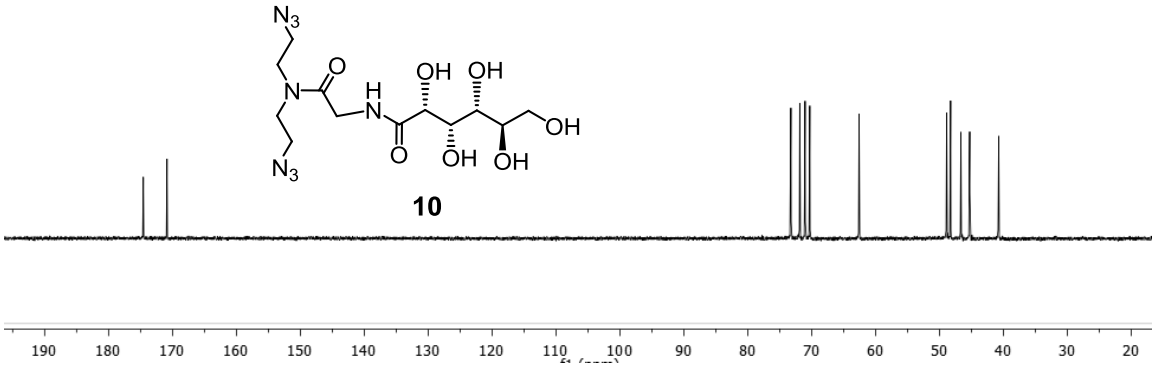

References

(1) Atwood, J. L.; Lehn, J. M., *Comprehensive Supramolecular Chemistry*. Pergamon: New York, 1996.

(2) Steed, J. W.; Gale, P. A., *Supramolecular Chemistry: From Molecules to Nanomaterials*. Wiley: Weinheim, 2012.

(3) Schneider, H.-J.; Yatsimirsky, A. K., *Principles and Methods in Supramolecular Chemistry*. Wiley: New York, 2000.

(4) Juwarker, H.; Suk, J. M.; Jeong, K. S., *Chem. Soc. Rev.* **2009,** *38*, 3316-3325.

(5) Chang, K. J.; Kang, B. N.; Lee, M. H.; Jeong, K. S., *J. Am. Chem. Soc.* **2005,** *127*, 12214-12215.

(6) Hua, Y.; Liu, Y.; Chen, C.-H.; Flood, A. H., *J. Am. Chem. Soc.* **2013,** *135*, 14401-14412.

(7) Gan, Q. A.; Ferrand, Y.; Bao, C. Y.; Kauffmann, B.; Grelard, A.; Jiang, H.; Huc, I., *Science* **2011,** *331*, 1172-1175.

(8) Zhao, Y.; Zhong, Z., *J. Am. Chem. Soc.* **2006,** *128*, 9988-9989.

(9) Chandramouli, N.; Ferrand, Y.; Lautrette, G.; Kauffmann, B.; Mackereth, C. D.; Laguerre, M.; Dubreuil, D.; Huc, I., *Nat. Chem.* **2015,** *7*, 334-341.

(10) Hou, J. L.; Shao, X. B.; Chen, G. J.; Zhou, Y. X.; Jiang, X. K.; Li, Z. T., *J. Am. Chem. Soc.* **2004,** *126*, 12386-12394.

(11) Zhong, Z.; Li, X.; Zhao, Y., *J. Am. Chem. Soc.* **2011,** *133*, 8862-8865.

(12) Zhao, Y., *ChemPhysChem* **2013,** *14*, 3878-3885.

(13) Wulff, G., *Chem. Rev.* **2001,** *102*, 1-28.

(14) Haupt, K.; Mosbach, K., *Chem. Rev.* **2000,** *100*, 2495-2504.

(15) Lakshmi, D.; Bossi, A.; Whitcombe, M. J.; Chianella, I.; Fowler, S. A.; Subrahmanyam, S.; Piletska, E. V.; Piletsky, S. A., *Anal. Chem.* **2009,** *81*, 3576-3584.

(16) Hao, Y.; Gao, R.; Shi, L.; Liu, D.; Tang, Y.; Guo, Z., *J. Chromatogr. A* **2015,** *1396*, 7-16.

(17) Kuwata, T.; Uchida, A.; Takano, E.; Kitayama, Y.; Takeuchi, T., *Anal. Chem.* **2015,** *87*, 11784-11791.

(18) Liu, J.; Yin, D.; Wang, S.; Chen, H. Y.; Liu, Z., *Angew. Chem. Int. Ed.* **2016,** *55*, 13215-13218.

(19) Chen, L.; Wang, X.; Lu, W.; Wu, X.; Li, J., *Chem. Soc. Rev.* **2016,** *45*, 2137-2211.

(20) Horikawa, R.; Sunayama, H.; Kitayama, Y.; Takano, E.; Takeuchi, T., *Angew. Chem. Int. Ed.* **2016,** *55*, 13023-13027.

(21) Panagiotopoulou, M.; Salinas, Y.; Beyazit, S.; Kunath, S.; Duma, L.; Prost, E.; Mayes, A. G.; Resmini, M.; Bui, B. T. S.; Haupt, K., *Angew. Chem. Int. Ed.* **2016,** *55*, 8244-8248.

(22) Yin, D.; Li, X.; Ma, Y.; Liu, Z., *Chem. Commun.* **2017,** *53*, 6716-6719.

(23) Paul, P. K.; Treetong, A.; Suedee, R., *Acta Pharm.* **2017,** *67*, 149-168.

(24) Bertolla, M.; Cenci, L.; Anesi, A.; Ambrosi, E.; Tagliaro, F.; Vanzetti, L.; Guella, G.; Bossi, A. M., *ACS Appl. Mater. Interfaces* **2017,** *9*, 6908-6915.

(25) Cecchini, A.; Raffa, V.; Canfarotta, F.; Signore, G.; Piletsky, S.; MacDonald, M. P.; Cuschieri, A., *Nano Lett.* **2017,** *17*, 2307-2312.

(26) Jiang, L.; Messing, M. E.; Ye, L., *ACS Appl. Mater. Interfaces* **2017,** *9*, 8985-8995.

(27) Zimmerman, S. C.; Wendland, M. S.; Rakow, N. A.; Zharov, I.; Suslick, K. S., *Nature* **2002,** *418*, 399-403.

(28) Zimmerman, S. C.; Zharov, I.; Wendland, M. S.; Rakow, N. A.; Suslick, K. S., *J. Am. Chem. Soc.* **2003,** *125*, 13504-13518.

(29) Li, Z.; Ding, J.; Day, M.; Tao, Y., *Macromolecules* **2006,** *39*, 2629-2636.

(30) Hoshino, Y.; Kodama, T.; Okahata, Y.; Shea, K. J., *J. Am. Chem. Soc.* **2008,** *130*, 15242-15243.

(31) Priego-Capote, F.; Ye, L.; Shakil, S.; Shamsi, S. A.; Nilsson, S., *Anal. Chem.* **2008,** *80*, 2881-2887.

(32) Cutivet, A.; Schembri, C.; Kovensky, J.; Haupt, K., *J. Am. Chem. Soc.* **2009,** *131*, 14699-14702.

(33) Yang, K. G.; Berg, M. M.; Zhao, C. S.; Ye, L., *Macromolecules* **2009,** *42*, 8739-8746.

(34) Zeng, Z. Y.; Patel, J.; Lee, S. H.; McCallum, M.; Tyagi, A.; Yan, M. D.; Shea, K. J., *J. Am. Chem. Soc.* **2012,** *134*, 2681-2690.

(35) Ma, Y.; Pan, G. Q.; Zhang, Y.; Guo, X. Z.; Zhang, H. Q., *Angew. Chem. Int. Ed.* **2013,** *52*, 1511-1514.

(36) Zhang, Y.; Deng, C.; Liu, S.; Wu, J.; Chen, Z.; Li, C.; Lu, W., *Angew. Chem. Int. Ed.* **2015,** *54*, 5157-5160.

(37) Biffis, A.; Graham, N. B.; Siedlaczek, G.; Stalberg, S.; Wulff, G., *Macromol. Chem. Phys.* **2001,** *202*, 163-171.

(38) Maddock, S. C.; Pasetto, P.; Resmini, M., *Chem. Commun.* **2004**, 536-537.

(39) Wulff, G.; Chong, B. O.; Kolb, U., *Angew. Chem. Int. Ed.* **2006,** *45*, 2955-2958.

(40) Carboni, D.; Flavin, K.; Servant, A.; Gouverneur, V.; Resmini, M., *Chem. -Eur. J.* **2008,** *14*, 7059-7065.

(41) Servant, A.; Haupt, K.; Resmini, M., *Chem.-Eur. J.* **2011,** *17*, 11052-11059.

(42) Çakir, P.; Cutivet, A.; Resmini, M.; Bui, B. T.; Haupt, K., *Adv. Mater.* **2013,** *25*, 1048-1051.

(43) Cho, H.; Zhao, Y., *J. Am. Chem. Soc.* **2010,** *132*, 9890-9899.

(44) Gunasekara, R. W.; Zhao, Y., *J. Am. Chem. Soc.* **2015,** *137*, 843-849.

(45) Gunasekara, R. W.; Zhao, Y., *Chem. Commun.* **2016,** *52*, 4345-4348.

(46) Awino, J. K.; Zhao, Y., *J. Am. Chem. Soc.* **2013,** *135*, 12552-12555.

(47) Awino, J. K.; Zhao, Y., *Chem.-Eur. J.* **2015,** *21*, 655-661.

(48) Awino, J. K.; Zhao, Y., *ACS Biomater. Sci. Eng.* **2015,** *1*, 425-430.

(49) Awino, J. K.; Gunasekara, R. W.; Zhao, Y., *J. Am. Chem. Soc.* **2016,** *138*, 9759-9762.
(50) Gunasekara, R. W.; Zhao, Y., *J. Am. Chem. Soc.* **2017,** *139*, 829-835.

(51) Fa, S.; Zhao, Y., *Chem. Mater.* **2017,** *29*, 9284-9291.

(52) Awino, J. K.; Gunasekara, R. W.; Zhao, Y., *J. Am. Chem. Soc.* **2017,** *139*, 2188-2191.
(53) Fa, S.; Zhao, Y., *Chem. -Eur. J.*, DOI: 10.1002/chem.201703760.

(54) Zhang, S.; Zhao, Y., *Macromolecules* **2010,** *43*, 4020-4022.

(55) Peng, H.-Q.; Chen, Y.-Z.; Zhao, Y.; Yang, Q.-Z.; Wu, L.-Z.; Tung, C.-H.; Zhang, L.-P.; Tong, Q.-X., *Angew. Chem. Int. Ed.* **2012,** *51*, 2088-2092.

(56) Li, X.; Zhao, Y., *Bioconjugate Chem.* **2012,** *23*, 1721-1725.

(57) Zhao, Y., *Curr. Opin. Colloid Interface Sci.* **2007,** *12*, 92-97.

(58) Li, X.; Zhao, Y., *Langmuir* **2012,** *28*, 4152-4159.

(59) Li, Y. H.; Chan, L. M.; Tyer, L.; Moody, R. T.; Himel, C. M.; Hercules, D. M., *J. Am. Chem. Soc.* **1975,** *97*, 3118-3126.

(60) Schmidtchen, F. P., Isothermal Titration Calorimetry in Supramolecular Chemistry. In *Supramolecular Chemistry: From Molecules to Nanomaterials*, Steed, J. W.; Gale, P. A., Eds. Wiley: Online, 2012.

(61) The cross-reactivity in the binding has been reported previously for $MINP_3$(**7**). See ref 46 for details.

(62) Danielsson, H.; Sjövall, J., *Sterols and Bile Acids*. Elsevier: Amsterdam, 1985.

(63) Carey, M. C., Physical-Chemical Properties of Bile Acids and Their Salts. In *Sterols and Bile Acids*, Danielsson, H.; Sjövall, J., Eds. Elsevier: Amsterdam, 1985; pp 345-403.

(64) For **7**, we suspect the higher density of surface hydrophilic groups also made it more difficult for them to adopt the folded conformation shown in Figure 3 to interact with the bound template. This could be another reason why the binding was weaker with **10** as the surface cross-linker.

(65) Oshovsky, G. V.; Reinhoudt, D. N.; Verboom, W., *Angew. Chem. Int. Ed.* **2007,** *46*, 2366-2393

(66) Kataev, E. A.; Müller, C., *Tetrahedron* **2014,** *70*, 137-167.

(67) Fa, S.; Zhao, Y., *Chem. -Eur. J.* **2018,** *24*, 150-158.

(68) Nisic, F.; Speciale, G.; Bernardi, A., *Chem. -Eur. J.* **2012,** *18*, 6895-6906.

(69) Kumar, S.; Ranjan, N.; Kellish, P.; Gong, C.; Watkins, D.; Arya, D. P., *Org. Biomol. Chem.* **2016,** *14*, 2052-2056.

(70) Radau, G.; Schermuly, S.; Fritsche, A., *Arch. Pharm.* **2003,** *336*, 300-309.

(71) Wiseman, T.; Williston, S.; Brandts, J. F.; Lin, L. N., *Anal. Biochem.* **1989,** *179*, 131-137.

(72) Jelesarov, I.; Bosshard, H. R., *J. Mol. Recognit.* **1999,** *12*, 3-18.

(73) Velazquez-Campoy, A.; Leavitt, S. A.; Freire, E., *Methods Mol. Biol.* **2004,** *261*, 35-54.

CHAPTER 4. ARTIFICIAL ZINC ENZYMES WITH FINE-TUNED CATALYTIC ACTIVE SITES FOR HIGHLY SELECTIVE HYDROLYSIS OF ACTIVATED ESTERS

Modified from a paper published in *ACS Catalysis* **2018**, 8, 8154−8161

MD Arifuzzaman and Yan Zhao

Department of Chemistry, Iowa State University, Ames, Iowa 50011-3111, United States

Abstract

Zinc enzymes are ubiquitous in nature and frequently used to catalyze the hydrolysis of carboxylic acid esters, phosphate esters, and amides. Although many models and mimics of zinc enzymes have been reported, it remains difficult to construct active sites with accurately positioned catalytic groups and tunable substrate selectivity. By imprinting a substrate-like amino template coordinated to a polymerizable zinc complex inside cross-linked micelles, we prepared water-soluble nanoparticles with well-defined active sites. The position of the zinc ion could be tuned systematically with respect to the ester bond to be leaved in the substrate (*p*-nitrophenyl esters), as well as the rigidity of the active site. Our imprinted zinc catalysts was able to distinguish substrates that differed by the position of a single methyl group, chain length of the acyl chain, and substitution of the phenyl ring. The turnover number (>460 at pH 7) was one order of magnitude higher than those previously reported for artificial zinc enzymes in the literature.

Introduction

Zinc is used by >1000 enzymes to perform vital catalytic tasks in biology.[1,2] Of these enzymes, the largest group is hydrolases that catalyze the hydrolysis of carboxylic acid esters, peptides, and phosphate esters under physiological conditions.[3,4] In the last decades, numerous small-molecule zinc complexes have been synthesized to mimic the coordination environments of zinc in the natural enzymes and understand its potential role in the catalysis.[5-7] Reproducing their catalytic behavior in aqueous solution, however, is hampered by the poor water solubility of common organic ligands, dimerization of zinc complexes, and product inhibition.[8]

To overcome these challenges, researchers turned to peptidic materials in recent years to construct artificial zinc enzymes and have synthesized by far the most active mimics of the natural catalysts.[8-13] Peptidic structures have a number of attractive features for biomimetic catalysis. Aqueous solubility, for example, can be easily achieved. Identical ligands such as histidine and aspartate found in the zinc enzymes could be used to bind the metal to better simulate the coordination environments. Steric protection by the peptide framework can prevent the dimerization of zinc complexes effectively. Indeed, with a zinc ion placed in the hydrophobic region of protein interfaces,[9,11] coiled coils,[8,10] self-assembled amyloid fibers,[12] or α-helical barrels,[13] Michalis-Menten kinetics has been observed in the hydrolysis of model substrates. For the most commonly used activated ester *para*-nitrophenyl acetate (PNPA), the catalytic efficiency often came close to that of carbonic anhydrase, a natural zinc enzyme.

One of the biggest challenges forward in the creation of artificial enzymes is in the design of the active site. For bottom-up-constructed small-molecule enzyme models, tremendous synthetic efforts are needed for a highly functionalized binding pocket,

especially if water-solubility, steric protection, and other features all need to be included. Although a large database of naturally folded structures, automated synthesis, and computational tools are available to peptide-based materials, fine-tuning of the active site for substrates of different shapes remains a formidable task.

Herein, we report a rational, facile construction of artificial zinc enzymes by a bottom-up approach through micellar imprinting.[14] Although molecularly imprinted catalysts are known in the literature,[15-24] traditional molecularly imprinted polymers (MIPs) face a number of challenges[25] to be used as mimics of natural enzymes, partly due to limited precision in the construction of the active sites, heterogeneous distribution of the binding sites, and/or poor solubility of highly cross-linked materials. Our molecularly imprinted nanoparticle (MINP) catalysts are characterized by their resemblance to natural enzymes in the nanodimension and water-solubility. The discrete active site, tunable in size and shape, is located in the hydrophobic core of the MINP. The highlight of our method is the systematic tuning of the catalytic zinc metal with respect to the ester bond to be cleaved in the substrate. The shape of the active site could be made to match the substrate precisely, to the point that the position of a single methyl group and the chain length of the substrate could be distinguished with ease. Artificial zinc enzymes often face strong product inhibition because the hydrolyzed products coordinate to zinc more strongly than the starting materials.[8] In our catalysts, product inhibition was effectively prevented, resulting in turnover numbers one order of magnitude higher than those reported in previous systems.

Results and Discussion

Design and Synthesis of Zn Catalyst

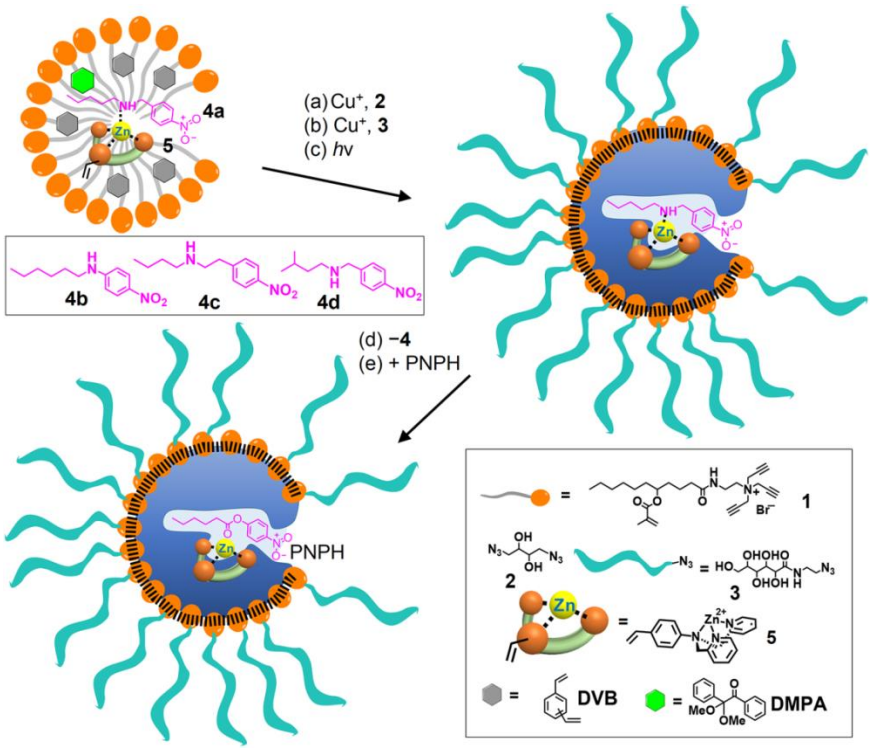

Scheme 1. Preparation of catalytic Zn-MINP as an artificial esterase for PNPH hydrolysis.

Scheme 1 illustrates the preparation of our artificial zinc enzymes. Cross-linkable surfactant **1** has two sets of orthogonal reactive groups—the tripropargyl groups in the head for surface-cross-linking with diazide **2** by the click reaction and the methacrylate on the hydrophobic tail for core-cross-linking with divinyl benzene (DVB) by free radical polymerization.[14] Surface ligand **3** is generally added after the surface-cross-linking, to decorate the cross-linked micelles with a layer of hydrophilic groups.[26] The entire synthesis was a one-pot reaction complete in less than two days and the procedures have been described in our previous publications.[14,27-29] Generally, the surface and core-cross-linking were monitored by ^{1}H NMR spectroscopy. The size and molecular weight of the MINP were measured by dynamic light scattering (DLS). The DLS size has been confirmed by

transmission electron microscopy (TEM, Figure 17). The surface cross-linking has been verified by mass spectrometry after cleavage of the 1,2-diol surface cross-linkages by periodate.[26] Formation of the templated binding pockets has been confirmed by fluorescence titration and/or isothermal titration calorimetry (ITC) for many different types of templates.[14,30-33]

Amines **4a**–**4d** are the templates used in this study. Their complexation with functional monomer (FM) **5** fixes the position of the amino nitrogen with respect to Zn^{2+}. The tridentate ligand has been a popular zinc-binding motif.[3] The surface/core double-cross-linking of the micelle then fixes the position of the zinc ion in the pocket, which is shaped as the template by the molecular imprinting process. Templates **4a**–**4c** are all designed to mimic the hydrolytic substrate *para*-nitrophenyl hexanoate (PNPH) in size and shape. We used the amines as the template to mimic PNPH because they are better ligands for the zinc complex than the activated ester itself and hydrolytically stable in the presence of zinc.

In the literature, PNPA is the most commonly used substrate in artificial zinc enzymes.[8-13] We chose to use PNPH to test our design of the active site and its selectivity, because we wanted to modify the alkyl chain and examine its effect on the catalysis (vide infra). The difference of **4a**–**4c** is in the position of the nitrogen on the alkyl chain. Through these templates, we can adjust the position of zinc systematically with respect to the ester group of PNPH to be bound in the active site. Additionally, we can tune the shape of the active site, independent of the zinc position using branched template **4d** as an example.

Binding Properties of Zn Catalysts

Although the micellar imprinting has worked successfully for many templates including hydrophobic sulfonates and carboxylates,[14,34] carbohydrates,[30,32] and

peptides,[29,31,35] this is the first time a metal complex was installed in the cross-linked micelle. We were not sure whether the metal complexes would survive the double cross-linking to afford the amine-imprinted binding pocket.

To gain insight into the metal-assisted molecular imprinting,[36-38] we first studied the binding of the Zn-containing MINP by ITC, one of the most reliable methods to measure intermolecular interactions in solution.[39] When we studied the binding of fluorescent guest molecules by MINPs in many previous examples, the ITC-determined binding constants generally showed excellent agreements with those determined by fluorescence titrations.[14,31,33,40]

As shown in Table 1, Zn-MINP prepared with **4a** as the template bound its template in 25 mM HEPES buffer (pH 7.0) with a binding constant (K_a) of $(24.0 \pm 1.1) \times 10^4$ M^{-1}. The buffer was same as that used in the hydrolysis (vide infra). The binding site also had a reasonable level of selectivity, with K_a 3–6-fold lower for the other amine guests (**4b**–**4d**) than for template **4a** (Table 1, entries 1–4). These results confirmed that molecular imprinting occurred successfully and the binding site of the MINP was able to distinguish the shift of the amino nitrogen or the shift of the methyl group by 1 carbon.

Zn-MINP(**4a**) bound **4b** more weakly than **4c**, even though both amines has a mismatch of the nitrogen by 1 carbon from the original template. The most likely reason for this probably was the weaker electron-donating power of amine **4b** from its *para*-nitro group. This conclusion was verified by determining the binding of **4b** by its own imprinted receptor, i.e., Zn-MINP(**4b**): the binding constant (9.9×10^4 M^{-1}) was 1.7–2.4 times weaker than that of **4a** by Zn-MINP(**4a**) or **4c** by Zn-MINP(**4c**).

Table 1. Binding data for Zn-MINP in 25 mM HEPES buffer (pH 7.0) obtained by ITC.[a]

Entry	Host	Guest	K_a ($\times 10^4$ M^{-1})	N	ΔG (kcal/mol)	$-\Delta H$ (kcal/mol)	$T\Delta S$ (kcal/mol)
1	Zn-MINP(4a)	4a	23.9 ± 0.9	0.9 ± 0.2	7.3	1.4 ± 0.3	5.9
2	Zn-MINP(4a)	4b	4.3 ± 0.2	0.9 ± 0.1	6.3	1.1 ± 0.1	5.2
3	Zn-MINP(4a)	4c	8.9 ± 0.1	0.9 ± 0.2	6.7	1.5 ± 0.1	5.2
4	Zn-MINP(4a)	4d	6.8 ± 0.2	0.9 ± 0.2	6.6	2.4 ± 0.4	4.2
5	Zn-MINP(4b)	4b	10.0 ± 0.2	1.0± 0.2	6.8	4.9 ± 0.2	1.9
6	Zn-MINP(4c)	4c	17.0 ± 1.1	1.0 ± 0.1	7.1	9.1 ± 0.1	-2.0
7	Zn-MINP(4d)	4d	26.2 ± 0.9	0.9 ± 0.2	7.4	1.8 ± 0.3	5.3
8	Zn-MINP(4d)	4a	6.9 ± 0.1	1.1 ± 0.1	6.6	0.8 ± 0.01	5.8

[a] The titrations were generally performed in duplicates and the errors between the runs were <10%. *N* was the number of binding site per nanoparticle. All MINPs were prepared with a 1:1 ratio between the cross-linkable surfactant and DVB.

It should be mentioned that our ITC titrations consistently showed an average of 0.9–1.1 binding sites (*N*) per nanoparticle. We were able to control this number by keeping the ratio between the surfactant and the template the same as the micelle aggregation number (~50). If needed, the number of binding sites could be tuned using different surfactant/template ratio.[14]

To further confirm the binding selectivity, we prepared Zn-MINP(**4d**), from the branched amine template. It bound its template (**4d**) better than the mismatched **4a** by a ratio of 26:6.9 or 3.8:1 (entries 7–8). Thus, the imprinting was very reliable and the imprinted micelle always preferred the original template, branched or linear. The results also suggest both the position of the nitrogen and the shape of the substrate were important to the binding of the zinc-functionalized MINPs.

The binding data reported in Table 1 were all obtained in 25 mM HEPES buffer at pH 7. We have also determined the binding in water and the difference between the two sets of binding data were within 10–20% and all the trends discussed above remained the same (Table 3). We have repeatedly found that normally pH-sensitive bindings become less sensitive (on insensitive) inside MINP. Examples include the binding of peptides containing multiple acid and basic groups[31,35] and carbohydrates by boronic acids.[30,32]

Activity and Selectivity of Zn Catalysts

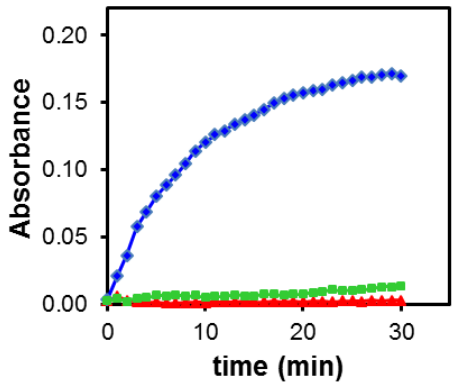

Figure 1. Absorbance at 400 nm as a function of time for the hydrolysis of PNPH in a 25 mM HEPEs buffer (pH 7.0) at 40 °C. The data sets correspond to hydrolysis catalyzed by Zn-MINP(**4a**) (◆), zinc complex **5** (▲), and nanoparticles prepared without **4a** and **5** (■). The data for the background hydrolysis in the buffer overlapped with those with **5** (▲) and were not shown for clarity of the figure. [PNPH] = 40 μM. [catalyst] = 8 μM.

p-Nitrophenyl esters are frequently used as the substrates for zinc enzyme mimics, even though they are not natural substrates for zinc enzymes.[8-13] The reason for the choice was their high activity and convenient monitoring of hydrolysis by the UV absorption of the phenoxide product at 400 nm. As shown in Figure 1, PNPH hydrolyzed very slowly in 25 mM HEPES buffer (pH 7.0) at 40 °C, in the presence of FM **5** or nonimprinted nanoparticles prepared without the template and FM. (The hydrolysis with or without FM **5** in buffer was

essentially the same.) In the presence of the same concentration of Zn-MINP(**4a**), however, the hydrolysis occurred rapidly, indicating that both MINP and the zinc ion were needed for the catalysis.[41,42]

Table 2 shows that, with 1 equiv DVB, Zn-MINP(**4a**) catalyzed the hydrolysis of PNPH with a pseudo-first-order rate constant of $k = 1.21 \times 10^{-4}$ s^{-1} in 25 mM HEPES buffer (pH 7.0) at 40 °C. Interestingly, as shown by entries 4 and 5, the reaction slowed down when the amino nitrogen of the template moved either to the right (in **4b**) or left (in **4c**). The result shows that the activity of our artificial zinc enzyme could be tuned by the position of the amino nitrogen in the template, as we had hypothesized. In addition, the catalytic activity could be tuned by the shape of the active site. Zn-MINP(**4d**), prepared from the branched template, showed a slower reaction in the hydrolysis of PNPH (entry 6).

When we constructed MINPs as receptors, we typically kept the ratio of DVB to the cross-linkable surfactant at 1:1 because an earlier study showed that the high level of DVB gave the micellar core rigidity essential to the binding selectivity.[14] This amount of DVB was the highest the surfactant can solubilize in water. In this study, we reasoned that some flexibility might be important to the fast binding of the substrate and the release of the product and thus varied the amount of DVB used in the MINP preparation.

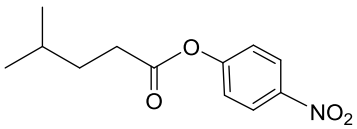

6

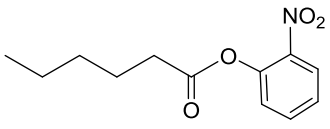

7

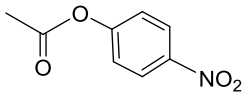

8

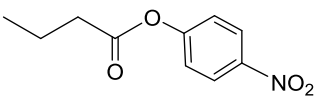

9

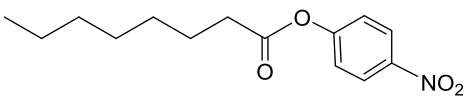

10

Table 2. Pseudo-first-order rate constants for the hydrolysis of activated esters catalyzed by Zn-MINPs in 25 mM HEPES buffer (pH 7.0).[a]

Entry	Catalyst	DVB:1	Substrate	k ($\times 10^{-4}$ s^{-1})
1	Zn-MINP(**4a**)	1:1	PNPH	1.21 ± 0.11
2	Zn-MINP(**4a**)	0.5:1	PNPH	4.31 ± 0.19
3	Zn-MINP(**4a**)	0:1	PNPH	0.71 ± 0.06
4	Zn-MINP(**4b**)	1:1	PNPH	0.68 ± 0.09
5	Zn-MINP(**4c**)	1:1	PNPH	0.89 ± 0.08
6	Zn-MINP(**4d**)	1:1	PNPH	1.01 ± 0.08
7	Zn-MINP(**4d**)	0.5:1	PNPH	0.89 ± 0.08
8	Zn-MINP(**4d**)	0:1	PNPH	1.10 ± 0.08
9	Zn-MINP(**4a**)	0.5:1	6	--[b]
10	Zn-MINP(**4a**)	0.5:1	7	--[b]
11	Zn-MINP(**4a**)	0.5:1	8	0.70 ± 0.04
12	Zn-MINP(**4a**)	0.5:1	9	0.48 ± 0.05
13	Zn-MINP(**4a**)	0.5:1	10	0.58 ± 0.04
14	none	-	8	0.21 ± 0.01
15	none	-	**9**	0.14 ± 0.01
16	none	-	PNPH	0.07 ± 0.01
17	none	-	**10**	0.06 ± 0.005
18	Zn-MINP(**4d**)	1:1	**6**	2.46 ± 0.14
19	Zn-MINP(**4d**)	0.5:1	**6**	7.15 ± 0.15
20	Zn-MINP(**4d**)	0:1	**6**	0.51 ± 0.04

[a] Reaction rates were measured in 25 mM HEPES buffer at 40 °C and pH 7.0. [PNPH] = 40 μM. [catalyst] = 8.0 μM unless otherwise indicated. The numbers given were averages from triplicate titrations at the 90% confidence level. [b] The hydrolysis was negligible under the reaction conditions.

The hypothesis was confirmed. Zn-MINP(**4a**) was optimized for PNPH, with its template resembling the substrate closely in size and shape. Cutting the amount of DVB by half increased the rate by 3.6-fold. Eliminating DVB decreased the rate by 1.7-fold (Table 1, entries 1–3).

Interestingly, when the active site was not optimized—i.e., when Zn-MINP(**4d**) was used to catalyze the hydrolysis of PNPH—the activity of the catalyst did not respond to the change in cross-linking density as much. The trend can be seen in entries 6–8, as the catalyst prepared with 1 or 0.5 DVB gave essentially the same rate constant within our experimental error. Without DVB, Zn-MINP(**4a**) was actually a slightly worse catalyst than Zn-MINP(**4d**) (entries 3 and 8). Apparently, when the MINP core was too flexible, the imprinting effect became very weak.

The above results suggest that, to successfully transfer the structural information from the template to the active site and then to the catalysis, we need a significant cross-linking density in the MINP core but too rigid an active site lowers the efficiency of the catalyst. It is illuminating to see that 0.5 equiv DVB in the MINP preparation afforded not only the highest activity (entries 1–3) but also the highest selectivity (compare entries 2 and 7) in catalysis. The result suggests that catalytic activity did not have to suffer at the expense of the selectivity in our artificial esterases, at least in the current example.

Substrates **6** and **7** differ from PNPH in the alkyl and phenyl side, respectively. The difference was especially subtle in **6** where a methyl group moved from the chain end by one carbon in comparison to PNPH. Yet, both substrates were completely inactive in the presence of Zn-MINP(**4a**), highlighting the selectivity of our synthetic esterase (entries 9–10).[43] It seems the Zn-MINP was far more sensitive to the structure of substrates during catalysis than

to the structure of guests during binding (**4a** and **4d**). The results are reasonable, because binding between a receptor and its ligand is a single event, whereas conversion of a substrate to the product by a catalyst requires many turnovers and may have amplified the difference. In our recent studies, MINP receptors were able to distinguish leucine and isoleucine which also differ by the position of a single methyl,[31] as well as mono- and oligosaccharides that differ by the inversion of a single hydroxyl.[30,32] We were pleased to see that similar precision was observed in catalysis.

The active site of Zn-MINP(**4a**) was designed to bind PNPH precisely. Thus, it should be able to distinguish substrates with a shorter or longer acyl chain. Without any catalysts, the hydrolysis of *p*-nitrophenyl ester slowed down as the acyl chain went from C2 to C8 (Table 2, entries 14–17). The MINP-catalyzed reactions, however, followed the order of C6 > C2 > C8 > C4 with a ratio of 1 : 0.16 : 0.13 : 0.11 (compare entry 2 with entries 11–13). The selectivity of the catalyst seemed to result from both the preference of the catalyst for PNPH and the inherent reactivity.[44] Thus, the catalyst was able to pick the correct substrate from very similar structural analogues. Take PNPA and PNPH as examples. The inherent reactivity of the two esters was PNPA/PNPH = 3/1 but the catalyst reversed the reactivity, to PNPA/PNPH = 1/6.

The chain-length selectivity of our catalyst was highlighted by a competition experiment. The data points in open circles (○) in Figure 2 indicate the hydrolysis of 40 μM butyrate **9** catalyzed by 8 μM Zn-MINP(**4a**). The reaction was quite slow as expected, shown by the small increase of absorbance at 400 nm for the *p*-nitrophenoxide. For the data points in triangles (△), 40 μM **9** was added in the beginning and then again at 30 min. The higher absorbance came from a higher total concentration of the substrate in the solution. For the

data points in squares (□), 40 μM **9** was added in the beginning but 40 μM PNPH was added to the solution at 30 min. The absorbance immediately began to rise after the PNPH addition, consistent with the selectivity of the catalysts for the C6 substrate.

Since the branched template **4d** resembled the branched substrate **6**, it is not surprising that Zn-MINP(**4d**) displayed good activity in the hydrolysis of **6** (entries 18–20). The balance of rigidity and flexibility was observed once again, and 0.5 equiv DVB afforded the highest activity. With this catalyst, **6** became more reactive than PNPH (compare entries 19 and 7, for example). Thus, we can tune the reactivity of the linear and the branched substrates at will, using the MINP catalyst with the matched active site.

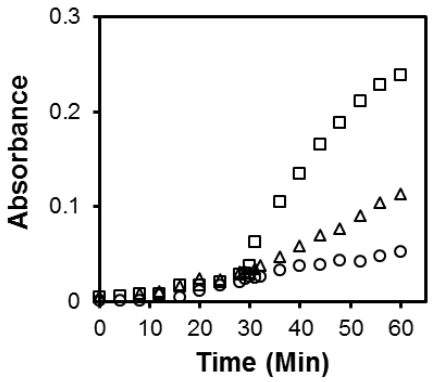

Figure 2. Absorbance at 400 nm as a function of time for the hydrolysis of 40 μM 4-nitrophenyl butyrate (**9**) catalyzed by Zn-MINP(**4a**) in a 25 mM HEPES buffer (pH 7.0) at 40 °C (○). In the data series marked with squares (□), 40 μM PNPH was added again at 30 min. In the data series marked with triangles (△), 40 μM PNPH was added at 30 min. [MINP(**4a**)] = 8 μM.

Michaelis-Menten kinetics of Zn Catalysts

Zn-MINP(**4a**) displayed enzyme-like behavior in its hydrolysis, following Michaelis-Menten kinetics at different pH values (Table 3).[45] The artificial zinc enzyme gave K_m = 0.09 mM and k_{cat} = 3.4 × 10^{-3} S^{-1} at pH 8 (entry 3), comparable to those of a natural zinc enzyme

(bovine carbonic anhydrase or BCA) under the same conditions (entry 7). Although there could be enzymes and modified enzymes with higher activities for *p*-nitrophenyl esters,[46,47] BCA was often used as the point of reference for artificial zinc enzymes because of its catalytic zinc in the active site.[8-13] In our hands, due to the slightly stronger binding of the substrate, the catalytic efficiency (k_{cat}/K_m) of Zn-MINP(**4a**) more than doubled that of the natural enzyme (entries 3 and 7).

Table 3. Michaelis-Menten parameters for the hydrolysis of PNPH catalyzed by Zn-MINP(4a) at different pHs.[a]

Entry	pH	V_{max} ($\times 10^{-7}$ mol/s)	K_m (mM)	k_{cat} ($\times 10^{-3}$ s^{-1})	k_{cat}/K_m ($M^{-1}s^{-1}$)
1	7.0	0.42 ± 0.04	0.21 ± 0.003	5.19 ± 0.44	25
2	7.5	0.33 ± 0.03	0.16 ± 0.01	4.15 ± 0.35	26
3	8.0	0.27 ± 0.05	0.09 ± 0.009	3.40 ± 0.65	38
4	8.5	0.92 ± 0.10	0.07 ± 0.01	11.5 ± 1.5	160
5	9.5	2.19 ± 0.09	0.13 ± 0.01	27.3 ± 1.3	210
6	10	2.98 ± 0.28	0.17 ± 0.01	36.5 ± 3.8	220
7	8.0[b]	0.33 ± 0.03	0.23 ± 0.04	4.15 ± 0.35	18
8	8.0[c]	1.04 ± 0.05	0.14 ± 0.01	13.0 ± 0.7	93

[a] The hydrolysis was catalyzed by [Zn-MINP(**4a**)] in 25 mM HEPES buffer at 40 °C unless indicated otherwise. [Zn-MINP(**4a**)] = 8.0 μM. [b] The hydrolysis was catalyzed by bovine carbonic anhydrase (BCA) in 25 mM HEPEs buffer (pH 8.0) at 40 °C. [BCA] = 8.0 μM. [c] The catalyst was Zn-MINP(**4a**/**11**).

With the background rate constants (k_{uncat}) measured at 0.07×10^{-4} S^{-1} at pH 7 and 0.15×10^{-4} S^{-1} at pH 8), the rate acceleration factor (k_{cat}/k_{uncat}) was calculated to be 740 at pH 7 and 230 at pH 8. The catalytic proficiency—$(k_{cat}/K_m)/k_{uncat}$—was 3.5×10^6 M^{-1} at pH 7 and 2.6×10^6 M^{-1} at pH 8.

We also found that the coordination environment of the zinc also influenced the catalysis. Zn-MINP(**4a**/**11**) was prepared using amine **4a** as the template but a different zinc complex (**11**) as the FM. As shown by the kinetic data (entry 8), this artificial zinc enzyme exhibited a higher activity than either the original Zn-MINP(**4a**) or BCA, with a calculated k_{cat}/k_{uncat} value of 870 at pH 8.

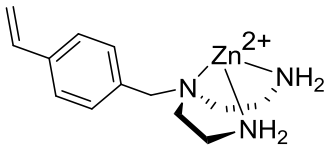

11

The pH profile of the hydrolysis of PNPH by Zn-MINP(**4a**) is shown in Figure 3. The profile is similar to the peptide-based artificial zinc enzymes reported in the literature.[8-13] The curve suggests a single protonation/deprotonation step for the active-site water with a pK_a of 8.36 ± 0.15. The number is higher than those of zinc-bound water in carbonic anhydrase B and C (6.8–7.3)[48] but comparable to those of other artificial zinc enzymes.[8-13]

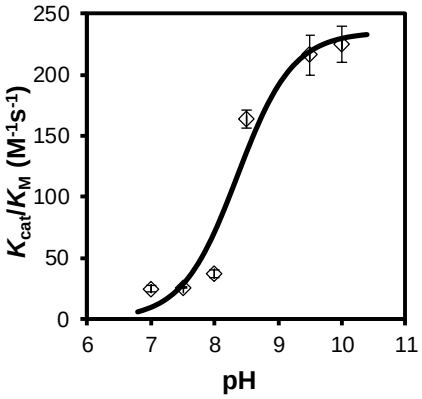

Figure 3. pH dependence of the hydrolysis of PNPH by Zn-MINP(**4a**). The smooth curve was obtained by nonlinear least-squares curve fitting to the equation, $k_{cat}/K_m = (k_{cat}/K_m)_{max} \times 10^{-pKa}/(10^{-pH} + 10^{-pKa})$, with the inflection point corresponding to the pK_a of the zinc-bound water (8.36 ± 0.15).[12]

One of the challenges with previous artificial zinc enzymes was product inhibition,[8] because the products (carboxylates and phenoxides) are stronger ligands for zinc than the starting materials (water and ester). Figure 4a shows the catalytic activity of 0.2 μM Zn-MINP(**4a**) in the presence of a large excess of PNPH (100 μM). Figure 4b shows the amount of product formed as a function of time. The amount was calculated based on an extinction coefficient of ε_{400} = 0.0216 μM^{-1} cm^{-1} for *p*-nitrophenoxide at pH 8.0. A turnover number of 324 was calculated at 300 min. At pH 7, the turnover number was found to be 460 at 540 min.[49] Even at high conversion (>95%), the reaction showed very little signs of slowing down (Figure 41). Our design gives an active site precisely constructed for the substrate (PNPH). Although carboxylate and the phenoxide should coordinate better to a cationic zinc more strongly than the starting materials, the active site of MINP(**4a**) must have prevented their complexation, possibly because the preferred coordination geometry could not be achieved in the tight binding site.

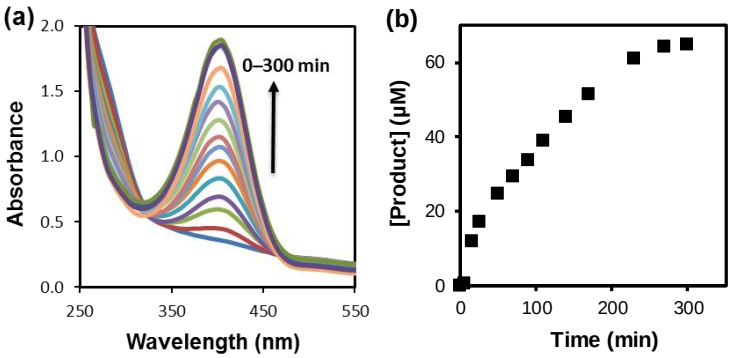

Figure 4. (a) UV-Vis spectra of PNPH (100 μM) in a 25 mM HEPEs buffer (pH 8.0) at 40 °C, after addition of 0.2 μM Zn-MINP(**4a**). (b) Amount of *p*-nitrophenoxide formed as a function of time, calculated based on an extinction coefficient of ε_{400} = 0.0216 μM^{-1} cm^{-1}.

Table 4. Catalytic data for the hydrolysis of PNPA catalyzed by artificial zinc enzymes.[a]

Entry	Catalysts	pH	pK_a	k_{cat}/K_m ($M^{-1}s^{-1}$)	TON
1[9]	MID1-Zn	8	8.2	180	>50
2[8]	Modified TRI peptide-Zn[b]	8	8.8	3	>10
3[12]	Ac-IHIHIQI-$CONH_2$	8	9.3	62	>20
4[11]	^{A104}AB3	9	9.0	32	-
5[13]	CC-Hept–Cys–His–Glu	8	9.0	18	>12
6	Zn-MINP(**4a**) for PNPH	8	8.4	38	>320 (>460)[c]
7	Zn-MINP(**4a**/**11**) for PNPH	8	-	93	-

[a] The data for the artificial zinc enzymes reported in the literature were obtained at 22–25 °C for PNPA and the data for the Zn-MINPs at 40 °C for PNPH. [b] The catalyst was $[Hg(II)]_S[Zn(II)(H_2O/OH^-)]_N(TRIL9CL23H)_3^{n+}$. [c] The turnover number in parentheses was obtained at pH 7 at 540 min.

Table 4 compares the catalytic performance of the Zn-MINP catalysts with artificial zinc enzymes reported in the literature, at comparable pHs if the corresponding data were available. Since small-molecule zinc enzyme mimics typically have poor catalytic turnovers, we only included peptidic catalysts that have displayed the Michaelis-Menten kinetics and good catalytic activities.[8-13] Although our Zn-MINPs were designed specifically for PNPH and the other artificial zinc enzymes were only tested for PNPA, the comparison gives a reasonable perspective on our catalysts, given that PNPH is generally less reactive than PNPA in the absence of catalysts (vide supra).

Generally speaking, the pK_a of the zinc-bound water was on the low side for our Zn-MINPs among their peers and the catalytic efficiency on the medium to high side, depending on the nature of the tridentate ligand used in the Zn-MINPs (Table 4). Although the TON numbers reported were the minima in all cases, our catalysts certainly looked very favorable in this property that has been a particular challenge with traditional artificial zinc enzymes. [8]

Conclusions

In summary, through micellar imprinting, we could prepare zinc-based artificial enzymes from simple building blocks in a highly efficient manner. The entire synthesis and purification could be done in less than 2 days once all the starting materials are available. The catalyst displayed enzyme-like kinetics and pH profile, and was able to distinguish the position of a single methyl group and the chain length of the substrate, as well as substitution pattern of the phenyl group. High turnovers were achieved as the active site prevented the products from re-binding the zinc.

The most significant feature of our artificial enzymes is the ability to fine-tune the size and shape of the active site in a rational manner, as well as the position of the catalytic metal ion with respect to the reactive functionality. These features gave us an unusual level of control in the construction of active site and allowed us to switch the relative reactivity of substrates with similar intrinsic reactivities. Although one wishes to move beyond activated esters in the catalytic hydrolysis,[50] efficient construction of a substrate-specific functionalized active site is important to the development of any artificial enzymes. The principle demonstrated in this study should not be limited to hydrolysis and could be used to design other biomimetic catalysts with enzyme-like activity and selectivity.

Acknowledgement

We thank NSF (DMR-1464927 and CHE-1708526) for financial support of this research.

Experimental Section

General Method

Routine ^{1}H and ^{13}C NMR spectra were recorded on a Bruker DRX-400, on a Bruker AV II 600 or on a Varian VXR-400 spectrometer. ESI-MS mass was recorded on Shimadzu

LCMS-2010 mass spectrometer. Dynamic light scattering (DLS) data were recorded at 25 °C using PDDLS/ CoolBatch 90T with PD2000DLS instrument. Isothermal titration calorimetry (ITC) was performed using a MicroCal VP-ITC Microcalorimeter with Origin 7 software and VPViewer2000 (GE Healthcare, Northampton, MA). UV-vis spectra were recorded on a Cary 100 Bio UV-visible spectrophotometer.

Syntheses

Syntheses of compounds **1**[51], **2**[51], **3**[51] and **12**[60] have been reported previously.

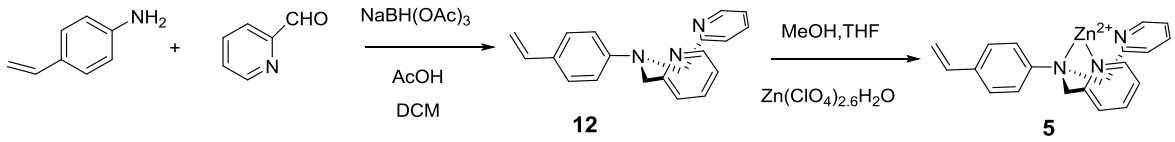

Scheme 2. Synthesis of compound **5**

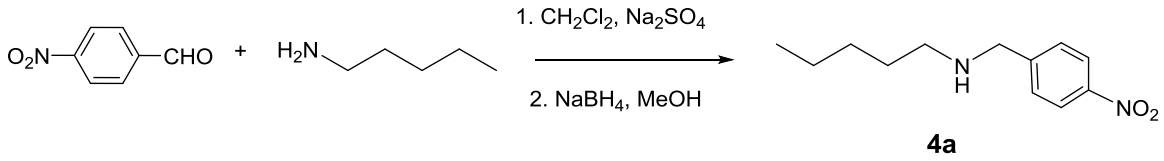

Scheme 3. Synthesis of compound **4a**

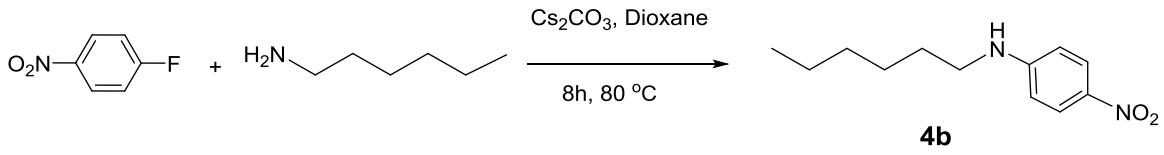

Scheme 4. Synthesis of compound **4b**

4c

Scheme 5. Synthesis of compound **4c**

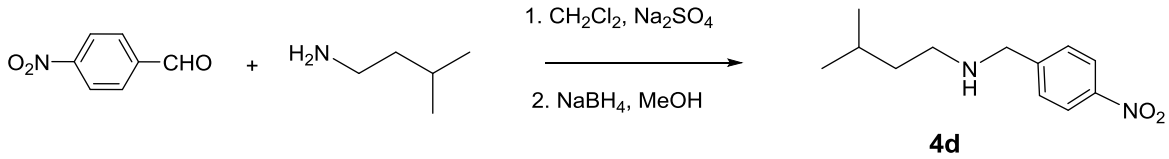

4d

Scheme 6. Synthesis of compound **4d**

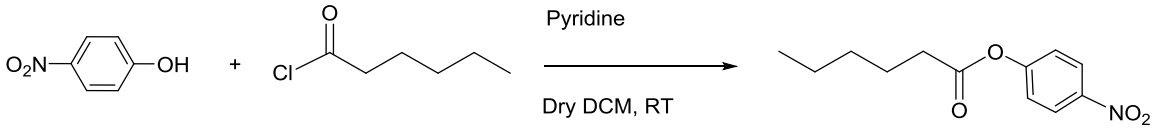

Scheme 7. Synthesis of compound **PNPH**

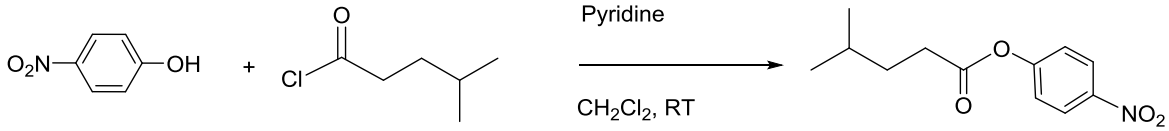

6

Scheme 8. Synthesis of compound **6**

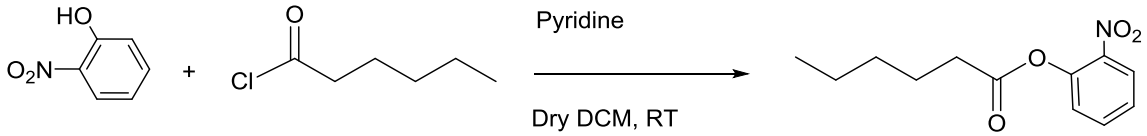

7

Scheme 9. Synthesis of compound **7**

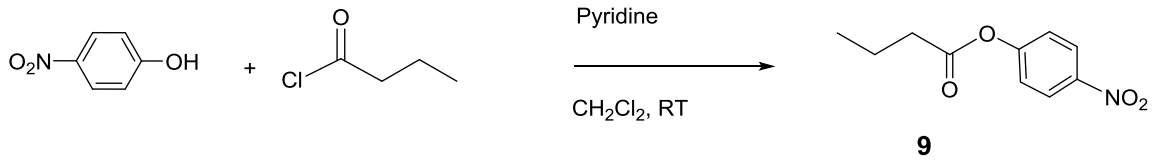

9

Scheme 10. Synthesis of compound **9**

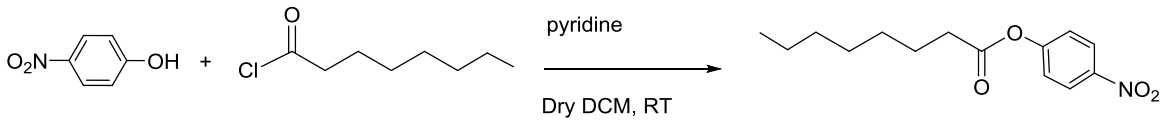

10

Scheme 11. Synthesis of compound **10**

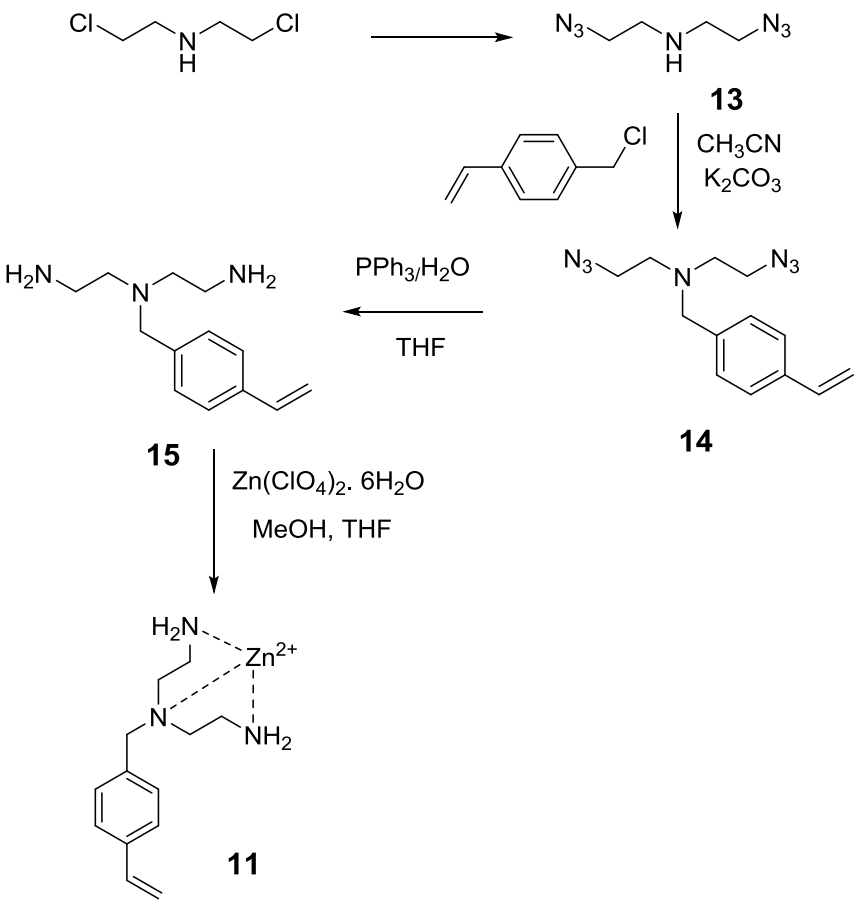

Scheme 11. Synthesis of compound **11**

Compound 12.[52] A mixture of 4-vinylaniline (0.25 g, 2.10 mmol), pyridine-2-carbaldehyde (0.60 g, 5.60 mmol), and acetic acid (0.40 g, 6.60 mmol) in 10 mL dry CH_2Cl_2 was stirred at room temperature for 30 min before sodium borohydride triacetate (1.50 g, 7.00 mmol) was added. Stirring was continued for 20 h, after which the mixture was diluted with 20 mL of CH_2Cl_2. The combined organic phase was washed with 20 mL of 1M NaOH aqueous solution, separated, and dried over $MgSO_4$. After the solvent was removed under reduced pressure, the residue was purified by column chromatography over silica gel using 5:1 methylene chloride/ethyl acetate as the eluent to afford an off-white powder (0.40 g, 62 %).^{1}HNMR (400 MHz, $CDCl_3$, δ): 8.52 (d, *J* = 8.0 Hz, 2H), 7.53-7.56 (m, 2H), 7.15-7.18 (m, 4H), 7.08-4.12 (m, 2H), 6.56-6.60 (m, 2H), 6.51 (dd, *J* = 20.0 & 12.0 Hz, 1H), 5.43 (d, *J* = 20.0 Hz, 1H), 4.93 (d, *J* = 12.0 Hz, 1H), 4.77 (s, 4H). ^{13}C NMR (100 MHz, $CDCl_3$, δ): 158.6, 149.7, 147.8, 136.9, 136.3, 127.3, 122.1, 120.8, 112.4, 109.9, 57.3. ESI-HRMS (*m/z*): $[M+H]^+$ calcd for $C_{20}H_{20}N_3$, 302.1652; found 302.1655.

Compound 5.[53] $Zn(ClO_4)_2 \cdot 6H_2O$ (14.9 mg, 0.04 mmol) was dissolved in a solution of compound **8** (1.20 mg, 0.04 mmol) in MeOH (2 mL) and THF (2 mL). After the mixture was stirred at room temperature for 4 h, the solvent was removed under reduced pressure to give a white powder (26.0 mg, 98%).^{1}H NMR (400 MHz, DMSO-d6, δ): 8.55 (d, *J* = 8.0 Hz, 2H), 7.72-7.24 (m, 2H), 7.26-7.28 (m, 4H), 7.17 (d, *J* = 8.0 Hz, 2H), 6.60 (d, *J* = 8.0 Hz, 2H), 6.51 (dd, *J* = 20.0 & 12.0 Hz, 1H), 5.48 (d, *J* = 20.0 Hz, 1H), 4.93 (d, *J* = 12.0 Hz, 1H), 4.83 (s, 4H).

Compound 4a.[54] A mixture of 4-nitrobenzaldehyde (0.50 g, 3.30 mmol), pentylamine (0.44 g, 5.00 mmol), and Na_2SO_4 (0.71g, 5.00 mmol) in dry CH_2Cl_2 (10 mL) was stirred at room temperature for 5 h. The solid was removed by filtration and the filtrate was removed under

reduced pressure. Sodium borohydride (0.07g, 1.70 mmol) was then added to the solution of this residue (imine) in MeOH (10 mL) and stirred at room temperature for additional 5 h. The organic solvents were removed under reduced pressure and the residue was combined with CH_2Cl_2, washed with water (3 x 10 mL) and dried with $MgSO_4$ to afford a pure yellow liquid (0.57 g, 78 %).[1]HNMR (400 MHz, $CDCl_3$, δ): 8.12 (d, *J* = 8.6 Hz, 2H), 7.47 (d, *J* = 8.4 Hz, 2H), 3.86 (s, 2H), 2.58 (t, *J* = 7.2 Hz, 2H), 1.47 (q, *J* = 7.2 Hz, 2H), 1.33 – 1.23 (m, 4H), 0.85 (t, *J* = 7.2 Hz, 3H). ^{13}C NMR (100 MHz, $CDCl_3$, δ): 148.6, 146.7, 128.5, 123.5, 53.2, 49.5, 29.8, 29.4, 22.6, 14.0. ESI-HRMS (*m/z*): $[M+H]^+$ calcd for $C_{12}H_{19}N_2O_3$, 223.1441; found 223.1444.

Compound 4b.[55] A mixture of 4-fluoronitrobenzene (0.25 g, 1.77 mmol), 1-hexylamine (0.40 g, 4.0 mmol), and cesium carbonate (1.75 g, 5.30 mmol) in 1,4-dioxane (10 mL) was stirred overnight at 90 °C. After cooled to room temperature, the mixture was poured into water. The product was extracted with ethyl acetate (3 × 15 mL). The combined organic phase was washed with water (3 × 10 mL), brine (3 × 10 mL), and dried over anhydrous Na_2SO_4. After ethyl acetate was removed under reduced pressure, the residue was purified by column chromatography over silica gel using 3:100 EA/hexane as the eluent to afford a yellow powder (0.22 g, 56%). ^{1}HNMR (400 MHz, $CDCl_3$, δ): 8.09 (d, *J* = 8.0 Hz, 2H), 6.51 (d, *J* = 8.0 Hz, 2H), 3.20 (t, *J* = 7.2 Hz, 2H), 1.65-1.56 (m, 4H), 1.38-1.41 (m, 4H), 0.91 (t, *J* = 6.1 Hz, 3H). ^{13}C NMR (100 MHz, $CDCl_3$, δ): 153.9, 138.1, 126.9, 111.3, 43.7, 31.9, 29.5, 27.1, 23.0, 14.4. ESI-HRMS (*m/z*): $[M+H]^+$ calcd for $C_{12}H_{19}N_2O_3$, 223.1441; found 223.1444.

Compound 4c.[56] A mixture of 1-(2-bromoethyl)-4-nitrobenzene (0.43g, 1.87 mmol) and 1-butylamine (0.30 g, 4.11 mmol) in DMSO (20 mL) was stirred at room temperature for 8 h.

The mixture was poured into water and extracted with ethyl acetate (3 × 20 mL). The combined organic phase was washed with water (3 × 15 mL), brine (3 × 10 mL), and dried over anhydrous Na_2SO_4. The solvent was removed under reduced pressure to afford a yellow oil (0.40 g, 99%). ^{1}HNMR (400 MHz, $CDCl_3$, δ): 8.13 (d, *J* = 8.0 Hz, 2H), 7.36 (d, *J* = 8.0 Hz, 2H), 2.90 (s, 4H), 2.61 (t, *J* = 7.2 Hz, 2H), 1.48 – 1.39 (m, 2H), 1.22-1.35 (m, 2H), 0.88 (t, *J* = 7.3 Hz, 3H). ^{13}C NMR (100 MHz, $CDCl_3$, δ): 148.6, 146.9, 129.9, 124.1, 51.1, 50.0, 36.9, 32.6, 20.9, 14.4. ESI-HRMS (*m/z*): $[M+H]^+$ calcd for $C_{12}H_{18}N_2O_3$, 223.1441; found 223.1438.

Compound 4d.[54] A mixture of 4-nitrobenzaldehyde (0.50 g, 3.30 mmol), isopentylamine (0.44 g, 5.00 mmol), and Na_2SO_4 (0.71g, 5.00 mmol) in CH_2Cl_2 (10.0 mL) was stirred at room temperature for 5 h. The solid was removed by filtration and the filtrate was concentrated under reduced pressure. The residue was dissolved in MeOH (10 mL) to which sodium borohydride (0.07g, 1.70 mmol) was added. The mixture was stirred at room temperature for additional 5 h. The organic solvent was removed under reduced pressure and the residue was dissolved with CH_2Cl_2. The organic phase was washed with water (3 × 10 mL) and dried with $MgSO_4$ to afford a reddish oil (0.60 g, 82 %) ^{1}H NMR (400 MHz, $CDCl_3$ δ): 8.08 (d, *J* = 8.7 Hz, 2H), 7.43 (d, *J* = 8.7 Hz, 2H), 3.83 (s, 2H), 2.58 – 2.54 (m, 2H), 1.56-1.60 (m , 1H), 1.38 – 1.30 (m, 2H), 0.82 (d, *J* = 6.7 Hz, 6H). ^{13}C NMR (100 MHz, $CDCl_3$, δ): 161.2, 147.2 , 128.9, 123.4, 52.4, 46.9, 38.1, 25.9, 24.9, 22.5. ESI-HRMS (*m/z*): $[M+H]^+$ calcd for $C_{12}H_{19}N_2O_3$, 223.1441; found 223.1440.

Compound PNPH. Hexanoyl chloride (0.53 g, 4.00 mmol) was added slowly to a solution of *p*-nitrophenol (0.56 g, 4.00 mmol) and pyridine (0.38g, 4.00 mmol) in dry CH_2Cl_2 (25 mL) at 0 °C. The mixture was stirred for another 1 h at 0 °C and allowed to warm to room

temperature. After the mixture was stirred for 8 h, it was washed with brine (3 × 10 mL) and dried over anhydrous Na_2SO_4. The solvent was removed under reduced pressure and the residue was purified by column chromatography over silica gel using ethyl 4:1 ethyl acetate/hexane as the eluent to afford a colorless oil (0.65 g, 68%). (400 MHz, $CDCl_3$, δ): 8.25 (d, *J* = 8.0 Hz, 2H), 7.27 (d, *J* = 8.0 Hz, 2H), 2.59 (t, *J* = 7.5 Hz, 2H), 1.80 – 1.69 (m, 2H), 1.46 – 1.29 (m, 4H), 0.92 (t, *J* = 7.5 Hz, 3H).^{13}C NMR (100 MHz, $CDCl_3$, δ): 171.3, 155.5, 145.2, 125.2, 122.4, 34.3, 31.2, 24.4, 22.3, 13.9.

Compound 6.[57] 4-Methylpentanoyl chloride (0.55 g, 4.20 mmol) was added slowly to a solution of *p*-nitrophenol (0.56 g, 4.00 mmol) and pyridine (0.38g, 4.00 mmol) in dry CH_2Cl_2 (25 mL) at 0 °C. The mixture was stirred for another 1 h at 0 °C and allowed to warm to room temperature. After the mixture was stirred for 8 h, it was washed with brine (3 × 10 mL) and dried over anhydrous Na_2SO_4. The solvent was removed under reduced pressure and the residue was purified by column chromatography over silica gel using ethyl 4:1 ethyl acetate/hexane as the eluent to afford a white powder (0.70 g, 74%). ^{1}HNMR (400 MHz, $CDCl_3$, δ): 8.19 (d, *J* = 8.0 Hz, 2H), 7.20 (d, *J* = 8.0 Hz, 2H), 2.57 – 2.49 (m, 2H), 1.66 – 1.52 (m, 3H), 0.93 (t, *J* = 7.5 Hz, 3H). ^{13}C NMR (100 MHz, $CDCl_3$, δ): 171.5, 155.5, 145.2, 125.2, 122.4, 32.9, 27.7, 22.2.

Compound 7. Hexanoyl chloride (0.31 mL, 2.0 mmol) was added slowly to a solution of *o*-nitrophenol (0.20 g, 1.4 mmol) and triethylamine (0.22 mL, 1.4 mmol) in dry CH_2Cl_2 (10 mL). The mixture was stirred for another 1 h at 0 °C and allowed to warm to room temperature. After the mixture was stirred for 8 h, it was washed with brine (3 × 10 mL) and dried over anhydrous Na_2SO_4. The solvent was removed under reduced pressure and the residue was purified by column chromatography over silica gel using 20:1

dichloromethane/methanol as the eluent to afford a colorless oil (0.26 g, 78%). ^{1}HNMR (400 MHz, $CDCl_3$, δ): 8.00 (dd, *J* = 8.0, 2.0 Hz, 1H), 7.57 (ddd, *J* = 8.0, 2.0 Hz, 1H), 7.31 (ddd, *J* = 7.5, 1.3 Hz, 1H), 7.15 (dd, *J* = 8.0, 1.3 Hz, 1H), 2.56 (t, *J* = 7.5 Hz, 2H), 1.73-1.66 (m, 2H), 1.38-1.25 (m, 4H), 0.85 (t, *J* = 7.0 Hz, 3H). ^{13}C NMR (100 MHz, $CDCl_3$, δ): 171.3, 144.1, 141.8, 134.7, 126.5, 125.7, 125.2, 77.5, 77.1, 76.8, 33.9, 31.1, 24.1, 22.3, 13.9. ESI-HRMS (m/z): [M + H]+ calcd for $C_{12}H_{16}NO_4$, 238.2641; found, 238.2645.

Compound 9. [57,58] Butyryl chloride (0.42 g, 4.00 mmol) was added slowly to a solution of *p*-nitrophenol (0.56 g, 4.00 mmol) and pyridine (0.38g, 4.00 mmol) in dry CH_2Cl_2 (25 mL) at 0 °C. The mixture was stirred for another 1 h at 0 °C and allowed to warm to room temperature. After the mixture was stirred for 8 h, it was washed with brine (3 × 10 mL) and dried over anhydrous Na_2SO_4. The solvent was removed under reduced pressure and the residue was purified by column chromatography over silica gel using ethyl 4:1 ethyl acetate/hexane as the eluent to afford a colorless oil (0.70 g, 83%). ^{1}HNMR (400 MHz, $CDCl_3$, δ): 8.26 (d, *J* = 9.1 Hz, 2H), 7.27 (d, *J* = 9.1 Hz, 2H), 2.58 (t, *J* = 7.4 Hz, 2H), 1.79 (q, *J* = 7.4 Hz 2H), 1.05 (t, *J* = 7.4 Hz, 3H). ^{13}C NMR (100 MHz, $CDCl_3$, δ): 171.1, 155.5, 145.1, 125.1, 122.45 , 36.0, 18.2, 13.5.

Compound 10. [57,59] Octanoyl chloride (0.6 g, 4 mmol) in CH_2Cl_2 (2 mL) was added slowly to a solution of *p*-nitrophenol (0.50g, 4 mmol) and pyridine (0.28g, 4 mmol) in dry CH_2Cl_2 (25 mL) at 0°C. The mixture was stirred for another 1 h at 0 °C and allowed to warm to room temperature. After the mixture was stirred for 8 h, it was washed with brine (40 mL) and dried over anhydrous Na_2SO_4. The solvent was removed under reduced pressure and the residue was purified by column chromatography over silica gel using ethyl 4:1 ethyl acetate/hexane as the eluent to afford a colorless oil (0.63 g, 83%). ^{1}HNMR (400 MHz,

$CDCl_3$, δ): 8.26 (d, *J* = 9.1 Hz, 2H), 7.27 (d, *J* = 9.1 Hz, 2H), 2.57 (t, *J* = 7.4 Hz, 2H), 1.71-1.75 (m, 2H), 1.20-1.28 (m, 8H), 0.86 (t, 7.4 Hz,3H). ^{13}C NMR (100 MHz, $CDCl_3$, δ): 171.2, 155.5, 145.1, 125.1, 122.4, 34.2, 31.6, 28.9, 28.5, 24.7, 22.6, 14.1.

Compound 14. 4-Vinylbenzyl chloride (0.47 g, 3.1 mmol) was added slowly to a solution of bis(2-azidoethyl)amine (**13**) (0.40 g, 2.6 mmol) and potassium carbonate (0.42 g, 3.1 mmol) in dry CH_3CN (15 mL) 5 at 0 °C. The mixture was stirred overnight at 50 °C and cooled to room temperature. Water (30 mL) was added. The solution was extracted with CH_2Cl_2 (3 × 30 mL) and the combined organic phase was dried over anhydrous Na_2SO_4. The solvent was removed under reduced pressure and the residue was purified by column chromatography over silica gel using 3:0 dichloromethane/hexane as the eluent to afford a colorless oil (0.50 g, 70%). ^{1}HNMR (400 MHz, $CDCl_3$, δ): 7.38 (d, *J* = 8.1 Hz, 2H), 7.30 (d, *J* = 8.2 Hz, 2H), 6.71 (dd, *J* = 17.6, 10.9 Hz, 1H), 5.74 (d, *J* = 17.6, 1H), 5.24 (d, *J* = 10.9 Hz, 1H), 3.69 (s, 2H), 3.30 (t, *J* = 6.2 Hz, 4H), 2.76 (t, *J* = 6.2 Hz, 4H). ^{13}C NMR (100 MHz, $CDCl_3$, δ): 138.1, 136.9, 136.6, 128.9, 126.3, 113.7, 53.7, 49.5. ESI-HRMS (*m/z*): $[M+H]^+$ calcd for $C_{13}H_{18}N_7$, 272.1618; found 272.1611.

Compound 15. Triphenylphosphine (0.50 g, 1.9 mmol) was added slowly to a solution of compound **13** (0.17 g, 0.6 mmol) in H_2O (10 mL) and THF (5 mL). The mixture was stirred at 50 °C overnight. The solvents were removed under reduced pressure and the residue was purified by column chromatography over silica gel using 50:1 methanol/ammonium hydroxide as the eluent to afford a colorless oil (0.06 g, 60%). ^{1}HNMR (400 MHz, $CDCl_3$, δ): 7.38 (d, *J* = 8.2 Hz, 2H), 7.29 (d, *J* = 8.2 Hz, 2H), 6.70 (dd, *J* = 17.6 & 10.9 Hz, 1H), 5.73 (d, *J* = 17.6 Hz, 1H), 5.17 (d, *J* = 10.9 Hz, 1H), 3.60 (s, 2H), 2.75 (t, *J* = 6.1 Hz, 4H), 2.57

(t, *J* = 6.1 Hz, 4H). ^{13}C NMR (100 MHz, $CDCl_3$, δ): 140.3, 138.5, 138.2 130.9, 127.7, 114.2, 60.2, 56.6, 40.0. ESI-HRMS (*m/z*): $[M+H]^+$ calcd for $C_{13}H_{22}N_3$, 220.1808; found 220.1808.

Compound 11.[53] $Zn(ClO_4)_2 \cdot 6H_2O$ (3.40 mg, 0.009 mmol) was dissolved in a solution of compound **15** (1.20 mg, 0.04 mmol) in MeOH (2 mL) and THF (2 mL). After the mixture was stirred at room temperature for 4 h, the solvent was removed under reduced pressure to get a white powder (26.0 mg, 98%).^{1}HNMR (400 MHz, $CDCl_3$, δ): 7.30 (d, *J* = 8.0 Hz, 2H), 7.41 (d, *J* = 8.0 Hz, 2H), 6.70 (dd, *J* = 20.0 & 12.0 Hz, 1H), 5.75 (d, *J* = 20.0 Hz, 1H), 5.25 (d, *J* = 12.0 Hz, 1H), 3.82 (s, 2H), 2.92 (d, *J* = 6.2 Hz, 4H), 2.85 (d, *J* = 6.2 Hz, 4H).

Synthesis of Zn-MINP(4a). To a micellar solution of compound **1** (10.4 mg, 0.02 mmol) in H_2O (2.00 mL), divinylbenzene (DVB, 2.80 μL, 0.02 mmol), Zn-complex **5** in DMSO (15.0 μL of a solution of 8.00 mg/500 μL DMSO, 0.0004 mmol) and 2,2-dimethoxy-2-phenylacetophenone (DMPA,10 μL of a 12.80 mg/mL solution in DMSO, 0.0005 mmol) were added. The mixture was subjected to ultrasonication for 10 min before compound **2** (4.13 mg, 0.024 mmol), $CuCl_2$ (10 μL of a 6.70 mg/mL solution in H_2O, 0.0005 mmol) and sodium ascorbate (10 μL of a 99 mg/mL solution in H_2O, 0.005 mmol) were added. After the reaction mixture was stirred slowly at room temperature for 12 h, compound **3** (10.6 mg, 0.04 mmol), $CuCl_2$ (10 μL of a 6.70 mg/mL solution in H_2O, 0.0005 mmol l) and sodium ascorbate (10 μL of a 99 mg/mL solution in H_2O, 0.005 mmol) were added. After being stirred for another 6 h at room temperature, the reaction mixture was transferred to a glass vial, purged with nitrogen for 15 min, sealed with a rubber stopper and irradiated in a Rayonet reactor for 12 h. ^{1}H NMR spectroscopy was used to monitor the progress of reaction. The reaction mixture was poured into acetone (8.00 mL). The precipitate was collected by

centrifugation and washed with a mixture of acetone/water (5 mL/1 mL) three times. The crude produce was washed by methanol/acetic acid (5 mL/0.1 mL) three times. The off white powder was dried in air to afford the final MINPs (11 mg).

Kinetic Measurements. Stock solutions (10 mM) of *p*-nitrophenyl hexanoate (PNPH) and other activated esters in methanol were prepared. The stock solutions were stored in a refrigerator and used within 3 d. Stock solutions of Zn-MINP (80 μM) in 25 mM HEPES buffer were prepared. For the kinetic experiment, a typical procedure is as follows: An aliquot of 200 μL of the Zn-MINP stock solution was combined with 1790 μL of the same HEPES buffer in a cuvette. The cuvette was placed in a UV-vis spectrometer and equilibrated to 40.0 °C. After 5 min, an aliquot of 10 μL of the PNPH stock solution was added. The concentration of the substrate (PNPH or other activated ester) in the reaction mixture was 40 μM and the concentration of the MINP was 8.0 μM in all cases. The hydrolysis was monitored by the absorbance of *p*-nitrophenoxide anion at 400 nm. The amount of the product formed was calculated from a calibration curve obtained from *p*-nitrophenol at the specified pH.

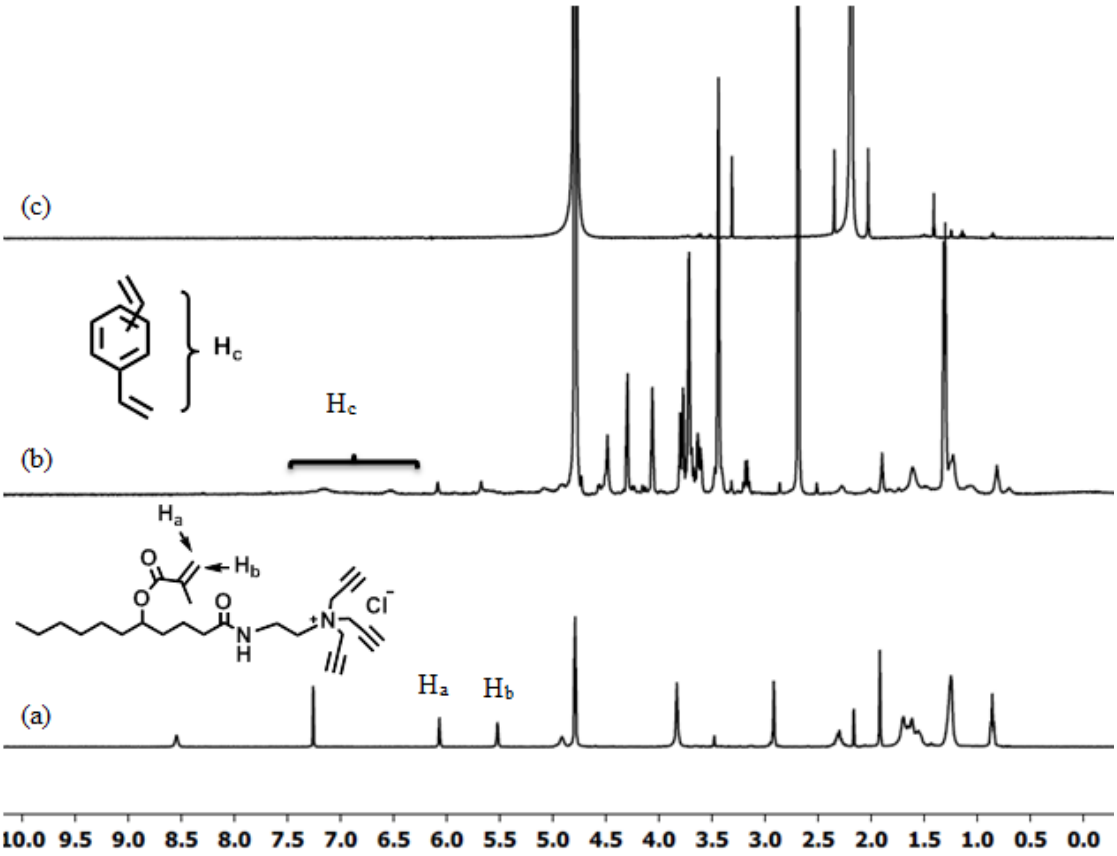

Figure 5. ^{1}H NMR spectra of (a) **1** in $CDCl_3$ (b) alkynyl-SCM in D_2O and (c) Zn-MINP(**4a**) in D_2O.

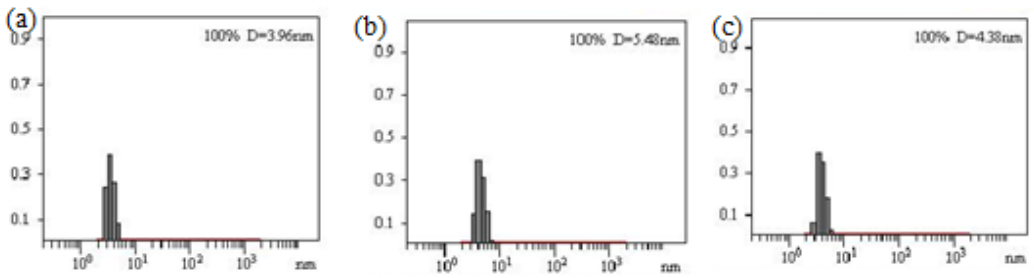

Figure 6. Distribution of the hydrodynamic diameters of the nanoparticles in water as determined by DLS for (a) alkynyl-SCM (b) surface-functionalized SCM and (c) Zn-MINP(**4a**) after purification.

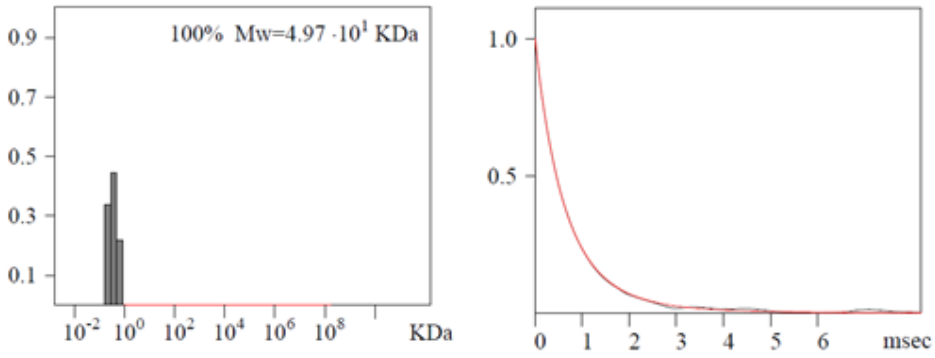

Figure 7. Distribution of the molecular weights of Zn-MINP(**4a**) and the correlation curves for DLS. The molecular weight distribution was calculated by the PRECISION DECONVOLVE program assuming the intensity of scattering is proportional to the mass of the particle squared. If each unit of building block for the Zn-MINP(**4a**) is assumed to contain one molecule of compound **1** (MW = 521 g/mol), 1.2 molecules of compound **2** (MW = 172 g/mol), one molecule of DVB (MW = 130 g/mol), 0.8 molecules of compound **3** (MW = 264 g/mol), and 0.02 molecules of compound **5** (MW = 365 g/mol), the molecular weight of Zn-MINP(**4a**) translates to 47 [= 49700/(521+1.2×172+130+0.8×264+ 0.02×365)] of such units.

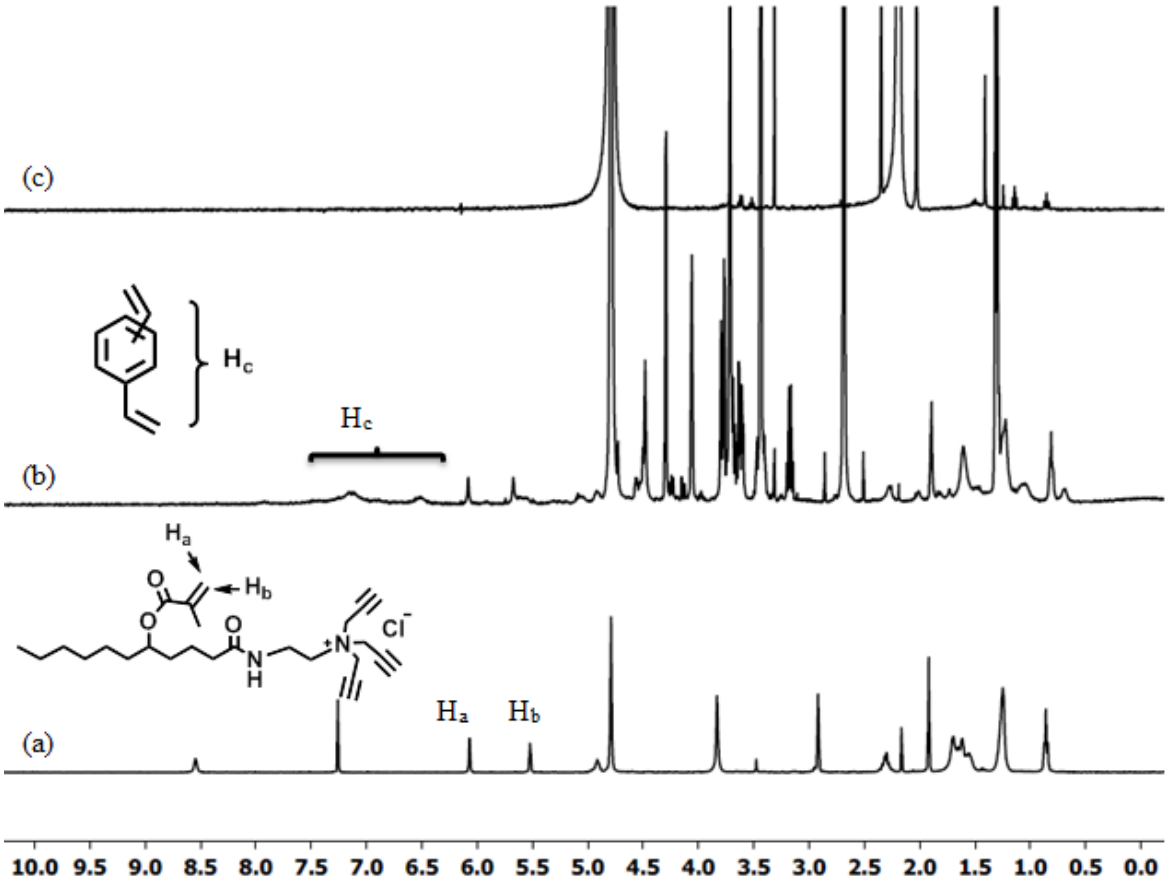

Figure 8. ^{1}H NMR spectra of (a) **1** in $CDCl_3$ (b) alkynyl-SCM in D_2O and (c) Zn-MINP(**4b**) in D_2O.

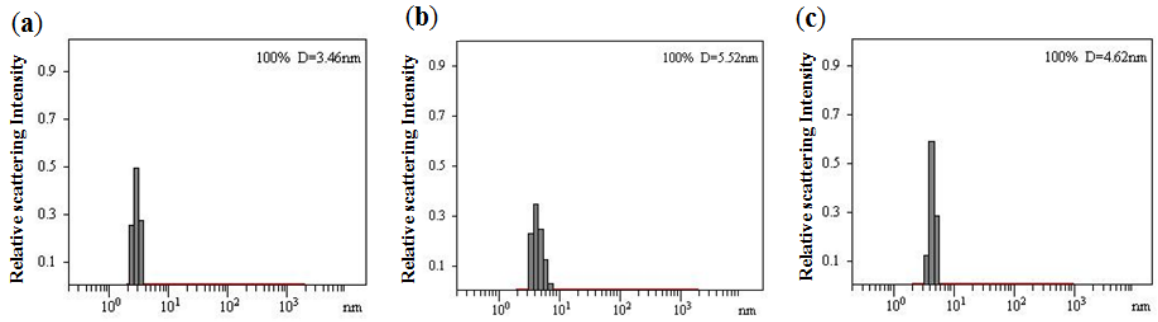

Figure 9. Distribution of the hydrodynamic diameters of the nanoparticles in water as determined by DLS for (a) alkynyl-SCM (b) surface-functionalized SCM and (c) Zn-MINP(**4b**) after purification.

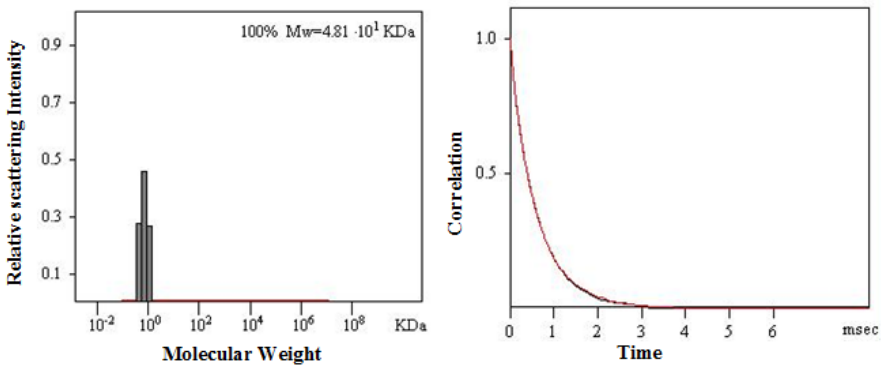

Figure 10. Distribution of the molecular weights of Zn-MINP(**4b**) and the correlation curves for DLS. The molecular weight distribution was calculated by the PRECISION DECONVOLVE program assuming the intensity of scattering is proportional to the mass of the particle squared. If each unit of building block for the Zn-MINP(**4b**) is assumed to contain one molecule of compound **1** (MW = 521 g/mol), 1.2 molecules of compound **2** (MW = 172 g/mol), one molecule of DVB (MW = 130 g/mol), 0.8 molecules of compound **3** (MW = 264 g/mol), and 0.02 molecules of compound **5** (MW = 365 g/mol), the molecular weight of MINP-Zn-(**4b**) translates to 45 [= 48100/(521+1.2×172+130+0.8×264,+ 0.02×365)] of such units.

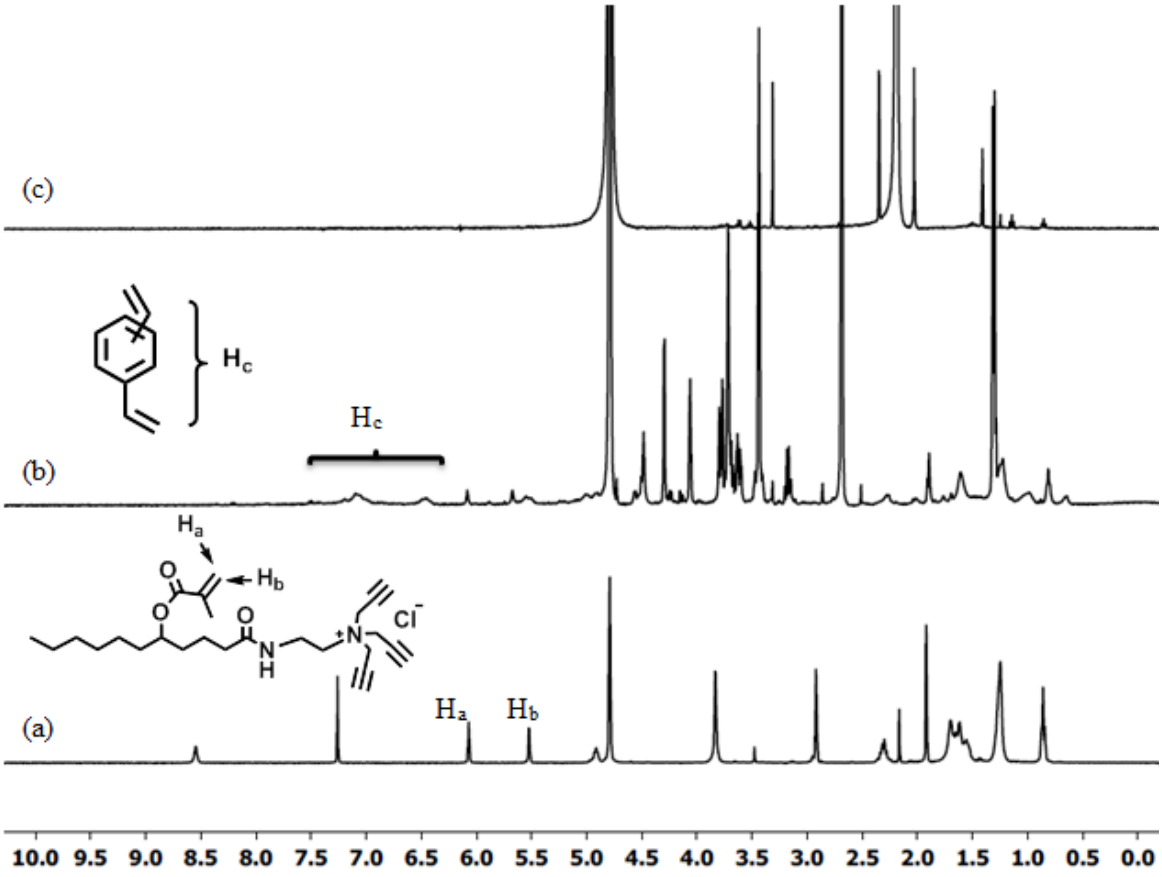

Figure 11. ^{1}H NMR spectra of (a) **1** in $CDCl_3$ (b) alkynyl-SCM in D_2O and (c) Zn-MINP(**4c**) in D_2O.

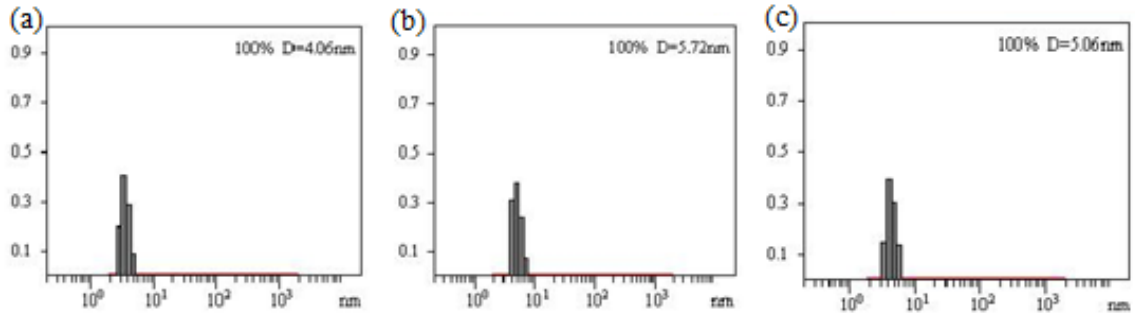

Figure 12. Distribution of the hydrodynamic diameters of the nanoparticles in water as determined by DLS for (a) alkynyl-SCM (b) surface-functionalized SCM and (c) Zn-MINP(**4c**) after purification.

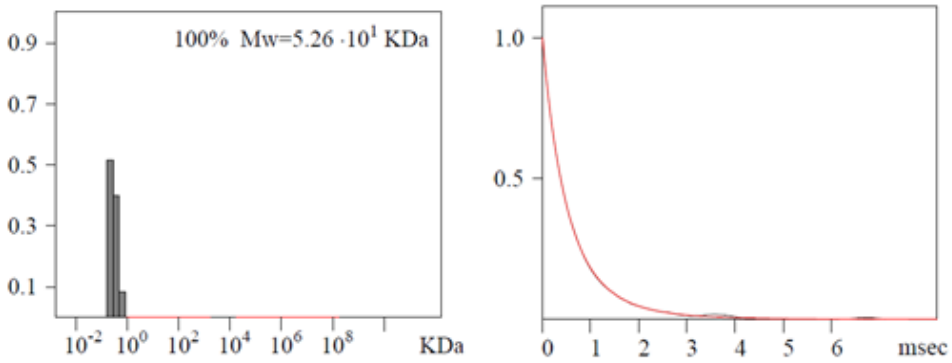

Figure 13. Distribution of the molecular weights of Zn-MINP(**4c**) and the correlation curves for DLS. The molecular weight distribution was calculated by the PRECISION DECONVOLVE program assuming the intensity of scattering is proportional to the mass of the particle squared. If each unit of building block for the Zn-MINP(**4c**) is assumed to contain one molecule of compound **1** (MW = 521 g/mol), 1.2 molecules of compound **2** (MW = 172 g/mol), one molecule of DVB (MW = 130 g/mol), 0.8 molecules of compound **3** (MW = 264 g/mol), and 0.02 molecules of compound **5** (MW = 365 g/mol), the molecular weight of Zn-MINP(**4c**) translates to 49 [= 52600/(521+1.2×172+130+0.8×264+0.02×365)] of such units.

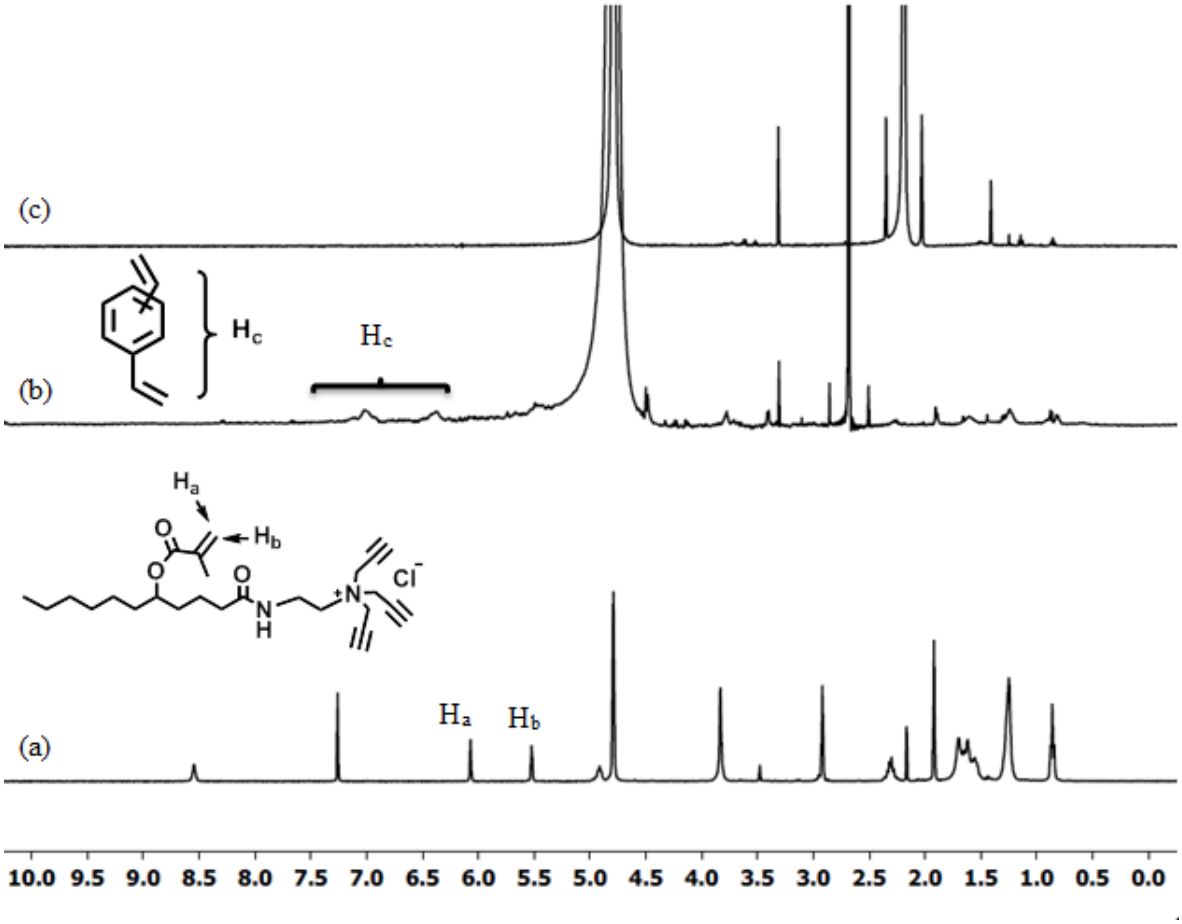

Figure 14. ^{1}H NMR spectra of (a) **1** in $CDCl_3$ (b) alkynyl-SCM in D_2O and (c) Zn-MINP(**4d**) in D_2O.

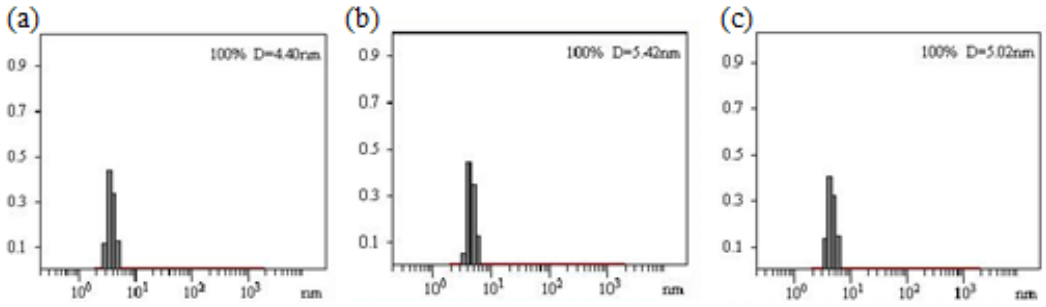

Figure 15. Distribution of the hydrodynamic diameters of the nanoparticles in water as determined by DLS for (a) alkynyl-SCM (b) surface-functionalized SCM, and (c) Zn-MINP(**4d**) after purification.

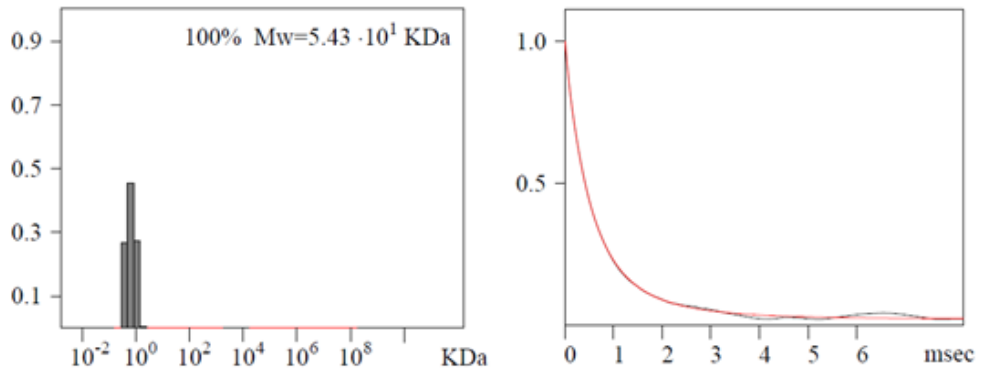

Figure 16. Distribution of the molecular weights of Zn-MINP(**4d**) and the correlation curves for DLS. The molecular weight distribution was calculated by the PRECISION DECONVOLVE program assuming the intensity of scattering is proportional to the mass of the particle squared. If each unit of building block for the Zn-MINP(**4d**) is assumed to contain one molecule of compound **1** (MW = 521 g/mol), 1.2 molecules of compound **2** (MW = 172 g/mol), one molecule of DVB (MW = 130 g/mol), 0.8 molecules of compound **3** (MW = 264 g/mol), and 0.02 molecules of compound **5** (MW = 365 g/mol), the molecular weight of Zn-MINP(**4d**) translates to 51 [= 54300/(521+1.2×172+130+0.8×264 + 0.02×365)] of such units.

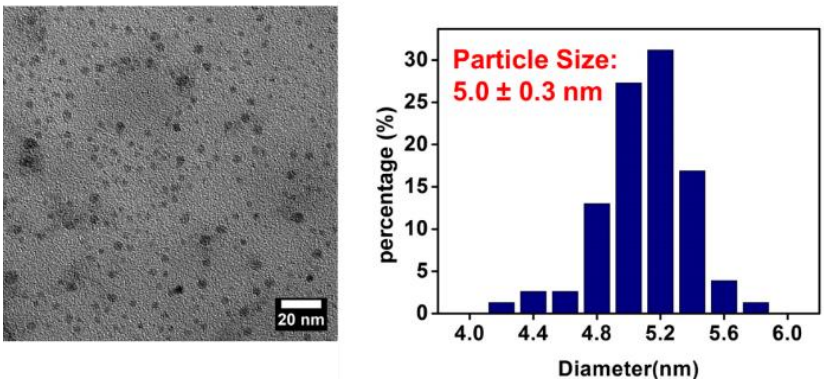

Figure 17. TEM image of typical MINPs and the distribution of size.

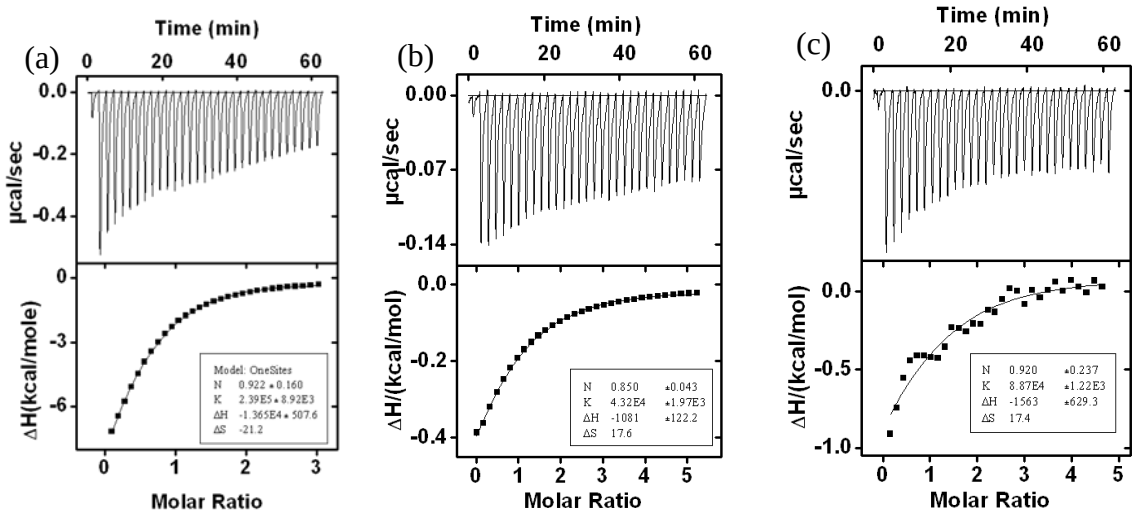

Figure 18. ITC titration curves obtained at 298 K for the binding of (a) **4a** with Zn-MINP(**4a**) (b) **4b** with Zn-MINP(**4a**) (c) **4c** with Zn-MINP(**4a**) prepared with 1 equiv. of DVB in HEPES buffer (25 mM HEPES, pH = 7). The data correspond to entries 1–3, respectively, in Table 1. The top panel shows the raw calorimetric data. The area under each peak represents the amount of heat generated at each ejection and is plotted against the molar ratio of MINP to the substrate. The solid line is the best fit of the experimental data to the sequential binding of N equal and independent binding sites on the MINP. The heat of dilution for the substrate, obtained by adding the substrate to the buffer, was subtracted from the heat released during the binding. Binding parameters were auto-generated after curve fitting using Microcal Origin 7.

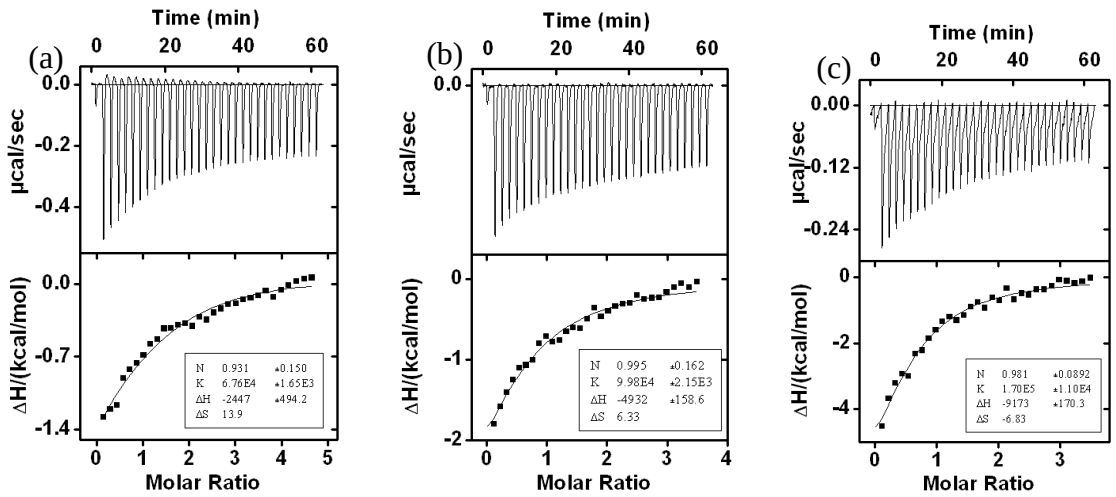

Figure 19. ITC titration curves obtained at 298 K for the binding of (a) **4d** with Zn-MINP(**4a**) (b) **4b** with Zn-MINP(**4b**) (c) **4c** with Zn-MINP(**4c**) prepared with 1 equiv. of DVB in HEPES buffer (25 mM HEPES, pH = 7). The data correspond to entries 4–6, respectively, in Table 1. The top panel shows the raw calorimetric data. The area under each peak represents the amount of heat generated at each ejection and is plotted against the molar ratio of MINP to the substrate. The solid line is the best fit of the experimental data to the sequential binding of N equal and independent binding sites on the MINP. The heat of dilution for the substrate, obtained by adding the substrate to the buffer, was subtracted from the heat released during the binding. Binding parameters were auto-generated after curve fitting using Microcal Origin 7.

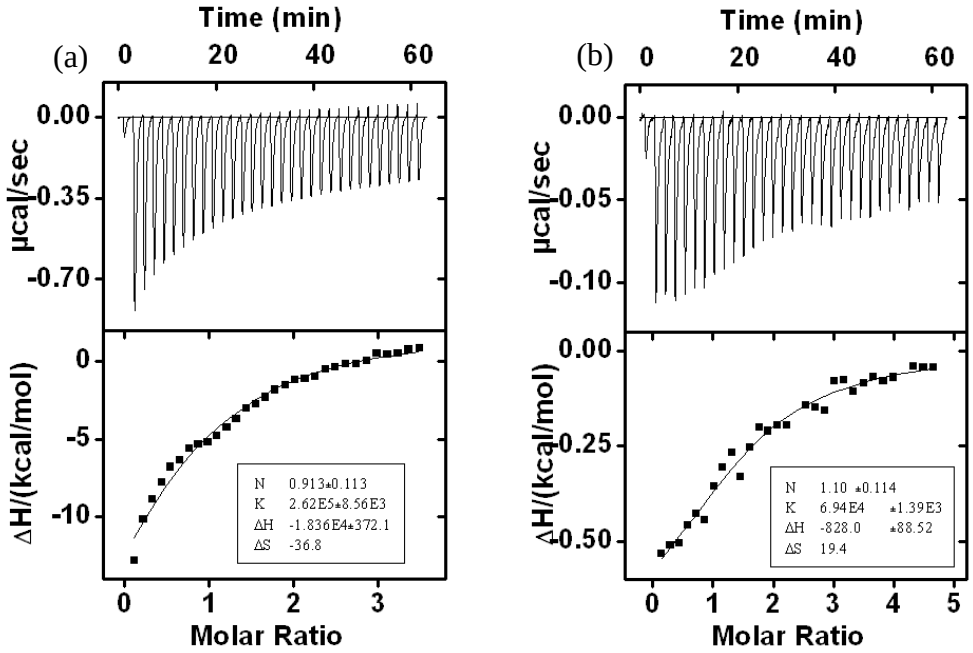

Figure 20. ITC titration curves obtained at 298 K for the binding of (a) **4d** with Zn-MINP(**4d**) (b) **4a** with Zn-MINP(**4d**) prepared with 1 equiv. of DVB in HEPES buffer (25 mM HEPES, pH = 7). The data correspond to entries 7–8, respectively, in Table 1. The top panel shows the raw calorimetric data. The area under each peak represents the amount of heat generated at each ejection and is plotted against the molar ratio of MINP to the substrate. The solid line is the best fit of the experimental data to the sequential binding of N equal and independent binding sites on the MINP. The heat of dilution for the substrate, obtained by adding the substrate to the buffer, was subtracted from the heat released during the binding. Binding parameters were auto-generated after curve fitting using Microcal Origin 7.

Table 3. Binding data for Zn-MINP in milipore water obtained by ITC.[a]

Entry	MINPs	Guest	-Δ*G* (kcal/mol)	*N*	K_a (10^4 M^{-1})	-Δ*H* (kcal/mol)	TΔ*S* (kcal/mol)
1	Zn-MINP(**4a**)	**4a**	7.3	1.1 ± 0.1	23.4 ± 1.9	2.9 ± 0.2	4.4
2	Zn-MINP(**4a**)	**4b**	6.1	1.1 ± 0.1	3.1 ± 0.1	1.8 ± 0.2	4.3
3	Zn-MINP(**4a**)	**4c**	6.6	1.0 ± 0.1	7.2 ± 0.2	1.5 ± 0.1	5.1
4	Zn-MINP(**4a**)	**4d**	6.6	1.2 ± 0.1	7.0 ± 0.4	0.3 ± 0.06	6.3
5	Zn-MINP(**4b**)	**4b**	6.8	0.9 ± 0.2	8.7 ± 0.1	0.6 ± 0.02	6.2
6	Zn-MINP(**4c**)	**4c**	7.3	1.0 ± 0.1	21.8 ± 1.8	1.1 ± 0.1	6.2
7	Zn-MINP(**4d**)	**4d**	7.3	1.0 ± 0.2	24.1 ± 0.2	1.3 ± 0.1	6.0
8	Zn-MINP(**4d**)	**4a**	6.6	1.0 ± 0.1	7.1 ± 0.1	2.6 ± 0.1	4.0

[a] The titrations were generally performed in duplicates and the errors between the runs were <10%. *N* was the number of binding site per nanoparticle.

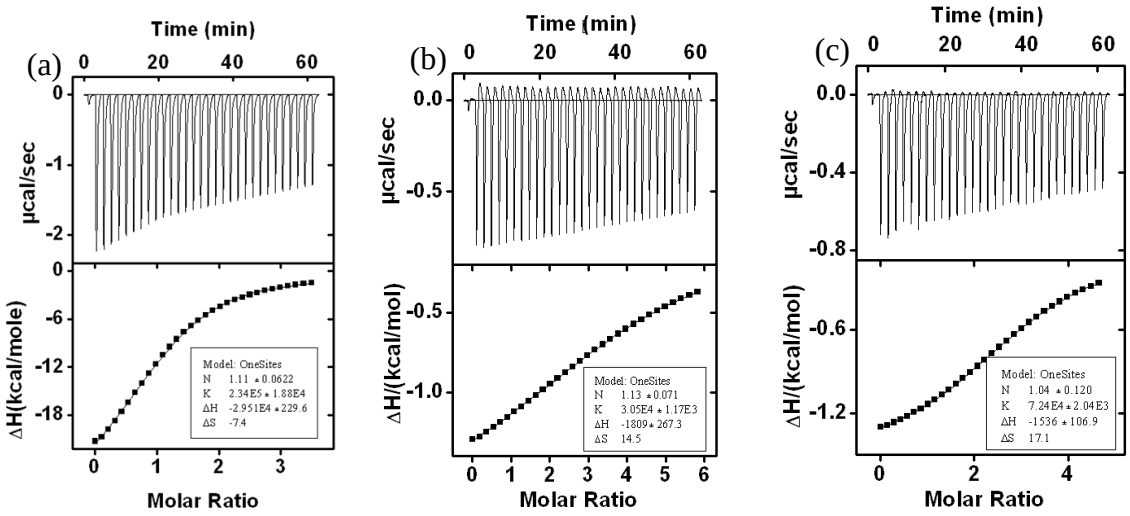

Figure 21. ITC titration curves obtained at 298 K for the binding of (a) **4a** with Zn-MINP(**4a**) (b) **4b** with Zn-MINP(**4a**) (c) **4c** with Zn-MINP(**4a**) prepared with 1 equiv. of DVB in millipore water. The data correspond to entries 1–3, respectively, in Table S1. The top panel shows the raw calorimetric data. The area under each peak represents the amount of heat generated at each ejection and is plotted against the molar ratio of MINP to the substrate. The solid line is the best fit of the experimental data to the sequential binding of N equal and independent binding sites on the MINP. The heat of dilution for the substrate, obtained by

adding the substrate to the buffer, was subtracted from the heat released during the binding. Binding parameters were auto-generated after curve fitting using Microcal Origin 7.

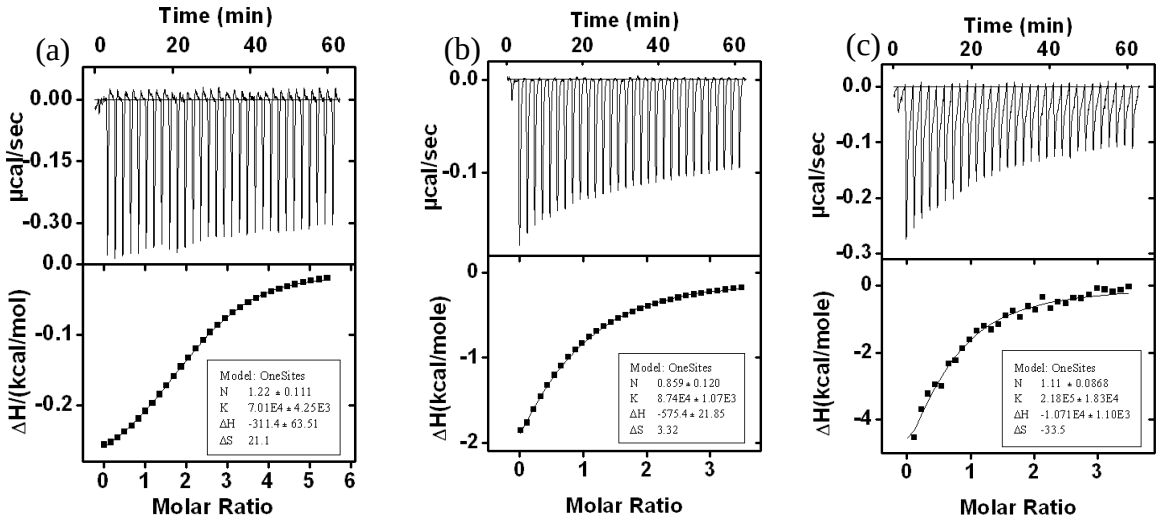

Figure 22. ITC titration curves obtained at 298 K for the binding of (a) **4d** with Zn-MINP(**4a**) (b) **4b** with Zn-MINP(**4b**) (c) **4c** with Zn-MINP(**4c**) prepared with 1 equiv. of DVB in millipore water. The data correspond to entries 4–6, respectively, in Table S1. The top panel shows the raw calorimetric data. The area under each peak represents the amount of heat generated at each ejection and is plotted against the molar ratio of MINP to the substrate. The solid line is the best fit of the experimental data to the sequential binding of N equal and independent binding sites on the MINP. The heat of dilution for the substrate, obtained by adding the substrate to the buffer, was subtracted from the heat released during the binding. Binding parameters were auto-generated after curve fitting using Microcal Origin 7.

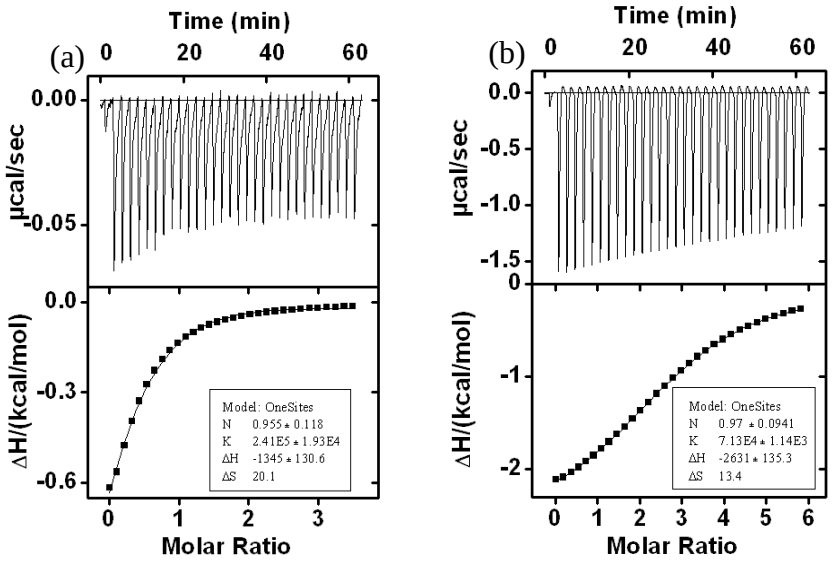

Figure 23. ITC titration curves obtained at 298 K for the binding of (a) **4d** with Zn-MINP(**4d**) (b) **4a** with Zn-MINP(**4d**) prepared with 1 equiv. of DVB in water. The data correspond to entries 7 and 8, respectively, in Table S1. The top panel shows the raw calorimetric data. The area under each peak represents the amount of heat generated at each ejection and is plotted against the molar ratio of MINP to the substrate. The solid line is the best fit of the experimental data to the sequential binding of N equal and independent binding sites on the MINP. The heat of dilution for the substrate, obtained by adding the substrate to the buffer, was subtracted from the heat released during the binding. Binding parameters were auto-generated after curve fitting using Microcal Origin 7.

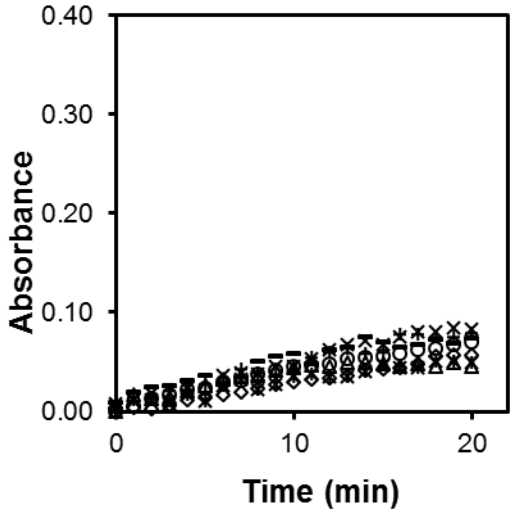

Figure 24. Absorbance at 400 nm as a function of time for the hydrolysis of PNPH in a 25 mM HEPES buffer (pH 7.0) at 40 °C. The data sets correspond to hydrolysis catalyzed by Zn-MINP(**4a**) by adding 0.0 equiv. (o), 0.25 equiv.(-), 0.50 equiv.(+), 1.00 equiv.(×), 5.00 equiv.(Δ), 10.0 equiv.(*) and 20.0 equiv.(◇) of $Zn(ClO_4)_2.6H_2O$. [PNPH] = 40 µM. [catalyst] = 8 µM.

Table 4. Kinetic data for the hydrolysis of PNPH by Zn-MINP (**4a**) in 25 mM HEPES buffer (pH 7.0).[a]

Entry	Amount of Zn Salt (µM)	k ($\times 10^{-4}$ s^{-1})
1	0.0	1.21 ± 0.11
2	2.0	1.30 ± 0.16
3	4.0	1.26 ± 0.08
4	8.0	1.31 ± 0.16
5	40	1.22 ± 0.15
6	80	0.96 ± 0.12
7	160	0.84 ± 0.11

[a] Reaction rates were measured in 25 mM HEPES buffer at 40 °C and pH 7.0. [PNPH] = 40 µM. [catalyst] = 8.0 µM unless otherwise indicated.

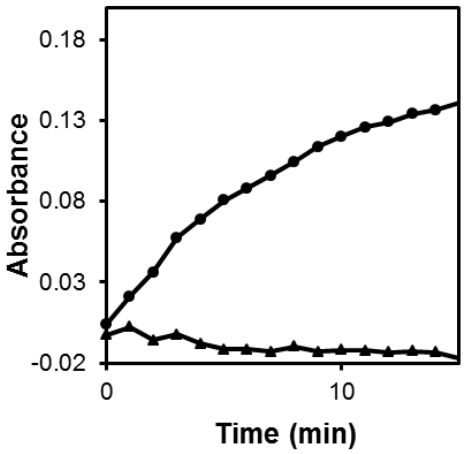

Figure 25. Absorbance at 400 nm as a function of time for the hydrolysis of **6** (▲) in comparison to PNPH (●) in a 25 mM HEPES buffer (pH 7.0) at 40 °C. The small, negative change of absorption in **6** presumably was caused by the scattering of UV light by the phase-separated ester starting material due to is hydrophobicity. [Substrate] = 40 μM. [catalyst] = 8 μM.

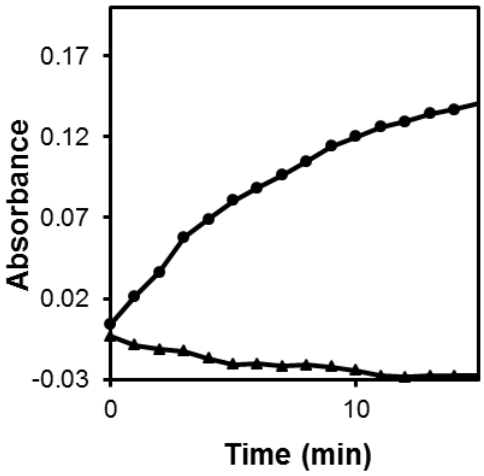

Figure 26. Absorbance at 400 nm as a function of time for the hydrolysis of **7** (▲) in comparison to PNPH (●) in a 25 mM HEPES buffer (pH 7.0) at 40 °C. The small, negative change of absorption in **7** presumably was caused by the scattering of UV light by the phase-separated ester starting material due to is hydrophobicity. [Substrate] = 40 μM. [catalyst] = 8 μM.

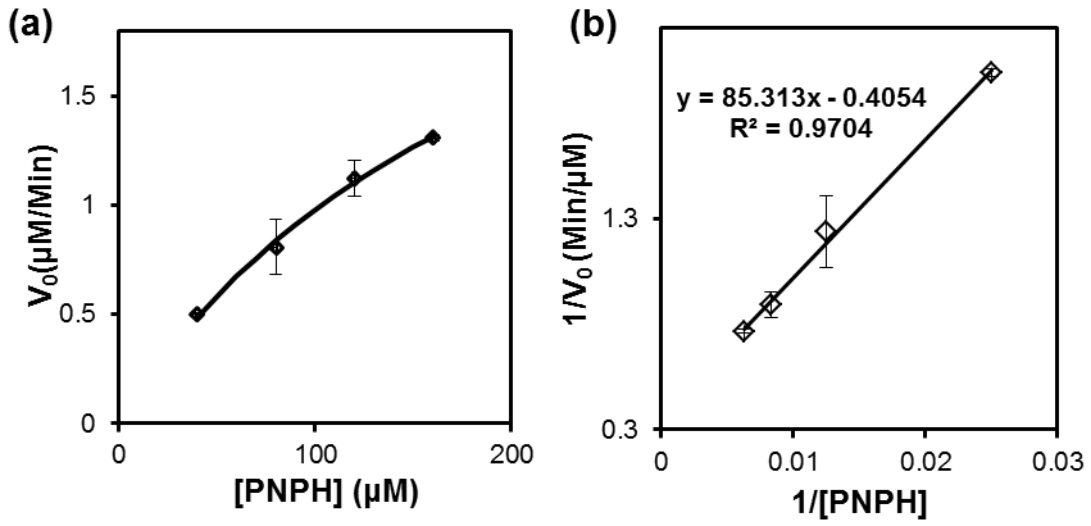

Figure 27. (a) Michaelis-Menten plot of the hydrolysis of PNPH by Zn-MINP (**4a**). (b) Double-reciprocal plot (Lineweaver-Burk) of the hydrolysis of PNPA by Zn-MINP (**4a**) in a 25 mM HEPES buffer at 40 °C and pH 7.0. [MINP] = 40 μM.

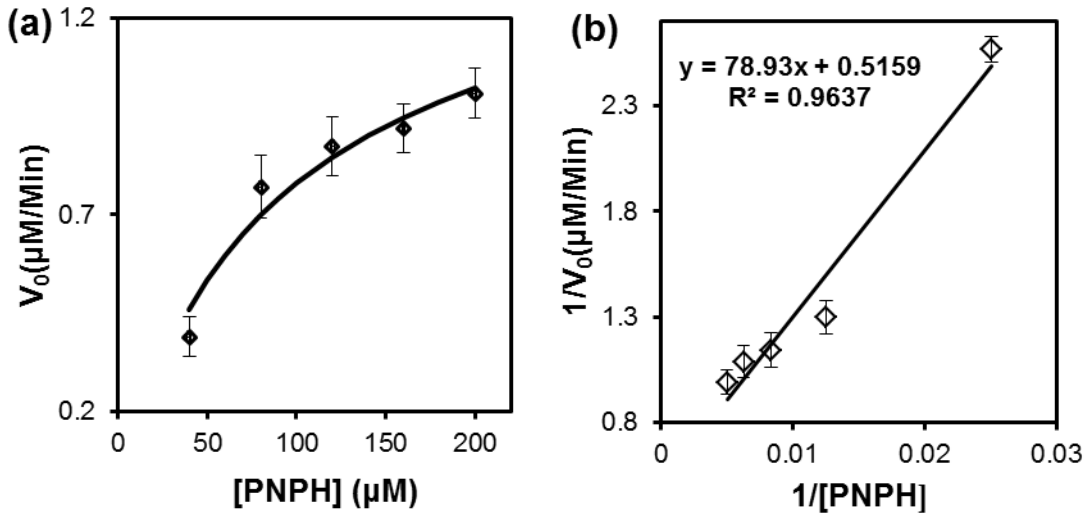

Figure 28. (a) Michaelis-Menten plot of the hydrolysis of PNPH by Zn-MINP (**4a**). (b) Double-reciprocal plot (Lineweaver-Burk) of the hydrolysis of PNPA by Zn-MINP (**4a**) in a 25 mM HEPES buffer at 40 ° C and pH 7.5. [MINP] = 40 μM.

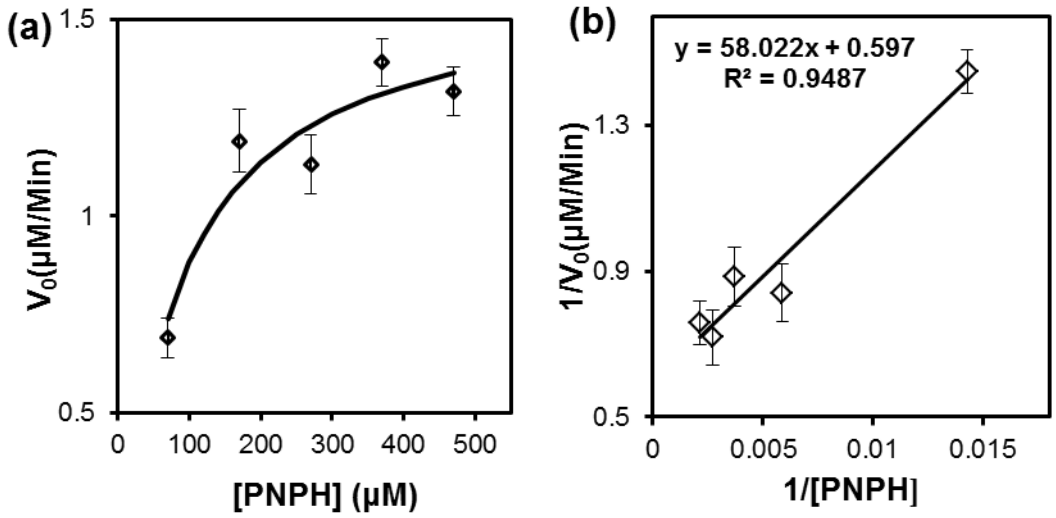

Figure 29. (a) Michaelis-Menten plot of the hydrolysis of PNPH by Zn-MINP (**4a**). (b) Double-reciprocal plot (Lineweaver-Burk) of the hydrolysis of PNPA by Zn-MINP (**4a**) in a 25 mM HEPES buffer at 40 ° C and pH 8.0. [MINP] = 40 μM.

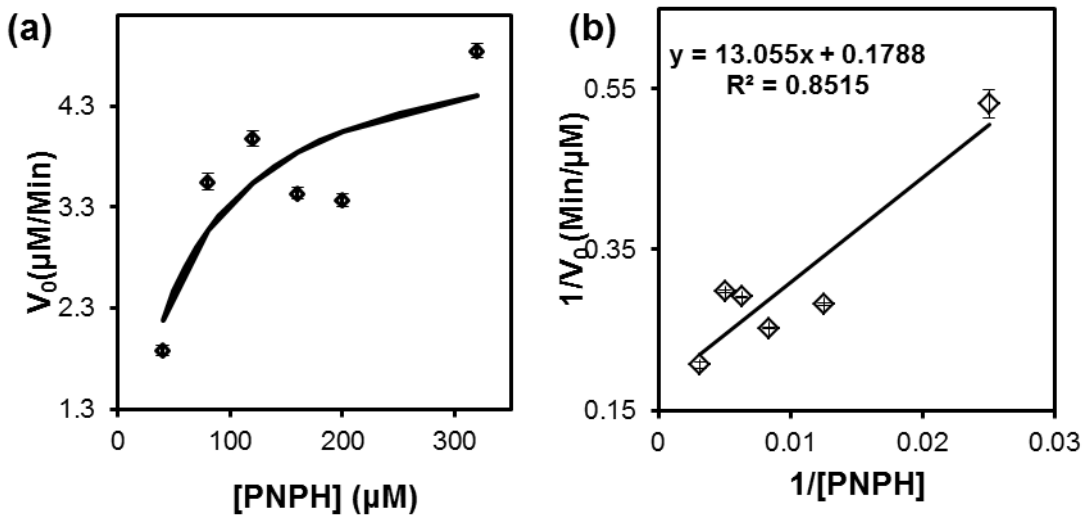

Figure 30. (a) Michaelis-Menten plot of the hydrolysis of PNPH by Zn-MINP (**4a**). (b) Double-reciprocal plot (Lineweaver-Burk) of the hydrolysis of PNPA by Zn-MINP (**4a**) in a 25 mM HEPES buffer at 40 °C and pH 8.5. [MINP] = 40 μM.

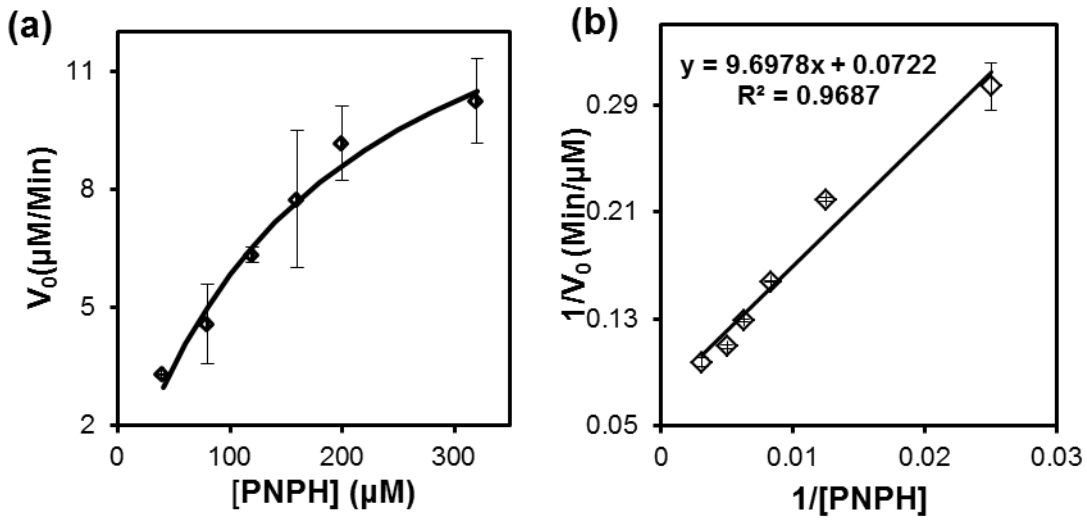

Figure 31. (a) Michaelis-Menten plot of the hydrolysis of PNPH by Zn-MINP (**4a**). (b) Double-reciprocal plot (Lineweaver-Burk) of the hydrolysis of PNPA by Zn-MINP (**4a**) in a 25 mM HEPES buffer at 40 °C and pH 9.5. [MINP] = 40 μM.

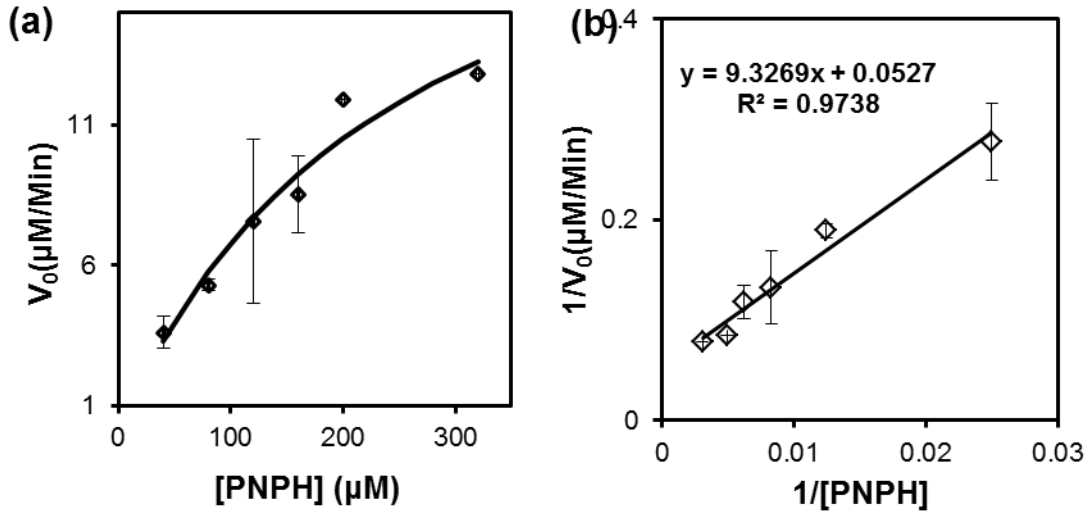

Figure 32. **(**a) Michaelis-Menten plot of the hydrolysis of PNPH by Zn-MINP (**4a**). (b) Double-reciprocal plot (Lineweaver-Burk) of the hydrolysis of PNPA by Zn-MINP (**4a**) in a 25 mM HEPES buffer at 40 °C and pH 10.0. [MINP] = 40 μM.

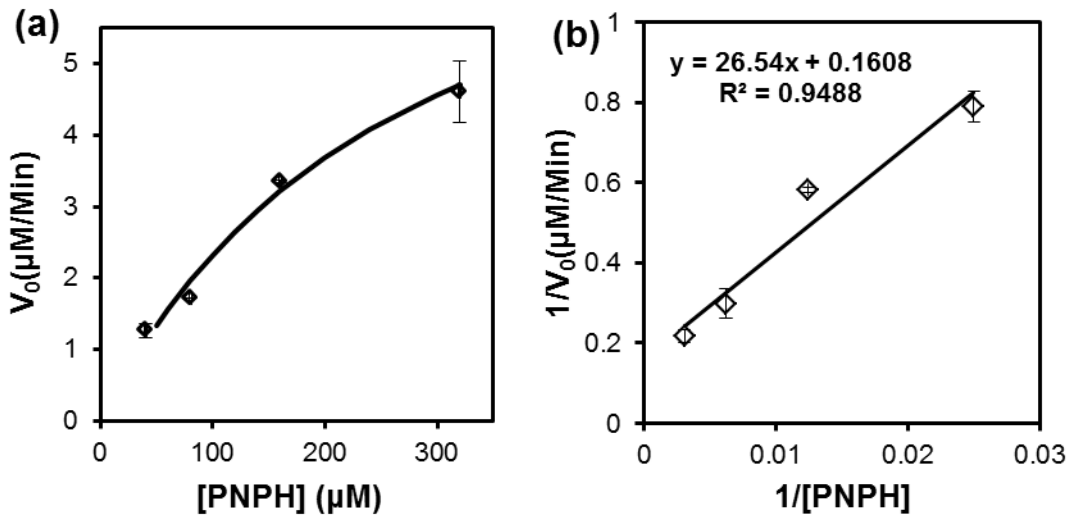

Figure 33. **(**a) Michaelis-Menten plot of the hydrolysis of PNPH by Zn-MINP (**4a/11**). (b) Double-reciprocal plot (Lineweaver-Burk) of the hydrolysis of PNPA by Zn-MINP (**4a/11**) in a 25 mM HEPES buffer at 40 °C and pH 8.0. [MINP] = 40 μM.

Table 5**.** Michaelis-Menten parameters for the hydrolysis of PNPH catalyzed by Zn-MINP(**4a**) at different pHs.[a]

Entry	pH	V_{max} (× 10^{-7} M/s)	K_m (mM)	k_{cat} (× 10^{-3} s^{-1})	k_{cat}/K_m ($M^{-1}s^{-1}$)
1	7	0.51 ± 0.04	0.21 ± 0.03	6.33	30
2	7.5	0.25 ± 0.03	0.09 ± 0.02	3.06	34
3	8.0	0.27 ± 0.02	0.08 ± 0.02	3.33	42
4	8.5	0.86 ± 0.12	0.06 ± 0.01	10.73	179
5	9.5	2.75 ± 0.25	0.18 ± 0.03	34.39	191
6	10	3.90 ± 0.71	0.25± 0.07	48.70	195
7	8[b]	1.46 ± 0.21	0.27 ± 0.07	18.29	68

[a] The hydrolysis was catalyzed by [Zn-MINP(**4a**)] in 25 mM HEPES buffer at 40 °C unless indicated otherwise. [Zn-MINP(**4a**)] = 8.0 μM. [b] The hydrolysis was catalyzed by [Zn-MINP(**4a/11**)] = 8.0 μM 25 mM HEPES buffer (pH 8.0) at 40 °C.

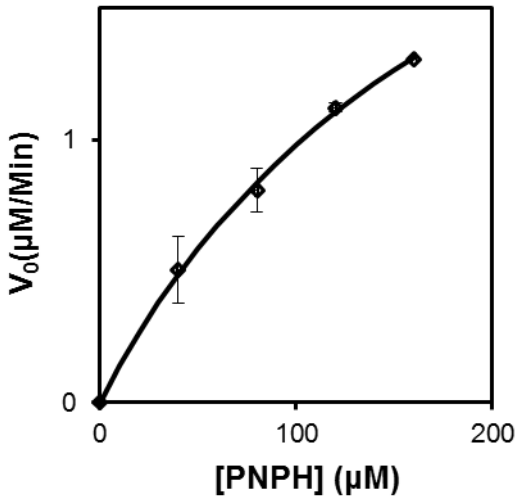

Figure 34. Michaelis-Menten plot of the hydrolysis of PNPH by Zn-MINP (**4a**) in a 25 mM HEPES buffer at 40 °C and pH 7.0. [MINP] = 8.0 μM.

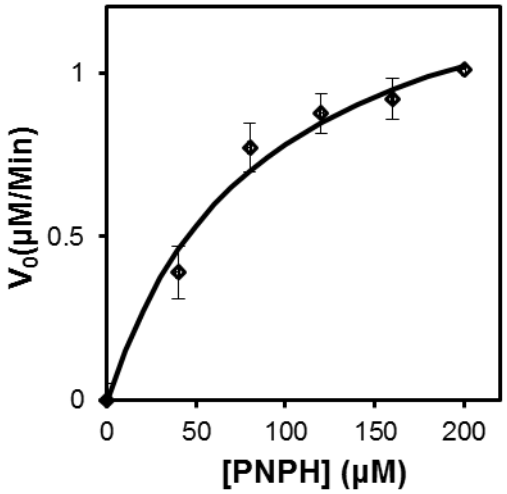

Figure 35. Michaelis-Menten plot of the hydrolysis of PNPH by Zn-MINP (**4a**) in a 25 mM HEPES buffer at 40 °C and pH 7.5. [MINP] = 8.0 μM.

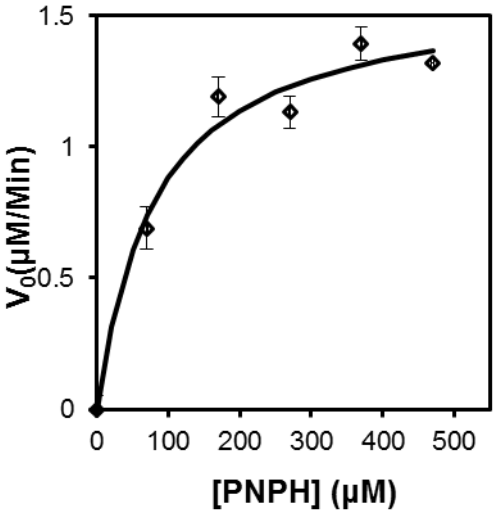

Figure 36. Michaelis-Menten plot of the hydrolysis of PNPH by Zn-MINP (**4a)** in a 25 mM HEPES buffer at 40 °C and pH 8.0. [MINP] = 8.0 μM.

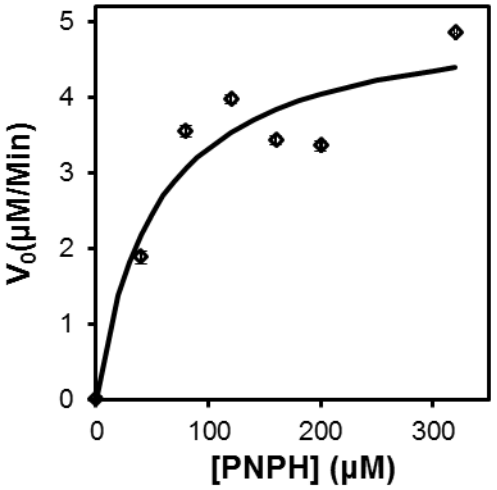

Figure 37. Michaelis-Menten plot of the hydrolysis of PNPH by Zn-MINP (**4a**) in a 25 mM HEPES buffer at 40 °C and pH 8.5. [MINP] = 8.0 μM.

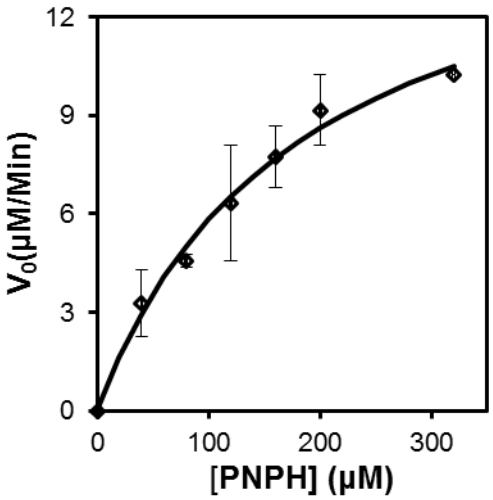

Figure 38. Michaelis-Menten plot of the hydrolysis of PNPH by Zn-MINP (**4a**) in a 25 mM HEPES buffer at 40 °C and pH 9.5. [MINP] = 8.0 μM.

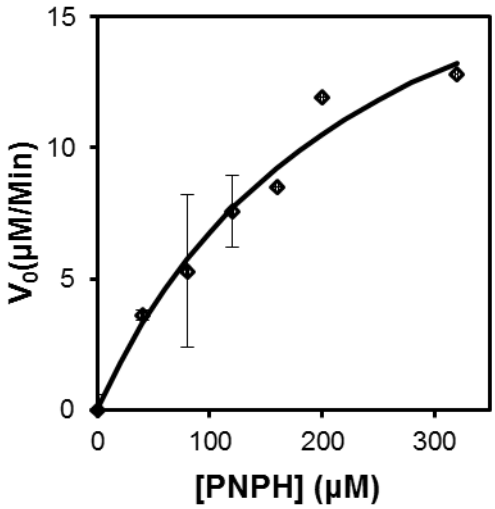

Figure 39. Michaelis-Menten plot of the hydrolysis of PNPH by MINP-Zn^{2+}-(**4a**) in a 25 mM HEPES buffer at 40 °C and pH 10.0. [MINP] = 8.0 μM.

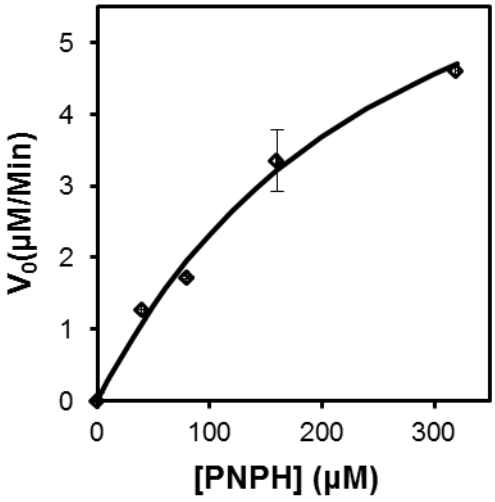

Figure 40. Michaelis-Menten plot of the hydrolysis of PNPH by Zn-MINP (**4a/11**) in a 25 mM HEPES buffer at 40 °C and pH 8.0. [MINP] = 40 μM.

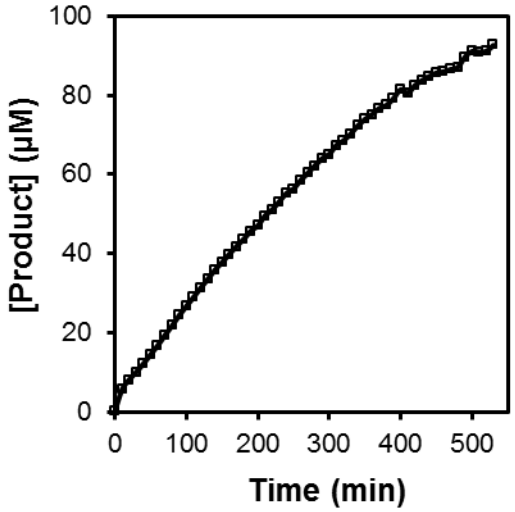

Figure 41. Amount of *p*-nitrophenoxide formed as a function of time in a 25 mM HEPEs buffer (pH 7.0) at 40 °C, after addition of 0.2 μM Zn-MINP(**4a**), calculated based on an extinction coefficient of ε_{400} = 0.0091 μM^{-1} cm^{-1}.

^{1}H NMR spectrum of compound **12**

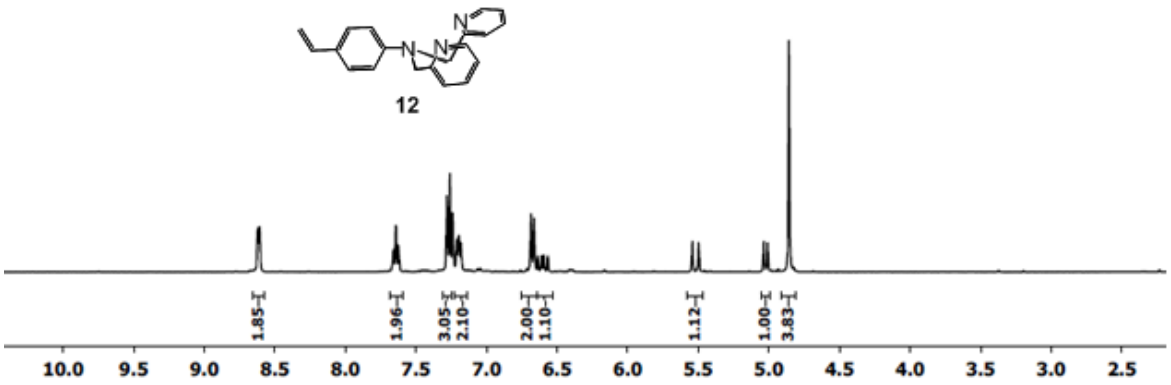

^{13}C NMR spectrum of compound **12**

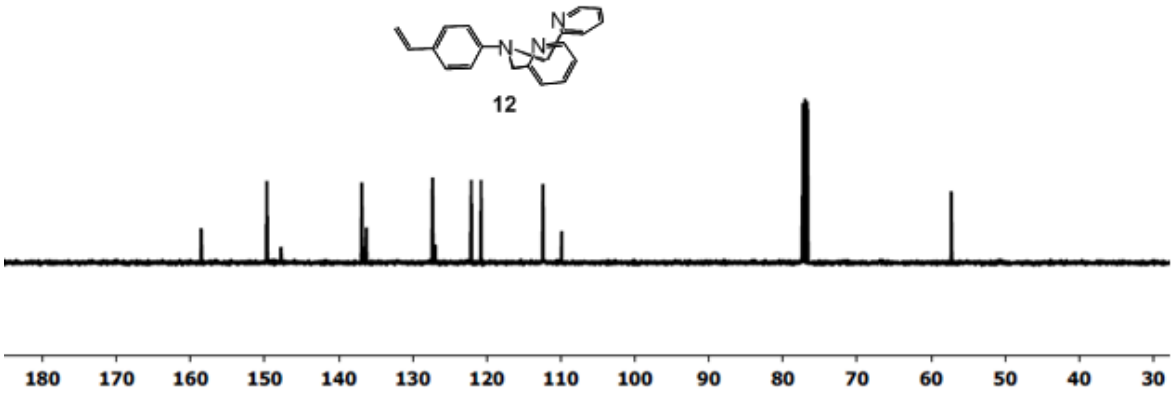

^{1}H NMR spectrum of compound **5** &**12**

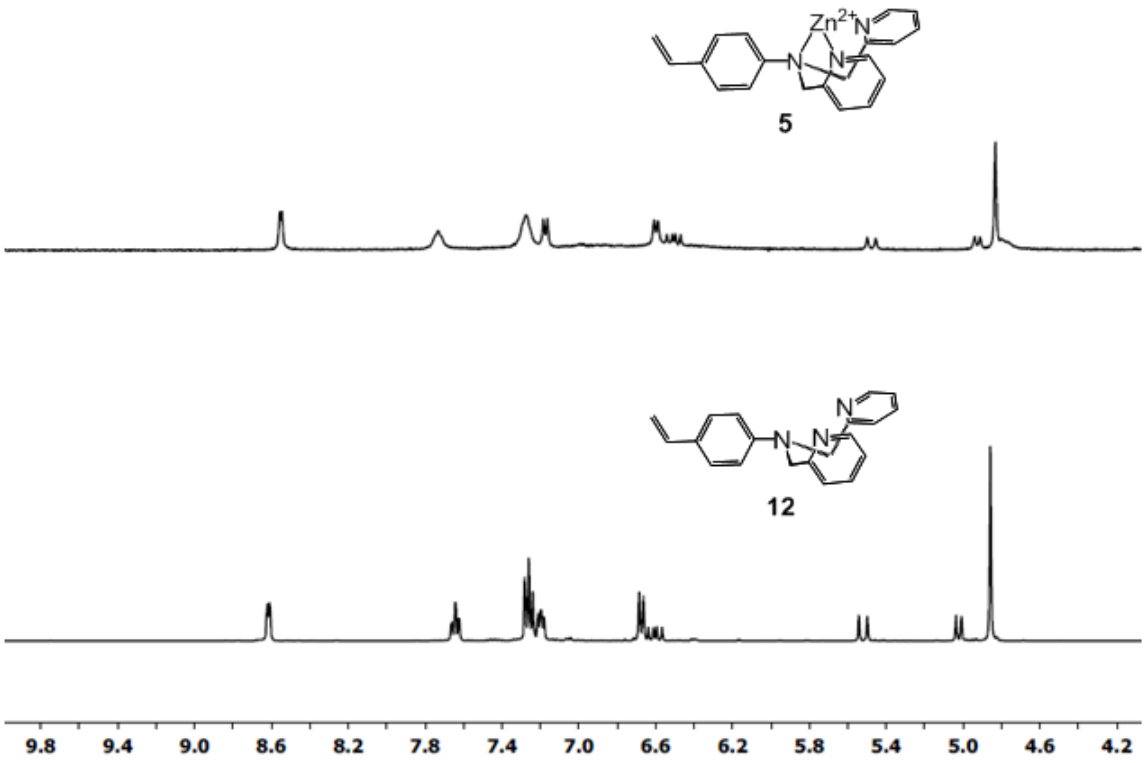

^{1}H NMR spectrum of compound **4a**

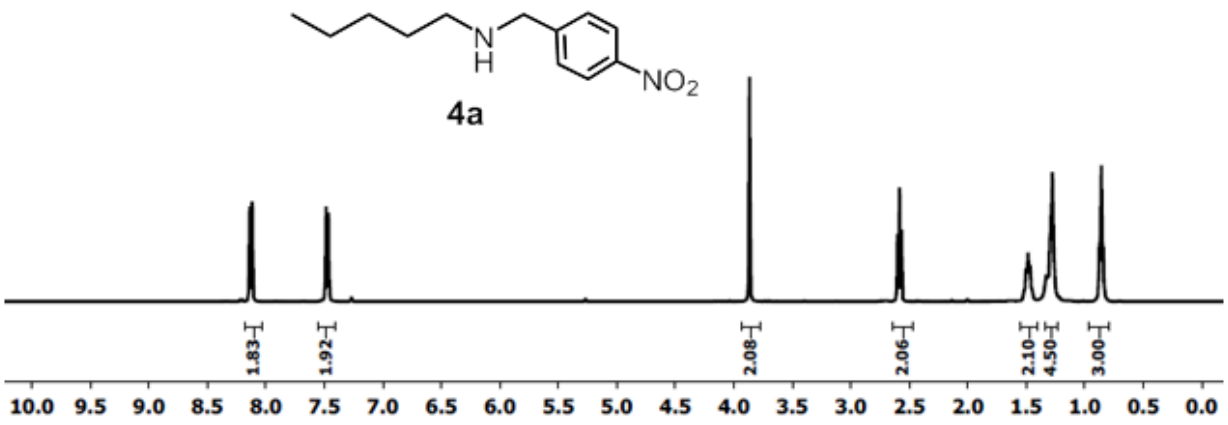

^{13}C NMR spectrum of compound **4a**

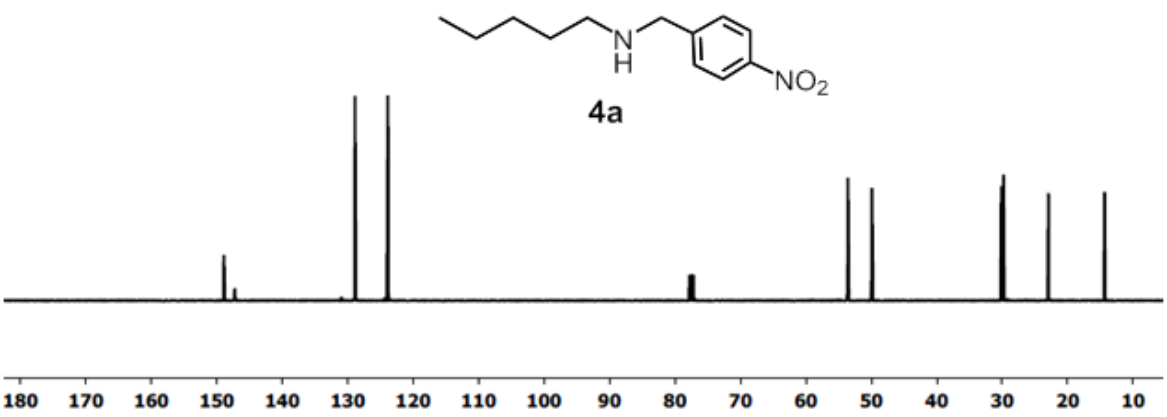

^{1}H NMR spectrum of compound **4b**

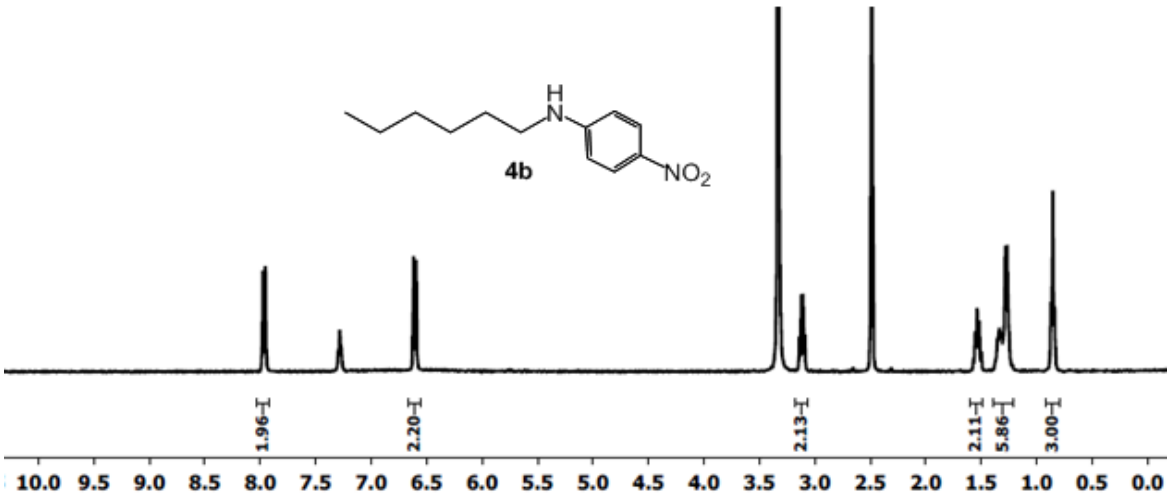

^{13}C NMR spectrum of compound **4b**

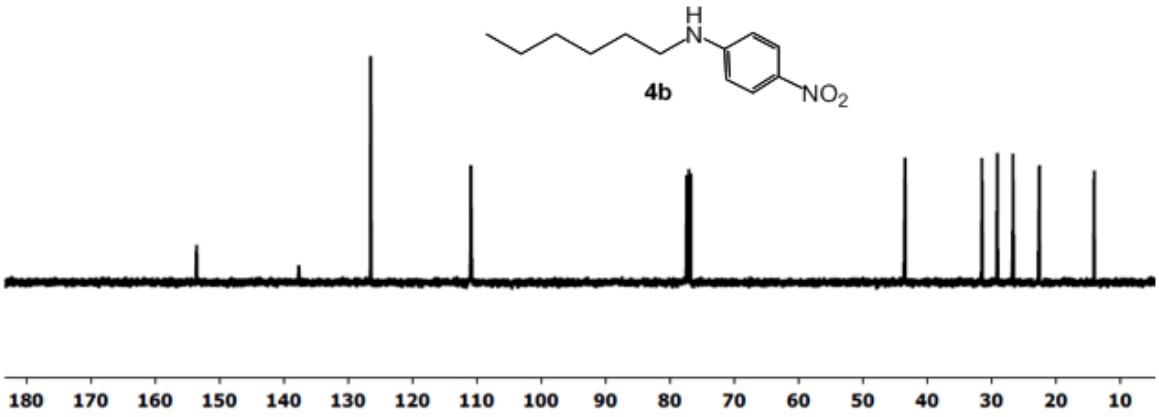

^{1}H NMR spectrum of compound **4c**

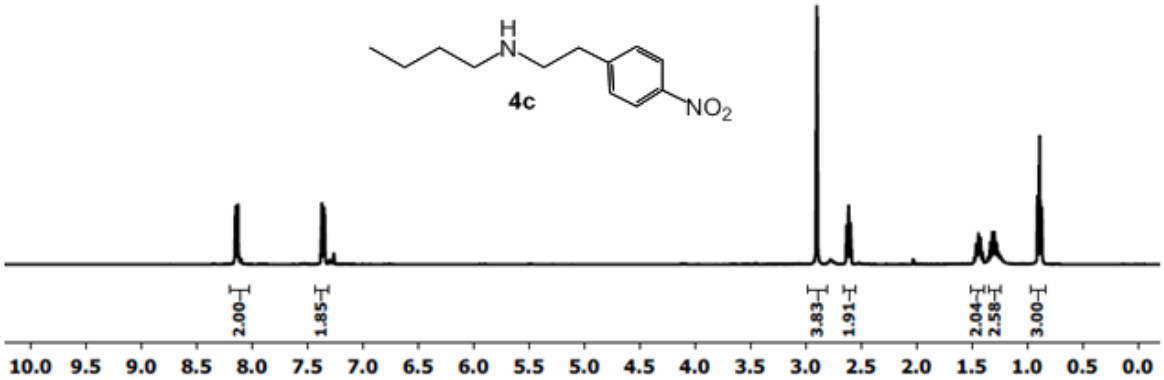

^{13}C NMR spectrum of compound **4c**

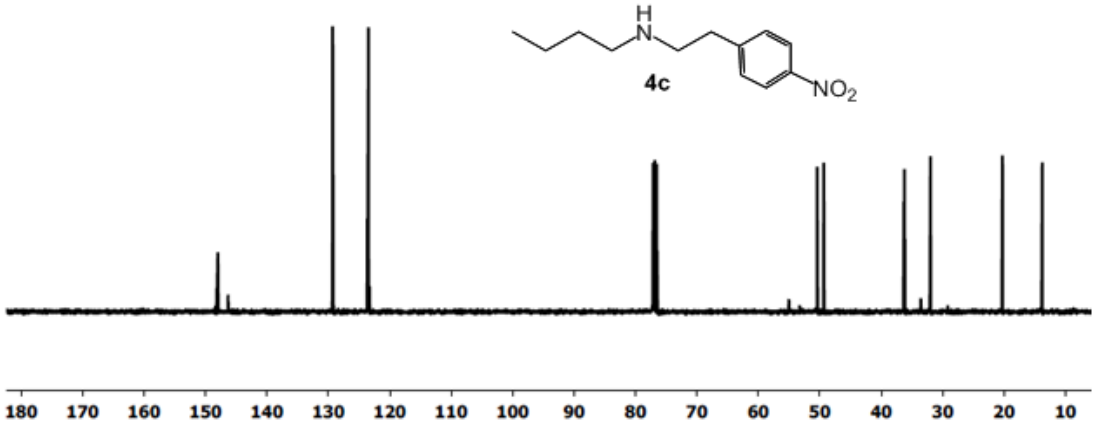

^{1}H NMR spectrum of compound **4d**

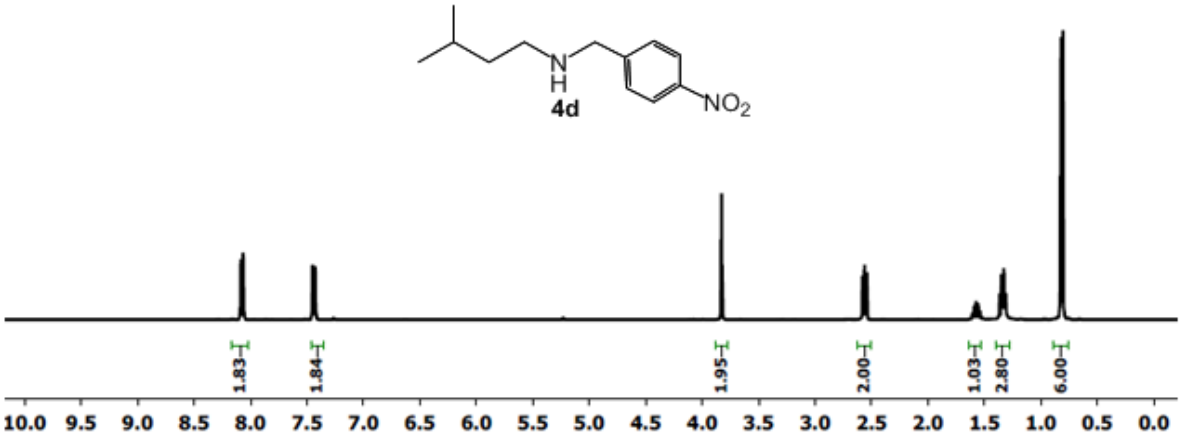

^{13}C NMR spectrum of compound **4d**

^{1}H NMR spectrum of compound **PNPH**

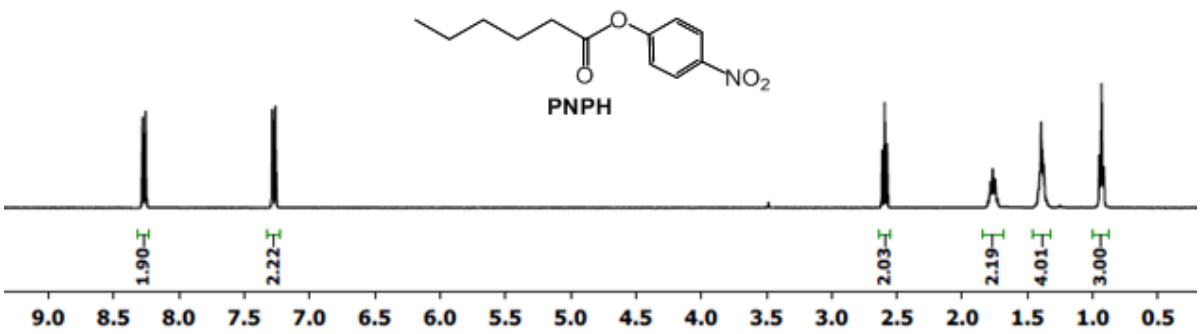

^{1}H NMR spectrum of compound **6**

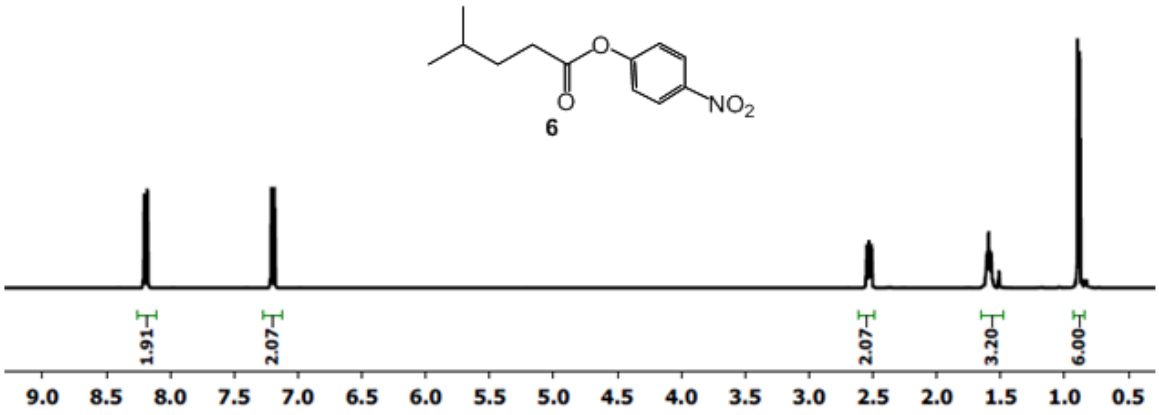

^{13}C NMR spectrum of compound **6**

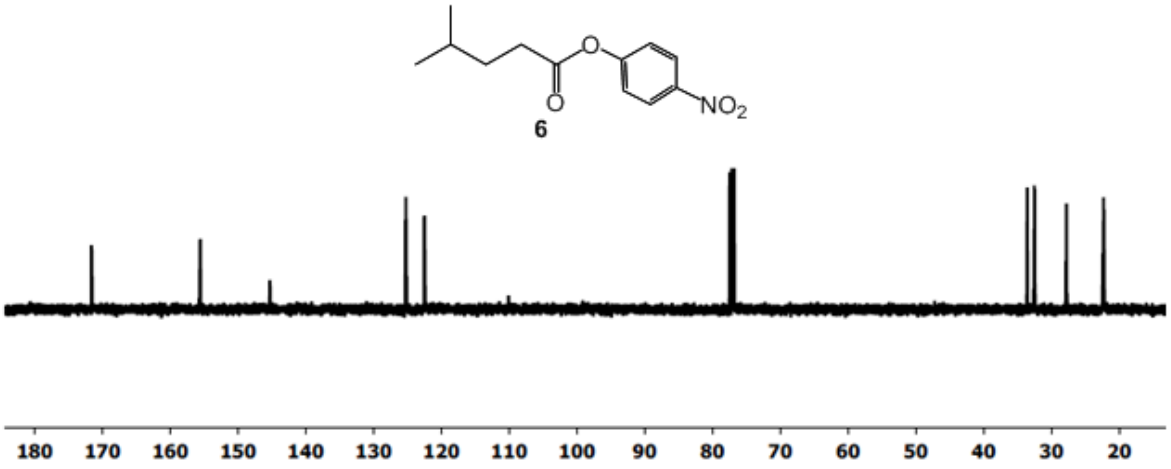

^{1}H NMR spectrum of compound **7**

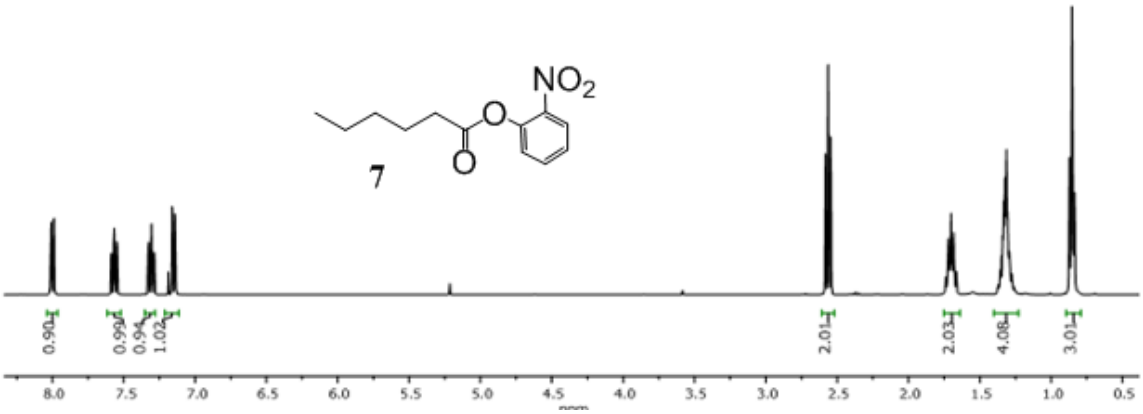

^{13}C NMR spectrum of compound **7**

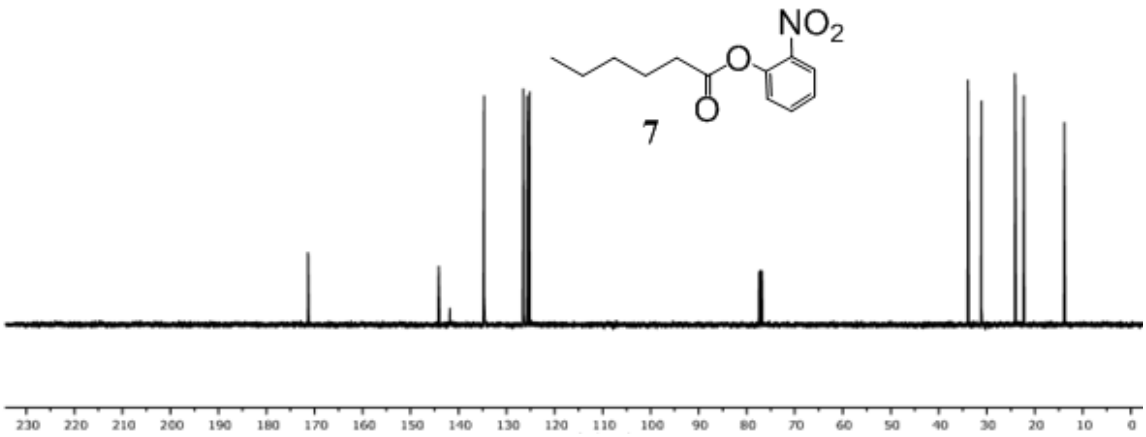

^{1}H NMR spectrum of compound **9**

^{13}C NMR spectrum of compound **9**

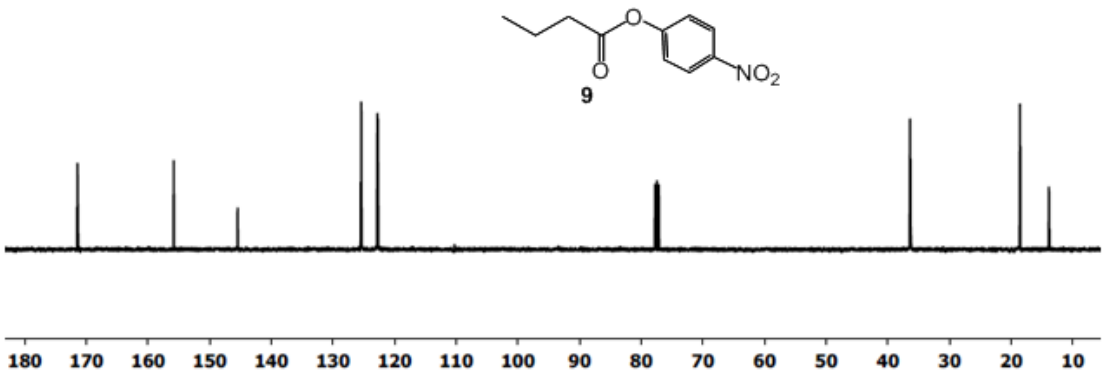

^{1}H NMR spectrum of compound **10**

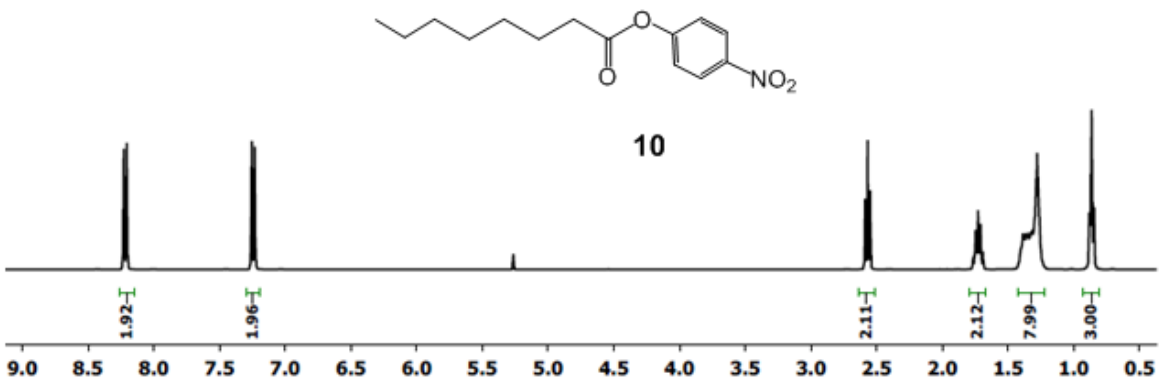

^{13}C NMR spectrum of compound **10**

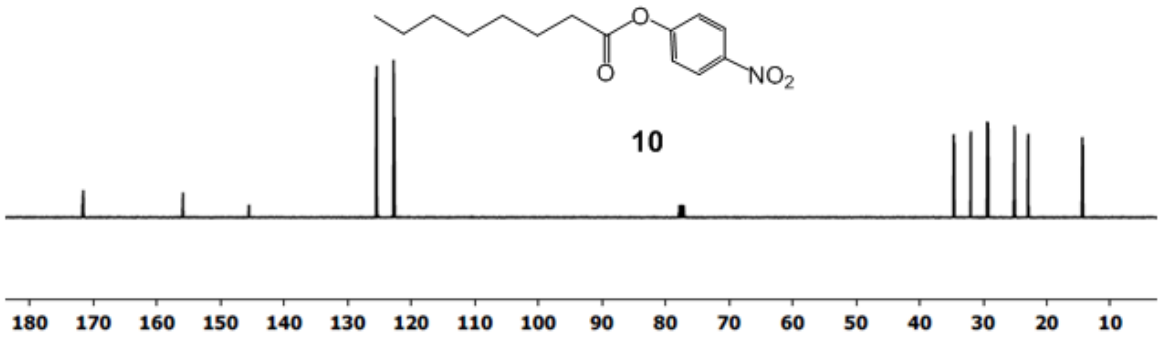

^{1}H NMR spectrum of compound **15**

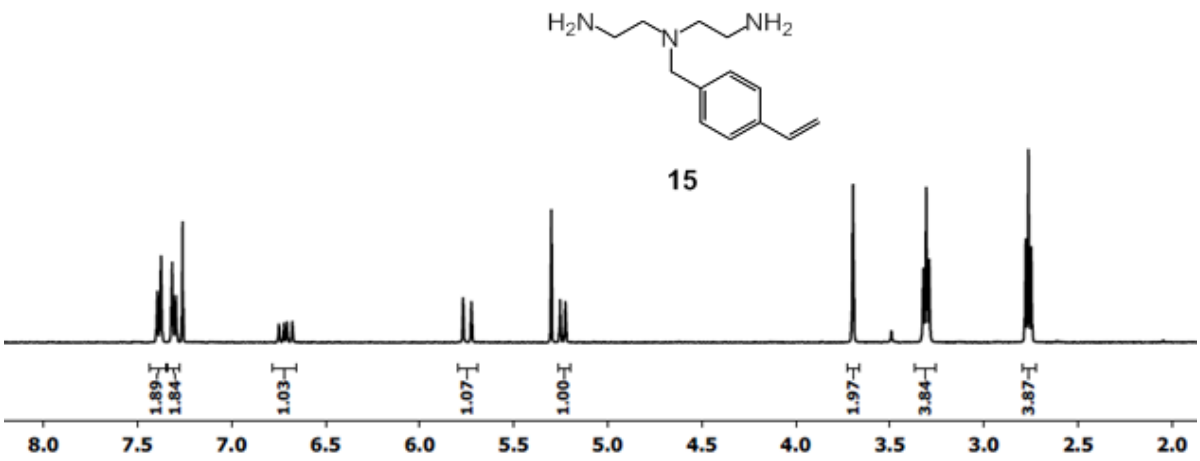

^{13}C NMR spectrum of compound **15**

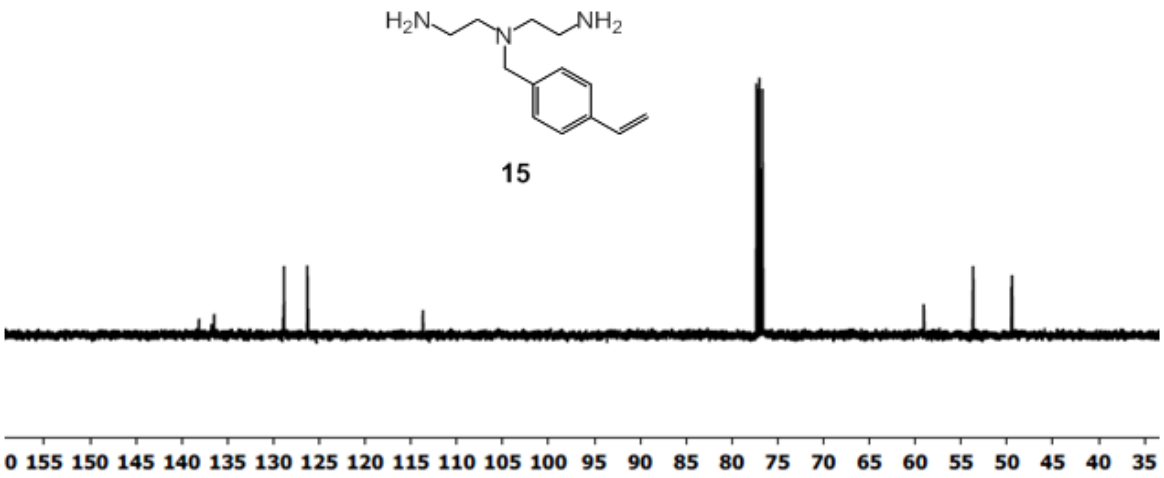

^{1}H NMR spectrum of compound **11**

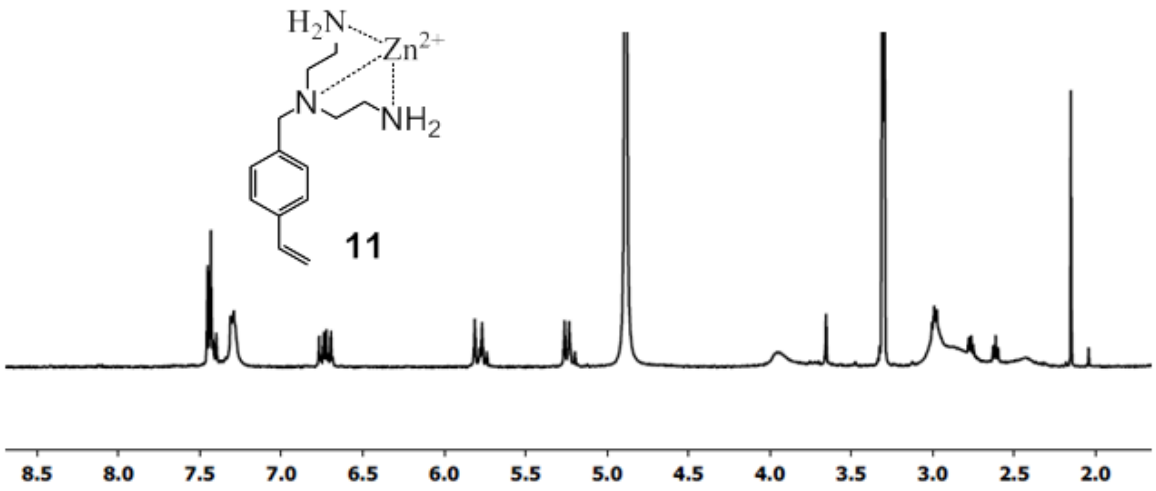

References

(1) Auld, D. S.: In *Encylopedia of Inorganic Chemistry, 2nd Ed.*; King, R. B., Ed.; Wiley: New York, 2007; pp 5885-5927.

(2) Vallee, B. L.; Auld, D. S. Zinc: Biological Functions and Coordination Motifs. *Acc. Chem. Res.* **1993**, *26*, 543-551.

(3) Vallee, B. L.; Auld, D. S. Zinc Coordination, Function, and Structure of Zinc Enzymes and Other Proteins. *Biochemistry* **1990**, *29*, 5647-5659.

(4) Coleman, J. E. Zinc Enzymes. *Curr. Opin. Chem. Biol.* **1998**, *2*, 222-234.

(5) Parkin, G. Synthetic Analogues Relevant to the Structure and Function of Zinc Enzymes. *Chem. Rev.* **2004**, *104*, 699-768.

(6) Kimura, E.; Hashimoto, H.; Koike, T. Hydrolysis of Lipophilic Esters Catalyzed by a Zinc(II) Complex of a Long Alkyl-Pendant Macrocyclic Tetraamine in Micellar Solution. *J. Am. Chem. Soc.* **1996**, *118*, 10963-10970.

(7) Vahrenkamp, H. Transitions, Transition States, Transition State Analogues: Zinc Pyrazolylborate Chemistry Related to Zinc Enzymes. *Acc. Chem. Res.* **1999**, *32*, 589-596.

(8) Zastrow, M. L.; Peacock, A. F. A.; Stuckey, J. A.; Pecoraro, V. L. Hydrolytic Catalysis and Structural Stabilization in a Designed Metalloprotein. *Nat. Chem.* **2012**, *4*, 118-123.

(9) Der, B. S.; Edwards, D. R.; Kuhlman, B. Catalysis by a De Novo Zinc-Mediated Protein Interface: Implications for Natural Enzyme Evolution and Rational Enzyme Engineering. *Biochemistry* **2012**, *51*, 3933-3940.

(10) Zastrow, M. L.; Pecoraro, V. L. Influence of Active Site Location on Catalytic Activity in De Novo-Designed Zinc Metalloenzymes. *J. Am. Chem. Soc.* **2013**, *135*, 5895-5903.

(11) Song, W. J.; Tezcan, F. A. A Designed Supramolecular Protein Assembly with in Vivo Enzymatic Activity. *Science* **2014**, *346*, 1525-1528.

(12) Rufo, C. M.; Moroz, Y. S.; Moroz, O. V.; Stohr, J.; Smith, T. A.; Hu, X. Z.; DeGrado, W. F.; Korendovych, I. V. Short Peptides Self-Assemble to Produce Catalytic Amyloids. *Nat. Chem.* **2014**, *6*, 303-309.

(13) Burton, A. J.; Thomson, A. R.; Dawson, W. M.; Brady, R. L.; Woolfson, D. N. Installing Hydrolytic Activity into a Completely De Novo Protein Framework. *Nat. Chem.* **2016**, *8*, 837-844.

(14) Awino, J. K.; Zhao, Y. Protein-Mimetic, Molecularly Imprinted Nanoparticles for Selective Binding of Bile Salt Derivatives in Water. *J. Am. Chem. Soc.* **2013**, *135*, 12552-12555.

(15) Wulff, G. Enzyme-Like Catalysis by Molecularly Imprinted Polymers. *Chem. Rev.* **2001**, *102*, 1-28.

(16) Wulff, G.; Liu, J. Design of Biomimetic Catalysts by Molecular Imprinting in Synthetic Polymers: The Role of Transition State Stabilization. *Acc. Chem. Res.* **2012**, *45*, 239-247.

(17) Emgenbroich, M.; Wulff, G. A New Enzyme Model for Enantioselective Esterases Based on Molecularly Imprinted Polymers. *Chem.-Eur. J.* **2003**, *9*, 4106-4117.

(18) Maddock, S. C.; Pasetto, P.; Resmini, M. Novel Imprinted Soluble Microgels with Hydrolytic Catalytic Activity. *Chem. Commun.* **2004**, 536-537.

(19) Liu, J.-q.; Wulff, G. Functional Mimicry of Carboxypeptidase a by a Combination of Transition State Stabilization and a Defined Orientation of Catalytic Moieties in Molecularly Imprinted Polymers. *J. Am. Chem. Soc.* **2008**, *130*, 8044-8054.

(20) Carboni, D.; Flavin, K.; Servant, A.; Gouverneur, V.; Resmini, M. The First Example of Molecularly Imprinted Nanogels with Aldolase Type I Activity. *Chem. -Eur. J.* **2008**, *14*, 7059-7065.

(21) Kirsch, N.; Hedin-Dahlström, J.; Henschel, H.; Whitcombe, M. J.; Wikman, S.; Nicholls, I. A. Molecularly Imprinted Polymer Catalysis of a Diels-Alder Reaction. *J. Mol. Catal. B: Enzym.* **2009**, *58*, 110-117.

(22) Chen, Z. Y.; Xu, L.; Liang, Y.; Zhao, M. P. Ph-Sensitive Water-Soluble Nanospheric Imprinted Hydrogels Prepared as Horseradish Peroxidase Mimetic Enzymes. *Adv. Mater.* **2010**, *22*, 1488-1492.

(23) Servant, A.; Haupt, K.; Resmini, M. Tuning Molecular Recognition in Water-Soluble Nanogels with Enzyme-Like Activity for the Kemp Elimination. *Chem.-Eur. J.* **2011**, *17*, 11052-11059.

(24) Shen, X.; Huang, C.; Shinde, S.; Jagadeesan, K. K.; Ekström, S.; Fritz, E.; Sellergren, B. Catalytic Formation of Disulfide Bonds in Peptides by Molecularly Imprinted Microgels at Oil/Water Interfaces. *ACS Appl. Mater. Interfaces* **2016**, *8*, 30484-30491.

(25) Zimmerman, S. C.; Lemcoff, N. G. Synthetic Hosts Via Molecular Imprinting—Are Universal Synthetic Antibodies Realistically Possible? *Chem. Commun.* **2004**, 5-14.

(26) Zhang, S.; Zhao, Y. Facile Synthesis of Multivalent Water-Soluble Organic Nanoparticles Via "Surface Clicking" of Alkynylated Surfactant Micelles. *Macromolecules* **2010**, *43*, 4020-4022.

(27) Awino, J. K.; Zhao, Y. Imprinted Micelles for Chiral Recognition in Water: Shape, Depth, and Number of Recognition Sites. *Org. Biomol. Chem.* **2017**, *15*, 4851-4858.

(28) Gunasekara, R. W.; Zhao, Y. Intrinsic Hydrophobicity Versus Intraguest Interactions in Hydrophobically Driven Molecular Recognition in Water. *Org. Lett.* **2017**, *19*, 4159-4162.

(29) Fa, S.; Zhao, Y. Peptide-Binding Nanoparticle Materials with Tailored Recognition Sites for Basic Peptides. *Chem. Mater.* **2017**, *29*, 9284-9291.

(30) Awino, J. K.; Gunasekara, R. W.; Zhao, Y. Selective Recognition of D-Aldohexoses in Water by Boronic Acid-Functionalized, Molecularly Imprinted Cross-Linked Micelles. *J. Am. Chem. Soc.* **2016**, *138*, 9759-9762.

(31) Awino, J. K.; Gunasekara, R. W.; Zhao, Y. Sequence-Selective Binding of Oligopeptides in Water through Hydrophobic Coding. *J. Am. Chem. Soc.* **2017**, *139*, 2188-2191.

(32) Gunasekara, R. W.; Zhao, Y. A General Method for Selective Recognition of Monosaccharides and Oligosaccharides in Water. *J. Am. Chem. Soc.* **2017**, *139*, 829-835.

(33) Duan, L.; Zhao, Y. Selective Binding of Folic Acid and Derivatives by Imprinted Nanoparticle Receptors in Water. *Bioconjugate Chem.* **2018**, *29*, 1438-1445.

(34) Awino, J. K.; Zhao, Y. Molecularly Imprinted Nanoparticles as Tailor-Made Sensors for Small Fluorescent Molecules. *Chem. Commun.* **2014**, *50*, 5752-5755.

(35) Fa, S.; Zhao, Y. Water-Soluble Nanoparticle Receptors Supramolecularly Coded for Acidic Peptides. *Chem. -Eur. J.* **2018**, *24*, 150-158.

(36) Matsui, J.; Higashi, M.; Takeuchi, T. Molecularly Imprinted Polymer as 9-Ethyladenine Receptor Having a Porphyrin-Based Recognition Center. *J. Am. Chem. Soc.* **2000**, *122*, 5218-5219.

(37) Becker, J. J.; Gagné, M. R. Exploiting the Synergy between Coordination Chemistry and Molecular Imprinting in the Quest for New Catalysts. *Acc. Chem. Res.* **2004**, *37*, 798-804.

(38) Muratsugu, S.; Tada, M. Molecularly Imprinted Ru Complex Catalysts Integrated on Oxide Surfaces. *Acc. Chem. Res.* **2013**, *46*, 300-311.

(39) Schmidtchen, F. P.: Isothermal Titration Calorimetry in Supramolecular Chemistry. In *Supramolecular Chemistry: From Molecules to Nanomaterials*; Steed, J. W., Gale, P. A., Eds.; Wiley: Online, 2012.

(40) Awino, J. K.; Zhao, Y. Polymeric Nanoparticle Receptors as Synthetic Antibodies for Nonsteroidal Anti-Inflammatory Drugs (NSAIDs). *ACS Biomater. Sci. Eng.* **2015**, *1*, 425-430.

(41) In our synthesis, we assumed the tridentate ligand in **5** was able to retain the zinc during the preparation and purification of the MINPs. Consistent with the notion, hydrolysis of PNPH by Zn-MINP(**4a**) showed no improvement upon the addition of up to 20 equiv of Zn^{2+} (Figure 24, Table 4), suggesting that the active site was fully metallated in Zn-MINP(**4a**).

(42) The Zn-MINP complex showed no catalytic activity for unactivated para-isopropylphenyl hexanoate under similar experimental conditions.

(43) In our hands, when the activated ester was not hydrolyzed, the absorbance at 400 nm often displayed small, negative changes over time (Figures 25-26, presumably caused by the scattering of UV light by the phase-separated ester starting material, due to its hydrophobicity.

(44) The difference between the C4 and C8 *p*-nitrophenyl esters was within experimental error.

(45) The numbers were obtained from linear curve-fitting to the Lineweaver-Burk plots (Figures 27-33). The data were mostly within 20% of those obtained by directing fitting to the Michaelis-Menten equation (Table 5, Figures 34-40).

(46) Yano, Y.; Shimada, K.; Okai, J.; Goto, K.; Matsumoto, Y.; Ueoka, R. Fairly Marked Enantioselectivity for the Hydrolysis of Amino Acid Esters by Chemically Modified Enzymes. *J. Org. Chem.* **2003**, *68*, 1314-1318.

(47) Engström, K.; Nyhlén, J.; Sandström, A. G.; Bäckvall, J.-E. Directed Evolution of an Enantioselective Lipase with Broad Substrate Scope for Hydrolysis of A-Substituted Esters. *J. Am. Chem. Soc.* **2010**, *132*, 7038-7042.

(48) Verpoorte, J. A.; Mehta, S.; Edsall, J. T. Esterase Activities of Human Carbonic Anhydrases B and C. *J. Biol. Chem.* **1967**, *242*, 4221-4229.

(49) We did not attempt to achieve even higher turnover numbers due to the limited solubility of PNPH in aqueous buffer.

(50) Menger, F. M.; Ladika, M. Origin of Rate Accelerations in an Enzyme Model: The P-Nitrophenyl Ester Syndrome. *J. Am. Chem. Soc.* **1987**, *109*, 3145-3146.

(51) Arifuzzaman, M.; Zhao, Y. Water-Soluble Molecularly Imprinted Nanoparticles Receptors with Hydrogen-Bond-Assisted Hydrophobic Binding. *J. Org. Chem*. **2016**, *81*, 7518–7526.

(52) Parrott, M. C.; Benhabbour, S. R.; Saab, C.; Lemon, J. A.; Parker, S.; Valliant, J. F.; Andronov, A. Synthesis, Radiolabeling, and Bio-imaging of High-Generation Polyester Dendrimers. *J. Am. Chem. Soc.* **2009**, *131*, 2906–2916.

(53) Chao, H. K.; Lee, D. H.; Hong, J.-I. A fluorescent pyrophosphate sensor via excimer formation in water. *Chem. Commun*. **2005**, *13*, 1690–1692.

(54) Orito, K.; Horibata, A.; Nakamura, T.; Ushito, H.; Nagasaki, H.; Yuguchi, M.; Yamashita, S.; Tokuda, M. Preparation of Benzolactams by $Pd(OAc)_2$-Catalyzed Direct Aromatic Carbonylation. *J. Am. Chem. Soc.* **2004**, *126*, 14342–14343.

(55) Tsuboi, K.; Bachovchin, D. A.; Speers, A. E.; Spicer, T. P.; Fernandez-Vega, V.; Hodder, P.; Rosen, H.; Cravatt, B. F. Potent and Selective Inhibitors of Glutathione S-Transferase Omega 1 That Impair Cancer Drug Resistance. *J. Am. Chem. Soc.* **2011**, *133*, 16605–16616.

(56) Boyle, R. G.; Boyle, R. J. PCCT. Int. Appl. 2013072502, 2013.

(57) Qian, L.; Liu, J.-Y.; Liu, J.-Y.; Yu, H.-L.; Li, C.-X.; Xu, J.-H. Fingerprint lipolytic enzymes with chromogenic p-nitrophenyl esters of structurally diverse carboxylic acids. *J. Mol. Catal., B Enzym.* **2011**, *73*, 22–26.

(58) Ghosh, U.; Ganessunker, D.; Sattigeri, V.J.; Carlson, K.E.; Mortensen, D.J.; Katzenellenbogen, B.S.; Katzenellenbogen, J.A. Estrogenic Diazenes: Heterocyclic Non-steroidal Estrogens of Unusual Structure with Selectivity for Estrogen Receptor Subtypes. *Bioorganic Med. Chem.* **2003**, *11*, 629–657.

(59) Kim, S.; Lee, K. J.; Kim, Y. C. A Simple and Mild Esterification Method for Carboxylic Acids Using Mixed Carboxylic-Carbonic Anhydrides. *J. Org. Chem.* **1985**, *50*, 560–565.

(60) Chen, Y.; Liu, Y.; Yao, Y.; Zhang, S.; Gu. Z. Reverse micelle-based water-soluble nanoparticles for simultaneous bioimaging and drug delivery. *Org. Biomol. Chem.* **2017**, *15*, 3232–3238.

CHAPTER 5. SYNTHETIC ESTERASE WITH BIOINSPIRED OXYANION HOLE FOR SELECTIVE HYDROLYSIS OF NONACTIVATED ARYL ESTERS

Modified from a paper is ready to submit in *ACS Catalysis*

MD Arifuzzaman and Yan Zhao

Department of Chemistry, Iowa State University, Ames, Iowa 50011-3111, United States

Abstract

One of the most remarkable features of enzymes is their ability to use ordinary functional groups to achieve extraordinary catalysis. Despite tremendous interest in such synthetic catalysts, it has been difficult for chemists to construct synthetic catalysts with active sites with molecular recognition features and multiple catalytic groups working in cooperation. Molecular imprinting in the nanospace of a cross-linked micelle using easy-to-synthesize small-molecule templates served as a convenient method to build a multifunctionalized, modifiable active site within the micellar core. A combination of noncovalent templating and post-modification enabled systematic, fine-tuning of the active site, yielding artificial esterases that selectively hydrolyzed aryl esters with minute structural differences under neutral conditions.

Introduction

Enzymes have fascinated generations of scientists by their extraordinary abilities to catalyze some of the most challenging reactions under mild conditions. Central to these achievements is their active sites, created through folding of peptide chains and sometimes

additionally through aggregation of protein subunits. It is in this special nanospace where the desired substrate is bound and cooperative actions of ordinary functionalities such as carboxylic acid and hydroxyl converge to enable extraordinary catalysis, in terms of both efficiency and selectivity.

With increasing knowledge in enzymatic mechanisms and access to high-resolution x-ray crystal structures of many enzymes, the opportunity is better than ever for chemists to create bioinspired catalysts with enzyme-like catalytic efficiency and selectivity. Nonetheless, despite the tremendous progress of supramolecular chemistry[1] and immense interest in artificial enzymes,[2] it remains difficult for chemists to create fine-tuned active sites with enzyme-like cooperative catalysis and high substrate selectivity. The challenge is understandable because coordinated actions of multiple groups requires highly precise placements of these groups. Moreover, if building an effective catalytic center needs tremendous design, synthesis, and sometimes good luck, having such a center with additional molecular recognition features demands even higher sophistication.[2b] For artificial enzymes prepared in a bottom-up fashion, the traditional principles of preorganization and complementarity, when coupled with catalytic functions, become very difficult to implement for substrates even of moderate complexity.

We herein report a rational, facile method to construct functionalized active sites within protein-sized water-soluble organic nanoparticles. The active site was able to recruit specific aryl esters from solution and had a nucleophilic pyridyl positioned for their hydrolysis. Our strategy enabled us to install a thiourea group precisely near the carbonyl of the ester substrate, to mimic the oxyanion hole in natural serine protease to stabilize the tetrahedral anionic intermediate in the hydrolysis. The distance of the pyridyl to the carbonyl,

as well as the electronic properties of the thiourea, could be tuned systematically, enabling nonactivated aryl esters to be hydrolyzed selectivity.

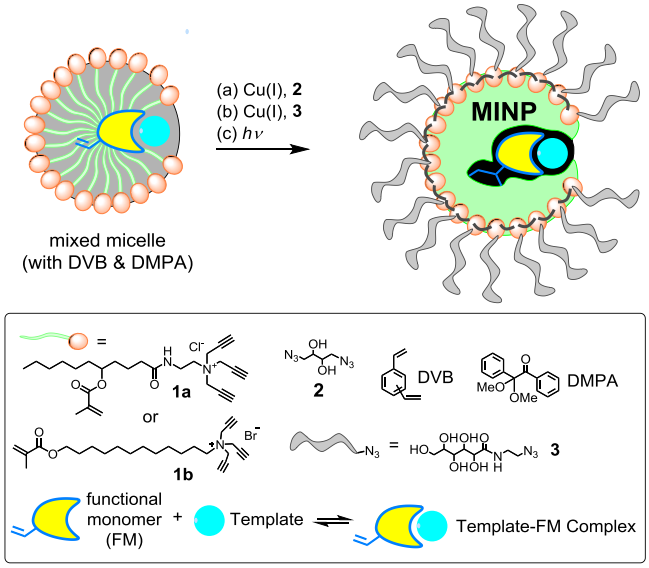

Scheme 1. Preparation of MINP by surface–core double cross-linking of surfactant **1** in the presence of template.

Scheme 1 shows the preparation of our artificial esterases, through micellar imprinting developed by our group in recent years.[3] Although molecularly imprinted polymers have been used for catalysis,[4] imprinting in this case was performed in the nanospace of a micelle, formed by a doubly cross-linkable surfactant **1a** or **1b** (Scheme 1). The mixed micelle, containing the template, DVB, and DMPA (a photoinitiator), was first cross-linked on the surface with diazide **2** by the Cu(I)-catalyzed click reaction, followed by functionalization with a hydrophilic ligand (**3**) by another round of click reaction. Free radical core-cross-linking then "solidified" the core around the template. Our previous work showed that imprinting in the nanospace of a micelle had an extraordinary ability to reproduce features of the template. For example, the molecularly imprinted nanoparticles (MINPs) obtained could distinguish isoleucine and leucine in di- and tripeptides, isomers

different in the position of a single methyl.[5] They could also differentiate mono- and oligosaccharides different in the stereochemistry of a single hydroxyl.[6]

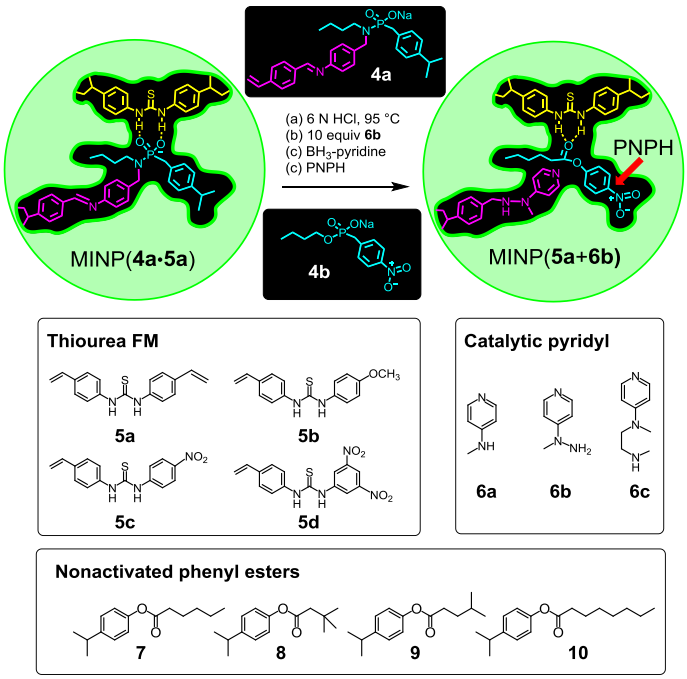

Scheme 2. Preparation of MINP catalysts with a thiourea and a catalytic pyridyl group in the active site.

The precision and high-fidelity in the micellar imprinting gave us a powerful way to construct functionalized nanospace for cooperative catalysis, using easy-to-synthesize small-molecule templates. To prove the concept, we designed phosphonamidate **4a**. The anionic template, shown in a black background, is color-coded: the cyan moiety resembles the transition state of an aryl ester in hydrolysis, after attack by a hydroxide nucleophile; the purple substructure contains a polymerizable imine as a space-holder for the subsequently installed catalytic group. The phosphonamidate, with two strong hydrogen-bond acceptors, is hypothesized to bind a polymerizable thiourea functional monomer (FM, **5a**–**5d**). Although it is challenging to use hydrogen-bonds directly for molecular recognition in water, micelles are known to enhance their stability by their local hydrophobicity.[7] In addition, when both

the template and FM have sufficient hydrophobicity, their inclusion into the micelle will greatly increase their local concentrations, further stabilizing their complex. We have shown that hydrogen-bonded complexes (between thiouronium and carboxylate) could be successfully imprinted within cross-linked micelles.[8]

Scheme 2 shows how a template-containing MINP can be converted into a designed artificial esterase. Preparation and characterization followed previously reported procedures.[9] MINP(**4a·5a**), i.e., MINP prepared with the template–FM complex **4a·5a**, was first treated with 6N HCl at 95 °C for 2 h. The condition was previously shown to hydrolyze polymerized imines within MINP without affecting the rest of the structure.[10] The aldehyde group obtained in the active site was then functionalized with various pyridyl derivatives (**6a**–**6c**, shown in purple) through reductive amination.[11] MINP(**5a**+**6b**) was obtained using FM **5a** in the synthesis and pyridyl **6b** in the post-functionalization. Because MINPs are soluble in water and selected organic solvents (e.g., DMF), they can be treated as macromolecules in standard reactions.[12] We typically use at least a 10-fold excess of reagents in such reactions (e.g., amidation and reductive amination) to promote the reaction.[11-12]

MINP(**5a**+**6b**) in principle should have an active site in the hydrophobic core of the cross-linked micelle to bind an aryl ester. Its structure in Scheme 2 contains a cyan-colored *p*-nitrophenyl hexanoate (PNPH), whose shape, size, and hydrophobicity closely match those of the cyan-colored segment of **4a**. The thiourea is designed to activate the carbonyl of the aryl ester and stabilize the anionic transition state, as the oxyanion hole of serine protease. The pyridyl can act as a nucleophilic catalyst or general base to assist the hydrolysis, with its distance to the carbonyl tuned by the different tethers in **6a**–**6c**.

Table 1. Pseudo-first-order rate constants for the hydrolysis of PNPH in 25 mM HEPES buffer (pH 7.0).[a]

Entry	Catalyst	k ($\times 10^{-4}$ s^{-1})	k_{rel}[b]
1	$MINP_{1a}$(**5a**+**6a**)	1.72 ± 0.01	43
2	$MINP_{1a}$(**5a**+**6b**)	4.50 ± 0.38	113
3	$MINP_{1a}$(**5a**+**6c**)	0.95 ± 0.06	24
4	$MINP_{1a}$(**5a**)	1.03 ± 0.06	26
5	$MINP_{1a}$(**6b**)	1.19 ± 0.08	30
6	$NINP_{1a}$	0.38 ± 0.03	10
7	none	0.04 ± 0.01	1
8	$MINP_{1b}$(**5a**+**6b**)	29.1 ± 2.18	728
9	$MINP_{1b}$(**5b**+**6b**)	27.5 ± 1.87	688
10	$MINP_{1b}$(**5c**+**6b**)	54.7 ± 1.50	1368
11	$MINP_{1b}$(**5d**+**6b**)	97.0 ± 9.18	2425
12	$MINP_{1b}$(**5d**)	3.55 ± 0.61	89
13	$MINP_{1b}$(**6b**)	5.82 ± 0.62	146
14	$NINP_{1b}$	1.30 ± 0.07	33

[a] Reaction rates were measured in a 25 mM HEPES buffer (pH 7.0) at 40 °C. [PNPH] = 50 μM. [catalyst] = 15 μM. The numbers given were averages from triplicate experiments at the 90% confidence level. [b] k_{rel} is the rate constant normalized to that in the buffer without any added catalyst.

To verify our catalytic design, we screened a number of MINPs in the catalytic hydrolysis of PNPH. The activated ester was chosen for the convenient monitoring of its hydrolysis by UV-vis spectroscopy at 400 nm for the formation of the product, *p*-nitrophenoxide (vide infra for nonactivated aryl esters). Table 1 shows the pseudo-first-order

rate constant for the hydrolysis, obtained with 50 μM of the substrate and 15 μM of MINP in 25 mM HEPES buffer (pH 7.0).

MINPs prepared with **1a** as the cross-linkable surfactant displayed modest activity for the PNPH hydrolysis. Compared to the background hydrolysis in the buffer, MINP$_{\mathbf{1a}}$(**5a**+**6a**) only accelerated the hydrolysis by 43 times (entry 1). The acceleration was quite insignificant given that the nonimprinted nanoparticle (NINP), prepared without any template, showed a k_{rel} of 10 (entry 6). Nonetheless, the pyridyl in the active site did participate in the catalysis, as varying the tether in the pyridyl derivative (**6a**–**6c**) did change the hydrolysis rate considerably, with MINP$_{\mathbf{1a}}$(**5a**+**6b**) being most active (entry 2). More importantly, the effects of the pyridyl and thiourea were positively cooperative. For example, MINP(**5a**), obtained with the imine hydrolyzed but without any reductive amination, gave a k_{rel} of 26 (entry 4). MINP$_{\mathbf{1a}}$(**6b**), prepared with **4** as the template in the absence of any thiourea FM, afforded a k_{rel} of 30 (entry 5). Together, they were more effective, with MINP$_{\mathbf{1a}}$(**5a**+**6b**) giving a rate acceleration of 113 (entry 2).

Although the data so far did support the cooperative actions between the pyridyl and the thiourea, the observed catalytic activity was too low. In our artificial esterase, installment of the thiourea group in the active site was determined by the degree molecular imprinting could capture the template–FM complex through double cross-linking of the micelle. The more stable the complex in the micelle, the better the chance will be for the final active site to have the two catalytic groups.

In agreement with the postulation, much larger rate acceleration was observed when **1b** instead of **1a** was used as the cross-linkable surfactant in the MINP preparation (Table 1, entries 8–13). The seemingly small change of surfactant enhanced the activity of

MINP$_{\mathbf{1a}}$(**5a**+**6b**) by nearly 7 times, affording a k_{rel} of 728 for MINP$_{\mathbf{1b}}$(**5a**+**6b**) (entry 8). With **1a** as the surfactant, the micelle has many hydrogen-bonding amide groups inside the micelle. These amide groups are expected to compete with the thiourea FM for the phosphonamidate template and also with the template for the FM. The template–FM complex, as a result, should be less stable in the micelle of **1a** than that of **1b** due to amide-competition.

Further improvement of our artificial esterase was achieved with additional fine-tuning of the active site. In contrast to FM **5a**, which has two polymerizable vinyl groups and will be doubly polymerized on both phenyl groups, **5b**–**5d** only had vinyl on one of the two phenyls. With only one side of the molecule attached to the MINP core, the thiourea is anticipated to have a higher mobility, which should be beneficial to the catalysis because it could adjust its position better to accommodate the anionic transition state.

Indeed, the mono-polymerized thiourea MINPs had a higher catalytic activity, especially those with electron-withdrawing groups on the phenyl (**5c** and **5d**). The thiourea was clearly key to the catalysis, as the activity of the catalyst correlated with the electronic nature of the substituent on the phenyl ring (entries 9–11). Our best catalyst was MINP$_{\mathbf{1b}}$(**5d**+**6b**), which showed a rate acceleration of 2425 under our experimental conditions. Synergism between the pyridyl and thiourea was maintained, since removing either from the active site lowered the activity by 17–27-fold (entries 12–13).

The presence of the thiourea in the active site was also supported by a binding study. Anionic phosphonate **4b** closely resembles the cyan part of template **4a** (Scheme 2), and thus should fit nicely into the active site created for the phosphonamidate template. In our hands, MINP$_{\mathbf{1b}}$(**5a**+**6b**) bound **4b** with a binding constant of $K_a = 2.12 \times 10^5$ M^{-1} according to

isothermal titration calorimetry (ITC). Once the thiourea FM was eliminated in the preparation, MINP$_{\mathbf{1b}}$(**6b**) displayed a weaker binding (K_a = 0.90 ± ×10^5 M^{-1}). Our best catalyst, MINP$_{\mathbf{1b}}$(**5d**+**6b**) showed the strongest binding for **4b** (K_a = 3.82 ± ×10^5 M^{-1}). The result was very reasonable considering that the two nitro groups made the thiourea more acidic and thus more strongly hydrogen-bonding.

MINP$_{\mathbf{1b}}$(**5d**+**6b**) showed enzyme-like Michaelis–Menten kinetics, with its hydrolysis followed equation $v_0 = V_{max}[S_0]/(K_m+[S_0])$, in which v_0 is the initial velocity, S_0 the initial substrate concentration, V_{max} the maximum velocity at a particular enzyme concentration, and K_m the Michaelis constant that measures the binding affinity of the substrate to the enzyme (SI).[13] Nonlinear least squares curve fitting of the kinetic data yielded K_m = (0.28 ± 0.07) mM and V_{max} = (4.55 ± 0.83) ×10^{-7} mol/s at a concentration of 8 μM for the catalyst. These data translate to $k_{cat} = V_{max}/[catalyst]$ = (56.9 ± 10.4) × 10^{-3} M^{-1} and a catalytic efficiency of k_{cat}/K_m = 203 M^{-1}s^{-1}. The k_{cat}/k_{uncat} value was calculated to be 14200.

Many reported synthetic esterases had low catalytic turnover numbers (TONs) because the products (carboxylate and phenoxide) tend to complex with the catalytic metal (often zinc) more strongly than the starting materials (ester and water). Even when peptidic structures as in natural enzymes were used to stabilize the metal, low TONs (10–50) were still obtained.[14] When a large excess (500 equiv) of PNPH was used in our case, MINP$_{\mathbf{1b}}$(**5d**+**6b**) showed little signs of slowing down even at high conversion (Figure 2). The TON was calculated to be 480 at 600 min.

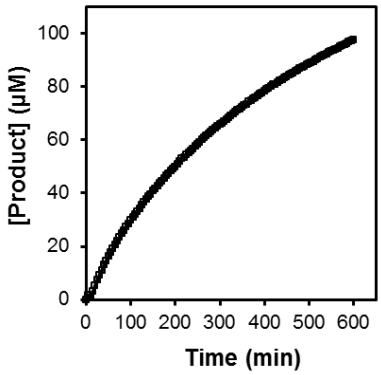

Figure 1. Amount of *p*-nitrophenoxide formed as a function of time in a 25 mM HEPES buffer (pH 7.0) at 40 °C, calculated based on an extinction coefficient of $\varepsilon_{400} = 0.0216\ \mu M^{-1}\ cm^{-1}$. [PNPH] = 100 μM. [$MINP_{1b}$(**5d**+**6b**)] = 0.2 μM.

Synthetic esterases historically have been criticized for their inability to hydrolyze anything beyond highly activated esters (i.e., the "*p*-nitrophenyl ester syndrome").[15] With a powerful nucleophile/general base in the active site near the ester bond to be cleaved and a biomimetic "oxyanion hole" formed from the thiourea, our artificial esterase was able to hydrolyze nonactivated aryl esters (Table 2).

Table 2. Pseudo-first-order rate constants for the hydrolysis of non-activated esters catalyzed by MINPs in 25 mM HEPES buffer (pH 7.0).[a]

Entry	Catalyst	Substrate	% yield
1	$MINP_{1b}$(5d+6b)	7	65
2	$MINP_{1b}$(5d)	7	12
3	$MINP_{1b}$(6b)	7	11
4	NIMP	7	n.R
5	$MINP_{1b}$(5d+6b)	8	9
6	$MINP_{1b}$(5b+6b)	9	15
7	$MINP_{1b}$(5d+6b)	10	22

[a] Reaction rates were measured in 25 mM HEPES buffer at 60 °C and pH 7.0 for 12 h. [PNPH] = 300 μM. [catalyst] = 15.0 μM unless otherwise indicated.

MINP$_{1b}$(**5d**+**6b**) should hydrolyze *p*-isopropylphenyl hexanoate **7**, due to its similarity to the cyan-colored substructure of template **4a**. At a 5 mol % catalyst loading, the artificial esterase indeed hydrolyzed 65% of the ester after 12 h in a 25 mM HEPES buffer at pH 7.0. Synergism of the pyridyl and thiourea was evident, as removing either functionality from the active site lowered the yield to 11–12% under the same conditions (Table 2, entries 2–3). More importantly, the catalyst displayed strong selectivity among closely related aryl esters (**7**–**10**). Minute changes in the substrate structure, including a shift of a remote methyl by 1 carbon as in **9** and an elongation of the acyl chain by two carbons as in **10**, lowered the yield of catalytic hydrolysis considerably.

To highlight the selectivity of our artificial esterase, we performed a competition experiment using MINP$_{1b}$(**5d**+**6b**) to hydrolyze a mixture of **7** and **9**. Because of the similarity of the two esters—different by the position of a single methyl remote from the reactive group—any catalysts would have difficulty hydrolyzing one without the other. Yet, as shown by the gas chromatographs of the reaction mixture at various times (Figure 2), **7** disappeared while **9** persisted very well over a period of 16 h.

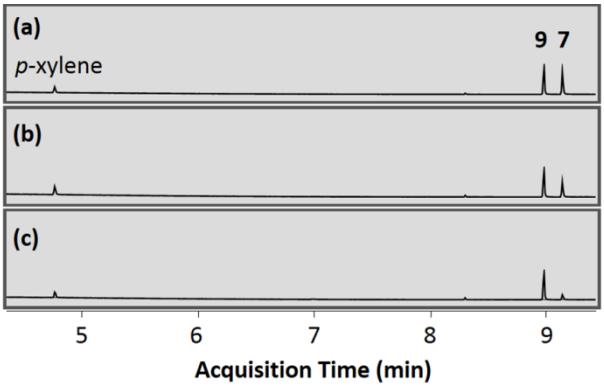

Figure 2. Hydrolysis of a mixture of **7** and **9** in 25 mM HEPES buffer (pH 7) at 60 °C after (a) 0 h, (b) 8 h, and (c) 16 h, monitored by gas chromatography using *p*-xylene (300 µM) as an internal standard. [**7**] = [**9**] = 300 µM. [MINP$_{1b}$(**5d**+**6b**)] = 15 µM.

We have demonstrated a rational, bottom-up synthesis of highly selective synthetic esterase. The highlight of the work is the facile construction of a substrate-tailored active site with cooperative catalytic groups. Our strategy allowed accurate placements of functional groups and systematic tuning of the active site. For many decades, synthetic esterases are limited to highly activated esters as substrates, which are known to "magnify" the catalytic effect.[15] With a powerful nucleophile and a bioinspired oxyanion hole in the active site, $MINP_{\mathbf{1b}}$(**5d**+**6b**) was able to hydrolyze nonactivated aryl esters under neutral conditions. Although our artificial esterase is still no match for their natural counterparts in activity, their tolerance for high temperature,[10-12] organic solvents,[10-12] and extreme pH conditions[10-11] far exceeds that of any natural enzymes. These MINP catalysts can already distinguish closely related substrates. With more advanced designs for the active site, it is possible that synthetic catalysts with enzyme-like efficiency and selectivity would no longer be an unreachable goal for chemists.

Acknowledgement

We thank NSF (CHE-1708526) for financial support of this research.

Experimental Section

General Method

All reagents and solvents were of ACS-certified grade or higher and used as received from commercial suppliers. Millipore water was used to prepare buffers and nanoparticles. ^{1}H and ^{13}C NMR spectra were recorded on a VARIAN MR-400 or on a VARIAN VXR-400 spectrometer. Dynamic light scattering (DLS) was performed on a PD2000DLSPLUS dynamic light scattering detector. Mass spectrometry was performed on AGILENT 6540

QTOF mass spectrometer. UV-vis spectra were recorded on a Cary 100 Bio UV-visible spectrophotometer.

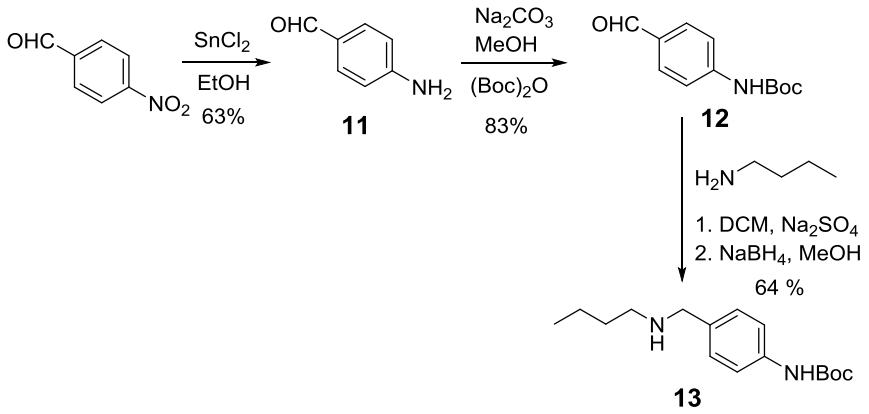

Scheme 3. Synthesis of Compound **13**

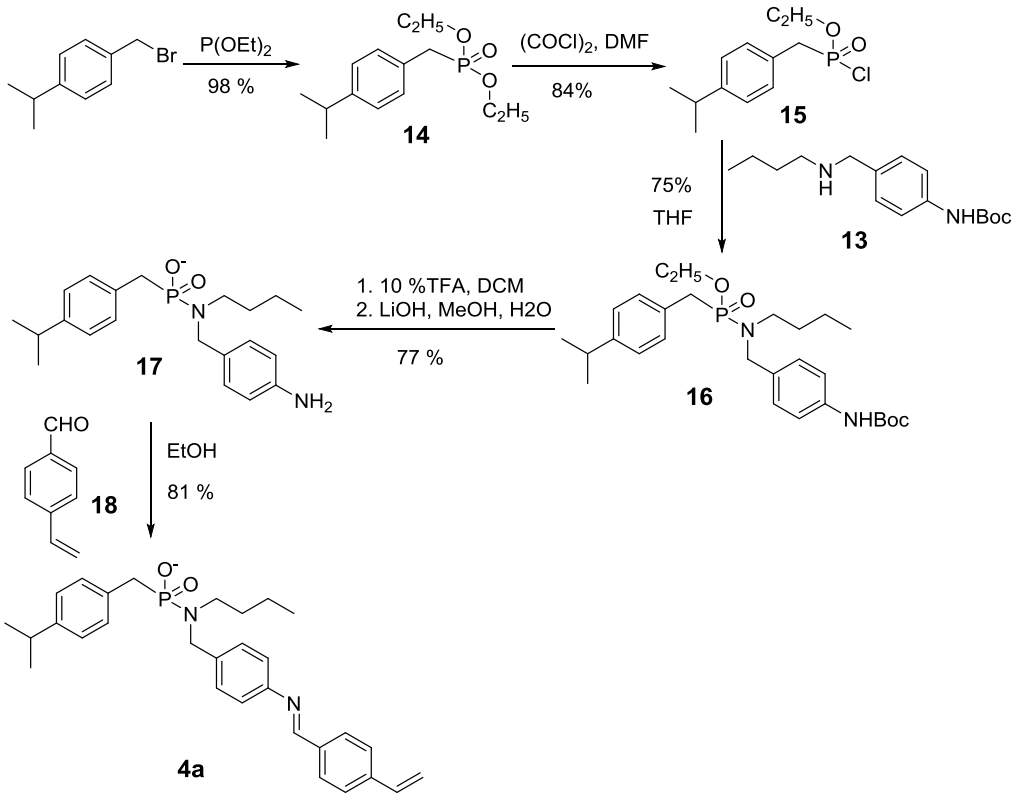

Scheme 4. Synthesis of Compound **4a**

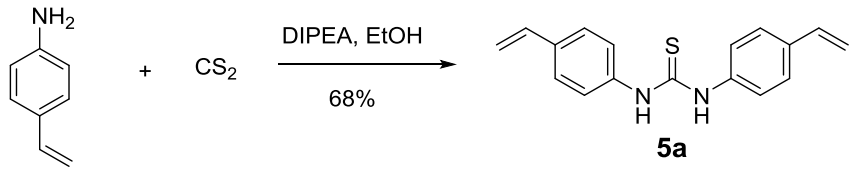

Scheme 5. Synthesis of Compound **5a**

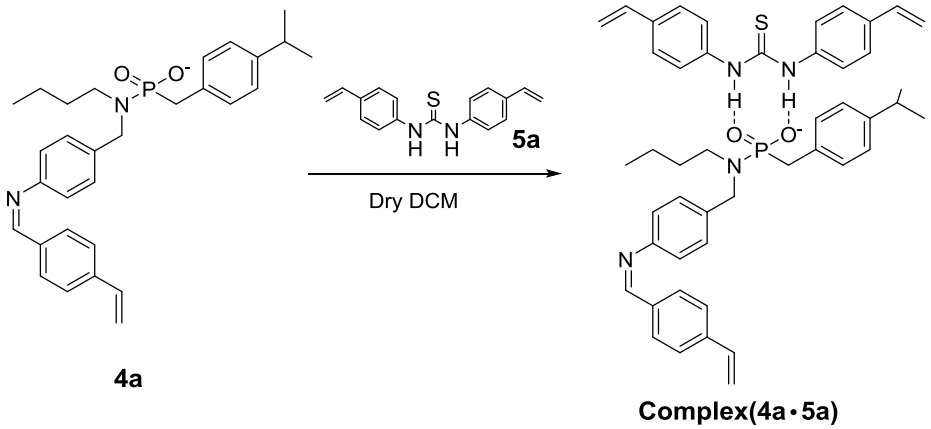

Scheme 6. Synthesis of Compound (**4a•5a)**

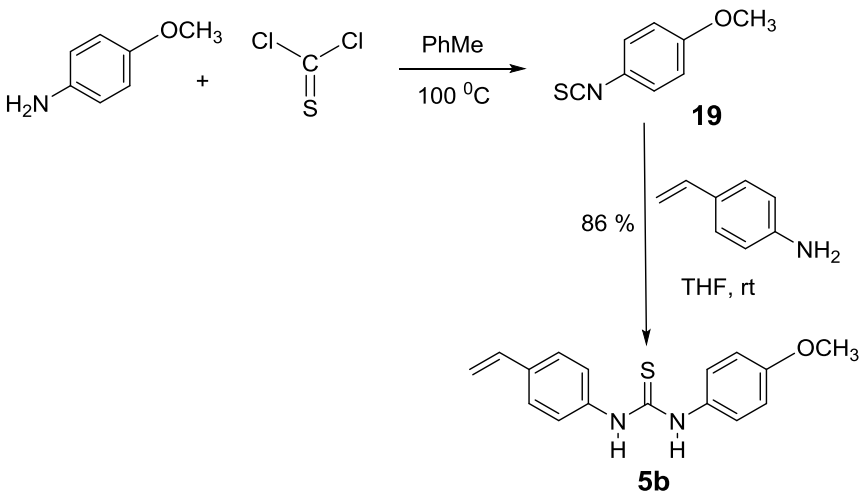

Scheme 7. Synthesis of Compound **5b**

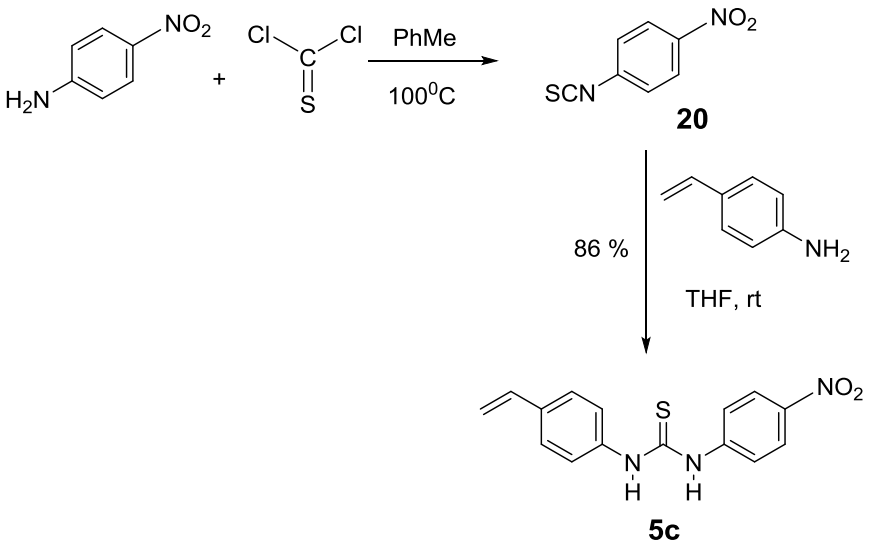

Scheme 8. Synthesis of Compound **5c**

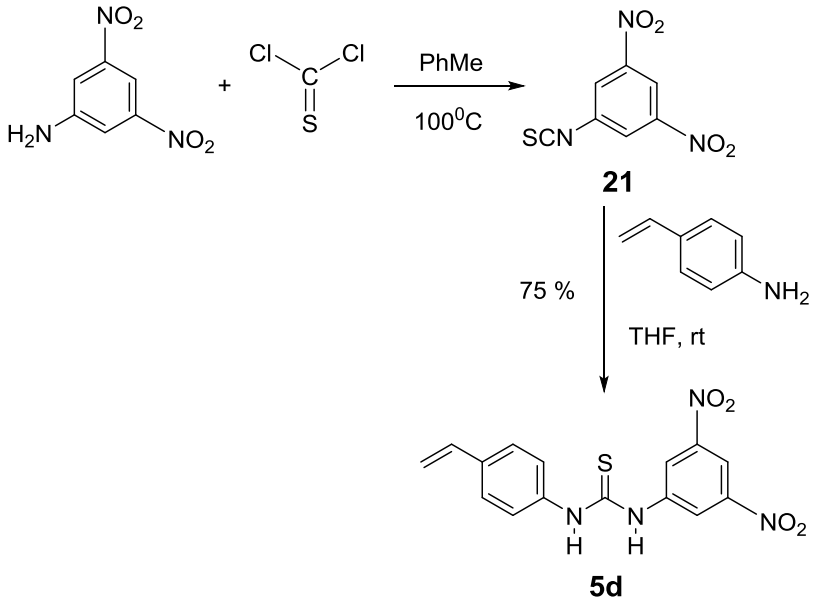

Scheme 9. Synthesis of Compound **5d**

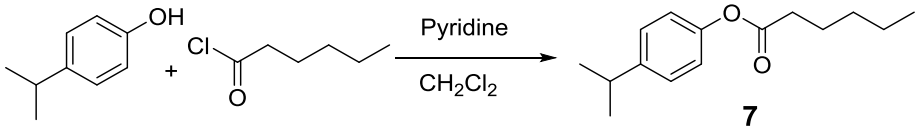

Scheme 10. Synthesis of Compound **7**

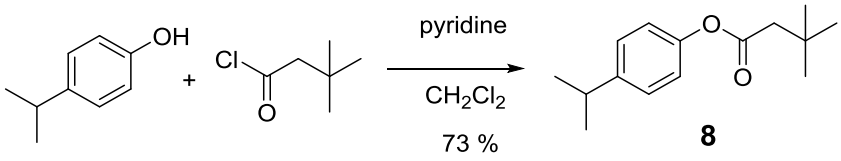

Scheme 11. Synthesis of Compound **8**

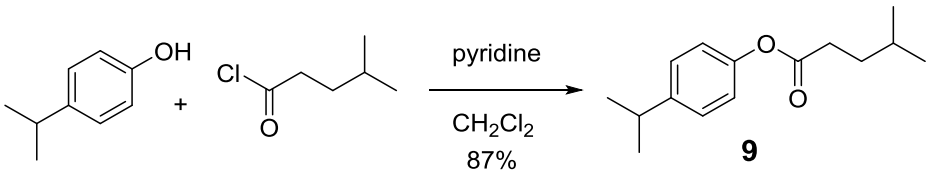

Scheme 12. Synthesis of Compound **9**

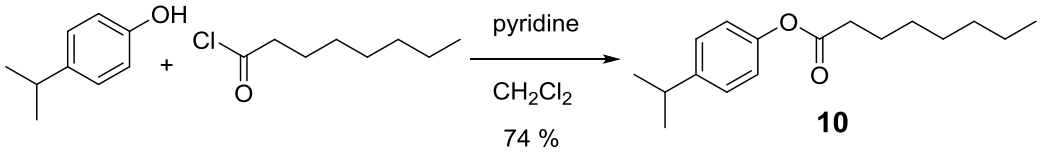

Scheme 13. Synthesis of Compound **10**

Syntheses

Syntheses of compounds **1a**,[16] **1b**,[17] **2**,[18] **3**,[19] **4b**,[20] **6b**,[21] **6c** [21] and **18**[22] followed previously reported procedures.

Compound 11.[23] A mixture of 4-nitrobenzaldehyde (0.5 g, 3.3 mmol) and $SnCl_2$ (3.75 g, 18.4 mmol) in ethanol (45 mL) was stirred at reflux for 4 h. After cooled to room temperature, the mixture was poured onto ice. The resulting mixture was treated with sat. $NaHCO_3$ until pH ~7-8, and was extracted with ethyl acetate (3 × 20 mL). The combined organic phase was washed with brine (3 × 20 mL) and dried over Na_2CO_3. The solvent was removed under reduced pressure to afford a white powder (0.25 g, 63%). ^{1}HNMR (400 MHz, $CDCl_3$, δ): 9.76 (s, 1H), 7.69 (d, J = 8.3 Hz, 2H), 6.70 (d, J = 8.3 Hz, 2H).

Compound 12.[24] A mixture of 4-aminobenzaldehyde (0.20 g, 1.65 mmol), di-*tert*-butyl dicarbonate (0.55 g, 2.5 mmol), and Na_2CO_3 (0.27g, 2.5 mmol) in MeOH (20 mL) was stirred at room temperature overnight. The solid was removed by filtration and the filtrate was concentrated under reduced pressure. The residue was dissolved in diethyl ether (50 mL). The solution was washed with $NaHCO_3$ (3 × 30 mL) and brine (3 × 30 mL), dried with Na_2SO_4, and concentrated *in vacuo*. The residue was purified by a short silica gel column to afford a white powder (0.30 g, 83%). ^{1}H NMR (400 MHz, $CDCl_3$ δ): 9.89 (s, 1H), 7.82 (d, *J* = 8.7 Hz, 2H), 7.53 (d, *J* = 8.6 Hz, 2H), 1.53 (s, 9H).

Compound 13. A mixture of compound **12** (0.73 g, 3.30 mmol), butylamine (0.20 g, 4.5 mmol), and Na_2SO_4 (0.35g, 4.5 mmol) in dry CH_2Cl_2 (10 mL) was stirred at room temperature for 5 h. The solid was removed by filtration and the filtrate was concentrated under reduced pressure. The residue was dissolved in MeOH (5 mL), to which sodium borohydride (0.02g, 1.1 mmol) was added slowly. The reaction mixture was stirred at room temperature for 5 h. The organic solvent was removed under reduced pressure and the residue was dissolved in CH_2Cl_2. The organic solution was washed with water (3 × 10 mL), dried with $MgSO_4$, and concentrated *in vacuo* to afford a yellow liquid (0.60 g, 64%).^{1}H-NMR (400 MHz, $CDCl_3$, δ): 7.34 (d, *J* = 8.5 Hz, 2H), 7.25 (d, *J* = 8.5 Hz, 2H), 6.61 (s, 1H), 3.75 (s, 2H), 2.63 (t, *J* = 7.3 Hz, 2H), 1.67 (m, 2H), 1.54 (s, 9H), 1.35 (m, 2H), 0.92 (t, *J* = 7.2 Hz, 3H). ^{13}C-NMR (100 MHz, $CDCl_3$, δ): 152.6, 137.4, 129.0, 118.4, 80.30, 52.60, 48.15, 31.11, 28.15, 20.21, 13.74. ESI-HRMS (*m/z*): $[M+H]^+$ calcd for $C_{16}H_{27}N_2O_2$, 279.2067; found 279.2076.

Compound 14.[25] A mixture of 4-isopropylbenzyl bromide (0.5 g, 2.35 mmol) and triethyl phosphite (0.98 g, 5.87 mmol) was heated to reflux for 24 h. Excess triethyl phosphate was

removed under reduced pressure to give the product as a brown oil (0.60 g, 98 %).^{1}H-NMR (400 MHz, $CDCl_3$, δ): 7.21 (d, *J* = 8.3 Hz, 2H), 7.16 (d, *J* = 8.3 Hz, 2H), 4.07 – 3.93 (m, 4H), 3.11 (d, *J* = 21.4 Hz, 2H),2.87 (p, *J* = 6.9 Hz, 1H), 1.26 – 1.21 (m, 13H).

Compound 15.[26] Oxalyl chloride (0.12 g, 1.0 mmol) was added to a solution of compound **14** (0.2 g, 0.8 mmol) in 1 mL DMF at 60 °C. After the reaction mixture was stirred at 60 °C for 5 h, the solvent was removed by rotary evaporation to yield a yellow powder (0.16 g, 84%) which was used in the next step without further purification. ^{1}H NMR (400 MHz, $CDCl_3$, δ): ^{1}H NMR (400 MHz, $CDCl_3$ δ): 7.32 – 7.09 (m, 4H), 4.10 – 3.90 (m, 2H), 3.13 (d, *J* = 21.3 Hz, 1H), 2.91 – 2.76 (m, 1H), 1.31 – 1.15 (m, 9H). ^{13}C-NMR (100 MHz, $CDCl_3$, δ): 147, 140, 131 124, 62.4, 53.5, 34.6, 33.2, 16.3.

Compound 16. Compound **15** (1.0 g, 4.0 mmol) was added to a solution of compound **13** (1.3 g, 4.6 mmol) in 2 mL of THF at room temperature. After the reaction mixture was stirred at 50 °C overnight, the solvent was removed by rotary evaporation. The residue was purified by column chromatography over silica gel using 5:1 methylene chloride/methanol as the eluent to give a light yellow powder (1.5 g, 75%). ^{1}H NMR (400 MHz, $CDCl_3$, δ) 9.65 (s, 1H), 7.48 (d, *J* = 8.1 Hz, 2H), 7.36 (d, *J* = 7.9 Hz, 2H), 7.22 (d, *J* = 7.9 Hz, 2H), 6.74 (d, *J* = 7.9 Hz, 2H), 4.03 – 3.99 (m, 2H), 3.98 – 3.96 (m, 2H), 3.11 (d, *J* = 21.5, Hz, 2H), 2.87 (m, 1H), 2.76 (t, *J* = 10.0 Hz, 2H), 1.93 (m, 3H), 1.49 (s, 9H), 1.33 (m, 4H), 1.23 (d, *J* = 7.0 Hz, 6H), 0.87 (t, *J* = 7.3 Hz, 3H).^{13}C NMR (100 MHz, $CDCl_3$, δ): 153, 148 , 140, 132, 130 129, 127, 125, 119, 81.3,77.1, 62.6, 51.2, 50.6, 46.3, 34.3, 32.9, 28.7, 28.2, 24.4 , 20.5, 16.8, 13.9. ESI-HRMS (*m/z*): $[M+Na]^+$ calcd for $C_{28}H_{43}N_2O_4PNa$, 525.2852; found 525.2875.

Compound 17. Trifluoroacetic acid (10% in THF) was added to compound **13** (0.05 g, 0.01 mmol) in 1 mL of THF at room temperature. After the reaction mixture was stirred at room

temperature for 8 h, the solvent was removed by rotary evaporation and the residue was mixed with LiOH (0.0036 g, 0.15 mmol) in 4:1 MeOH/H_2O (2 mL + 0.5 mL). After the reaction mixture was stirred for 6 h and the solvents were removed by rotary evaporation, the residue was purified by column chromatography over silica gel using 15:1 methylene chloride/methanol as the eluent to give a light yellow powder (3.4 mg, 77%).^{1}H NMR (400 MHz, $CDCl_3$, δ) 7.21 (d, *J* = 8.0 Hz, 2H), 7.09 (d, *J* = 8.1 Hz, 2H), 7.00 (d, *J* = 7.7 Hz, 2H), 6.57 (d, *J* = 8.0 Hz, 2H), 3.55 (s, 2H), 2.90 (d, *J* = 20.9 Hz, 2H), 2.76 (m, 1H), 2.23 (m, 2H), 1.42 (m, 2H), 1.16 – 1.05 (m, 9H), 0.82 – 0.72 (m, 3H).^{13}C NMR (100 MHz, $CDCl_3$, δ): 147, 131, 130,129, 126, 115, 114, 80.1, 48.2, 33.6, 27.3, 24.0, 20.3, 19.9, 13.6.ESI-HRMS (*m/z*): $[M+NH_4]^+$ calcd for $C_{21}H_{34}N_3O_2P$, 391.2388; found 391.2300.

Compound 4a. Compound **17** (4.0 mg, 0.01 mmol) and 4-vinylbenzaldehyde **18** (1.3 mg, 0.01 mmol) were dissolved in 1 mL of ethanol. The reaction mixture was heated to reflux overnight and cooled to room temperature. Diethyl ether (40 mL) was added slowly. The precipitate formed was collected by filtration and washed with 5 mL of diethyl ether to yield a yellow powder (5.0 mg, 81%). The product was used in the MINP preparation without further purification. ^{1}H NMR (400 MHz, $CDCl_3$, δ) 8.33 (s, 1H), 7.86 – 7.80 (m, 2H), 7.56 (dd, *J* = 8.1, 1.5 Hz, 1H), 7.50 (dd, *J* = 8.1, 1.5 Hz, 1H), 7.36 (d, *J* = 7.6 Hz, 1H), 7.21 (d, *J* = 7.7 Hz, 2H), 7.12 (d, *J* = 7.8 Hz, 2H), 7.01 (d, *J* = 7.6 Hz, 2H), 6.76 (td, *J* = 11.2, 5.6 Hz, 1H), 6.58 (d, *J* = 7.8 Hz, 1H), 5.90 (dd, *J* = 32.3, 10.8 Hz, 1H), 5.40 (dd, *J* = 32.3, 10.8 Hz, 1H), 3.70 (td, *J* = 6.3, 5.7, 2.2 Hz, 2H), 2.92 (d, *J* = 21.0 Hz, 2H), 2.76 (h, *J* = 7.0, 6.5 Hz, 1H), 2.27 (t, *J* = 21.7 Hz, 2H), 1.28 – 1.21 (m, 4H), 1.12 (d, *J* = 6.8 Hz, 6H), 0.77 (t, *J* = 7.3 Hz, 3H).

Compound 5a.[27] To a 500 mL three-neck round-bottom flask were added carbon disulfide (0.17 g, 2.26 mmol), DIPEA (0.72 g, 5.66 mmol), EtOH (10 mL), and 4-vinylaniline (0.6 g, 5.0 mmol). The reaction mixture was heated to reflux for 24 h and cooled to 5 °C, and the precipitate was collected by suction filtration. The filter cake was stirred with 50 mL of hexanes and the solid was collected again by suction filtration and air-dried to give a yellow powder (0.95 g, 68%). ^{1}H NMR (400 MHz, $CDCl_3$, δ): 8.36 (br, 1H), 7.40 (d, *J* = 2.1 Hz, 4H), 7.28 (d, *J* = 2.1 Hz, 4H), 6.70 (ddd, *J* = 17.6, 10.9, 2.1 Hz, 2H), 5.74 (dd, *J* = 17.6, 2.1 Hz, 2H), 5.26 (dd, *J* = 10.9, 2.1 Hz, 2H).

Compound (4a·5a). A mixture of **4a** (2.0 mg, 0.004 mml) and **5a** (1.15 mg, 0.004 mmol) was stirred in dry CH_2Cl_2 (3 mL) at room temperature for 1 h. The solvent was removed by rotary evaporation and the residue was used in MINP preparation without further purification. ^{1}H NMR (400 MHz, $CDCl_3$, δ): 8.34 (s, 1H), 7.84 (d, *J* = 8.3 Hz, 2H), 7.56 (d, *J* = 7.9 Hz, 2H), 7.51 (d, *J* = 8.1 Hz, 2H), 7.38 (d, *J* = 8.1 Hz, 4H), 7.20 (d, *J* = 7.7 Hz, 4H), 7.13 (d, *J* = 8.0 Hz, 2H), 7.01 (d, *J* = 7.6 Hz, 2H), 6.95 (s, 1H), 6.82 – 6.72 (dd, *J* = 17.5, 10.9 Hz, 1H), 6.67 (dd, *J* = 17.5, 10.9 Hz, 2H), 6.60 (d, *J* = 7.8 Hz, 2H), 4.64 (s, 2H), 3.76 – 3.69 (m, 2H), 2.91 (d, *J* = 21.3 Hz, 2H), 2.78 (h, *J* = 7.0 Hz, 1H), 2.32 (s, 2H), 1.27 – 1.22 (m, 4H), 1.13 (d, *J* = 6.9 Hz, 6H), 0.79 (t, *J* = 7.3 Hz, 3H).

Compound 19.[28] Thiophosgene (3.74 g, 32.5 mmol) was added dropwise to a solution of 4-methoxyaniline (2.0 g, 16.3 mmol) in toluene (20 mL). The mixture stirred at 100 °C under a nitrogen atmosphere for 8 h. After cooled to room temperature, the reaction mixture was neutralized with a saturated solution of K_2CO_3 and the mixture was stirred vigorously for 24 h at room temperature. The organic phase was separated, dried with anhydrous sodium sulfate, and concentrated by rotary evaporation. The residue was purified using column

chromatography over silica gel using 20:1 Hexane/EtOAc as the eluent to afford a yellowish oil (1.77 g, 68%). ^{1}H NMR (400 MHz, $CDCl_3$, δ): 7.15 (d, *J* = 9.0 Hz, 2H), 6.84 (d, *J* = 9.0 Hz, 2H), 3.79 (s, 3H). ^{13}C NMR (100 MHz, $CDCl_3$, δ): 158, 134, 127, 123, 115, 55.6.

Compound 5b. 4-Vinylaniline (0.12 g, 1.0 mmol) was added to a stirred solution of compound **19** (0.25 g, 1.5 mmol) in THF (5 mL) at 0 °C. The reaction mixture was warmed to room temperature and stirred for 9 h. The solvent was removed by rotary evaporation and the residue was purified by column chromatography over silica gel using 1:4 ethyl acetate/hexane as the eluent to give a yellow powder (0.37 g, 86%): ^{1}H NMR (400 MHz, $CDCl_3$ δ): 7.72 (s, 1H), 7.65 (s, 1H), 7.42 (d, *J* = 8.5 Hz, 2H), 7.35 (d, *J* = 8.5 Hz, 2H), 7.27 (d, *J* = 8.5 Hz, 2H), 6.94 (d, *J* = 8.5 Hz, 2H), 6.69 (m, 2H), 5.73 (dd, *J* = 17.6, 1.8 Hz, 2H), 5.27 (dd, *J* = 17.6, 1.8 Hz, 2H), 3.82 (s, 3H). ^{13}C NMR (100 MHz, DMSO-d_6, δ):180, 157, 140, 137, 133, 127, 126, 124, 114, 55.1. ESI-HRMS (*m/z*): $[M-H]^-$ calcd for $C_{16}H_{15}N_2OS$, 283.0911; found 283.0922.

Compound 20. [28] The same procedure as that for compound **19** was followed to give **20** as a yellowish oil (70%). ^{1}H NMR (400 MHz, $CDCl_3$, δ): 8.23 (d, *J* = 8.5 Hz, 1H), 7.34 (d, *J* = 8.5 Hz, 1H). ^{13}C NMR (100 MHz, $CDCl_3$, δ): 145,140, 138, 126, 125.

Compound 5c. The same procedure as that for compound **5b** was followed to give **5c** as a yellow powder (86%). ^{1}H NMR (400 MHz, $CDCl_3$ δ): 8.21 (d, *J* = 8.2 Hz, 2H), 8.10 (s, 1H), 7.85 (s, 1H), 7.73 (d, *J* = 8.2 Hz, 2H), 7.52 (d, *J* = 8.2 Hz, 2H), 7.29 (d, *J* = 8.1 Hz, 3H), 6.72 (dd, *J* = 17.6, 10.9 Hz, 1H), 5.80 (d, *J* = 17.6 Hz, 1H), 5.36 (d, *J* = 10.9 Hz, 1H).^{13}C NMR (100 MHz, DMSO-d_6, δ): 179., 144, 144, 137, 135, 135, 128, 125, 124, 123, 115. ESI-HRMS (*m/z*): $[M-H]^-$ calcd for $C_{15}H_{12}N_3O_2S$, 298.0656; found. 298.0665.

Compound 21.[27] The same procedure as that for compound **19** was followed to give **21** as a yellowish oil (66%). ^{1}H NMR (400 MHz, $CDCl_3$, δ): 8.86 (s, 1H), 8.36 (s, 2H). ^{13}C NMR (100 MHz, DMSO-d_6, δ):149, 143, 135, 126, 117.

Compound 5d. The same procedure as that for compound **5b** was followed to give **5c** as a yellow powder (75%). ^{1}H NMR (400 MHz, $CDCl_3$ δ) 8.83 (s, 3H), 8.18 (s, 1H), 8.09 (s, 1H), 7.54 (d, *J* = 8.2 Hz, 2H), 7.32 (d, *J* = 8.1 Hz, 2H), 6.73 (dd, *J* = 17.4, 10.9 Hz, 1H), 5.81 (d, *J* = 17.7 Hz, 1H), 5.37 (d, *J* = 11.0 Hz, 1H). ^{13}C NMR (100 MHz, DMSO-d_6, δ): 179, 144, 143, 138, 135, 135, 128, 125, 124, 123, 116. ESI-HRMS (*m/z*): $[M-H]^-$ calcd for $C_{15}H_{11}N_4O_4S$, 343.0506; found 343.0516.

Compound 7. A solution of 4-isopropylphenol (0.2 g, 1.5 mmol) and pyridine (0.12 g, 1.5 mmol) in dry CH_2Cl_2 (5 mL) was added slowly at 0°C to hexanoyl chloride (0.20 g, 1.5 mmol) in CH_2Cl_2 (1 ml). After stirred at 0°C for 1 h, the reaction mixture was warmed to room temperature and stirred for another 8 h. The mixture was washed with brine (40 mL), dried over anhydrous Na_2SO_4, concentrated by rotary evaporation, and purified by column chromatography over silica gel using 4:1 ethyl acetate/hexane as the eluent to afford a colorless liquid(0.25 g, 72%). ^{1}H NMR (400 MHz, $CDCl_3$, δ): 7.24 (d, *J* = 8.5 Hz, 2H), 7.01 (d, *J* = 8.5 Hz, 2H), 2.92 (hept, *J* = 7.0 Hz, 1H), 2.56 (t, *J* = 7.5 Hz, 2H), 1.78 (q, *J* = 8.5, 6.2 Hz, 2H), 1.45 – 1.38 (m, 4H), 1.26 (d, *J* = 6.9 Hz, 6H), 0.95 (t, *J* = 7.5 Hz, 3H).^{13}C NMR (100 MHz, DMSO-d_6, δ): 172, 149, 146, 127, 121, 34.4, 33.6, 31.3, 24.7, 24.0, 22.3, 13.9. ESI-HRMS (*m/z*): $[M+H]^+$ calcd for $C_{15}H_{23}O_2$, 235.1695; found 235.1709.

Compound 8. A solution of 4-isopropylphenol (0.2 g, 1.5 mmol) and pyridine (0.12 g, 1.5 mmol) in dry CH_2Cl_2 (5 mL) was added slowly at 0°C to 3,3-dimethylbutanoyl chloride (0.2 g, 1.5 mmol) in CH_2Cl_2 (2 ml). After stirred at 0°C for 1 h, the reaction mixture was warmed

to room temperature and stirred for another 8 h. The mixture was washed with brine (40 mL), dried over anhydrous Na_2SO_4, concentrated by rotary evaporation, and purified by column chromatography over silica gel using 4:1 ethyl acetate/hexane as the eluent to afford a colorless liquid (0.25 g, 73%). ^{1}H NMR (400 MHz, $CDCl_3$, δ): 7.27 (d, *J* = 8.5 Hz, 2H), 7.04 (d, *J* = 8.6 Hz, 2H), 3.00 – 2.89 (m, 1H), 2.48 (s, 2H), 1.29 (d, *J* = 7.0 Hz, 6H), 1.18 (s, 9H). ^{13}C NMR (100 MHz, DMSO-d_6, δ): 171, 148, 146, 127, 121, 47.7, 33.5, 30.9, 29.5, 23.9. ESI-HRMS (*m/z*): $[M+H]^+$ calcd for $C_{15}H_{23}O_2$, 235.1695; found 235.1699.

Compound 9. A solution of 4-isopropylphenol (1.5 g, 11 mmol) and pyridine (0.87g, 11 mmol) in dry CH_2Cl_2 (10 mL) was added slowly at 0°C to 4-methylpentanoyl chloride (1.0 g, 7.5 mmol) in CH_2Cl_2 (2 mL). After stirred at 0°C for 1 h, the reaction mixture was warmed to room temperature and stirred for another 8 h. The mixture was washed with brine (40 mL), dried over anhydrous Na_2SO_4, concentrated by rotary evaporation, and purified by column chromatography over silica gel using 4:1 ethyl acetate/hexane as the eluent to afford a colorless liquid (1.52 g, 87%). ^{1}H NMR (400 MHz, $CDCl_3$, δ): 7.22 (d, *J* = 8.4 Hz, 2H), 6.98 (d, *J* = 8.6 Hz, 2H), 2.90 (h, *J* = 7.0 Hz, 1H), 2.54 (ddd, *J* = 14.7, 6.1, 1.3 Hz, 1H), 2.34 (ddd, *J* = 14.7, 8.1, 1.3 Hz, 1H), 2.01 (dp, *J* = 13.2, 6.6 Hz, 1H), 1.46 (qt, *J* = 7.9, 6.2 Hz, 1H), 1.32 (dtd, *J* = 13.6, 7.4, 1.3 Hz, 1H), 1.24 (d, *J* = 6.9 Hz, 6H), 1.04 (d, *J* = 6.7 Hz, 3H), 0.95 (t, *J* = 7.4 Hz, 3H). ^{13}C NMR (100 MHz, DMSO-d_6, δ): 171, 147, 146, 128, 122, 41.9, 34.1, 32.6, 29.8, 24.5, 19.8, 11.8. ESI-HRMS (*m/z*): $[M+H]^+$ calcd for $C_{15}H_{23}O_2$, 235.1695; found 235.1686.

Compound 10. A solution of 4-isopropylphenol (0.2 g, 1.5 mmol) and pyridine (0.12 g, 1.5 mmol) in dry CH_2Cl_2 (5 mL) was added slowly at 0°C to octanoyl chloride (0.24 g, 1.5 mmol) in CH_2Cl_2 (1 mL). After stirred at 0°C for 1 h, the reaction mixture was warmed to room

temperature and stirred for another 8 h. The mixture was washed with brine (40 mL), dried over anhydrous Na_2SO_4, concentrated by rotary evaporation, and purified by column chromatography over silica gel using 4:1 ethyl acetate/hexane as the eluent to afford a colorless liquid (0.28 g, 74%). ^{1}H NMR (400 MHz, $CDCl_3$, δ): 7.30 (d, *J* = 8.5 Hz, 2H), 7.07 (d, *J* = 8.5 Hz, 2H), 2.98 (h, *J* = 6.9 Hz, 1H), 2.62 (t, *J* = 7.5 Hz, 2H), 1.90 – 1.80 (m, 2H), 1.57 – 1.36 (m, 8H), 1.32 (d, *J* = 6.9 Hz, 6H), 1.02 – 0.96 (t, *J* = 6.9 Hz, 3H). ^{13}C NMR (100 MHz, DMSO-d_6, δ): 172, 149, 146, 127, 121, 34.4, 33.7, 31.7, 29.1, 28.9, 25.0, 24.0, 22.6, 14.0. ESI-HRMS (*m/z*): $[M+H]^+$ calcd for $C_{17}H_{27}O_2$, 263.2005; found 263.2006.

Synthesis of MINP

MINPs were synthesized according to previously reported procedures.[16] To a micellar solution of **1** (10.2 mg, 0.02 mmol) in H_2O (2.0 mL), divinylbenzene (DVB, 1.4 μL, 0.01 mmol), the template–FM complex (**4·5a**) in DMSO (0.0004 mmol), and 2,2-dimethoxy-2-phenylacetophenone (DMPA) in DMSO (10 μL of a 12.8 mg/mL, 0.0005 mmol) were added. The mixture was sonicated for 10 min. Cross-linker **2** (4.1 mg, 0.024 mmol), $CuCl_2$ in H_2O (10 μL of 6.7 mg/mL, 0.0005 mmol), and sodium ascorbate in H_2O (10 μL of 99 mg/mL, 0.005 mmol) were then added and the reaction mixture was stirred slowly at room temperature for 12 h. Compound **3** (10.6 mg, 0.04 mmol), $CuCl_2$ (10 μL of a 6.7 mg/mL solution in H_2O, 0.0005 mmol), and sodium ascorbate (10 μL of a 99 mg/mL solution in H_2O, 0.005 mmol) were then added and the solution stirred for another 6 h at room temperature. The reaction mixture was transferred to a glass vial, purged with nitrogen for 15 min, sealed with a rubber stopper, and irradiated in a Rayonet reactor for 12 h. The reaction mixture was poured into acetone (8 mL). The precipitate was collected by centrifugation and washed with

three times each with 2 mL of acetone and methanol. The off-white product was dried in air to afford the final MINPs (> 80%).

Hydrolysis of Imine in MINP

Hydrolysis of imine in MINP was performed according to previously reported procedures.[29,30] The appropriate MINP (5.0 mg) was sonicated in 1.0 mL of 6 M hydrochloric acid for 20 min. The resulting solution was stirred at 95 °C for 2 h and then was poured into acetone (8 mL). The precipitate formed was collected by centrifugation and washed with a mixture of acetone/water (5 mL/1 mL) three times. The off-white product was dried in air to afford MINP-CHO, with the imine hydrolyzed (4.0 mg, 80%).

Synthesis of Pyridyl-Functionalized MINP

Pyridyl-functionalized MINPs were synthesized according to previously reported procedures. [29,30] The appropriate MINP-CHO (4.0 mg) was sonicated in 0.5 mL of anhydrous DMF for 20 min until it was fully dissolved. An aliquot (5.0 μL) of a stock solution of **6b** (25.0 mg in 1 mL DMSO) was added. The reaction mixture was stirred for 2 h at room temperature. An aliquot of sodium borohydride stock solution (40.0 mg in 1 mL anhydrous DMF) was added. After stirred overnight, the reaction mixture was poured into acetone (8 mL). The precipitate formed was collected by centrifugation and washed with three times each with 2 mL of acetone and methanol and air-dried to give an off-white powder (3.0 mg, 75%).

Determination of Binding Constants by ITC

In general, a solution of an appropriate guest in 25 mM HEPES buffer (pH 7.0) was injected in equal steps into 1.43 mL of the corresponding MINP in the same solution. The top panel shows the raw calorimetric data. The area under each peak represents the amount of

heat generated at each ejection and is plotted against the molar ratio of the MINP to the guest. The smooth solid line is the best fit of the experimental data to the sequential binding of *N* binding site on the MINP. The heat of dilution for the guest, obtained by titration carried out beyond the saturation point, was subtracted from the heat released during the binding. Binding parameters were auto-generated after curve fitting using Microcal Origin 7.

Kinetic Measurements

UV-vis spectroscopy method. Stock solutions (10 mM) of *p*-nitrophenyl hexanoate (PNPH) and other activated esters in methanol were prepared. The stock solutions were stored in a refrigerator and used within 3 d. Stock solutions of the appropriate catalytic MINPs (100 μM) in 25 mM HEPES buffer (pH 7.0) were prepared. For the kinetic experiment, a typical procedure is as follows: An aliquot of 300 μL of the catalytic MINP stock solution was combined with 1690 μL of the same HEPES buffer in a cuvette. The cuvette was placed in a UV-vis spectrometer and equilibrated to 40.0 °C. After 5 min, an aliquot of 10 μL of the PNPH stock solution was added. The concentration of the substrate (PNPH) in the reaction mixture was 50 μM and the concentration of the MINP was 15 μM in all cases. The hydrolysis was monitored by the absorbance of *p*-nitrophenoxide at 400 nm. The amount of the product formed was calculated from a calibration curve obtained from *p*-nitrophenol at pH 7.

GC-MS spectroscopy method. Stock solutions (20 mM) of nonactivated esters (**7**–**10**) in methanol were prepared. Stock solutions of the appropriate catalytic MINPs (100 μM) in 25 mM HEPES buffer were prepared. For the kinetic experiment, a typical procedure is as follows: An aliquot of 75 μL of the catalytic MINP stock solution and 7.5 μL of a nonactivated ester were combined with 418 μL of the same HEPES buffer in a vial. The

concentration of the ester in the reaction mixture was 300 µM and the concentration of the catalyst 15 µM. The sealed vial was kept at 60.0 °C in a heating block for 16 h. After 16 h, the reaction mixture was cooled to room temperature and extracted with diethyl ether (500 µL).The hydrolysis was monitored by the decrease of substrate (ester) peak intensity by using an internal standard (*p*-xylene, 300 µM).

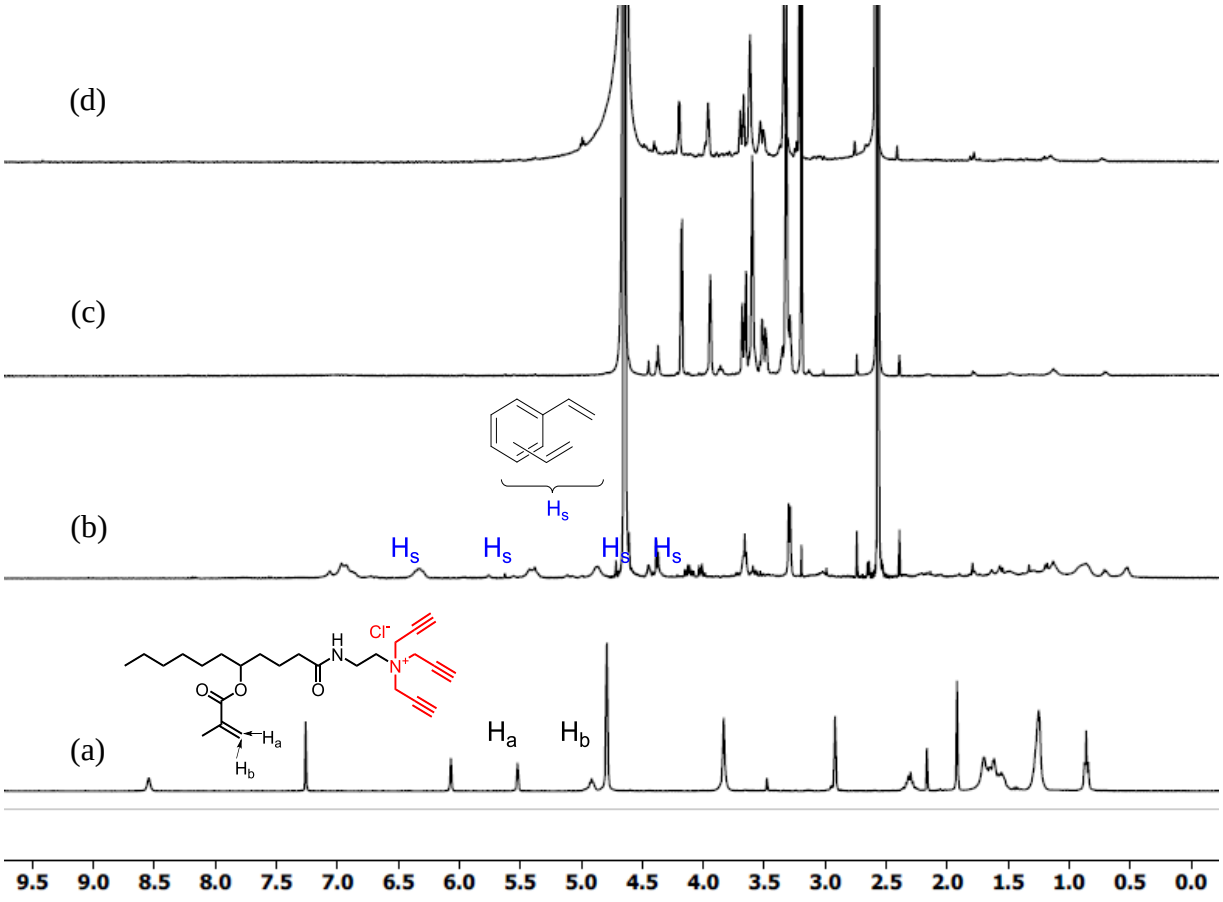

Figure 3. ^{1}H NMR spectra of (a) **1b** in $CDCl_3$, (b) alkynyl-SCM in D_2O, (c) after core-crosslinking in D_2O, (d) purified $MINP_{\mathbf{1a}}$(**5a**+**6b**) in D_2O.

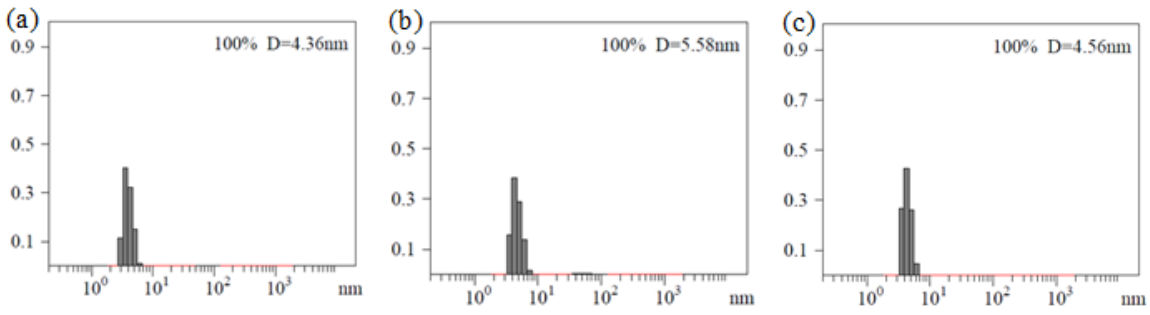

Figure 4. Distribution of the hydrodynamic diameters of the nanoparticles in water as determined by DLS for (a) alkynyl-SCM, (b) surface-functionalized SCM and (c) $MINP_{\mathbf{1a}}$ (**5a**+**6b**) after purification.

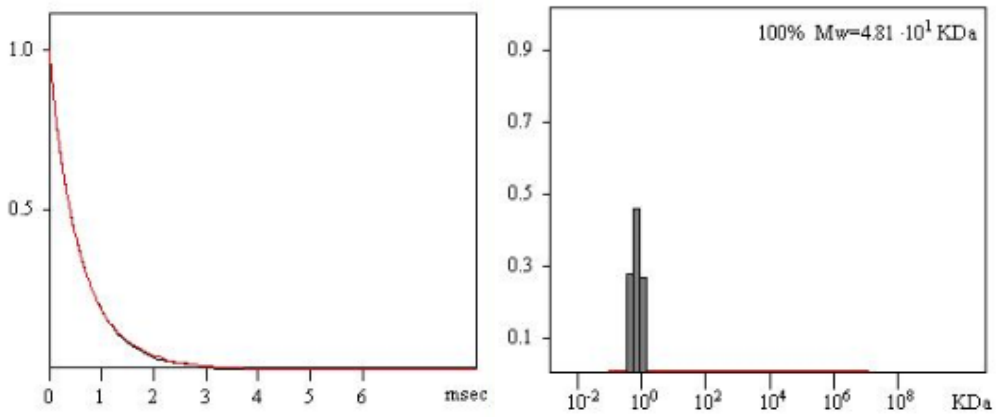

Figure 5. (a) Distribution of the molecular weights of the $MINP_{\mathbf{1a}}$(**5a**+**6b**). (b) The correlation curve for DLS. The molecular weight distribution was calculated by the PRECISION DECONVOLVE program assuming the intensity of scattering is proportional to the mass of the particle squared. If each unit of building block for the $MINP_{\mathbf{1a}}$ (**5a**+**6b**) is assumed to contain one molecule of compound **1a** (MW = 521 g/mol), 1.2 molecules of compound **2** (MW = 172 g/mol), 0.5 molecule of DVB (MW = 130 g/mol), 0.8 molecules of compound **4** (MW = 264 g/mol), 0.02 molecules (MW = 518 g/mol) of the complex (5s+18+6b), the molecular weight of $MINP_{\mathbf{1a}}$ (**5a**+**6b**) translates to 47 [=48100/(521 + 1.2×172 + 0.5×130 + 0.8×264+ 0.02×518)] of such units.

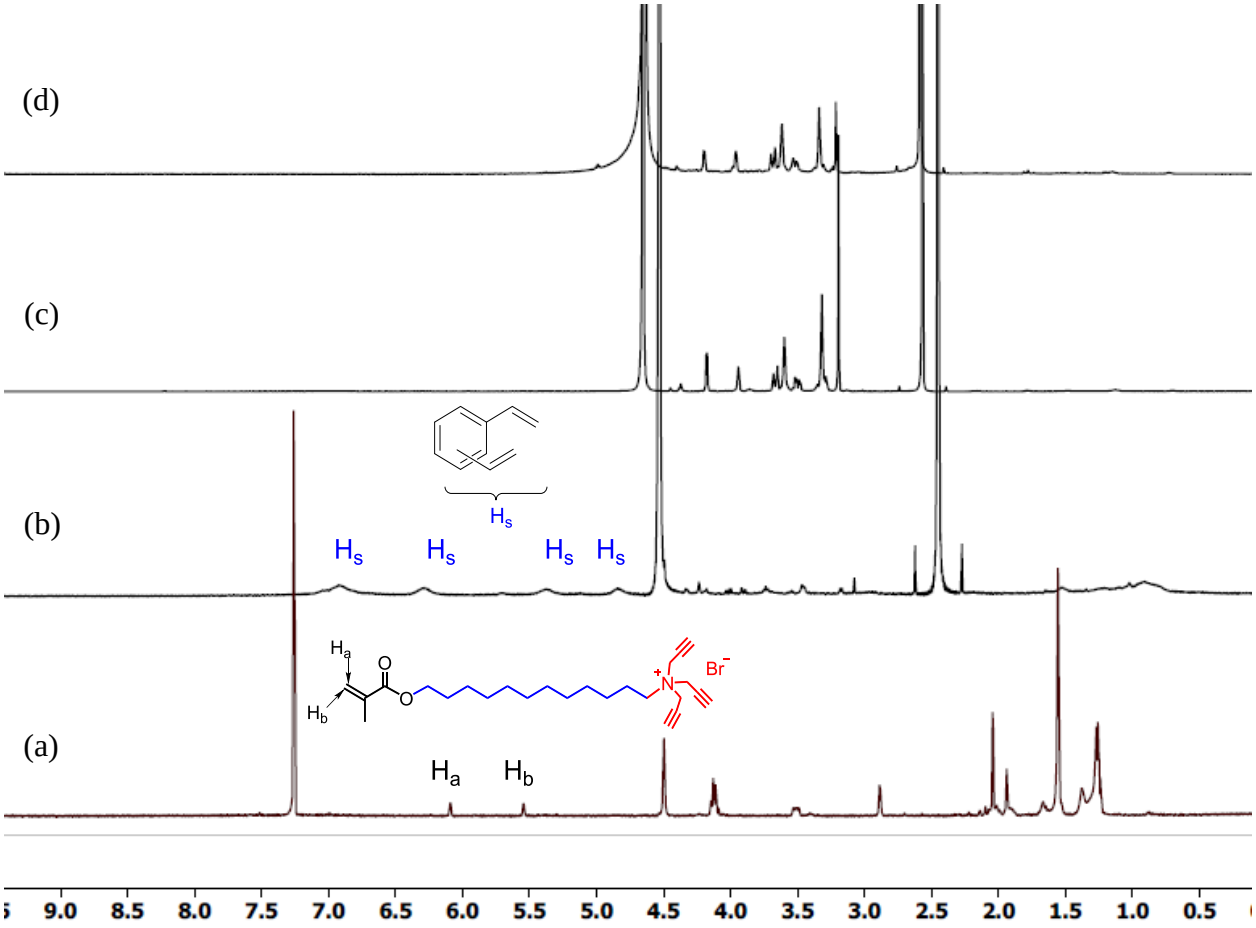

Figure 6. ^{1}H NMR spectra of (a) **1b** in $CDCl_3$, (b) alkynyl-SCM in D_2O, (c) after core-crosslinking in D_2O, (d) purified $MINP_{\mathbf{1b}}$(**5d**+**6b**) in D_2O.

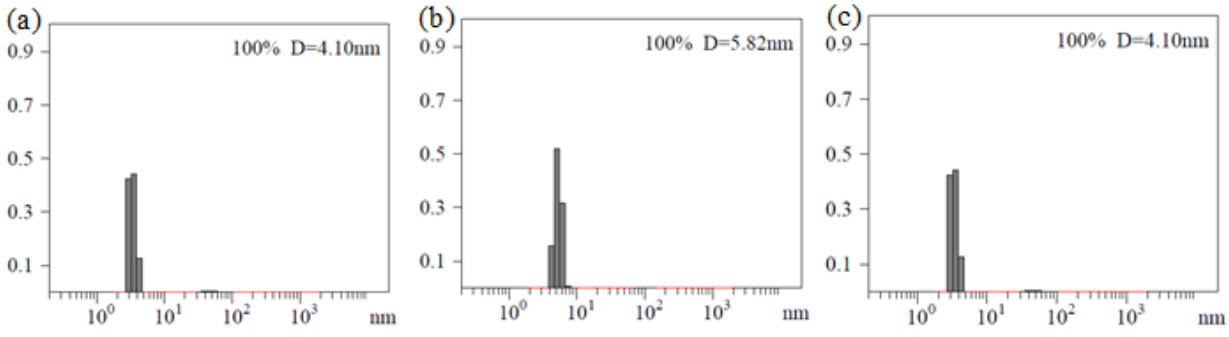

Figure 7. Distribution of the hydrodynamic diameters of the nanoparticles in water as determined by DLS for (a) alkynyl-SCM, (b) surface-functionalized SCM and (c) $MINP_{\mathbf{1b}}$ (**5d**+**6b**) after purification.

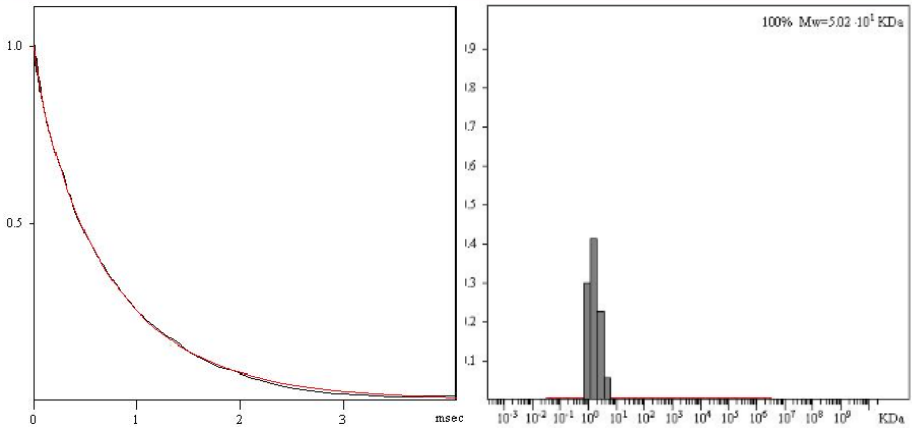

Figure 8. (a) Distribution of the molecular weights of the MINP$_{\mathbf{1b}}$ (**5d**+**6b**) (b) The correlation curve for DLS. The molecular weight distribution was calculated by the PRECISION DECONVOLVE program assuming the intensity of scattering is proportional to the mass of the particle squared. If each unit of building block for the MINP$_{\mathbf{1b}}$ (**5d**+**6b**) is assumed to contain one molecule of compound **1a** (MW = 521 g/mol), 1.2 molecules of compound **2** (MW = 172 g/mol), 0.5 molecule of DVB (MW = 130 g/mol), 0.8 molecules of compound **4** (MW = 264 g/mol), 0.02 molecules (MW = 518 g/mol) of the complex (5s+18+6b), the molecular weight of MINP$_{\mathbf{1b}}$ (**5d**+**6b**) translates to 52 [=50200 / (465 + 1.2×172 + 0.5×130 + 0.8×264+ 0.02×518)] of such units.

Table 3. Binding data for MINPs obtained by ITC[a]

Entry	MINPs	Guest	-Δ*G* (kcal/mol)	*N*	K_a (10^4 M^{-1})	-Δ*H* (kcal/mol)	TΔ*S* (kcal/mol)
1	MINP$_{\mathbf{1b}}$ (**5a**+**6b**)	**4b**	7.30	1.21 ± 0.02	21.2 ± 2.14	24.8 ± 1.88	-17.5
2	MINP$_{\mathbf{1b}}$ (**5d**+**6b**)	**4b**	7.64	1.27 ± 0.02	38.2± 3.51	5.04 ± 1.50	2.60
3	MINP$_{\mathbf{1a}}$ (**5a**+**6b**)	**4b**	6.98	1.19 ± 0.03	13.7 ± 0.97	4.88 ± 0.14	2.10
4	MINP$_{\mathbf{1b}}$ (**6b**)	**4b**	6.80	1.11 ± 0.31	9.04 ± 1.51	10.6 ± 1.81	-3.80
5	NINP$_{\mathbf{1a}}$	**4b**	-[b]	-[b]	-[b]	-[b]	-[b]
6	NINP$_{\mathbf{1b}}$	**4b**	-[b]	-[b]	-[b]	-[b]	-[b]

[a] The titrations were performed in duplicates in 25 mM HEPES buffer (pH 7.0) at 25 °C and the errors between the runs were <20%. [b]Binding (K_a <100 M^{-1}) was too weak to be measured accurately by ITC.

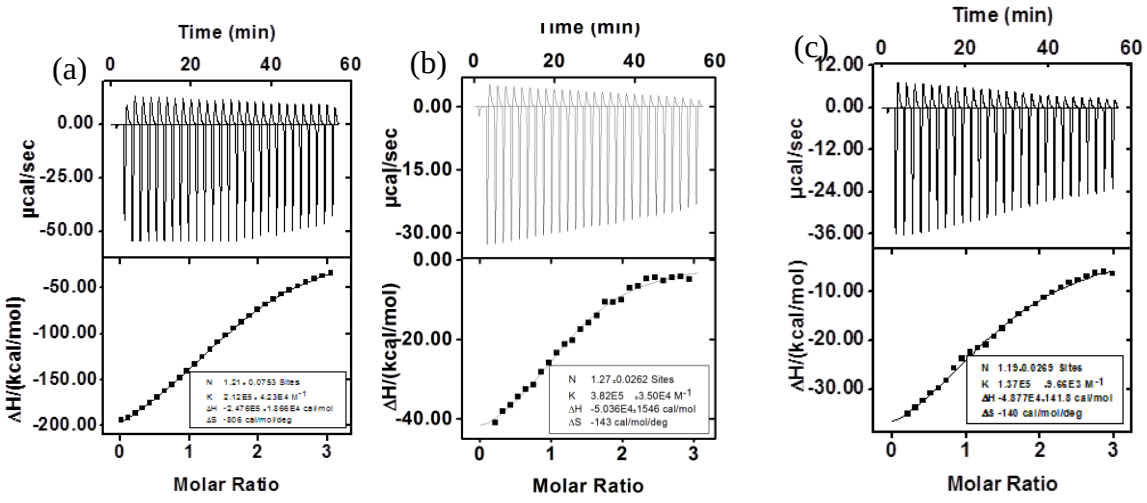

Figure 9. ITC titration curves obtained at 298 K for the binding of **4b** with (a) $MINP_{1b}$(**5a**+**6b**), (b) $MINP_{1b}$ **5d+6b**), and (b) $MINP_{1a}$(**5a**+**6b**) prepared in HEPES buffer (25 mM HEPES, pH = 7.0). The data correspond to entries 1–3, respectively, in Table S1. The top panel shows the raw calorimetric data. The area under each peak represents the amount of heat generated at each ejection and is plotted against the molar ratio of MINP to the substrate. The solid line is the best fit of the experimental data to the sequential binding of N equal and independent binding sites on the MINP. The heat of dilution for the substrate, obtained by adding the substrate to the buffer, was subtracted from the heat released during the binding. Binding parameters were auto-generated after curve fitting using Microcal Origin 7.0 substrate, obtained by adding the substrate to the buffer, and was subtracted from the heat released during the binding. Binding parameters were auto-generated after curve fitting using Microcal Origin 7.

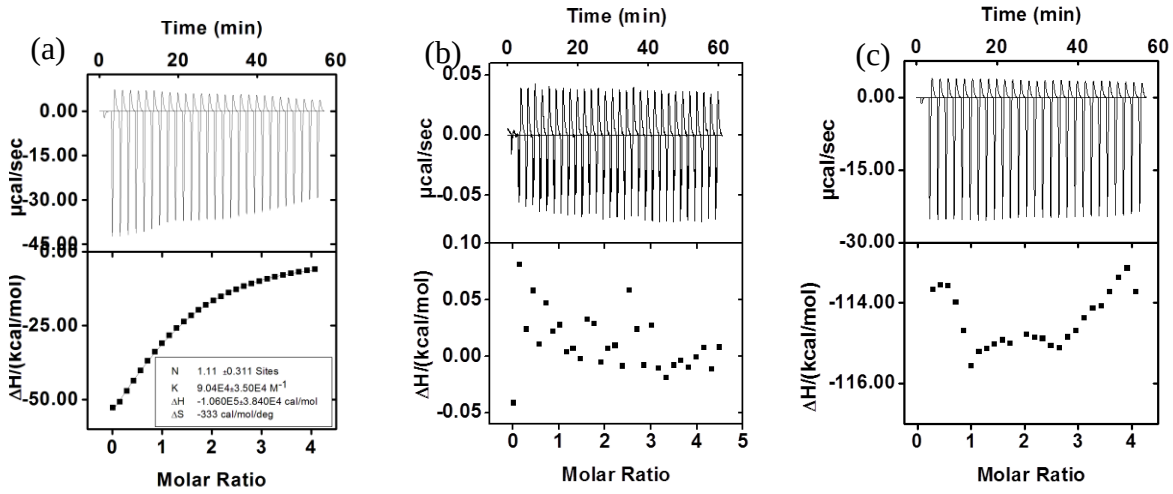

Figure 10. ITC titration curves obtained at 298 K for the binding of **4b** with (a) $MINP_{\mathbf{1b}}$ (**6b**), (b) $NINP_{\mathbf{1b}}$, and (c) $NINP_{\mathbf{1a}}$ prepared in HEPES buffer (25 mM HEPES, pH = 7.0). The data correspond to entries 4–6, respectively, in Table S1. The top panel shows the raw calorimetric data. The area under each peak represents the amount of heat generated at each ejection and is plotted against the molar ratio of MINP to the substrate. The solid line is the best fit of the experimental data to the sequential binding of N equal and independent binding sites on the MINP. The heat of dilution for the substrate, obtained by adding the substrate to the buffer, was subtracted from the heat released during the binding. Binding parameters were auto-generated after curve fitting using Microcal Origin 7.0 substrate, obtained by adding the substrate to the buffer, and was subtracted from the heat released during the binding. Binding parameters were auto-generated after curve fitting using Microcal Origin 7.

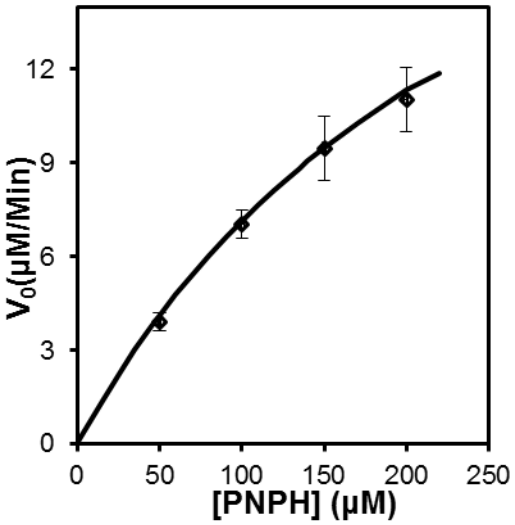

Figure 11. Michaelis-Menten plot of the hydrolysis of PNPH by $MINP_{1b}$ (**5d**+**6b**) in a 25 mM HEPES buffer at 40 °C and pH 7.0

^{1}H NMR of compound **11**

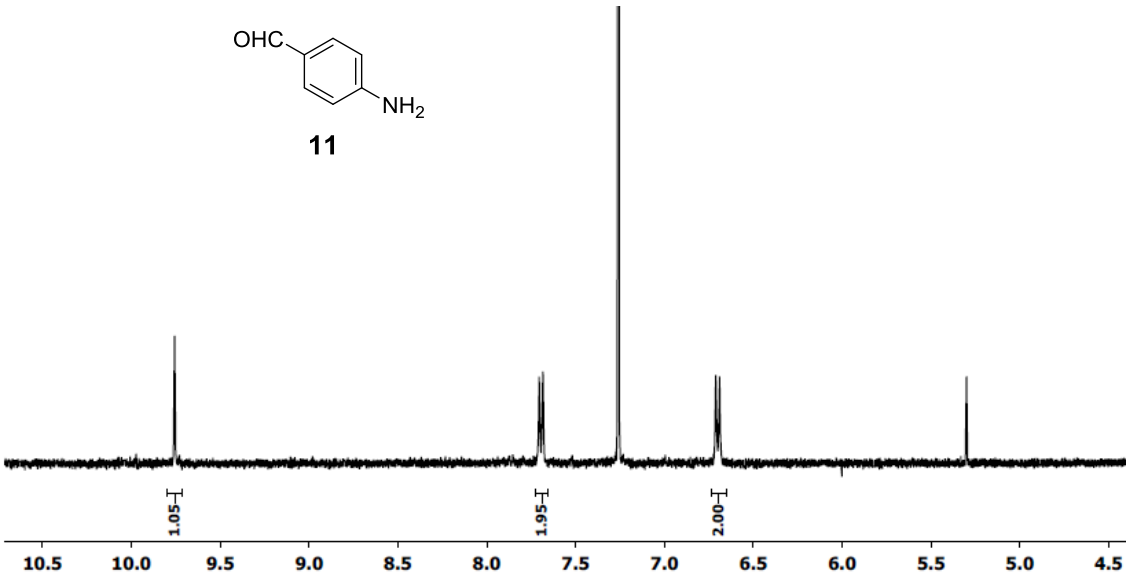

^{1}H NMR of compound **12**

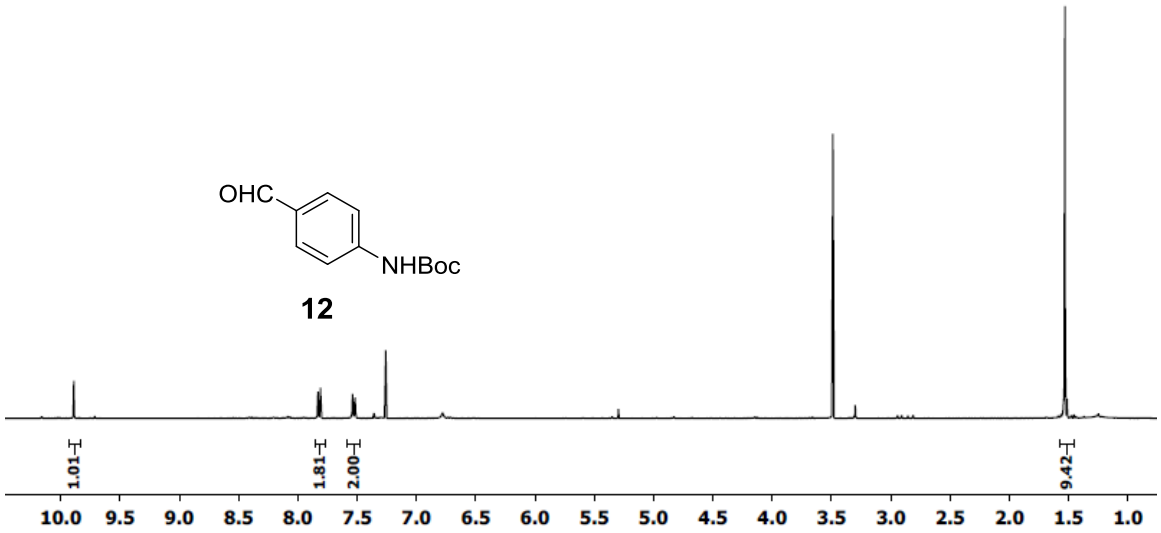

^{1}H NMR of compound **13**

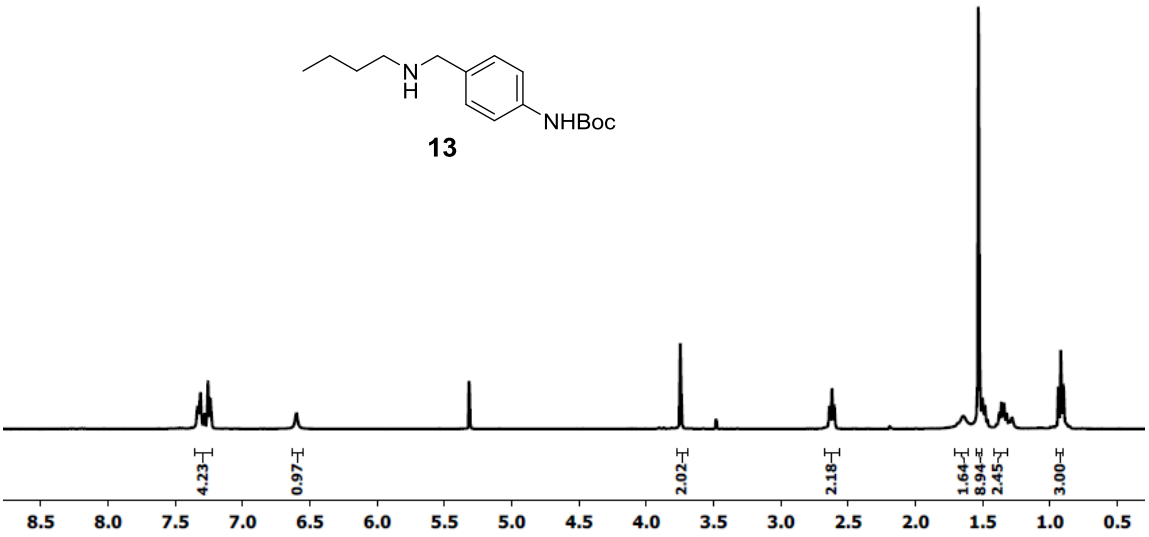

^{13}C NMR of compound **13**

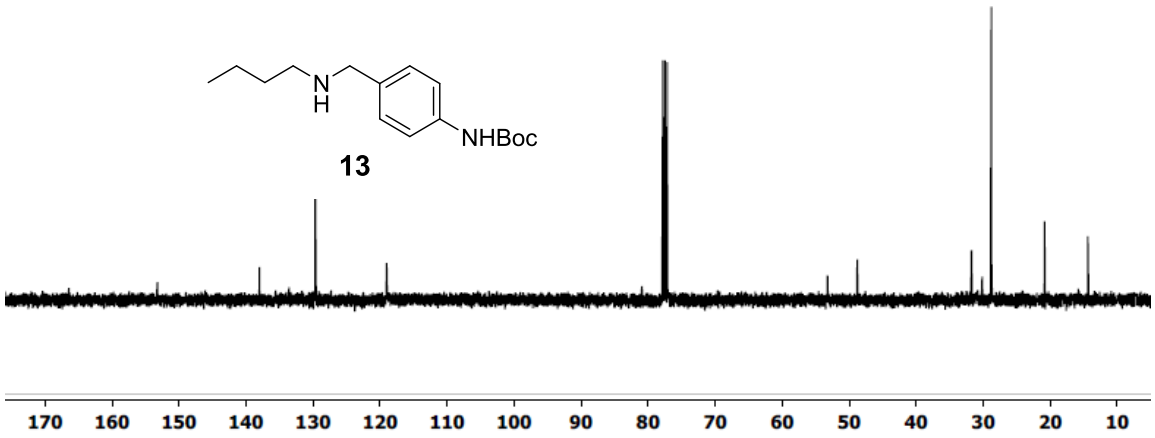

^{1}H NMR of compound **14**

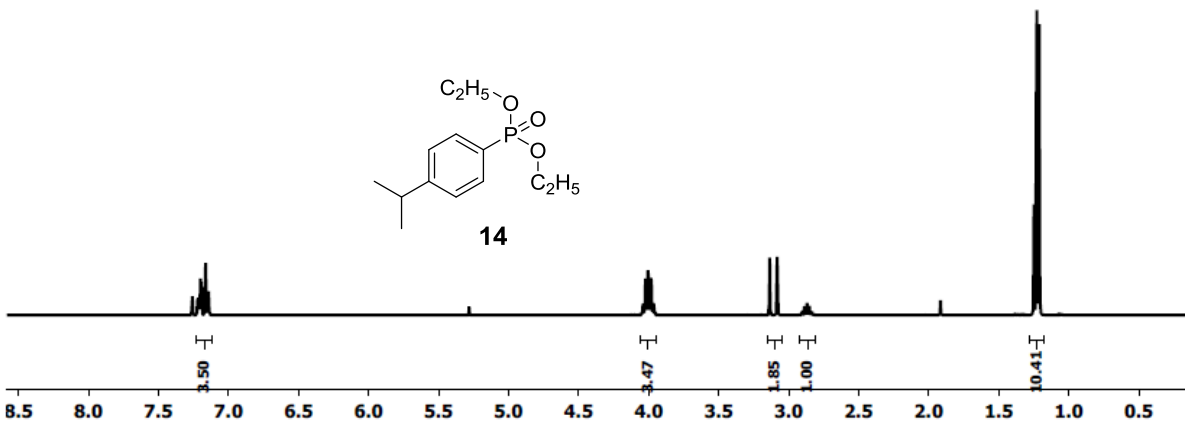

^{1}H NMR of compound **15**

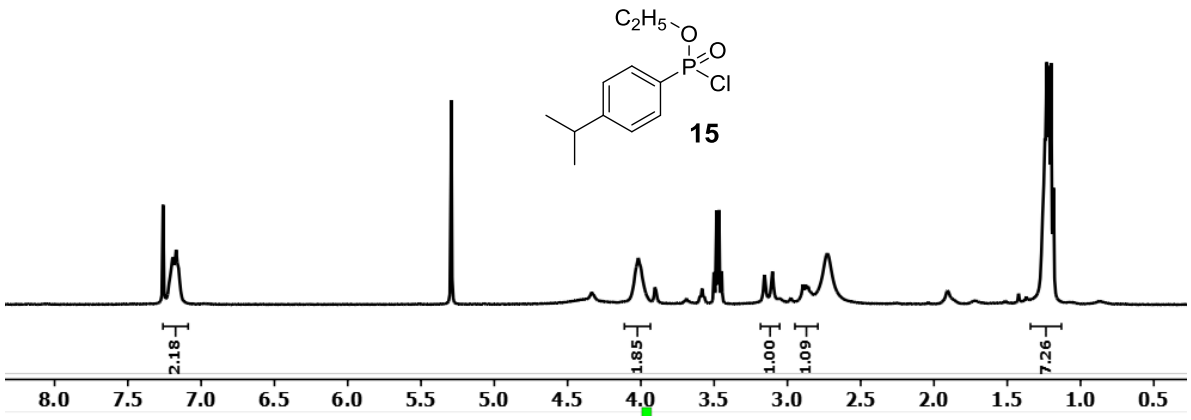

^{13}C NMR of compound **15**

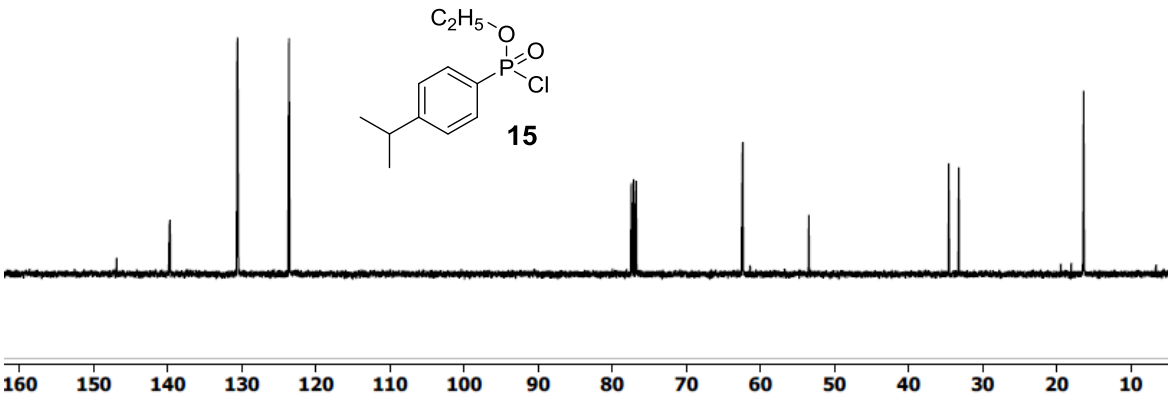

^{1}H NMR of compound **16**

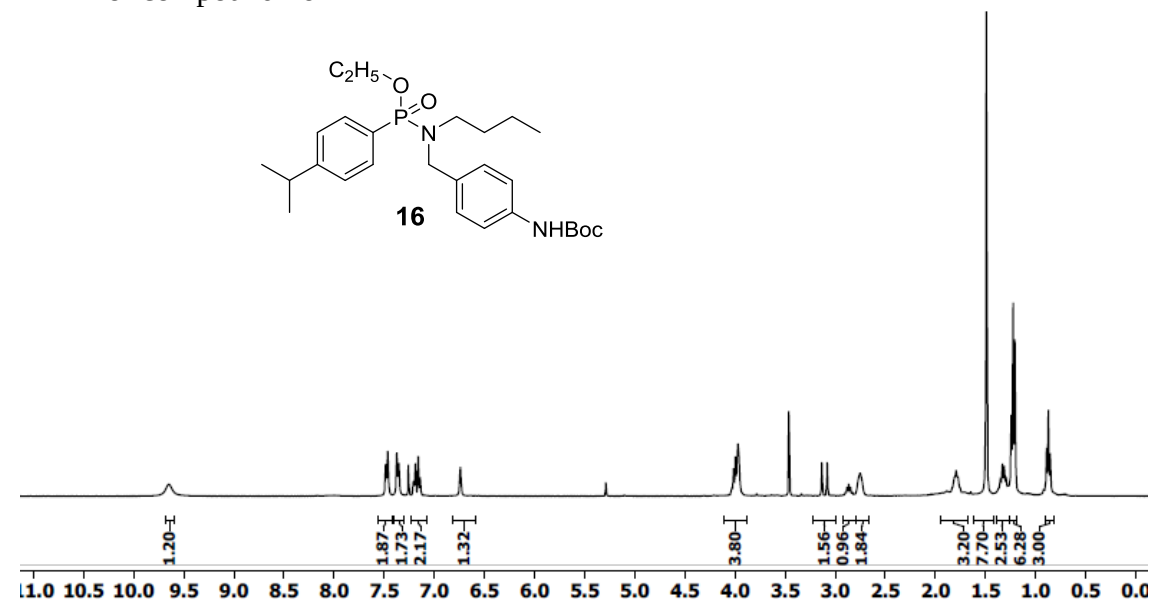

^{13}C NMR of compound **16**

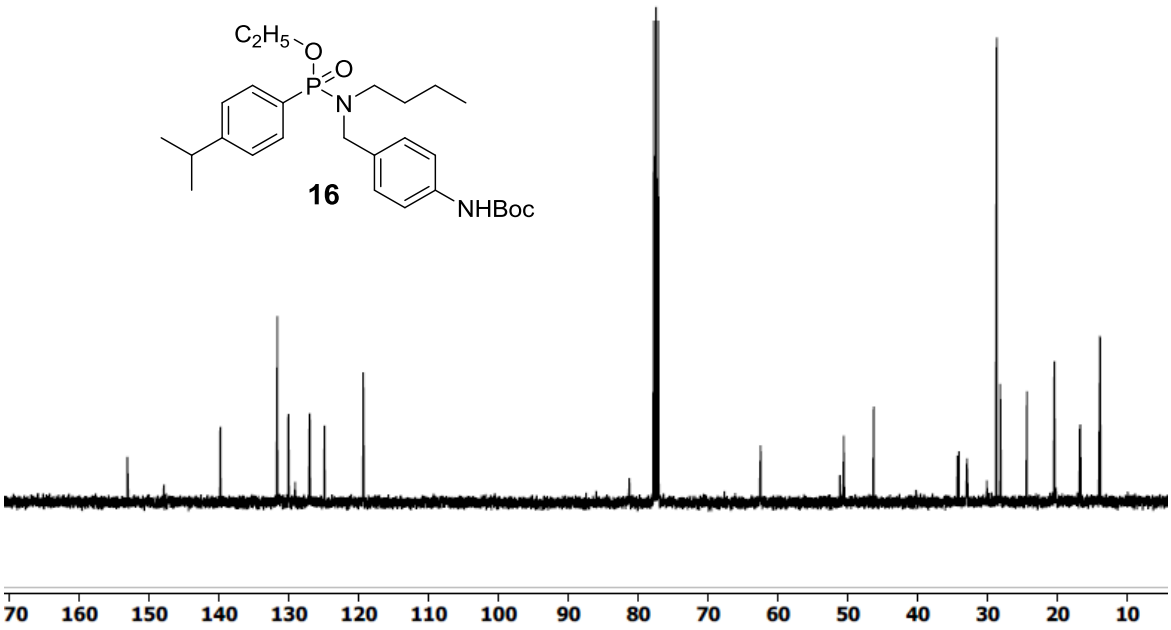

^{1}H NMR of compound **17**

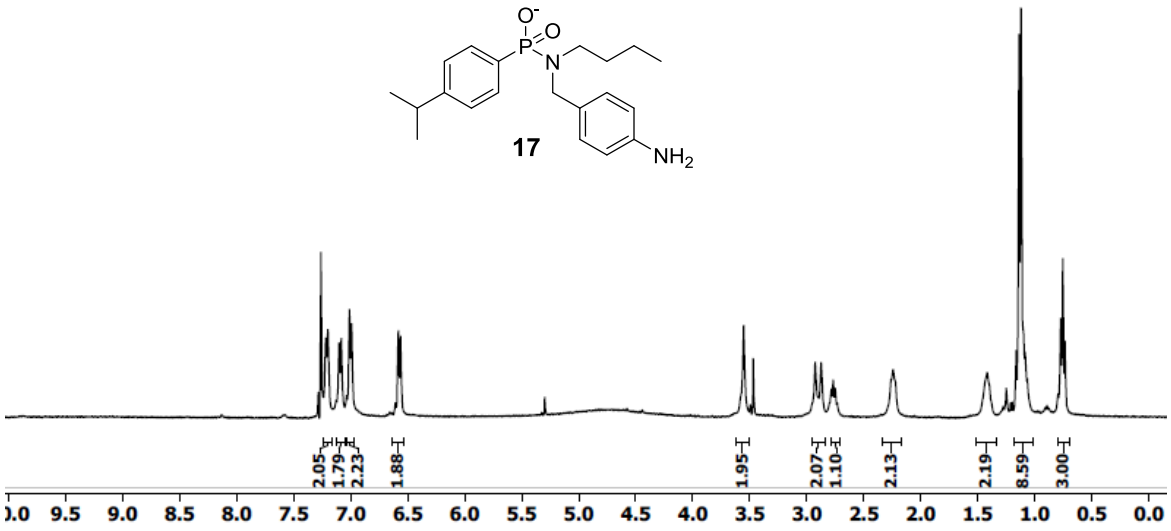

^{13}C NMR of compound **17**

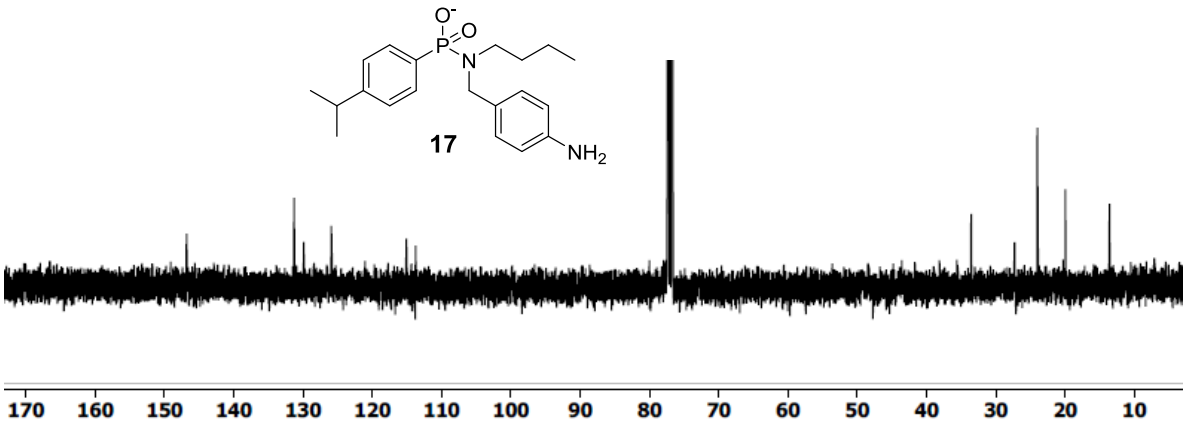

^{1}H NMR of compound **4a**

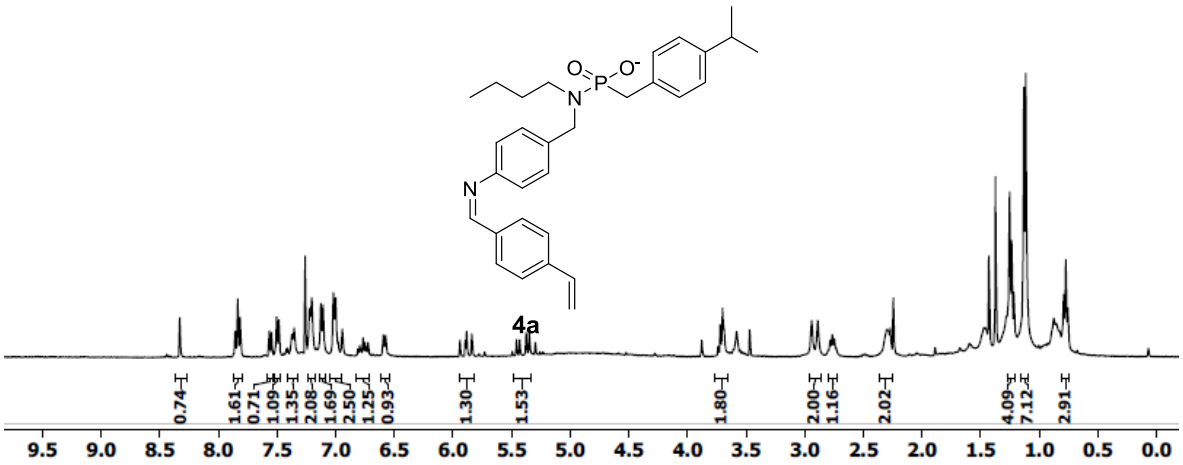

^{1}H NMR comparison between compound **4a &18**

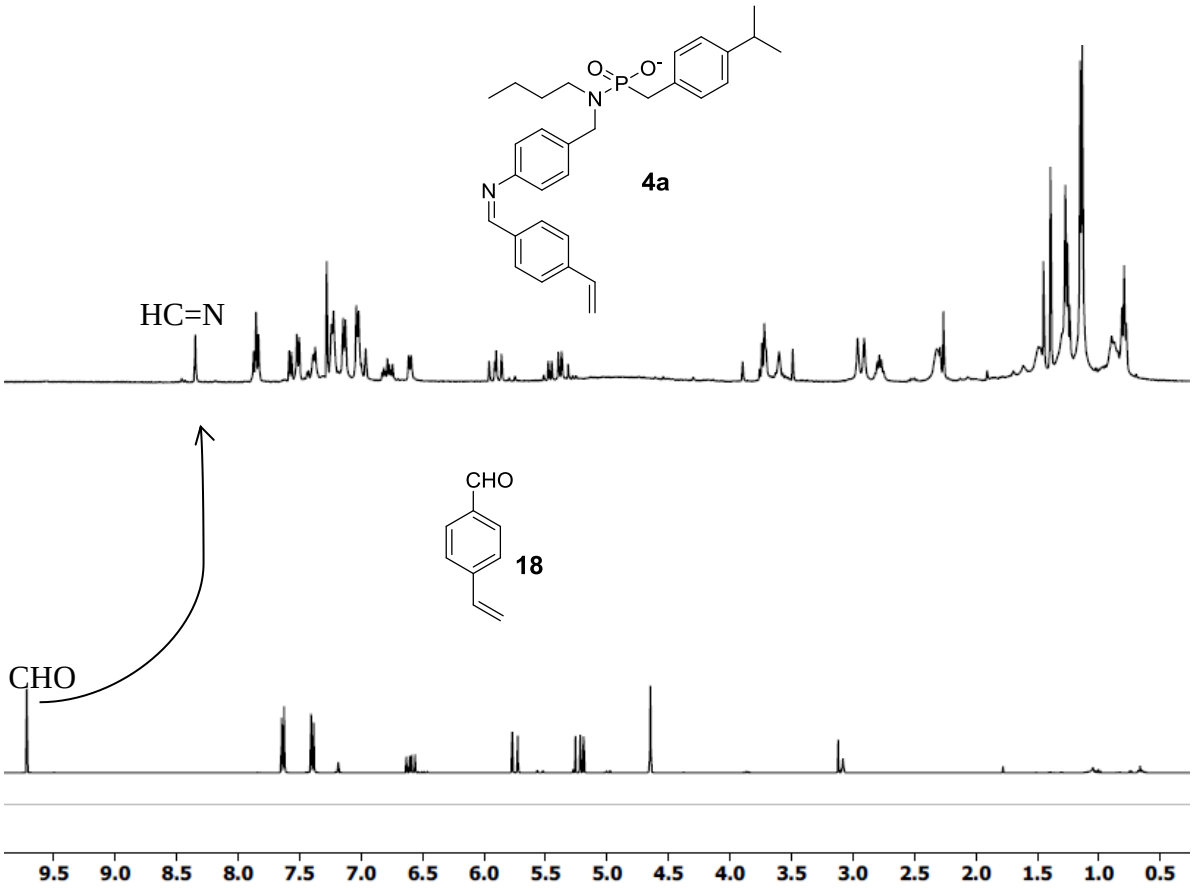

^{1}H NMR of compound **5a**

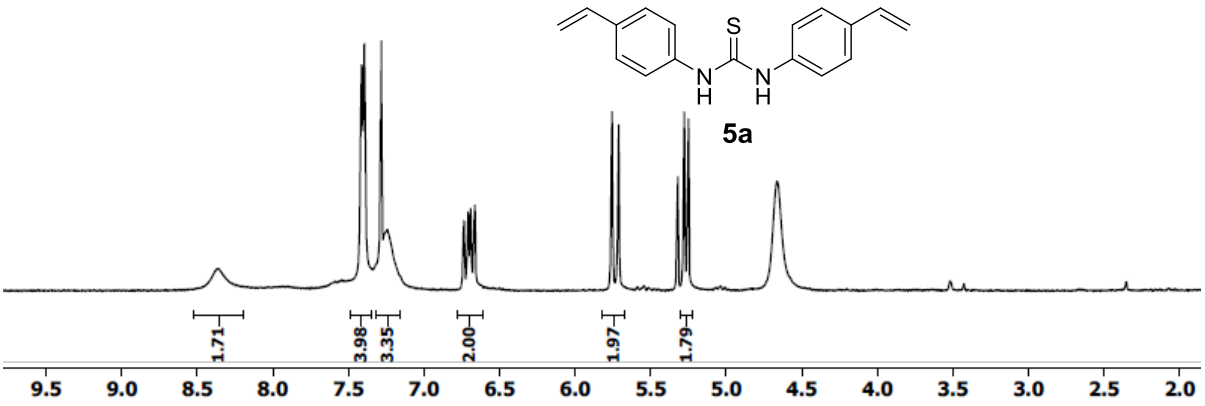

^{1}H NMR of complex (**4a•5a)**

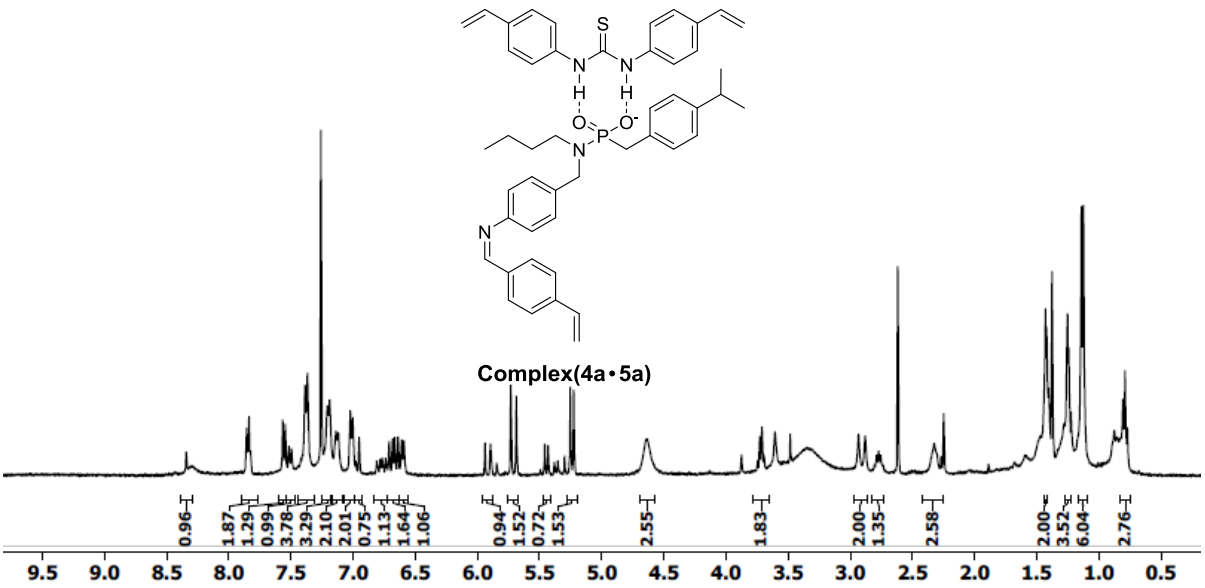

^{1}H NMR of compound **19**

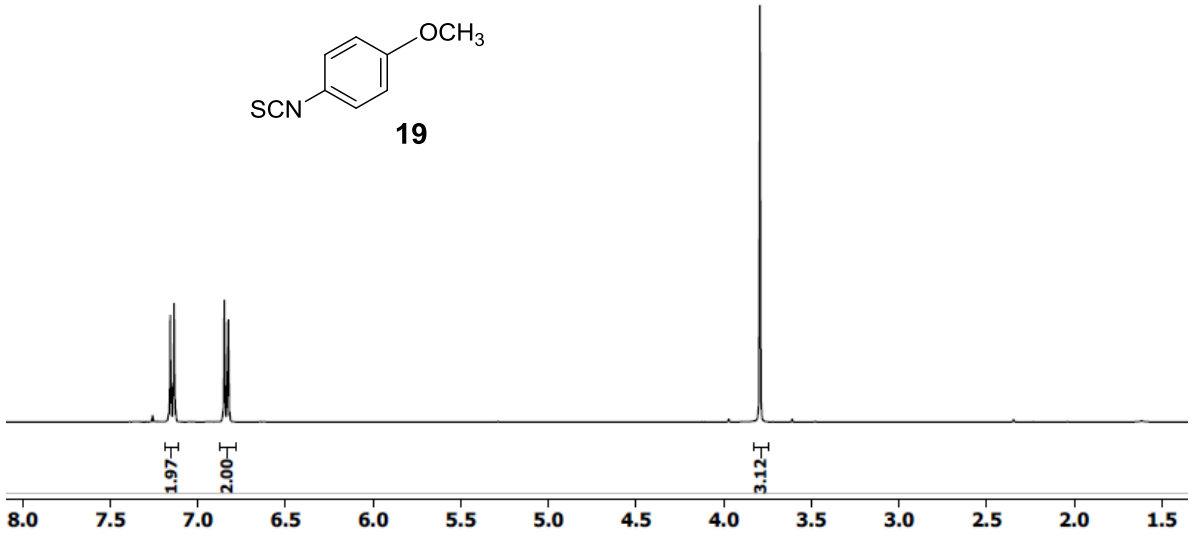

^{1}H NMR of compound **5b**

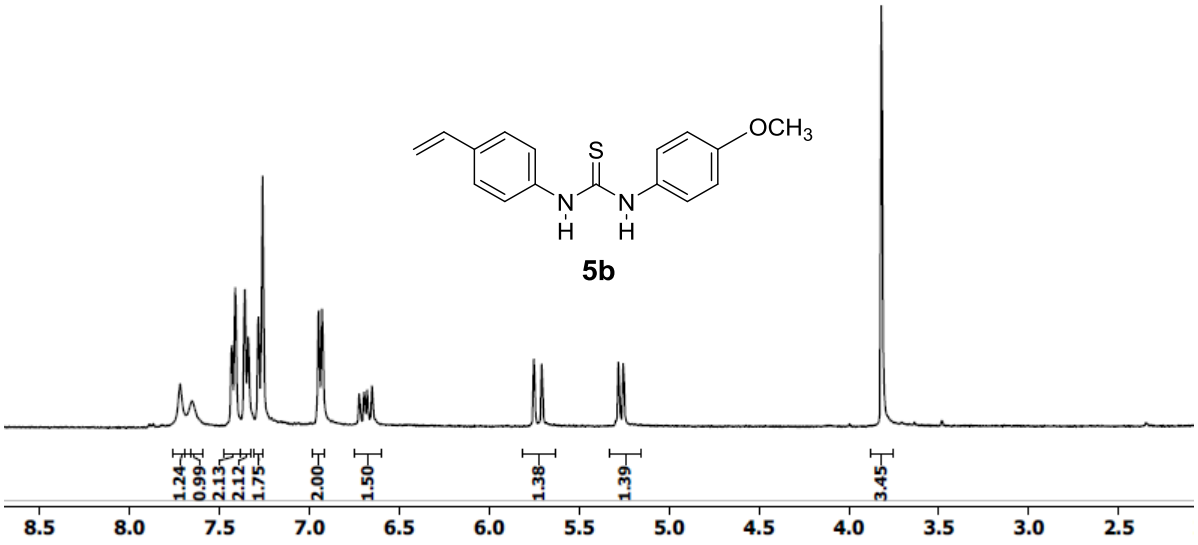

^{13}C NMR of compound **5b**

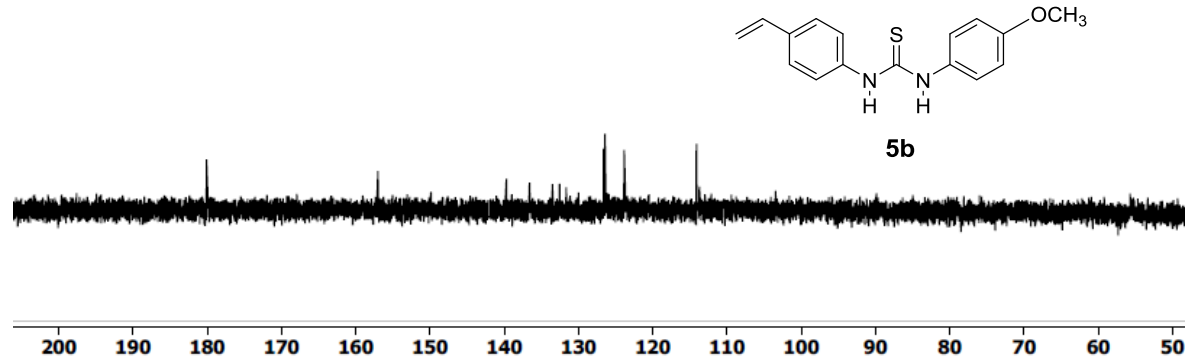

^{1}H NMR of compound **20**

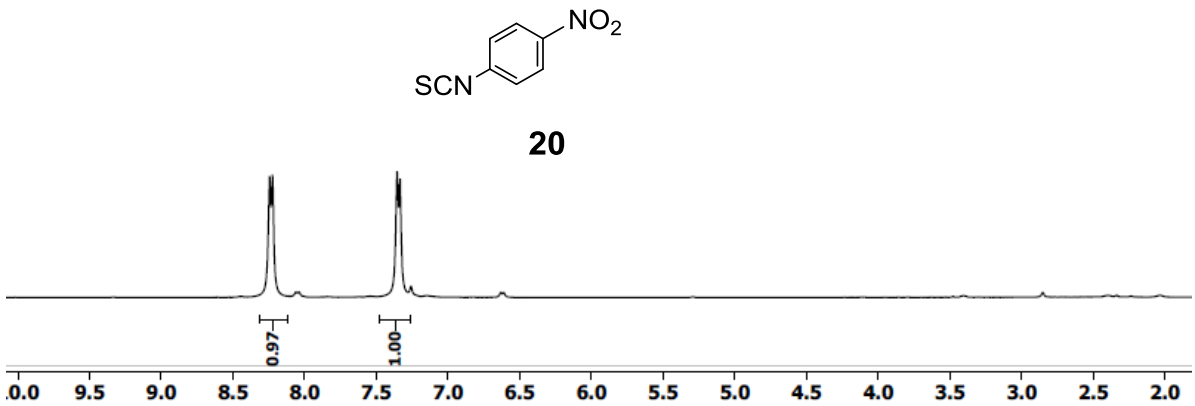

^{1}H NMR of compound **5c**

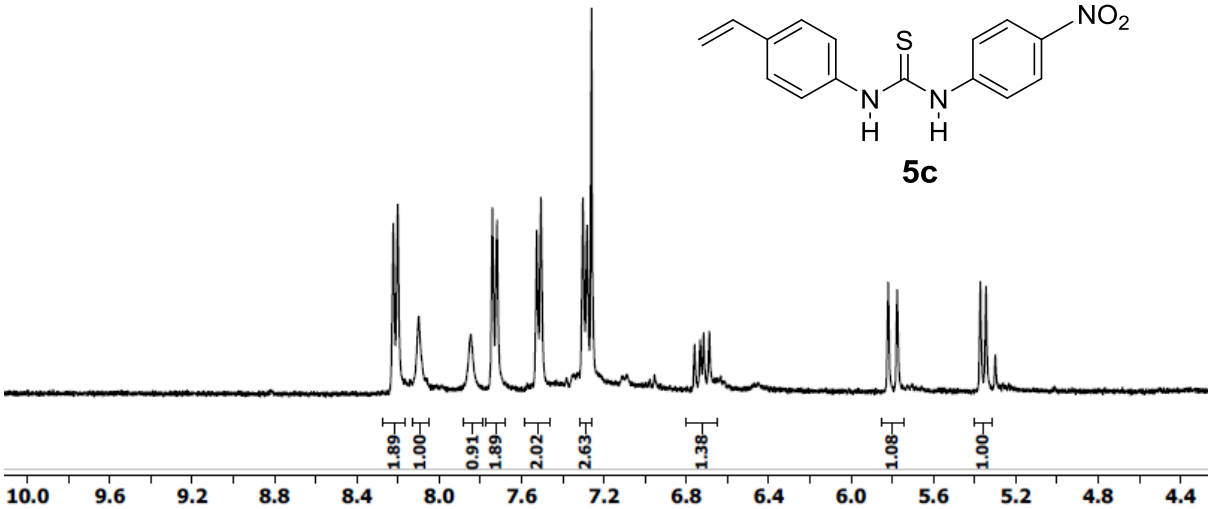

^{13}C NMR of compound **5c**

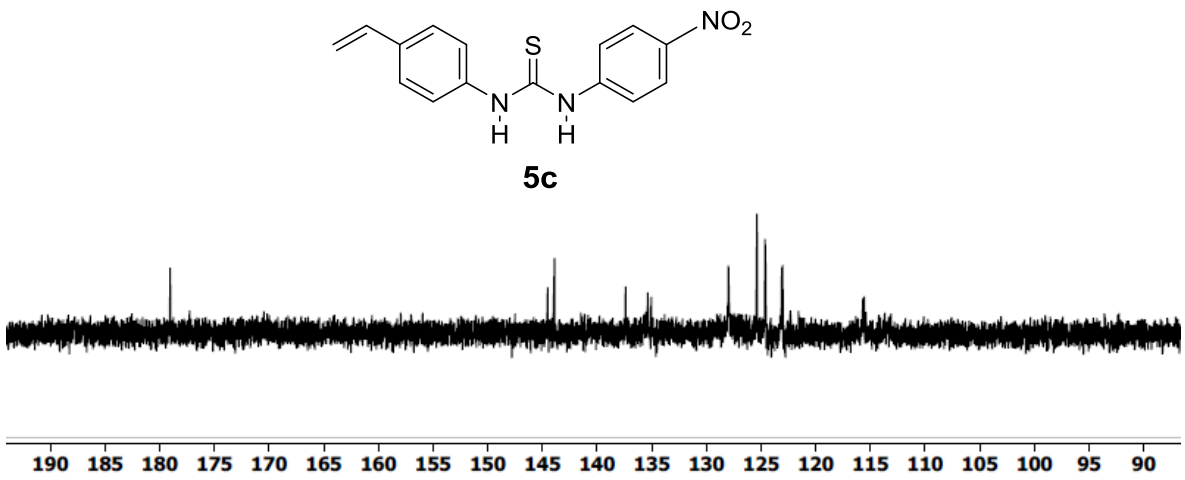

^{1}H NMR of compound **21**

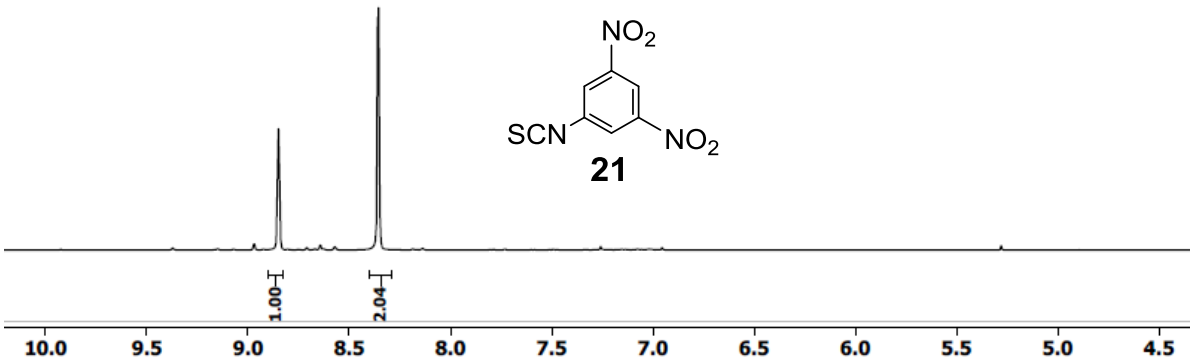

^{1}H NMR of compound **5d**

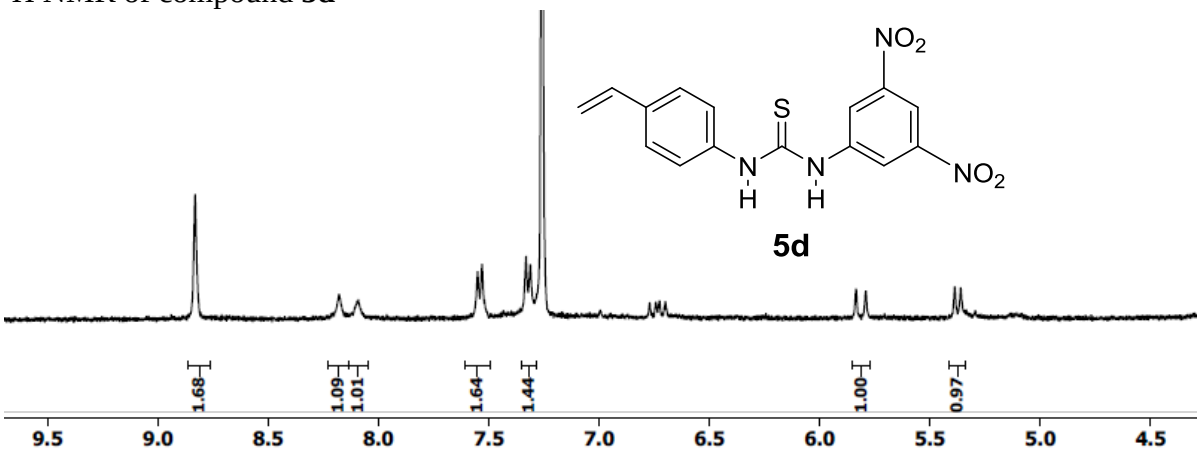

^{13}C NMR of compound **5d**

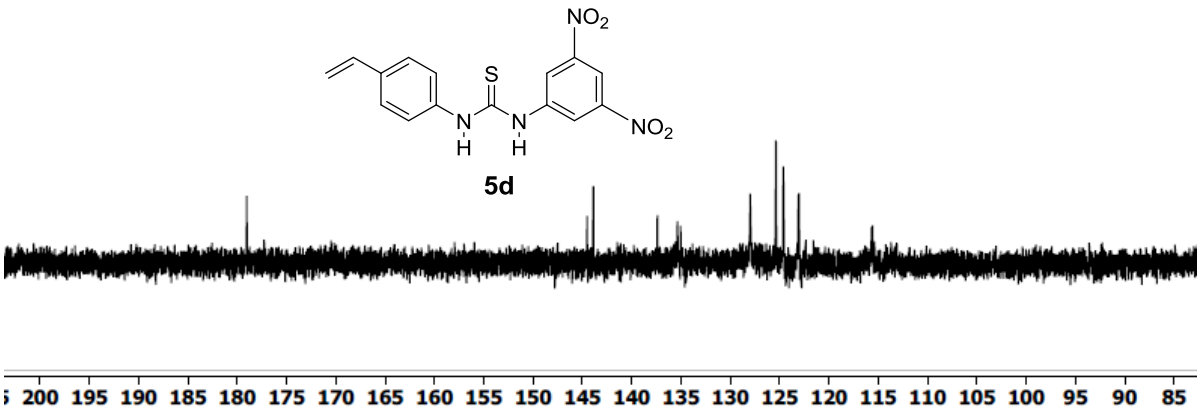

^{1}H NMR of compound **7**

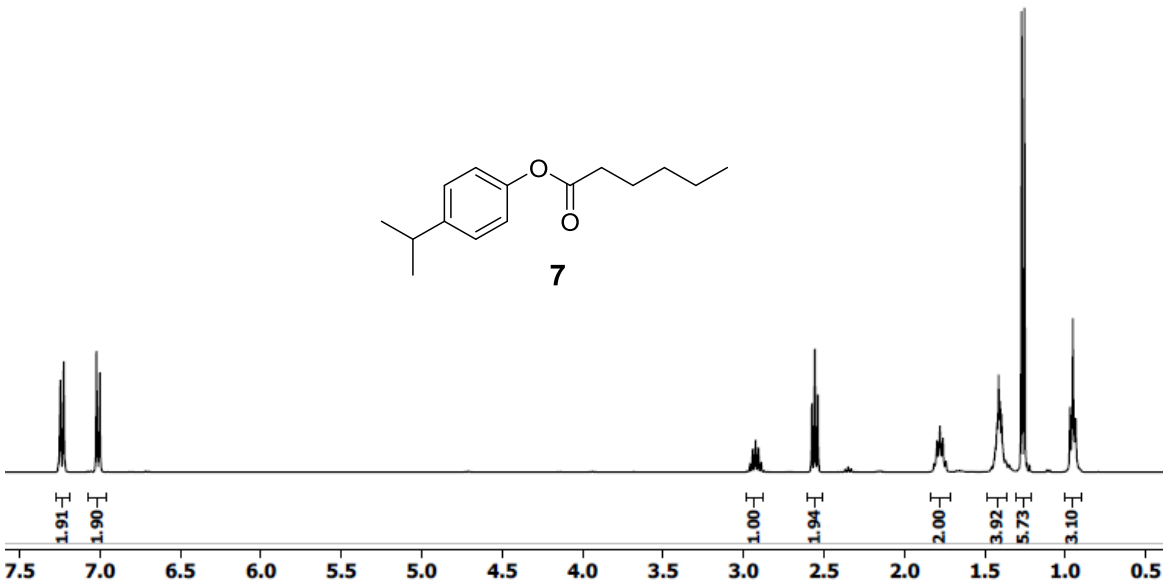

^{13}C NMR of compound **7**

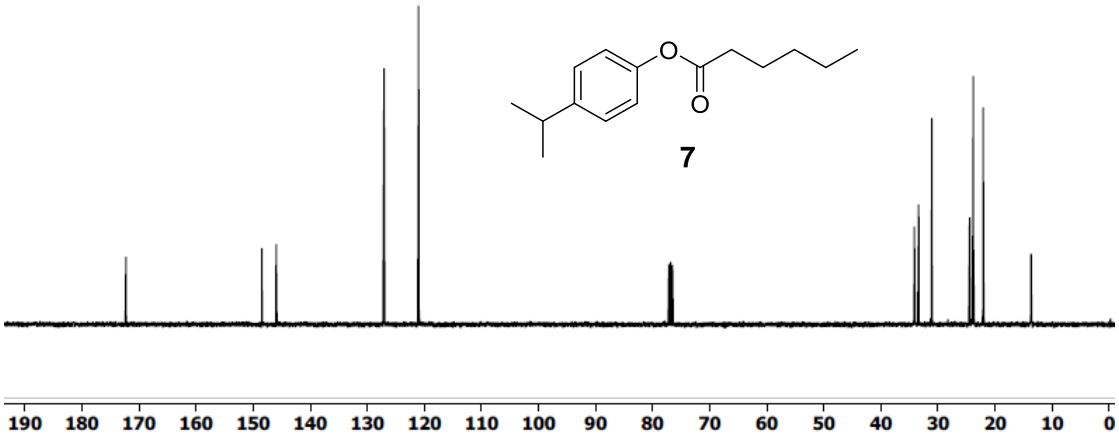

^{1}H NMR of compound **8**

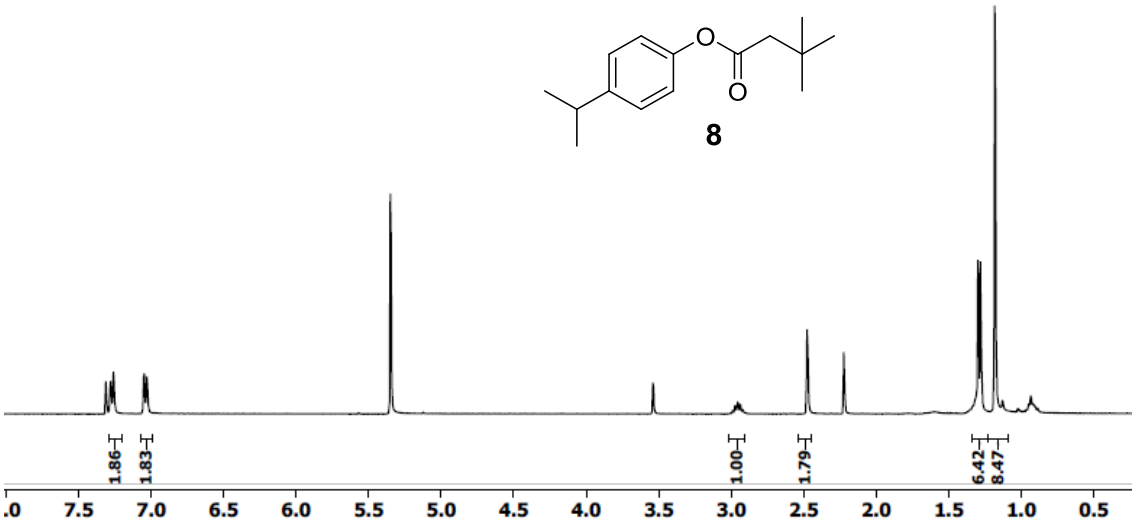

^{13}C NMR of compound **8**

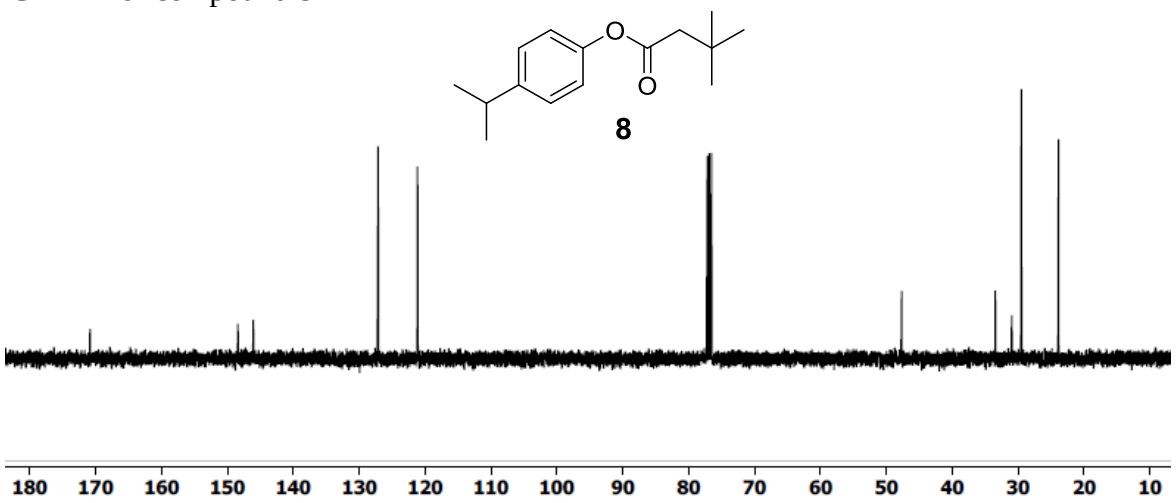

^{1}H NMR of compound **9**

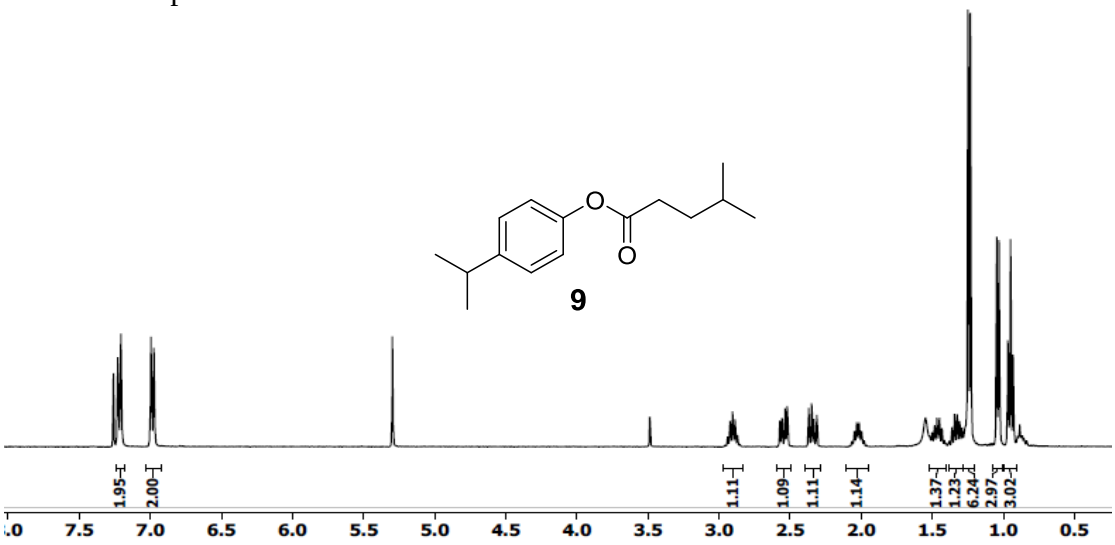

^{13}C NMR of compound **9**

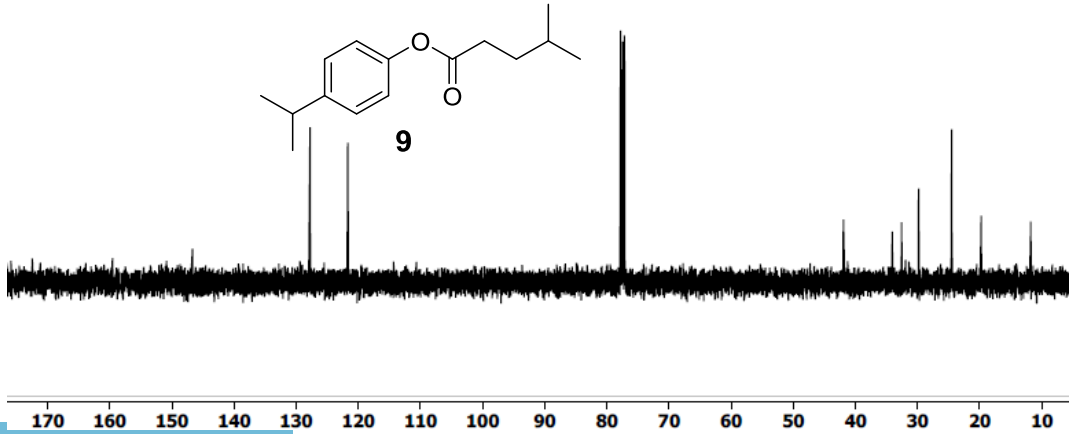

^{1}H NMR of compound **10**

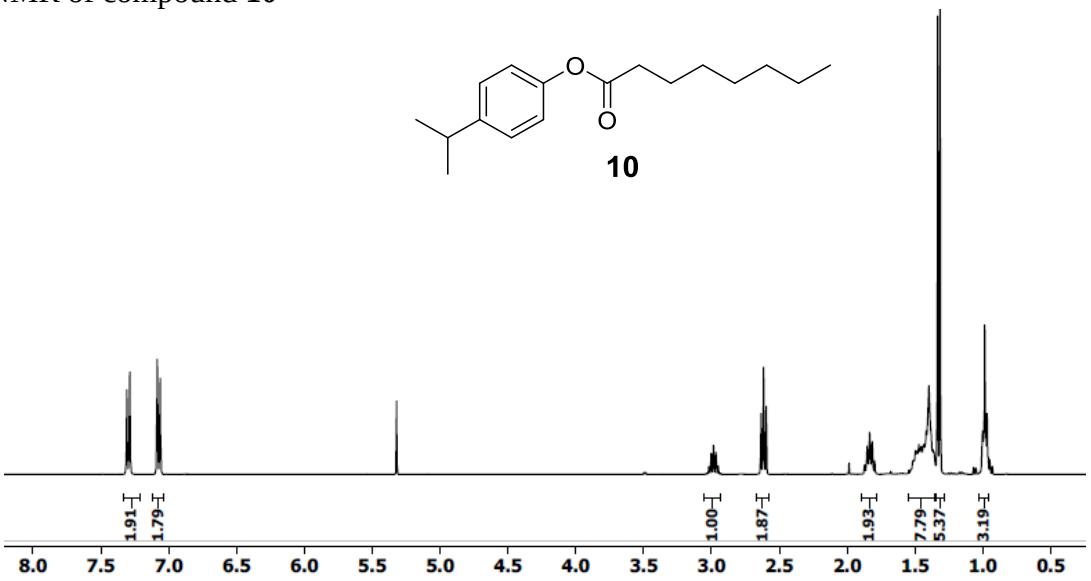

^{13}C NMR of compound **10**

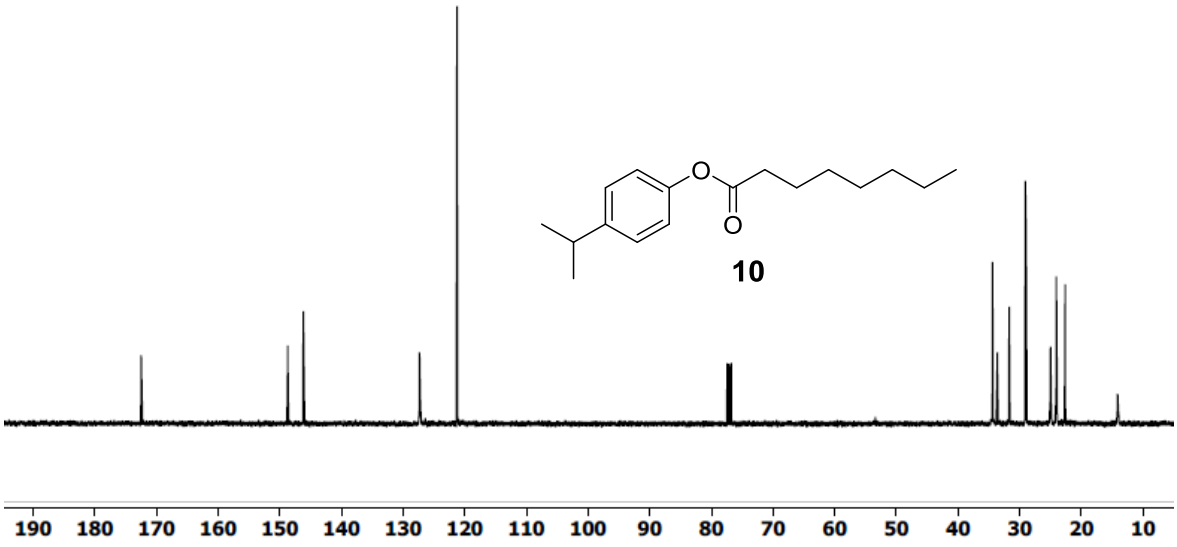

References

1. (a) Atwood, J. L.; Lehn, J. M.: *Comprehensive Supramolecular Chemistry*; Pergamon: New York, 1996. (b) Steed, J. W.; Gale, P. A.: *Supramolecular Chemistry: From Molecules to Nanomaterials*; Wiley: Weinheim, 2012. (c) Schneider, H.-J.; Yatsimirsky, A. K.: *Principles and Methods in Supramolecular Chemistry*; Wiley: New York, 2000.

2. (a) Breslow, R.: *Artificial Enzymes*; Wiley-VCH: Weinheim, 2005. (b) Das, S.; Brudvig, G. W.; Crabtree, R. H. Molecular Recognition in Homogeneous Transition Metal Catalysis: A Biomimetic Strategy for High Selectivity. *Chem. Commun.* **2008**, 413-424. (c) Rakowski DuBois, M.; DuBois, D. L. The Roles of the First and Second Coordination Spheres in the Design of Molecular Catalysts for H2 Production and Oxidation. *Chem. Soc. Rev.* **2009**, *38*, 62-72. (d) Meeuwissen, J.; Reek, J. N. H. Supramolecular Catalysis Beyond Enzyme Mimics. *Nat Chem* **2010**, *2*, 615-621. (e) Raynal, M.; Ballester, P.; Vidal-Ferran, A.; van Leeuwen, P. W. N. M. Supramolecular Catalysis. Part 2: Artificial Enzyme Mimics. *Chem. Soc. Rev.* **2014**, *43*, 1734-1787. (f) Bistri, O.; Reinaud, O. Supramolecular Control of Transition Metal Complexes in Water by a Hydrophobic Cavity: A Bio-Inspired Strategy. *Org. Biomol. Chem.* **2015**, *13*, 2849-2865.

3. Awino, J. K.; Zhao, Y. Protein-Mimetic, Molecularly Imprinted Nanoparticles for Selective Binding of Bile Salt Derivatives in Water. *J. Am. Chem. Soc.* **2013**, *135*, 12552-12555.

4. (a) Wulff, G. Enzyme-Like Catalysis by Molecularly Imprinted Polymers. *Chem. Rev.* **2001**, *102*, 1-28. (b) Wulff, G.; Liu, J. Design of Biomimetic Catalysts by Molecular Imprinting in Synthetic Polymers: The Role of Transition State Stabilization. *Acc. Chem. Res.* **2012**, *45*, 239-247. (c) Sellergren, B.; Karmalkar, R. N.; Shea, K. J. Enantioselective Ester Hydrolysis Catalyzed by Imprinted Polymers. 2. *J. Org. Chem.* **2000**, *65*, 4009-4027. (d) Emgenbroich, M.; Wulff, G. A New Enzyme Model for Enantioselective Esterases Based on Molecularly Imprinted Polymers. *Chem.-Eur. J.* **2003**, *9*, 4106-4117. (e) Liu, J.-q.; Wulff, G. Functional Mimicry of Carboxypeptidase a by a Combination of Transition State Stabilization and a Defined Orientation of Catalytic Moieties in Molecularly Imprinted Polymers. *J. Am. Chem. Soc.* **2008**, *130*, 8044-8054. (f) Kirsch, N.; Hedin-Dahlström, J.; Henschel, H.; Whitcombe, M. J.; Wikman, S.; Nicholls, I. A. Molecularly Imprinted Polymer Catalysis of a Diels-Alder Reaction. *J. Mol. Catal. B: Enzym.* **2009**, *58*, 110-117. (g) Chen, Z. Y.; Xu, L.; Liang, Y.; Zhao, M. P. Ph-Sensitive Water-Soluble Nanospheric Imprinted Hydrogels Prepared as Horseradish Peroxidase Mimetic Enzymes. *Adv. Mater.* **2010**, *22*, 1488-1492. (h) Servant, A.; Haupt, K.; Resmini, M. Tuning Molecular Recognition in Water-Soluble Nanogels with Enzyme-Like Activity for the Kemp Elimination. *Chem.-Eur. J.* **2011**, *17*, 11052-11059. (i) Shen, X.; Huang, C.; Shinde, S.; Jagadeesan, K. K.; Ekström, S.; Fritz, E.; Sellergren, B. Catalytic Formation of Disulfide Bonds in Peptides by Molecularly Imprinted Microgels at Oil/Water Interfaces. *ACS Appl. Mater. Interfaces* **2016**, *8*, 30484-30491. (j) Zheng, A.-x.; Gong, C.-b.; Zhang, W.-j.; Tang, Q.; Huang, H.-r.; Chow, C.-f.; Tang, Q. An Amphiphilic and Photoswitchable Organocatalyst for the Aldol Reaction Based on a Product-Imprinted Polymer. *Mol. Catal.* **2017**, *442*, 115-125.

5. Awino, J. K.; Gunasekara, R. W.; Zhao, Y. Sequence-Selective Binding of Oligopeptides in Water through Hydrophobic Coding. *J. Am. Chem. Soc.* **2017**, *139*, 2188-2191.

6. (a) Awino, J. K.; Gunasekara, R. W.; Zhao, Y. Selective Recognition of D-Aldohexoses in Water by Boronic Acid-Functionalized, Molecularly Imprinted Cross-Linked Micelles. *J. Am. Chem. Soc.* **2016**, *138*, 9759-9762. (b) Gunasekara, R. W.; Zhao, Y. A General Method for Selective Recognition of Monosaccharides and Oligosaccharides in Water. *J. Am. Chem. Soc.* **2017**, *139*, 829-835.

7. (a) Nowick, J. S.; Chen, J. S. Molecular Recognition in Aqueous Micellar Solution - Adenine Thymine Base-Pairing in Sds Micelles. *J. Am. Chem. Soc.* **1992**, *114*, 1107-1108. (b) Nowick, J. S.; Chen, J. S.; Noronha, G. Molecular Recognition in Micelles - the Roles of Hydrogen-Bonding and Hydrophobicity in Adenine Thymine Base-Pairing in Sds Micelles. *J. Am. Chem. Soc.* **1993**, *115*, 7636-7644.

8. (a) Fa, S.; Zhao, Y. Water-Soluble Nanoparticle Receptors Supramolecularly Coded for Acidic Peptides. *Chem. -Eur. J.* **2018**, *24*, 150-158. (b) Duan, L.; Zhao, Y. Selective Binding of Folic Acid and Derivatives by Imprinted Nanoparticle Receptors in Water. *Bioconjugate Chem.* **2018**, *29*, 1438-1445.

9. (a) Fa, S.; Zhao, Y. Peptide-Binding Nanoparticle Materials with Tailored Recognition Sites for Basic Peptides. *Chem. Mater.* **2017**, *29*, 9284-9291. (b) Zhao, Y. Sequence-Selective Recognition of Peptides in Aqueous Solution: A Supramolecular Approach through Micellar Imprinting. *Chem.-Eur. J.* **2018**, *24*, 14001-14009.

10. Xing, X.; Zhao, Y. Fluorescent Nanoparticle Sensors with Tailor-Made Recognition Units and Proximate Fluorescent Reporter Groups. *New J. Chem.* **2018**, *42*, 9377-9380.

11. Xing, X.; Zhao, Y. Binding-Promoted Chemical Reaction in the Nanospace of a Binding Site: Effects of Environmental Constriction. *Org. Biomol. Chem.* **2018**, *16*, 2855-2859.

12. (a) Awino, J. K.; Zhao, Y. Water-Soluble Molecularly Imprinted Nanoparticles (Minps) with Tailored, Functionalized, Modifiable Binding Pockets. *Chem.-Eur. J.* **2015**, *21*, 655-661. (b) Hu, L.; Zhao, Y. Molecularly Imprinted Artificial Esterases with Highly Specific Active Sites and Precisely Installed Catalytic Groups. *Org. Biomol. Chem.* **2018**, *16*, 5580-5584.

13. Palmer, T.: *Understanding Enzymes*; 4th ed.; Prentice Hall/Ellis Horwood: London ; New York, 1995.

14. (a) Der, B. S.; Edwards, D. R.; Kuhlman, B. Catalysis by a De Novo Zinc-Mediated Protein Interface: Implications for Natural Enzyme Evolution and Rational Enzyme Engineering. *Biochemistry* **2012**, *51*, 3933-3940. (b) Zastrow, M. L.; Peacock, A. F. A.; Stuckey, J. A.; Pecoraro, V. L. Hydrolytic Catalysis and Structural Stabilization in a Designed Metalloprotein. *Nat. Chem.* **2012**, *4*, 118-123. (c) Zastrow, M. L.; Pecoraro, V. L. Influence of Active Site Location on Catalytic Activity in De Novo-Designed Zinc Metalloenzymes. *J. Am. Chem. Soc.* **2013**, *135*, 5895-5903. (d) Song, W. J.; Tezcan, F. A. A Designed Supramolecular Protein Assembly with in Vivo Enzymatic Activity. *Science* **2014**, *346*, 1525-1528. (e) Rufo, C. M.; Moroz, Y. S.; Moroz, O. V.; Stohr, J.; Smith, T. A.; Hu, X. Z.; DeGrado, W. F.; Korendovych, I. V. Short Peptides Self-Assemble to Produce Catalytic Amyloids. *Nat. Chem.* **2014**, *6*, 303-309. (f) Burton, A. J.; Thomson, A. R.; Dawson, W. M.; Brady, R. L.; Woolfson, D. N. Installing Hydrolytic Activity into a Completely De Novo Protein Framework. *Nat. Chem.* **2016**, *8*, 837-844.

15. Menger, F. M.; Ladika, M. Origin of Rate Accelerations in an Enzyme Model: The P-Nitrophenyl Ester Syndrome. *J. Am. Chem. Soc.* **1987**, *109*, 3145-3146.

16. Arifuzzaman, M. and Zhao, Y. Water-Soluble Molecularly Imprinted Nanoparticles Receptors with Hydrogen-Bond-Assisted Hydrophobic Binding. *J. Org. Chem.* **2016**, *81*, 7518–7526.

17. Awino, J. K. and Zhao, Y. Protein-Mimetic Molecularly Imprinted Nanoparticles for Selective Binding of Bile Salt Derivatives in Water. *J. Am. Chem. Soc.* **2013**, *135*, 12552–12555.

17. Zhang, S. and Zhao, Y. Facile Synthesis of Multivalent Water-Soluble Organic Nanoparticles via Surface-Clicking of Alkylated Surfactant Micelles. *Macromolecules.* **2010**, *43*, 4020–4022.

19. Ryu, E-H. and Zhao, Y. Environmentally Responsive Molecular Baskets: Unimolecular Mimics of Both Micelles and Reversed Micelles. *Org. Lett.* **2004**, *6*, 3187–3189.

20. Chengyih, Y.; Weichen, Y. and Chienlu, W. Studies on Organophosphorous Compounds .VI. Monoester of *p*-Substituted Phenyl- and Benzylphosphonic Acids. *ACTA. CHIM. SINICA.* **1981**, 230–240.

21. Chao, H.; Zhong, Z.; and Zhao, Y. A DMAP-Functionalized Oligo-cholate Foldamer for Solvent-Responsive Catalysis. *Tetrahedron.* **2009**, *65*, 7311–7316.

22. Peyroux, P.; Berthiol, F. and Santelli, M. Suzuki Cross-coupling Reactions Between Alkenyl Boronic Acids and Aryl Bromides Catalyzed by Tetraphosphane-Palladium Catalyst. *Eur. J. Org. Chem.* **2004**, *5*, 1075–1082.

23. Schwob, T. and Kempe, R. Reusable Co Catalyst for Selective Hydrogenation of Functionalized Nitroarenes and Direct Synthesis of Imines and Benzimidazoles from Nitroarenes and aldehyde. *Angew. Chem. Int. Ed.* **2016**, *55*, 15175–15179.

24. Xiao, P.; Tang, Z,; Wang, K.; Chen, H.; Gue, Q.; Chu, Y.; Gao, L. and Song, Z. Chemoselective Reduction of Sterically Demanding *N,N*-Diisopropylamide to Aldehydes. *J. Org. Chem.* **2018**, *83*, 1687–1700.

25. Bellucci, C.; Gualtieri, F. and Chiartniz, A. Negative Inotropic Activity of *p/m*-Substituted Diethyl Benzylphosphonates Related to Fostedil. *Eur. J. Med. Chem.* **1987**, *22*, 473–477.

26. Bera, M.; Sahoo, S-K. and Maiti, D. Room-Temperature *meta*-Functionalization: Pd (II)-Catalyzed Synthesis of 1,3,6-Trialkenyl Arene and *meta*-Hydroxylated Olefin. *ACS. Catal.* **2016**, *6*, 3575–3579.

27. Shur, A. M. and Barba, N. A Chemical Transformation of Aminostyrenes. I. Synthesis of *p*-Styryl Isothiocyanate and Some Sunstituted Thioureas. *Russ. J. Org. Chem.* **1966**, *2*, 1819–1821.

28. Wroblewska, A. and Mloston, G. Synthesis of New Enantiopure Thioureas Derived from (s)-Proline. *Phosphorus, Sulfur silicon Relat. Elem.* **2013**, *188*, 509–5011.

29. Xing, X. and Zhao, Y. Tailor-Made Fluorescent Nanoparticles Sensor for Carboxylic Acids via Molecular Imprinting and Post Modification. *New. J. Chem.* **2018**, *42*, 9377–9380.

30. Xing, X. and Zhao, Y. Binding-Promoted Chemical Reaction in the Nanospace of a Binding Site: Effects of Environmental Constriction. *Org. Biomol. Chem.* **2018**, *16*, 2855–2859.

CHAPTER 6. GENERAL CONCLUSION

Overall, the research presented here explains an easy and effective way for the interaction between host and guest in the core and surface of the MINPs that are fully soluble and functional in water. MINPS were prepared from a tripropargylammonium headgroup and a methacrylate-functionalized surfactant with an amide near the surface. After surface cross-link, surface decoration with a sugar and core cross linked by using DVB, the MINPs contained guest-tailored pocket with a layer of hydrogen-bonding groups in the interior that strongly influenced their molecular recognition. To verify for the formation of the pocket, binding studies were performed using isothermal titration calorimetry and fluorescence spectroscopy. MINPs act as an antibody for the antigen, in which the antigen fit perfectly based on the chemical structure and their different kinds of chemical interaction like H-bond, pi-pi, hydrophobic etc. Amide layer containing nanoparticles resembled natural proteins in water-solubility, hydrophilic surface and hydrophobic core with H-bond capabilities, and in their discrete nanosized structure.

MINPs showed many interesting features including easy preparation, perfect imprinting by removal of the template, selective binding toward different guests based on fine-tune size imprinted hydrophobic core that fits to different guests as well as some nonsteroidal anti-inflammatory drugs (NSAIDs).

To investigate the binding interaction inside the amide-functionalized MINPs, a sizable template/guest is needed. Binding studies were performed using ITC and fluorescence spectroscopy revealed 1:1 binding with high affinity and selectivity for the corresponding

guest/template. The template with hydrogen-bonding groups can interact strongly inside the MINPs. The study gives us a clear view of different intermolecular interactions to enhance the binding of molecularly imprinted nanoparticle receptors.

Molecular recognition is difficult in water due to weak non-covalent interactions caused from competitive binding with water. Multiple interactions between the template and the binding site can increase the molecular recognition based on the structure of the guest. In this work we explore this application in our system. Our hydrophilic surface ligands on the nanoparticle could interact with the hydrophilic groups of the template. The resultant MINPs can bind the template by both hydrophobic interaction inside the core and hydrophilic interactions with the surface of the nanoparticle based on the structure of the template.

Enzyme showed very high catalytic activity and selectivity because the active sites of enzymes are usually hydrophobic which, enables hydrophobic substrates to bind in the interiors in high turnover i.e. less product inhibition due to the high affinity for the transition state rather than the reactants or products. In this dissertation, we prepared bio-inspired water soluble artificial Zn-enzyme to mimics catalysis in water. We were able to easily tuned the position of the active site of the substrate as well as the position of the catalyst .This active site could hydrolysis different kind of ester based on the size and shape of the pocket made from corresponding amine template. Our imprinted zinc catalysts were able to distinguish substrates that differed by the position of a single methyl group, chain length of the acyl chain, and substitution of the phenyl ring. The turnover number is higher than other artificial Zn-enzyme because of formation of the polar product leaching to the water.

The active site of the enzyme often contains multiple catalytic groups working cooperatively in the active site of a nanospace with multiple interactions including hydrogen

bonding, electrostatics, van der Waals interaction, p–p interaction, steric effect, shape complementarity and so on to control the motions of macromolecular structure, substrate recognition, transition state stabilization, and product release. We prepared nanoparticles imprinted by an imine-based template-functional monomer (T-FM) complex with thiourea containing anion hole to host an aldehyde group inside the MINP binding site. Post functionalized by amine containing DMAP derivatives leaves a hydrophobic pocket with thiourea as an anion hole. Our imprinted catalyst was able to increase the reaction rate for hydrolysis both active and non-active ester with some selectivity that differed by the position of a single methyl group and chain length of the acyl chain by assisting through H-bonding from the anion hole during the transition state of the reaction.

From this point, we have built plastic antibodies that could find many applications in chemistry and biology. We also prepared a very unique artificial enzyme that can be used to hydrolyze active and non-active substrate efficiently. Further improvement of the catalyst could be utilized in biological systems toward practical application.